investigations of the transonic flow around oscillating airfoils

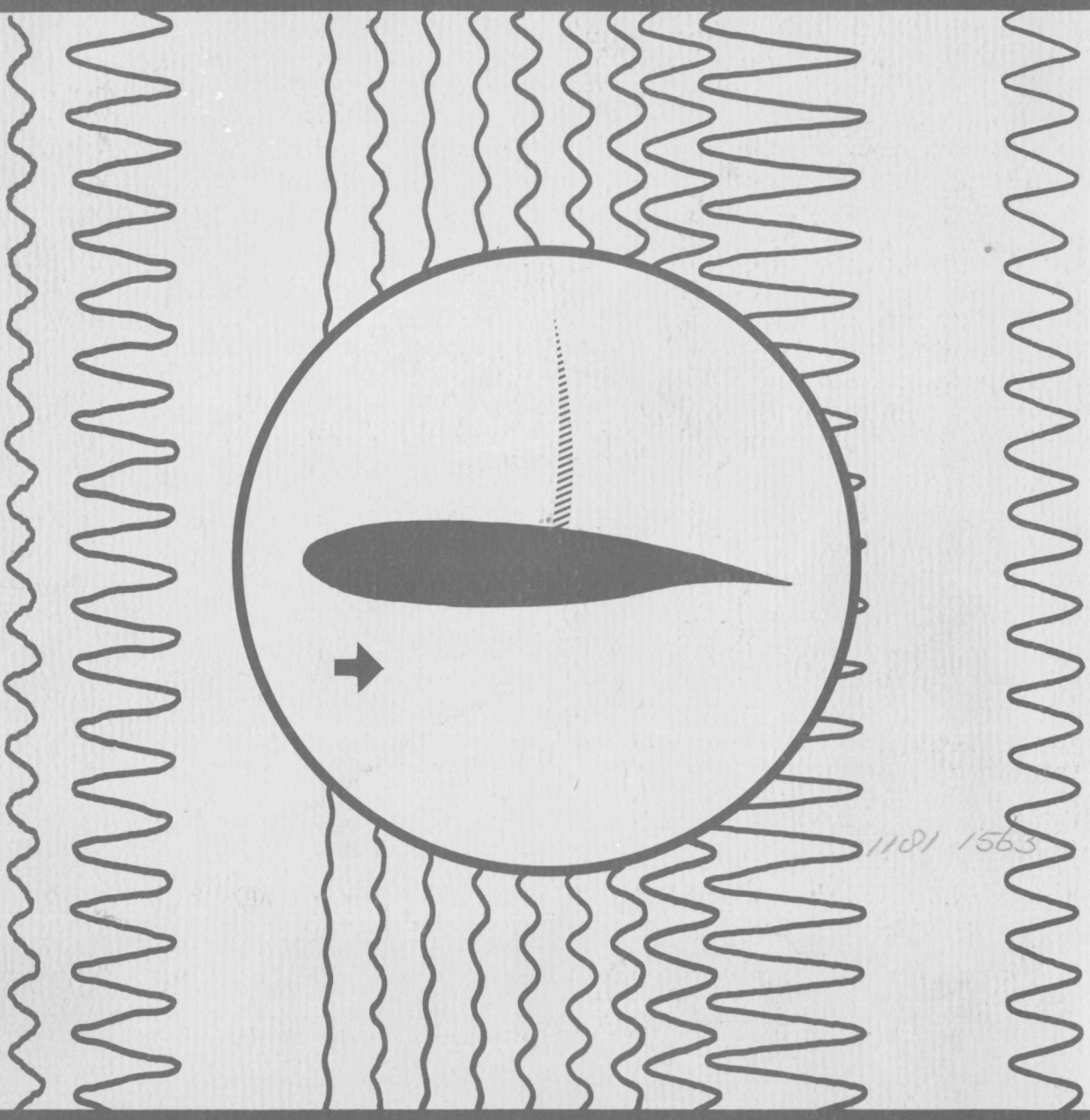

1181 1565

hendrik tijdeman

C10029
82948
P1181
1563
VERVALLEN

INVESTIGATIONS OF THE TRANSONIC FLOW AROUND OSCILLATING AIRFOILS

PROEFSCHRIFT

TER VERKRIJGING VAN DE GRAAD VAN DOCTOR IN DE TECHNISCHE WETENSCHAPPEN AAN DE TECHNISCHE HOGESCHOOL DELFT, OP GEZAG VAN DE RECTOR MAGNIFICUS PROF. IR. L. HUISMAN, VOOR EEN COMMISSIE AANGEWEZEN DOOR HET COLLEGE VAN DEKANEN TE VERDEDIGEN OP WOENSDAG 21 DECEMBER 1977 TE 16.00 UUR

DOOR

HENDRIK TIJDEMAN

vliegtuigbouwkundig ingenieur

geboren te Alkmaar

1181 1563

BIBLIOTHEEK DER TECHNISCHE HOGESCHOOL DELFT
78
000655
DOELENSTR. 101

BIBLIOTHEEK TU Delft
P 1181 1563
C 298294

DIT PROEFSCHRIFT IS GOEDGEKEURD DOOR DE PROMOTOR PROF. IR. H. BERGH

EN DE COPROMOTOR PROF. DR. IR. J.L. VAN INGEN

VOOR JEANNETTE

ACKNOWLEDGMENTS

The author is indebted to the Directors of the Nationaal Lucht- en Ruimtevaartlaboratorium (National Aerospace Laboratory NLR) for their permission to publish the results of the investigations in this form.

The experiments described in this paper have been carried out in collaboration with Fokker-VFW under contract with the Netherlands Agency for Aerospace Programs (NIVR). The permission of the NIVR and Fokker-VFW to use the results for the present purpose is gratefully acknowledged.

Severe gratitude is expressed to the many colleagues at NLR, who contributed in one way or another to the extensive program. The following persons should be mentioned specifically: Messrs. R.J. Zwaan, J.W. Slooff and Dr. R. Roos for the stimulating and fruitful discussions and Messrs. P. Schippers, J.W.G. van Nunen, A.J. Persoon and R. Poestkoke for their skilful assistance in preparing and executing the experiments. Further, the author owes many thanks to Mrs. Dr. A.A.C. Klaasse for critical reviewing and Mrs. J.H. Buttstedt for careful typing of the manuscript and to Messrs. H. Willigers, A. Timmer, R. Bons and J.T.A.M. Groos, who took care of the lay-out and assisted in preparing the many illustrations.

SUMMARY

Exploratory wind-tunnel experiments in high-subsonic and transonic flow on a conventional airfoil with oscillating flap and a supercritical airfoil oscillating in pitch are described. In the analysis of the experimental results, emphasis is placed upon the typical aspects of transonic flow, namely the interaction between the steady and unsteady flow fields, the periodical motion of the shock waves and their contribution to the overall unsteady airloads. Special attention is paid to the behaviour of the supercritical airfoil in its "shock-free" design condition. Moreover, it is discussed to what extent linearization of the unsteady transonic flow problem is allowed if the unsteady field is considered as a small perturbation superimposed upon a given mean steady-flow field. Finally, the current status of unsteady transonic flow theory is reviewed and the present test data are used to evaluate some of the recently developed calculation methods.

CONTENTS

		Page
1	BACKGROUND AND OUTLINE OF THESIS	9
	1.1 Background	9
	1.2 Outline of thesis	11
PART 1: INTRODUCTORY CHAPTERS		
2	THE FLOW AROUND OSCILLATING AIRFOILS	15
	2.1 Description of unsteady airloads	15
	2.2 Some notes on the unsteady-flow equations	16
	2.2.1 The unsteady-flow equations	
	2.2.2 Moderately subsonic and supersonic flow	
	2.2.3 Transonic flow	
	2.3 Present status of the research on unsteady transonic flow	19
3	MAIN CHARACTERISTICS OF THE STEADY TRANSONIC FLOW AROUND AIRFOILS	20
	3.1 Transonic flows with embedded shock waves	20
	3.1.1 Development of flow pattern with Mach number, flap angle, and incidence	
	3.1.2 Characteristics of a normal shock wave	
	3.2 Shock-free flow	22
	3.3 Some particular flow patterns on airfoils with flap	22
	3.4 Viscous aspects	24
PART II: SCOPE AND DESCRIPTION OF THE EXPERIMENTAL INVESTIGATIONS		
4	SCOPE OF THE NLR INVESTIGATIONS	29
	4.1 Problem definition	29
	4.2 Approach	29
5	TECHNIQUE FOR UNSTEADY PRESSURE MEASUREMENTS	30
	5.1 Principle of the measuring technique	30
	5.2 Theoretical model for the dynamic response of tube-transducer systems	31
	5.2.1 The propagation of pressure waves through cylindrical tubes	
	5.2.2 Solution for complete tube-transducer systems	
	5.3 The dynamic characteristics of tube-transducer systems	33
	5.3.1 The dynamic response in still air	
	5.3.2 Influence of the airflow	
	5.3.3 Verification in a joint ONERA-NLR investigation	
	5.4 Practical application in wind-tunnel tests	35
	5.4.1 Choice and calibration of tube-transducer systems	
	5.4.2 Measuring equipment and data reduction	
6	WIND-TUNNEL MODELS AND TEST SET-UP	38
	6.1 NACA 64A006 airfoil with flap	38
	6.2 NLR 7301 airfoil	39
	6.3 Wind tunnel	41
	6.4 Optical flow studies	41
7	TEST PROGRAM	42
	7.1 NACA 64A006 airfoil with flap	42
	7.2 NLR 7301 airfoil	42

Page

PART III: ANALYSIS OF RESULTS

8 THE INTERACTION BETWEEN THE STEADY AND UNSTEADY FLOW FIELD 47

8.1 Introductory remarks 47

8.2 The influence of Mach number on the airloads of the NACA 64A006 airfoil with flap 47

8.2.1 Steady pressure distributions
8.2.2 Unsteady pressure distributions
8.2.3 Unsteady aerodynamic coefficients

8.3 Graphical experiment 53

8.4 The influence of incidence and mean flap angle 54

8.4.1 Unsteady pressure distributions
8.4.2 Unsteady aerodynamic coefficients

8.5 The influence of frequency 58

8.5.1 Unsteady pressure distributions
8.5.2 Unsteady aerodynamic coefficients

9 ON THE PERIODICAL MOTION OF SHOCK WAVES 62

9.1 Introductory remarks 62

9.2 Shock strength and shock position in steady flow 62

9.3 Types of shock-wave motion observed in unsteady flow 64

9.4 Introduction of an analytical model 66

9.4.1 Relation between shock position and shock strength
9.4.2 Application of the analytical model

9.5 Additional remarks 69

9.5.1 Some properties of the unsteady shock relations
9.5.2 Possible use of the shock-wave model

10 THE UNSTEADY AERODYNAMIC CHARACTERISTICS OF THE "SHOCK-FREE" NLR 7301 AIRFOIL 70

10.1 Introductory remarks 70

10.2 Unsteady pressure distributions 71

10.2.1 Fully subsonic flow (condition I)
10.2.2 Transonic flow with shock wave (condition II)
10.2.3 The "shock-free" design condition (condition III)

10.3 Unsteady aerodynamic coefficients 75

10.4 Remarks on the motion of the shock wave 78

10.5 The influence of the transition strip 81

10.6 Some additional effects 83

10.6.1 The effect of Mach number
10.6.2 The effect of the amplitude of oscillation

10.7 Concluding remarks 84

11 SOME CONSIDERATIONS ON A LINEARIZED TREATMENT OF UNSTEADY TRANSONIC FLOWS 86

11.1 Introductory remarks 86

11.2 Flow conditions with an oscillating shock wave 86

11.2.1 Local effects of a shock wave
11.2.2 Contribution of a shock wave to the overall aerodynamic loads

11.3 Special flow conditions 89

11.3.1 "Shock-free" flow
11.3.2 Flow with a double shock
11.3.3 Flow around an airfoil with flap

11.4 Concluding remarks 92

PART IV: THE CURRENT STATUS OF UNSTEADY FLOW THEORY AND EVALUATION OF SOME NEW METHODS FOR UNSTEADY TRANSONIC FLOW

Page

12 REVIEW OF CALCULATION METHODS FOR TWO-DIMENSIONAL UNSTEADY FLOW 95

12.1 Classification of the various methods 95

12.2 Linearized subsonic lifting-surface theory 99

12.2.1 The integral equation relating downwash and load distribution
12.2.2 The Kernel-function method
12.2.3 The Doublet-Lattice method

12.3 Methods for high-subsonic flow 100

12.3.1 Local-Mach-number corrections in linearized lifting-surface theory
12.3.2 Methods based on the linearized transonic small-perturbation equation

12.4 Methods for near-sonic flow without shock waves 102

12.5 Methods for transonic flow with shock waves 102

12.5.1 General remarks
12.5.2 Methods based on the Euler equations
12.5.3 Methods based on the potential equation

12.6 Role of the NLR results 104

13 EVALUATION OF SOME NEW CALCULATION METHODS FOR UNSTEADY TRANSONIC FLOW 105

13.1 Introductory remarks 105

13.2 Comparisons between theory and experiment in steady and quasi-steady flow 106

13.2.1 Correction for tunnel-wall interference
13.2.2 Subsonic flow
13.2.3 Transonic flow with shock wave
13.2.4 "Shock-free" flow

13.3 Comparisons between theory and experiment in unsteady flow 111

13.3.1 Pressure distributions
13.3.2 Aerodynamic coefficients
13.3.3 Shock-wave motions

13.4 Concluding remarks 117

14 IMPACT OF THE NLR INVESTIGATIONS AND FUTURE PROSPECTS 118

14.1 Impact of the NLR investigations 118

14.2 Future prospects 118

15 REFERENCES 119

APPENDIX A: DEFINITION OF STEADY AND UNSTEADY AERODYNAMIC QUANTITIES 129

APPENDIX B: THE DYNAMIC RESPONSE OF TUBE-TRANSDUCER SYSTEMS 131

APPENDIX C: DERIVATION OF THE QUASI-STEADY AND UNSTEADY SHOCK RELATIONS 143

APPENDIX D: LIST OF SYMBOLS 145

APPENDIX E: SUMMARY IN DUTCH (SAMENVATTING IN HET NEDERLANDS) 147

1 BACKGROUND AND OUTLINE OF THESIS

1.1 BACKGROUND

Under certain conditions, structures like airplane wings and tail surfaces may experience vibrations of an unstable nature.
This phenomenon, called "flutter", is an aeroelastic problem, determined by the interaction of the elastic and inertial forces of the structure and the unsteady aerodynamic forces generated by the oscillatory motion of the structure itself. In general, two or more vibration modes are involved - for instance bending and torsional vibration of a wing - which, under the influence of the unsteady aerodynamic forces, interact with each other such that the vibrating structure extracts energy from the passing airstream. This leads to a progressive increase in amplitude of vibration, usually ending up in a disintegration of the structure.

As for a given configuration of a structure the unsteady aerodynamic forces increase rapidly with flight speed, while the elastic and inertia forces remain almost unchanged, normally there exists a critical flight speed ("flutter speed"), above which flutter occurs. Because of the disastrous character of the phenomenon, the aircraft manufacturers have to prove that the flutter speeds of their products are well outside the flight envelope, and in this respect they have to meet severe airworthiness requirements.

In many cases the demands for flutter freedom are the determining factors for the construction of wings and tail surfaces. For this reason, much attention has been paid to the development of adequate calculation methods to predict the flutter characteristics of aircraft. The vibration characteristics of the structure at zero airspeed can be determined accurately by sophisticated calculation methods or by ground vibration tests. Therefore, the accuracy of the flutter prediction depends mainly on the knowledge of the unsteady aerodynamic forces.

In the subsonic and supersonic flight regimes, the unsteady aerodynamic forces can be predicted reasonably well by theoretical means. For the transonic flight regime, with its mixed subsonic-supersonic flow patterns, these means are less developed. Here the aeroelastician is hampered seriously by the lack of effective calculation methods to determine the unsteady air loads. For wing sections in two-dimensional flow, calculation methods become available at the moment, but the current practice for wings of general planform still is that rather arbitrary interpolations and extrapolations are being made on the basis of calculated airloads for pure subsonic and supersonic flow. In many cases, one has to resort to very expensive wind-tunnel experiments.

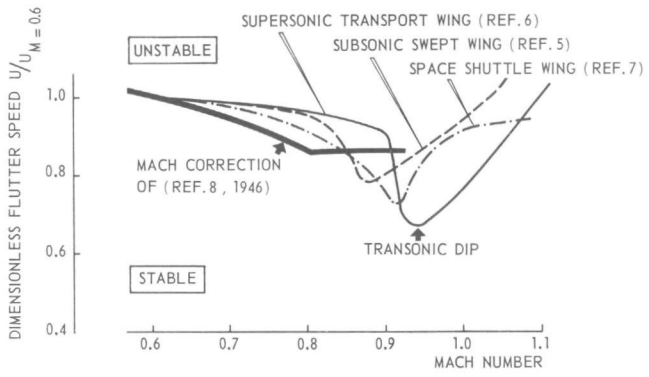

Fig. 1.1 Flutter speed versus Mach number curve showing the "transonic dip".

This situation is very unsatisfactory, especially since experience shows (Refs. 1-4) that flutter problems often become most critical for transonic-flow conditions. The main reason for this is the rather peculiar behaviour of the unsteady aerodynamic forces in transonic flows, in particular when strong shock waves are involved. This is reflected, for instance, in the behaviour of the flutter speed for bending-torsion flutter as a function of Mach number (Fig. 1.1), which shows the so-called "transonic dip", a region of relatively low flutter speeds in the transonic flight regime. In addition to the results of some wind-tunnel investigations (Refs. 5-7), also the Mach-number correction as proposed in 1946 for a flutter criterion for wing torsional stiffness (Ref. 8) is given in figure 1.1, which illustrates the presence of an old problem.

The first transonic-flutter problems were encountered during world war II by aircraft of advanced design at that time (Typhoon, Fury), which were able to penetrate the transonic regime during a diving flight. A number of aircraft lost ailerons and tails, sometimes ending up in fatal accidents. These early experiences gave the transonic regime its veil of mysticism and contributed to the many myths that came into being about the difficulties associated with crossing the "sound barrier". At that time it was impossible to get aerodynamic data for the transonic range, because there were no transonic wind tunnels available and there was little or no support by theoretical means.

During the first fifteen years after the war, the knowledge of transonic flows is improved considerably by the experience gained with a number of flying models and research aircraft, like the Bell X-1, and the development of transonic wind tunnels with slotted and porous walls, which greatly enlarged the possibilities for obtaining aerodynamic data under controlled conditions. The main interest in this period, however, was not the transonic regime itself. The attention was focussed primarily on the development of military aircraft for supersonic operations, and the transonic speed range was only a transient phase that had to be passed safely without excessive drag rise and without severe vibration and stability problems.

This situation has changed since the late sixties, when a renewed interest for transonic flight started. As far as military aviation is concerned, this increased interest stems from the demand for a new generation of "air-combat fighters", like the F-16 and F-17, which require an optimal manoeuvrability under transonic-flow conditions. In civil aviation, the interest is stimulated by the new concept of the so-called "supercritical wing", which should make it possible to cruise at transonic speeds without the usual drag penalty associated with the presence of shock waves. This can be achieved by shaping the wing geometry in such a way that the transition from local flow regions with supersonic flow to the adjacent subsonic regions does not take place with strong shock waves, as on the conventional-type wings, but with only very weak shock waves or even without them.

The advantages of local supersonic regions on the wing without noticeable wave drag can be utilized in several ways. For instance, in comparison with conventional wings, one may use thicker wings or reduced sweep angles at the same cruise Mach number. Another possibility is to increase the cruise Mach number at constant wing thickness and sweep angle. The first application will lead to a more efficient wing construction, the second will lead to an increased cruising speed, both without extra drag penalty.

In contrast with the first phase in the history of transonic flight, the recent developments are supported - at least as far as steady flow is concerned - by a number of highly computer-oriented calculation methods, which enable the prediction of transonic flow patterns around airfoils and wings, with and without shock waves. Important contributions in this respect are the methods developed by Nieuwland (Ref. 9) and Boerstoel (Ref. 10) for the design of supercritical airfoils. (For a review of computational methods for steady transonic flow, reference is made to references 11-16.) The extensive computations required for this purpose became possible by the enormous development in computer technology and numerical mathematics during the last two decades. In addition, the knowledge about the physical behaviour of steady transonic flows has been increased considerably by the fundamental experimental investigations of Holder (Ref. 17), Pearcy et al. (Refs. 18, 19) and Spee (Ref. 20).

As already mentioned, the situation with respect to unsteady flow is still very unsatisfactory. Stimulated, however, by the renewed interest in transonic flight and the encouraging progress in steady-flow computations, the efforts to solve the unsteady-flow problem have become stronger than ever before.

It is clear that the success of new calculation methods for unsteady transonic flow will depend largely on the reliability that can be achieved in describing phenomena typical for unsteady transonic flow. However, in contrast with

the steady-flow case, experimental data that are sufficiently detailed to verify fundamental theoretical assumptions or to confirm the validity of calculated results were very scarce, and it is in this respect that the present work aims to contribute.

1.2 OUTLINE OF THESIS

In an attempt to improve the physical insight into the nature of unsteady transonic flows and to furnish experimental evidence that could support the development of theoretical or semi-empirical methods, it was decided at NLR to perform a program of exploratory wind-tunnel investigations on oscillating airfoils in two-dimensional flow. With the aid of a special technique developed by Bergh (Refs. 21 and 22), detailed steady and unsteady pressure distributions were determined on an airfoil of conventional type (NACA 64A006) with an oscillating trailing edge flap and on an advanced-type supercritical airfoil (NLR 7301) performing oscillations in pitch. In addition, time histories of the shock-wave motions were recorded. The investigations were limited to attached flow, so unsteady-flow phenomena like "buffet" or "buzz", occurring in situations with severely separated flows, were left out of consideration.

The thesis is subdivided into four parts.

Part I starts with a general description of the flow around oscillating airfoils, which is followed by a consideration of specific problems associated with transonic flows. It is shown that in the transonic speed range an essential coupling exists between the steady and unsteady flow field, which does not occur for moderately subsonic and supersonic speeds. This coupling causes one of the main difficulties in transonic unsteady aerodynamics, since it implies that the unsteady-flow problem can be treated no longer independently of the steady-flow problem. For this reason, part I is concluded with a brief description of the main characteristics of steady transonic flows (chapter 3).

Part II describes the wind-tunnel investigations of both the NACA 64A006 airfoil with oscillating flap and the NLR 7301 airfoil performing oscillations in pitch. Details are discussed of the technique for unsteady pressure measurements developed at NLR (chapter 5), the models and test set-up (chapter 6), and the test program (chapter 7).

In part III, an analysis is given of the results of the experiments. In this analysis, emphasis is placed upon the effects that are typical for high subsonic and transonic flow. In chapter 8, results for the NACA 64A006 airfoil are used to illustrate the mechanism of the interaction between the steady and unsteady flow fields. Further it is demonstrated that the presence of oscillating shock waves may contribute significantly to the overall unsteady airloads. In chapter 9, the existence is shown of three different types of periodical shock-wave motion. These types are explained by means of a simple analytical model. Next, in chapter 10, some aspects of the unsteady flow around a supercritical airfoil are discussed with the aid of results for the NLR 7301 airfoil. In this chapter, results for oscillations around the "shock-free" design condition of this airfoil, as well as results for some typical off-design conditions, are considered. Finally, in chapter 11, the question is raised to what extent linearization of the unsteady-flow problem is possible, if the unsteady field is considered as a small perturbation of a given mean steady condition.

Part IV starts with a review of the current status of two-dimensional unsteady-flow theory, in which emphasis is placed upon the recent developments in this field (chapter 12). It is shown that in the past few years, especially in the USA, considerable progress has been achieved in solving the complicated unsteady-flow equations numerically. The exploratory investigations at NLR have been made just in time to support these developments, and at present the NLR data are being used extensively for the purpose of comparison in the majority of the recent theoretical studies. At the same time, this situation enables the author to conclude this work with a first evaluation of a number of new computational methods for unsteady transonic flow (chapter 13).

PART I INTRODUCTORY CHAPTERS

2 THE FLOW AROUND OSCILLATING AIRFOILS

2.1 DESCRIPTION OF UNSTEADY AIRLOADS

When an airfoil is performing sinusoidal oscillations around a given mean condition, the circulation and, hence, the lift force and local pressures show periodical variations. In order to keep the total vorticity constant (according to Helmholtz' theorem), each time-dependent change in circulation around the airfoil is compensated by the shedding of free vorticity from the trailing edge. This vorticity, which has the same strength as the change in circulation but is of opposite sign, is carried downstream by the flow (Fig. 2.1). Due to the velocities at the airfoil induced by the free vortices, the instantaneous incidence of the airfoil is changed in such a way that the oscillatory part of the lift lags behind the motion of the airfoil.

The main parameter governing the unsteady flow is the so-called reduced frequency, k, defined as $k = \omega\ell/U_\infty$, which is proportional to the ratio of the chord length 2ℓ and the wave length L (Fig. 2.1). This parameter is a measure for the unsteadiness of the flow. For similarity of the flow around an oscillating full-scale airfoil and its wind-tunnel model representation it is required that, besides the important parameters for steady flow (airfoil shape, incidence, Mach number and Reynolds number), also the reduced frequency for the model tests is the same as in reality.

As a typical example, figure 2.2 gives some time histories of the local pressures and the resulting lift and moment on an airfoil performing oscillations in pitch. Both the pressures and the overall loads show almost sinusoidal variations

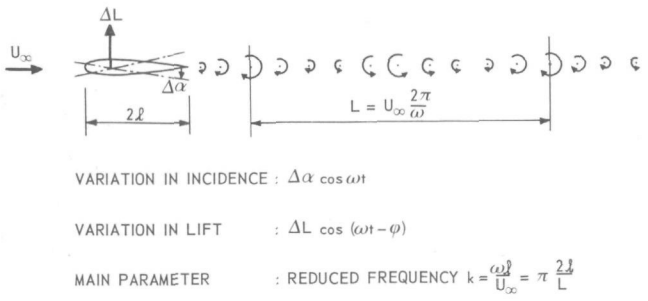

Fig. 2.1 Flow around an oscillating airfoil.

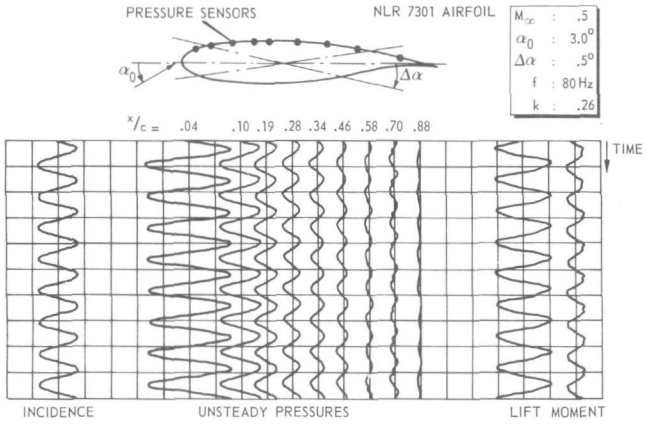

Fig. 2.2 Example of unsteady pressure signals and overall loads on a sinusoidally oscillating airfoil at subsonic speed.

around their mean values. To describe such harmonic variations, two quantities are needed, namely magnitude and phase shift with respect to the motion of the airfoil (Fig. 2.3). An equivalent way of description is in terms of a complex number. In the latter notation, the real part of a pressure perturbation (or load) is in phase with the motion of the airfoil, and the imaginary part is in quadrature with it. In other words, the real part is the actual pressure perturbation at the instant the oscillating airfoil reaches its maximum positive deflection, whereas the imaginary part represents the pressure perturbation at the instant the airfoil passes its mid position in positive direction. Of interest to the aeroelastician is the distribution of the unsteady pressures along the chord or over the wing and their integrated values, which represent the overall unsteady lift and moments. It is usual to present steady and unsteady pressures in the form of dimensionless coefficients, as defined in Appendix A. This Appendix also contains the definitions of the overall steady and unsteady aerodynamic coefficients; the sign conventions are according to the AGARD (Advisory Group for Aerospace Research and Development of the NATO) Manual on Aeroelasticity, Volume VI (Ref. 23).

This way of describing unsteady pressures or loads is only valid if the aerodynamic quantities vary sinusoidally in time, or, in other words, as long as a linear relationship exists between the

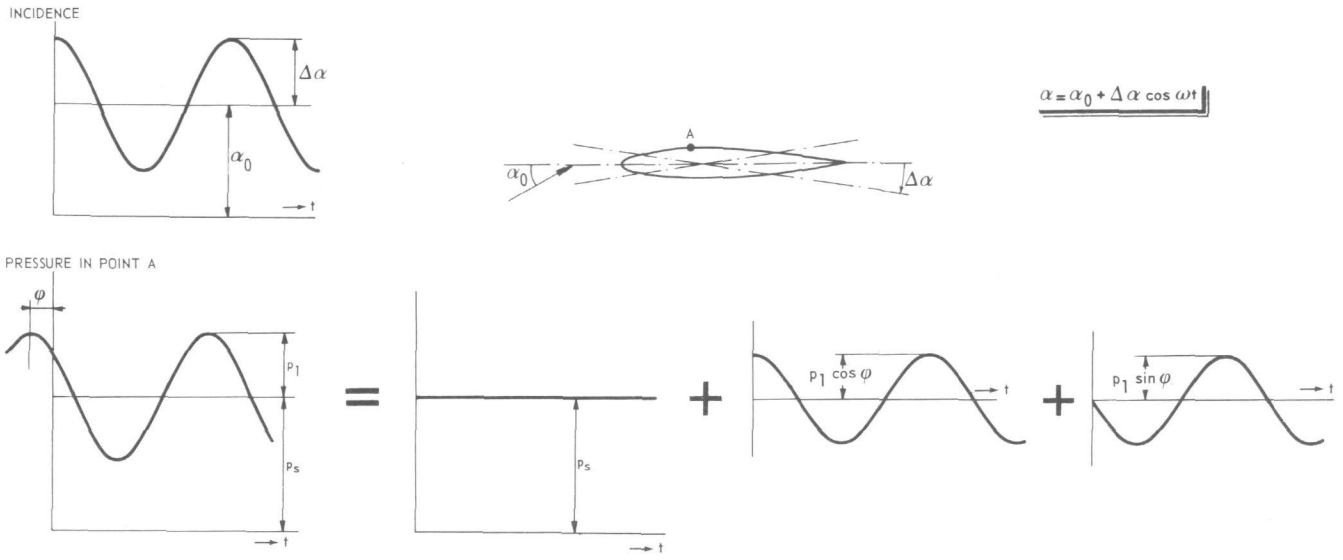

DESCRIPTION IN TERMS OF MAGNITUDE AND PHASE ANGLE

PRESSURE IN POINT A : $p = p_s + \Delta p = p_s + p_1 \cos(\omega t + \varphi)$

$= p_s + (p_1 \cos \varphi) \cos \omega t - (p_1 \sin \varphi) \sin \omega t$

WITH : p_1 = MAGNITUDE OF PRESSURE PERTURBATION

φ = PHASE ANGLE

DESCRIPTION IN TERMS OF A COMPLEX NUMBER

$p = p_s + \Delta p = p_s + p_1 \, \mathrm{Re} \left\{ e^{i(\omega t + \varphi)} \right\}$

$= p_s + \mathrm{Re} \left\{ (\Delta p' + i \Delta p'') \right\} e^{i\omega t}$

WITH : $\Delta p' = p_1 \cos \varphi$, REAL PART OF PRESSURE PERTURBATION

$\Delta p'' = p_1 \sin \varphi$, IMAGINARY PART

Fig. 2.3 Description of unsteady pressures.

displacement of the airfoil and the unsteady airloads. This is, however, not always true, especially not in separated flows or in regions near oscillating shock waves (see, for instance, the pressure variation at x/c = 0.46 in figure 2.4). In such cases, emphasis will be placed upon the first Fourier component of the signals, because in flutter investigations this is the only component that can generate net energy at the frequency of the airfoil motion.

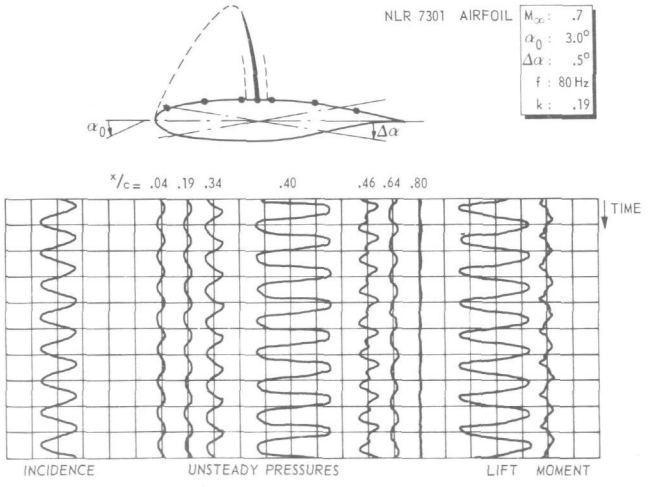

Fig. 2.4 Example of unsteady pressure signals and overall loads on an oscillating airfoil in transonic flow with a shock wave.

2.2 SOME NOTES ON THE UNSTEADY-FLOW EQUATIONS

The joint influence of airfoil thickness, incidence and amplitude of vibration is different for moderately subsonic and supersonic flow and for transonic flow. This will be demonstrated by considering the basic flow equations for all three speed regimes.

2.2.1 The unsteady-flow equations

The basic equations for an ideal two-dimensional inviscid flow, which express conservation of mass, momentum in x- and y-direction, and energy, can be written as:

$$\frac{\partial}{\partial t} \begin{Bmatrix} \rho \\ \rho U \\ \rho V \\ e \end{Bmatrix} + \frac{\partial}{\partial x} \begin{Bmatrix} \rho U \\ \rho U^2 + p \\ \rho UV \\ U(e+p) \end{Bmatrix} + \frac{\partial}{\partial y} \begin{Bmatrix} \rho V \\ \rho UV \\ \rho V^2 + p \\ V(e+p) \end{Bmatrix} = 0, \qquad (2.1)$$

where e represents the total energy per unit volume, given by

$$e = (\gamma - 1)^{-1} p + \tfrac{1}{2} \rho (U^2 + V^2), \qquad (2.2)$$

and where ρ and p are the density and pressure,

while U and V represent the velocity components in x- and y-direction, respectively. The quantity γ denotes the ratio of specific heats.

The boundary condition at the moving airfoil surface, $S(x,y,t) = 0$, requires the velocity component normal to the surface to be zero:

$$\frac{\partial S}{\partial t} + U \frac{\partial S}{\partial x} + V \frac{\partial S}{\partial y} = 0 \ . \qquad (2.3)$$

The solution satisfying (2.1) to (2.3) is made unique by the Kutta condition, which requires that at the trailing edge and across the trailing vortex sheet the pressure and flow direction are continuous.

Various degrees of approximation can be made to satisfy both equations (2.1) and the accompanying boundary conditions. A great simplification is attained when it is assumed that the flow is isentropic and irrotational:

$$p\rho^{-\gamma} = \text{constant} \qquad (2.4)$$

and

$$\frac{\partial V}{\partial x} - \frac{\partial U}{\partial y} = 0 \ . \qquad (2.4a)$$

The latter relation allows the introduction of a disturbance velocity potential Φ, defined by

$$U = U_\infty + \Phi_x \ , \qquad V = \Phi_y \ . \qquad (2.5)$$

Then equation (2.1), together with (2.4) and (2.5), can be combined into a single equation for Φ (Refs. 24, 25):

$$\begin{aligned}
&\nabla^2\Phi - M_\infty^2 \left[\Phi_{xx} + (2/U_\infty)\Phi_{xt} + (1/U_\infty^2)\Phi_{tt}\right] = \\
&= M_\infty^2 \Big[\left[(\gamma+1)/U_\infty\right] \Phi_x\Phi_{xx} + \left[(\gamma-1)/U_\infty\right] \Phi_x\Phi_{yy} + \\
&\quad + (2/U_\infty)\, \Phi_y\Phi_{xy} + \left[(\gamma-1)/U_\infty^2\right] \Phi_t\, \nabla^2\Phi + \\
&\quad + (2/U_\infty^2)(\Phi_x\Phi_{xt} + \Phi_y\Phi_{yt}) \Big] + \\
&+(M_\infty^2/U_\infty^2) \Big[\left[\tfrac{1}{2}(\gamma+1)\ \Phi_x^2 + \tfrac{1}{2}(\gamma-1)\ \Phi_y^2\right] \Phi_{xx} + \\
&\quad + \left[\tfrac{1}{2}(\gamma+1)\ \Phi_y^2 + \tfrac{1}{2}(\gamma-1)\ \Phi_x^2\right] \Phi_{yy} + 2\Phi_x\Phi_y\Phi_{xy} \Big] .
\end{aligned} \qquad (2.6)$$

Although equation (2.6) is only valid for isentropic flow, it remains a good approximation for flows with weak shock waves (Mach number just upstream of the shock wave less than about 1.3). The terms that are linear in Φ are placed on the left. The terms on the right-hand side are of the second and third degree.

2.2.2 Moderately subsonic and supersonic flow

When it is tried to further simplify the potential equation (2.6), the commonly used approach is to assume the perturbations to be small, so that terms of second and higher order can be neglected. The result for moderately subsonic and supersonic flow, where $|1 - M_\infty|$ is of the order 1, is the linear equation

$$\nabla^2\Phi - M_\infty^2 \left[\Phi_{xx} + (2/U_\infty)\Phi_{xt} + (1/U_\infty^2)\Phi_{tt}\right] = 0. \qquad (2.7)$$

The boundary of the airfoil can be expressed as

$$S(x,y,t) = y - \left[f^{\pm}(x) + \alpha(x) + g(x,t)\right] = 0, \qquad 0 \leq x \leq 2\ell \qquad (2.8)$$

in which $f^{\pm}(x)$ is the two-valued function denoting the thickness distribution, $\alpha(x)$ the incidence plus the camber distribution, and $g(x,t)$ the time-dependent deformation of the airfoil.

By introduction of (2.8), the boundary condition (2.3) reduces to

$$\Phi_y = U_\infty(f_x^{\pm} + \alpha_x + g_x) + g_t \quad \text{on} \quad 0 \leq x \leq 2\ell, \ y = 0. \qquad (2.9)$$

Both the differential equation (2.7) and the boundary condition (2.9) are linear in Φ. They form the basis of numerous calculation methods to determine aerodynamic loads on thin steady and oscillating airfoils. The linearity implies that solutions satisfying the unsteady part of boundary condition (2.9) can be considered separately from solutions satisfying the steady parts. In this decomposition, illustrated in figure 2.5, the oscillating airfoil is replaced by an infinitely thin airfoil oscillating in a uniform parallel flow.

For practical applications in flutter calculations, it is usual to consider only this unsteady part of the solution.

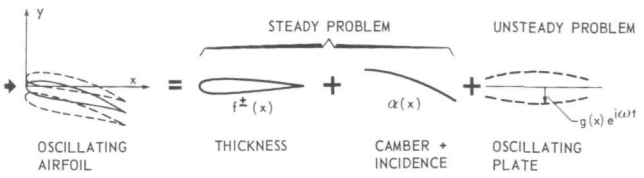

Fig. 2.5 Decomposition into a symmetrical nonlifting airfoil, an infinitely thin curved plate, and an infinitely thin oscillating plate.

When applied to sinusoidal motions, the time-dependent deformation is described by

$$g(x,t) = g(x)\, e^{i\omega t} . \qquad (2.10)$$

By splitting up the disturbance potential Φ in a steady and unsteady part

$$\Phi = \Phi_o(x,y) + \phi(x,y)\, e^{i\omega t} , \qquad (2.11)$$

the unsteady part of equation (2.7) becomes:

$$\nabla^2\phi - M_\infty^2\left[\phi_{xx} + 2ik\phi_x - k^2\phi\right] = 0, \qquad (2.12)$$

and the boundary condition (2.9) yields:

$$\phi_y = U_\infty\left[\partial g(x)/\partial x + ikg(x)\right], \qquad (2.13)$$

where $k = \omega\ell/U_\infty$ denotes the reduced frequency based on a reference length ℓ equal to 1.

In accordance with the linearization, the unsteady pressure jump across the airfoil surface can be found from

$$\overline{\Delta C_p} = \Delta C_{p+} - \Delta C_{p-} = -(2/U_\infty)(\partial\phi/\partial x + ik\phi), \qquad (2.14)$$

where ΔC_{p+} and ΔC_{p-} denote the unsteady pressure coefficients for the upper and lower surface, respectively.

From (2.12) and (2.13) it follows that the main parameters governing the unsteady problem are the reduced frequency k, the free-stream Mach number M_∞, and the vibration mode g(x).

Solutions of the thin-airfoil equations for both two- and three-dimensional subsonic and supersonic flows are documented very well in the literature and have been verified extensively by experiments (Refs. 23, 26-40). In general, it appears that satisfactory predictions can be obtained for attached moderately subsonic and supersonic flows. An exception is formed by oscillating trailing-edge flaps, for which the influence of viscosity is obviously dominant. In such cases, one has to rely on wind-tunnel tests.

2.2.3 Transonic flow

In the transonic regime, where the Mach number is close to one, the potential equation (2.6) can no longer be linearized completely. By assuming small perturbations, most of the nonlinear terms in (2.6) can be eliminated but, as derived by Landahl (Ref. 24), the following equation, which is essentially nonlinear, has to be retained:

$$\left[1 - M_\infty^2 - M_\infty^2\left[(\gamma+1)/U_\infty\right]\Phi_x\right]\Phi_{xx} + \Phi_{yy} + \\ - (2M_\infty^2/U_\infty)\Phi_{xt} - (M_\infty^2/U_\infty^2)\Phi_{tt} = 0 . \qquad (2.15)$$

The corresponding boundary condition remains the same as that given in (2.9).

The nonlinearity of (2.15) prevents a separate solution of Φ, due to airfoil thickness and incidence and to oscillations. This means that airloads on sinusoidally oscillating airfoils also depend on airfoil thickness and incidence. Consequently, the study of oscillating airfoils in transonic flow is much more complicated than in moderately subsonic and supersonic flow.

Formally, the nonlinearity of the unsteady flow field may be circumvented by assuming the unsteady effects to be vanishingly small disturbances of the steady flow around the airfoil in a given mean position.
When it is assumed that

$$\Phi = \Phi_o(x,y) + \phi(x,y)\, e^{i\omega t} , \qquad |\phi| \ll \Phi_o , \qquad (2.16)$$

equation (2.15) can be split into two parts, one

for the steady potential Φ_o and one for the superimposed unsteady potential ϕ.
For the potential Φ_o, the resulting equation reads:

$$\Phi_{oxx}\left[1 - M_\infty^2 - (M_\infty^2/U_\infty)(\gamma+1)\Phi_{ox}\right] + \Phi_{oyy} = 0, \quad (2.17)$$

which is the well-known transonic small-perturbation equation for steady transonic flow.
The equation governing the unsteady flow field becomes:

$$\phi_{xx}\left[1 - M_\infty^2 - M_\infty^2\left[(\gamma+1)/U_\infty\right]\Phi_{ox}\right] + \phi_{yy} - 2ikM_\infty^2\phi_x + \\ + k^2M_\infty^2\phi - (\gamma+1)(M_\infty^2/U_\infty)\Phi_{oxx}\phi_x = 0 . \quad (2.18)$$

The boundary condition on the airfoil is the same as that given in (2.13), and also the formula for the unsteady pressure coefficient (2.14) remains valid.

The unsteady-flow equation (2.18) is linear in ϕ. The equation, however, has nonconstant coefficients that depend on the mean steady flow field Φ_o. This demonstrates again that, in contrast with moderately subsonic and supersonic flow, the unsteady flow field in the transonic range can be no longer treated independently of the steady flow field. Because of the importance of this interaction, the main characteristics of the steady transonic flow around airfoils are briefly reviewed in chapter 3.

2.3 PRESENT STATUS OF THE RESEARCH ON UNSTEADY TRANSONIC FLOW

The mathematical complexity of the problem of unsteady transonic flow has prevented the development of efficient computation methods for many years.

Stimulated, however, by the renewed interest in transonic flight and the enormous developments in steady transonic flow computations, a number of attempts has been made in the last few years to solve the complicated unsteady flow equations (a review is given in chapter 12), and it may be expected that in the coming years considerable attention will be paid to this subject.

When the experimental evidence to support this fast development is considered, it can be concluded that very little material is available. With only a few exceptions, the numerous experimental investigations in the past are not suitable for this purpose, since they were limited to the determination of only one or two overall coefficients, like the hinge moment (Refs. 41-63) or the pitching moment (Refs. 64-68). In the majority of these investigations, the free-oscillation technique has been applied, in which the model or control surface is suspended in springs, in such a way that free oscillations can be performed. The aerodynamic moment is then determined from the change in frequency and damping with airspeed. A serious drawback of this relatively simple method is that no further information is obtained about the details of the unsteady pressure distribution and the corresponding mean steady flow field.

This type of information can be obtained only by measuring detailed steady and unsteady pressure distributions on a model that is forced into an oscillatory motion. For tests of this type, however, the test set-up, instrumentation and data-reduction procedures are much more complicated than for the free-oscillation method. This might explain that in the past unsteady pressure distributions very seldom have been determined.

A first attempt to measure local unsteady pressures on an oscillating wind-tunnel model in transonic flow was made by Erickson and Robinson (Ref. 41). Their method, in which electrical pressure cells installed flush with the model surface are used, has been applied successfully by Wyss, Sorenson, and their colleagues at NASA. Although they actually measured the pressures on oscillating control surfaces on two-dimensional and three-dimensional wings (Refs. 43, 53, 56, 57) and airfoils oscillating in pitch (Refs. 65-67), only overall aerodynamic coefficients have been published, except for some typical oscillograph records of local pressure fluctuations.

The first detailed unsteady pressure distributions in the transonic regime have been reported by Lessing, Troutman and Meness (Ref. 69) and by Leadbetter, Clevenson and Igoe (Ref. 70).

These two studies deal with three-dimensional flow. Probably the results given in reference 69 are not correct because of a fundamental error in the data-reduction procedure, where the effect of the main flow on the dynamic response of the pressure tubes is discarded (see chapter 5). To the author's knowledge, similar date for two-dimensional oscillating airfoils did not exist at the time NLR started its exploratory program on unsteady transonic flows.

3 MAIN CHARACTERISTICS OF THE STEADY TRANSONIC FLOW AROUND AIRFOILS

As an introduction to the discussion of the transonic flow around oscillating airfoils, a brief survey will be given of the behaviour of transonic flows around airfoils at rest. For more detailed considerations of plane steady transonic flow with embedded shock waves, the reader is referred to the publications of Holder (Ref. 17), Shapiro (Ref. 74) and Sears (Ref. 75), while, for the various aspects of shock-free flow, reference is made to the contributions of Nieuwland, Spee and Boerstoel (Refs. 13, 16, 20, 76).

3.1 TRANSONIC FLOWS WITH EMBEDDED SHOCK WAVES

3.1.1 Development of flow pattern with Mach number, flap angle, and incidence

When the free-stream Mach number of a purely subsonic flow around a symmetrical airfoil is increased, the flow pattern usually develops in a way as sketched in figure 3.1. The so-called critical Mach number, M^*, is reached when somewhere in the flow the local Mach number becomes unity. Beyond the critical Mach number, a supersonic region appears at the airfoil, which in general is terminated by a normal shock wave as soon as the maximum local Mach number exceeds a value of about 1.05. Through this shock wave, the flow velocity is reduced from supersonic to subsonic (Fig. 3.1b). With a further increase of the free-stream Mach number, the shock moves backwards, while both the shock strength and the size of the supersonic region increase. After the pressure jump through the shock wave has become sufficiently large, so-called shock-induced separation of the boundary layer occurs (Fig. 3.1c). For a turbulent boundary layer, this shock-induced separation starts when the local Mach number just upstream of the shock wave is about 1.25 to 1.3. When the boundary layer downstream of the shock wave separates completely, the flow around the airfoil is changed considerably, and often unsteady-flow phenomena like "buffet" and "buzz" start to occur.

For aeroelastic investigations, one is interested primarily in the changes in aerodynamic loading due to variations in downwash along the chord. Therefore, some examples will be given of the development of the flow pattern when the downwash is changed at constant free-stream Mach number.

The first example deals with a symmetrical airfoil with flap at zero incidence (Fig. 3.2). When the flap is deflected downwards over an angle δ_o, the speed over the upper surface is gradually increased, and the supersonic region and the shock wave develop in the same way as described above for increasing free-stream Mach

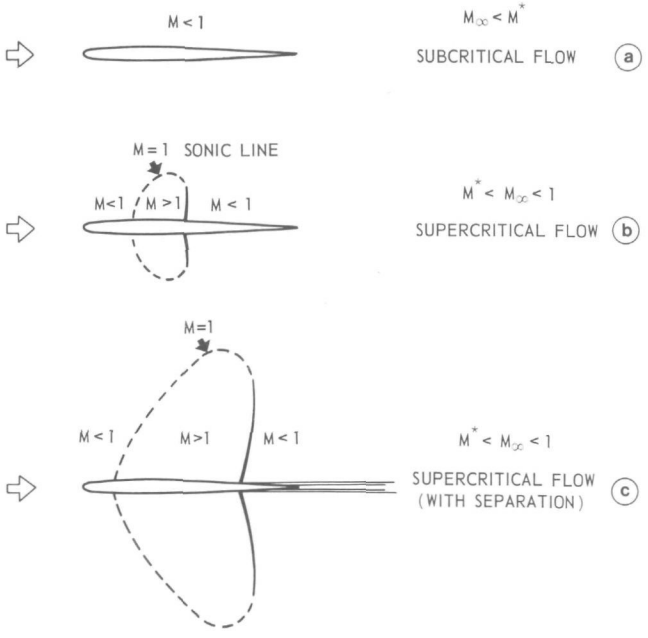

Fig. 3.1 Influence of Mach number on flow pattern.

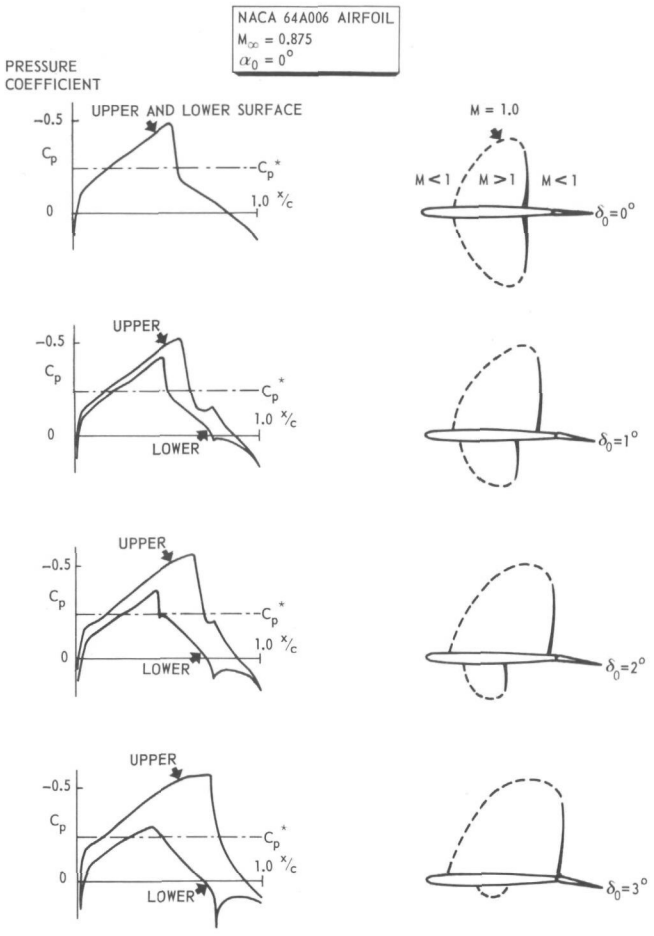

Fig. 3.2 Influence of flap deflection on pressure distribution and shock pattern in transonic flow.

number. At the lower surface the flow speed decreases and the development of the flow pattern is reversed: the size of the supersonic region decreases, the shock becomes weaker, and finally, beyond a certain flap deflection, the shock vanishes.

A similar development in flow pattern can be observed when the incidence of the airfoil is varied. An example is shown in figure 3.3, which deals with an airfoil that carries a well-developed supersonic region on its upper surface, terminated by a relatively strong shock wave. This example shows also that already small variations in incidence may lead to considerable changes in pressure distribution, shock position, and shock strength.

Fig. 3.3 Influence of incidence on pressure distribution and shock pattern in transonic flow. ➡

3.1.2 Characteristics of a normal shock wave

Through a normal shock wave, as occurring in one-dimensional flow, the velocity is reduced from supersonic to subsonic. The pressure jump across the shock wave is determined completely by the free-stream Mach number upstream of the shock (Fig. 3.4a). For an inviscid two-dimensional flow around an airfoil, the foot of the shock is normal to the contour of the airfoil, but the remaining part is curved forward. This can be explained as follows: On a convex contour, the velocity in y-direction has to decrease upstream as well as downstream of the shock wave. As shown by Zierep (Ref. 77), this requirement is not compatible with a completely straight shock, because, if the shock

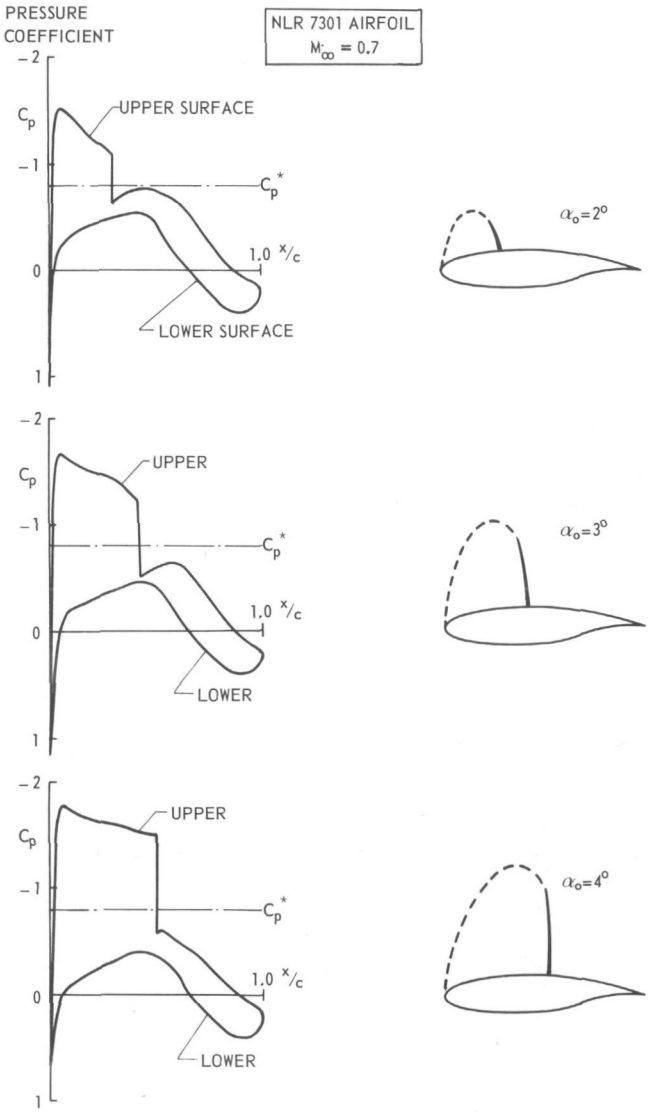

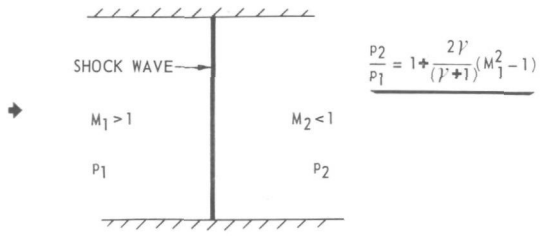

a: ONE - DIMENSIONAL FLOW

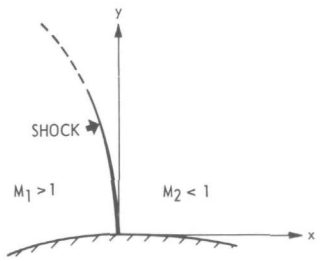

b-1 : SHOCK WAVE ON CONVEX SURFACE

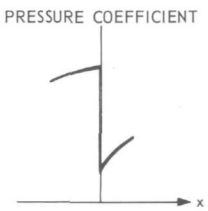

b-2 : RAPID EXPANSION DIRECTLY DOWNSTREAM OF SHOCK WAVE (*ZIEREP CUSP*)

b: TWO - DIMENSIONAL FLOW

Fig. 3.4 Normal shock waves in one- and in two-dimensional flow.

were straight, a decrease in velocity upstream of the shock would result in an increase in velocity downstream of the shock according to the relation for a normal shock wave (Fig. 3.4a). This leads to a reversed gradient in y-direction. According to Zierep, the shock wave therefore has to be curved in the sense as indicated in figure 3.4b-1, while, in addition, a readjustment of the pressure gradient is required just downstream of the shock wave, which results in a rapid expansion (Fig. 3.4b-2). Often this expansion can be noticed in surface pressure distributions of airfoils, where it manifests itself as the so-called Zierep cusp (see, for instance, figure 3.3). There are, however, circumstances, depending on the velocity gradients in y-direction, the curvature of the airfoil contour and the thickness of the boundary layer, in which this effect cannot be observed, as in the examples of figure 3.2.

3.2 SHOCK-FREE FLOW

The flow patterns discussed so far are characterized by the presence of a normal shock wave at either the upper or the lower surface of the airfoil, or at both surfaces at the same time. Occasionally, even two normal shock waves behind each other occur. An exception to this rule forms the flow around a so-called supercritical airfoil in its design condition. This type of airfoil is shaped in such a way that, for a specific combination of incidence and free-stream Mach number (the design condition), the transition of the supersonic region to the adjacent subsonic region takes place without noticeable shock wave. Away from this design condition, the flow remains no longer shock-free, and the airfoil behaves more or less like a *conventional-type airfoil*.

An example of the flow around a supercritical airfoil in its design condition is shown in figure 3.5, together with the flow patterns for some neighbouring values of incidence and Mach number. The figure reveals that already small changes in incidence and Mach number are sufficient to disturb the shock-free flow condition. Both the lowering and the increasing of the Mach number result in a flow pattern with a normal shock wave, while the same holds when the incidence is varied.

It is clear that an important question with respect to the practical application of supercritical airfoils is, how gradual the change from shock-free flow to the neighbouring flow conditions with shock waves is, or, in other words, what are the margins within which the Mach number and incidence may be varied around the design condition without serious deterioration of the favourable low-drag property (little or no wave drag) of the shock-free flow. For the aeroelastician, the important question becomes how the aerodynamic loading will change during oscillations around the design condition.

3.3 SOME PARTICULAR FLOW PATTERNS ON AIRFOILS WITH FLAP

Apart from the flow patterns discussed in the preceding sections, there are some additional shock configurations that may occur only on airfoils with a flap, since they are directly related

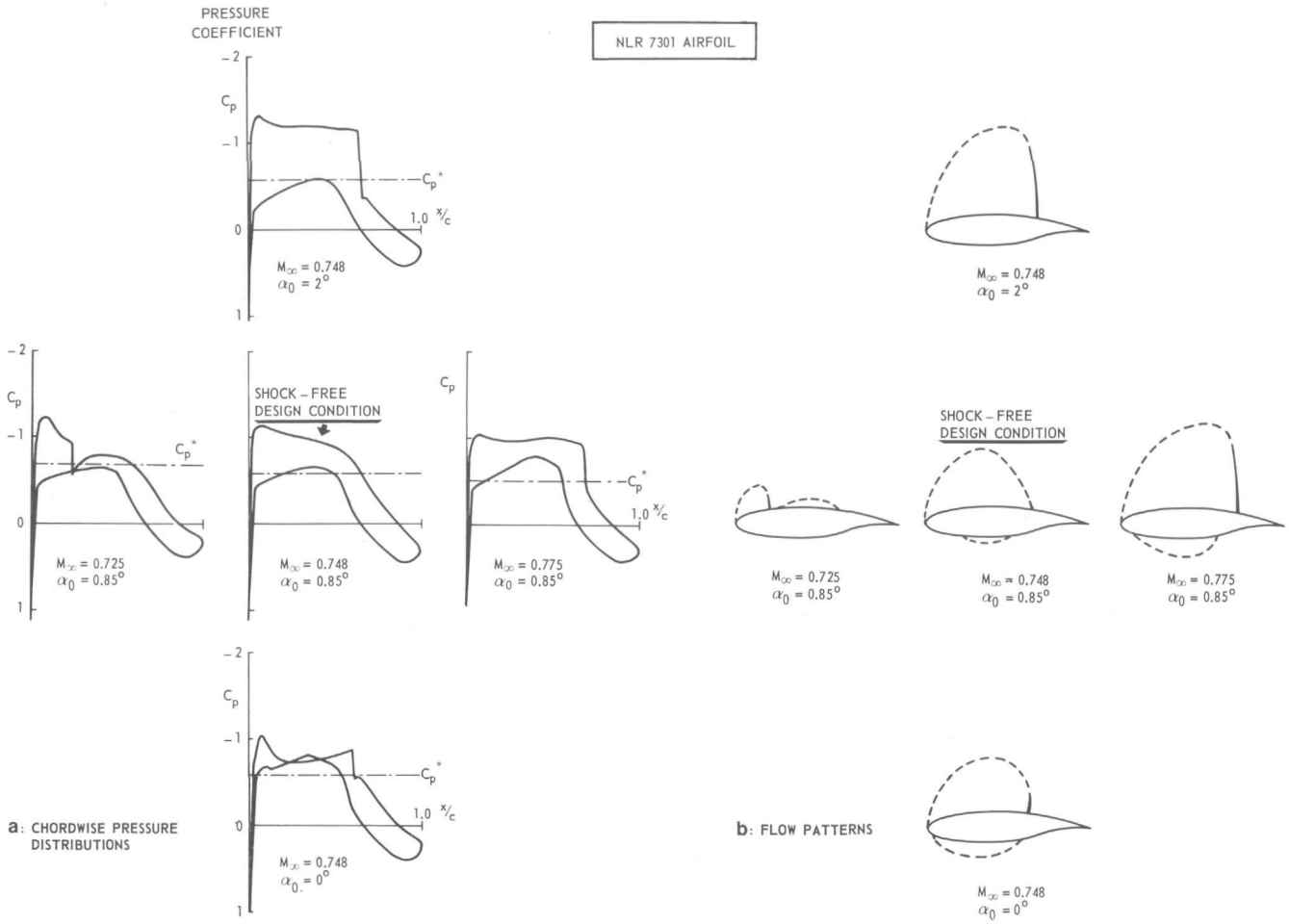

Fig. 3.5 Influence of Mach number and incidence on pressure distribution and flow pattern of a "shock-free" airfoil in its design condition.

to the abrupt change in downwash at the leading edge of the flap (Fig. 3.6). All additional possibilities contain one or more of the following elementary flow patterns, which are well-known from the behaviour of subsonic and supersonic flows around sharp-edged corners (Refs. 74, 75):

(a) Subsonic expansion around a sharp-edged convex corner. This results in a supersonic region and an oblique shock wave emanating from the corner. Since downstream of an oblique shock the flow remains supersonic, a second normal shock or a fan of compression waves is required to reduce the velocity to subsonic speed (Fig. 3.6a).

(b) Prandtl-Meyer expansion. When a supersonic flow passes a convex corner, the flow expands continuously, until the flow is directed along the contour downstream of the corner. In the examples of the airfoil with flap (Fig. 3.6b), the expansion has to be followed by a normal shock in order to reduce the flow velocity from supersonic to subsonic.

(c) Lambda shock wave. When a supersonic flow passes a concave corner, an oblique shock wave occurs, through which the flow remains supersonic but changes its direction. For the examples of figure 3.6c, the oblique shock will be followed by a normal one to arrive again at a subsonic mean flow. Both shocks merge into a so-called lambda shock.

During the present wind-tunnel experiments, almost every type of shock pattern as sketched in figure 3.6 has been realized. However, in order to simplify the analysis for the airfoil with flap, the flow patterns in which only normal shocks occur are emphasized.

3.4 VISCOUS ASPECTS

Normally, the effect of viscosity in an attached subsonic flow around an airfoil is confined to a thin layer adjacent to the surface of the airfoil, which is called the boundary layer, and to the wake. In the boundary layer, the velocity rises from zero at the surface to an almost constant value at the outer edge. Usually the boundary layer starts at the leading edge as a laminar boundary layer, which after a certain distance changes from laminar to turbulent (transition) (Fig. 3.7). The presence of the boundary layer changes the effective contour of the airfoil and, thus, has an effect on the pressure distribution and the aerodynamic loading. The magnitude of this effect depends, among others, on the geometry and the incidence of the airfoil and the Reynolds number, the latter being an important parameter for the growth of the boundary-layer thickness and the location of the transition point.

The behaviour of the boundary layer is of even more importance in transonic flow than in subsonic flow, since here it has a considerable influence on the position and strength of the shock wave. The pressure jump through the shock wave, in its turn, has a large influence on the development

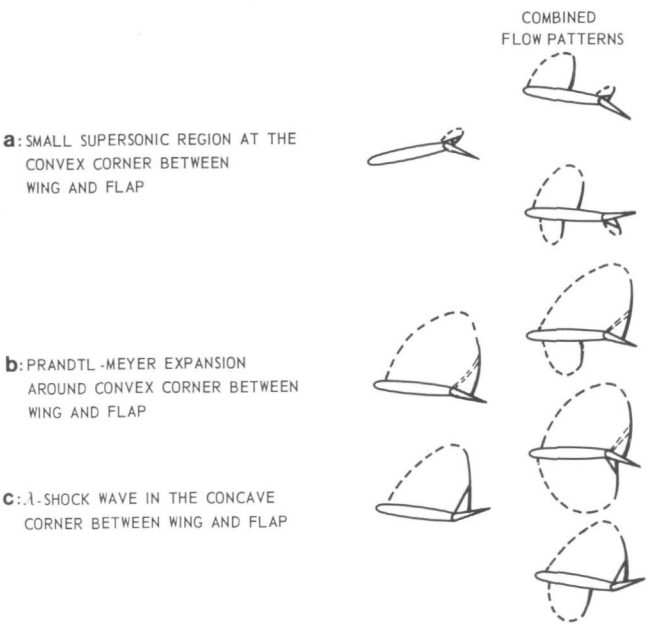

Fig. 3.6 Some particular flow patterns on an airfoil with flap.

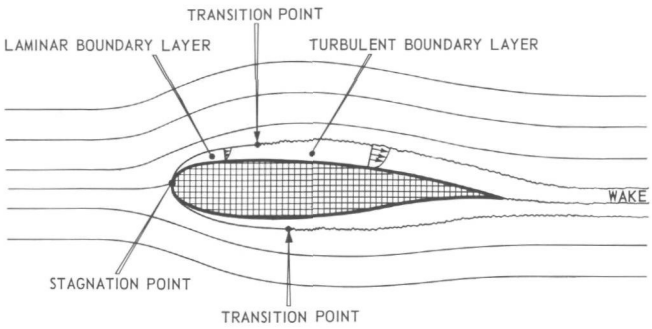

Fig. 3.7 Boundary layer in a subsonic attached flow.

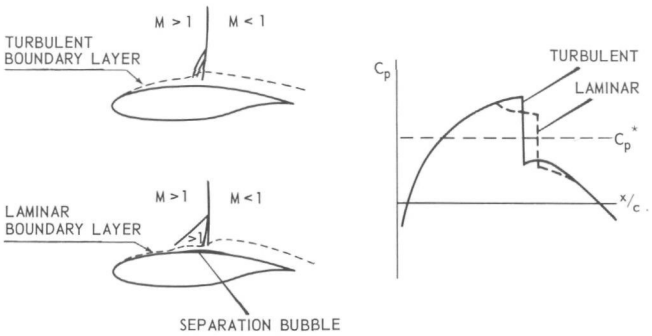

Fig. 3.8 Interaction of a shock wave with a turbulent and laminar boundary layer and its effect on the pressure distribution.

of the boundary layer. Of special importance is whether the shock wave interacts with a laminar or a turbulent boundary layer. As sketched in figure 3.8, this may lead to considerable differences in shock patterns and pressure distributions.

At the relatively low Reynolds numbers that usually can be reached in wind-tunnel tests, the boundary layer often remains laminar up to the shock wave, while, for full-scale Reynolds numbers, the boundary layer most probably will be turbulent when interacting with the shock. This gives rise to considerable scale effects. For conventional airfoils, a useful technique for reducing these scale effects is to artificially force transition of the boundary layer upstream of the shock by means of a transition strip. As will be explained below, this technique becomes questionable for the modern-type airfoils.

In the interaction between a shock wave and the boundary layer, different stages can be distinguished (Fig. 3.9). The interaction is called "weak" when the boundary layer remains attached, and "strong" when separation occurs.

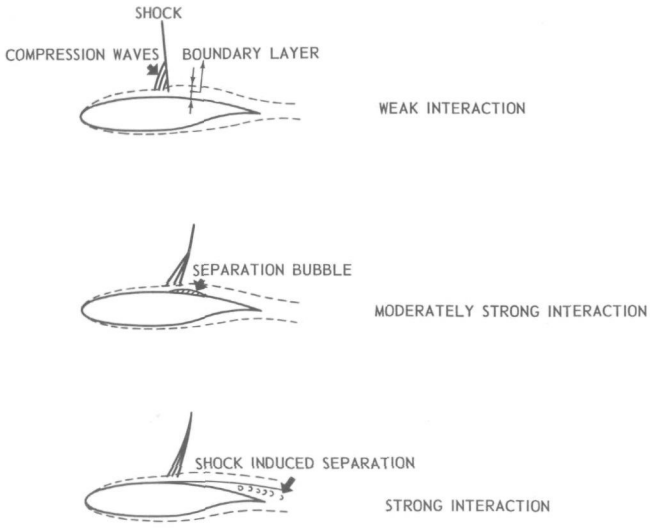

Fig. 3.9 Different stages of shock-wave/boundary-layer interaction (turbulent boundary layer).

For conventional airfoils, the separation process indicated by Pearcy et al. (Ref. 19) as type "A" normally proceeds as follows (Fig. 3.10): the pressure rise through the shock causes a thickening of the boundary layer at the foot. If the pressure rise is large enough, a local separation bubble develops just downstream of the shock. With further increase in the free-stream Mach number, at first the bubble remains localized, but then it spreads out rapidly towards the trailing edge, which leads to a sudden fall in pressure at the trailing edge (pressure divergence). This is accompanied by a significant drop in circulation, and often unsteady phenomena like "buffet" and "buzz" start to occur.

For modern airfoils, like the NLR 7301 (Fig. 3.5a), with their steep pressure gradients towards the trailing edge, a second type of separation may occur, which starts from the trailing edge (rear separation). Some possible developments of this so-called B-type separation are sketched in figure 3.10. The rear separation, which is of the classical subsonic type, depends strongly on the thickness and the velocity profile of the boundary layer approaching the trailing edge and on the pressure gradient. Therefore, in contrast with the preceding type of separation (type A), the type-B separation is very sensitive to the Reynolds number and to the location of the point where the transition of the boundary layer from laminar to turbulent takes place. This means that the advanced-type airfoils are very sensitive to the Reynolds number, while simulation of high Reynolds numbers with the help of artificial transition becomes very questionable.

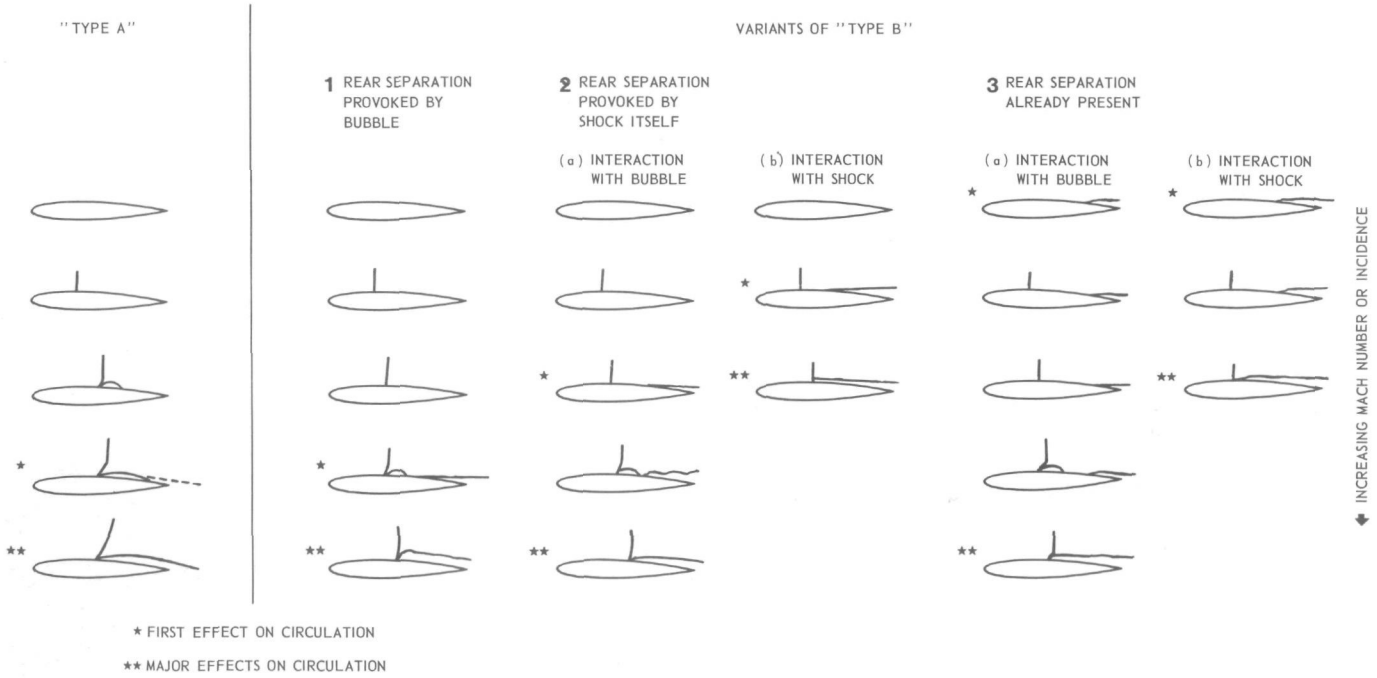

Fig. 3.10 Flow models for the initial development of shock-induced separation with Mach number or incidence for a turbulent boundary layer (Ref. 19).

Pearcy et al. (Ref. 19) developed a method to determine the type of separation for a specific airfoil and the conditions (Mach number and incidence) at which this occurs by presenting the pressures at fixed chord-wise stations as a function of the free-stream Mach number. In the present investigation, their method has been applied to determine the boundaries of separation for both the NACA 64A006 airfoil and the NLR 7301 airfoil, in order to assure that only flow conditions are studied without severe separation effects. The result for the NLR 7301 airfoil, as obtained in a detailed investigation of Zwaaneveld (Ref. 73), is reproduced in figure 3.11. Together with the boundaries for maximum lift and lift divergence, this figure gives a good illustration of the characteristics and limitations of a transonic airfoil.

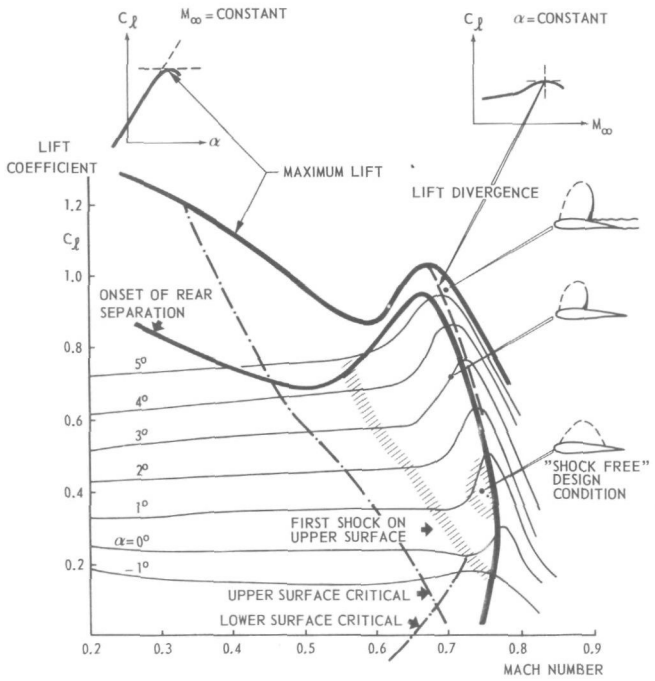

Fig. 3.11 *Main characteristics and boundaries for the onset of separation of the NLR 7301 airfoil (Ref. 73).*

PART II SCOPE AND DESCRIPTION OF THE EXPERIMENTAL INVESTIGATIONS

4 SCOPE OF THE NLR INVESTIGATIONS

4.1 PROBLEM DEFINITION

The aim of the investigations at NLR was to improve the physical insight into the nature of unsteady transonic flows and to support the development of theoretical or semi-empirical prediction methods. From the considerations in chapter 2, it is clear that such an exploratory investigation should be focussed on the following aspects.

Firstly, the discussions about the unsteady-flow equations have shown that in transonic flows an essential coupling exists between the steady and unsteady flow fields. This implies that, besides the usual parameters for unsteady flow (free-stream Mach number, reduced-frequency and vibration mode), also the airfoil shape, the mean incidence and the mean flap angle have to be considered. In an investigation of the influence of these additional parameters, detailed information should be obtained about both the unsteady and the mean steady flow.

Secondly, the unsteady transonic-flow problem is essentially nonlinear (see eq. 2.15). As shown in section 2.2.3, the problem can be reduced to a linear one, be it that the resulting equation (2.18) possesses spatially varying coefficients. This linearization was achieved by assuming the unsteady flow to be a small perturbation of the nonlinear steady flow field. Of course, this linearization can always be enforced by taking the amplitude of oscillation small enough, but the important question arises whether this can be achieved without a return to impractically small values. Therefore, the question how far linearization about a given mean steady-flow condition is justified should be a point of investigation. This is important, since in aeroelastic investigations, where the unsteady aerodynamic forces have to be combined with inertial, stiffness, and damping forces of the aircraft structure, all routine methods are linear. From that side there clearly exists a strong interest in some sort of linearization of the unsteady aerodynamic problem.

A third point of interest, related to the current developments in supercritical-wing design, is the question whether or not the new generation of supercritical airfoils possesses adverse unsteady aerodynamic characteristics, especially around their design condition.

A final aspect that inevitably has to be considered is the influence of the boundary layer. As described in chapter 3, the boundary layer is of crucial importance for steady transonic flow and, therefore, may have a significant influence also on the unsteady airloads.

4.2 APPROACH

In view of the afore-mentioned aspects, it was decided at NLR to perform steady and unsteady pressure measurements on some characteristic airfoils in two-dimensional flow. Priority has been given to the concentration on investigations in two-dimensional flow, since they are not only simpler than for three-dimensional flow, but also offer the opportunity to supplement the pressure measurements by optical flow studies of the periodical motion of the shock waves. Further it was anticipated that the development of theoretical methods - in analogy with the development of steady transonic computational methods - would also start with the two-dimensional flow problem.

An excellent tool to reach this goal was the experimental technique developed at NLR, which enables the measurement of a large number of mean steady and unsteady pressures on oscillating wind-tunnel models (details of this technique are given in chapter 5).

After some preliminary measurements on a circular arc airfoil with oscillating flap, which were not very successful because of severe flow-separation effects, a first series of extensive tests was conducted in 1966 on an NACA 64A006 airfoil provided with a 25 per cent chord trailing-edge flap that could be forced into sinusoidal motions. These tests, which were limited to zero mean lift conditions, revealed a number of interesting effects in the high-subsonic and transonic speed regime (Ref. 71). Unfortunately, a few years later it was discovered that an important effect had been over-

looked in the measuring technique, which had a considerable influence on the unsteady-flow data at high speed in a quantitative sense (Refs. 39, 72; see also section 5.3.2).

Because of the increased interest in unsteady transonic flow, it was decided to repeat the earlier tests and to extend the program to flow conditions with non-zero mean lift, to investigate the effects of mean incidence and mean flap angle on the unsteady airloads. These measurements took place in 1972. The main reasons to concentrate the investigation again on this specific airfoil with flap were:

- oscillatory changes of the downwash are confined to the rear part of the airfoil, which considerably facilitates the interpretation of the airloads on the whole airfoil;
- by variation of mean incidence, mean flap angle, and free-stream Mach number, a great variety of steady flow fields can be generated, about which oscillatory perturbations can be investigated (see also chapter 3);
- the unsteady airloads on control surfaces are still of current interest, not only for flutter purposes, but also in connection with the recent development of so-called "active-control" systems.

The following step in the exploration of unsteady transonic flows was an investigation on a supercritical airfoil that could be oscillated in pitch. For this purpose the "NLR 7301" airfoil was selected, which was designed for shock-free flow with the hodograph method of Boerstoel (Refs. 10, 78). This airfoil was chosen, because it is representative for the new generation of airfoils that is of interest for application in supercritical-wing design. Moreover, its steady-flow characteristics were known already from an extensive wind-tunnel investigation (Ref. 73). The unsteady-flow tests on the NLR 7301 airfoil were performed in 1976.

The experimental investigations will be described in this part of the thesis, while in the next part an analysis of the results will be given, in which the various aspects mentioned in section 4.1 are emphasized.

5 TECHNIQUE FOR UNSTEADY PRESSURE MEASUREMENTS

5.1 PRINCIPLE OF THE MEASURING TECHNIQUE

The method employed at NLR for the determination of unsteady pressure distributions on harmonically oscillating wind-tunnel models was developed about two decades ago by Bergh (Ref. 21). The quintessence of this method is that the pressure distribution over the model surface is measured through a large number of pressure tubes, which are connected in groups to only a few scanning valves (Fig. 5.1a). The use of tubes and scanning valves makes the method relatively inexpensive as compared with methods in which each tube is replaced by an in situ pressure sensor.

For steady pressure measurements, the required values can be determined directly with the transducers in the scanning valves, because the presence of the tubes does not affect the results. More complicated is the measurement of the sinusoidally varying pressures, because then the tubing

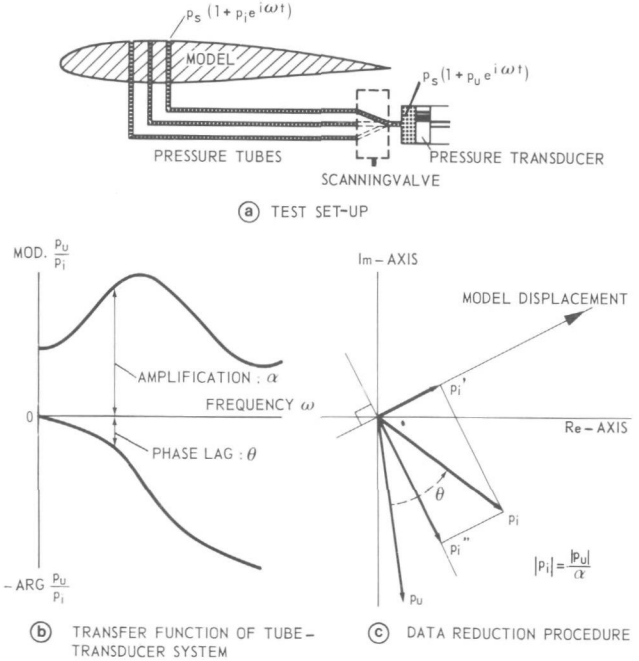

Fig. 5.1 Principle of measuring technique.

system leads to a considerable difference between the actual pressures at the model surface and the pressures as recorded by the transducers. Therefore, an essential step in the data-reduction procedure is the translation of the unsteady pressures p_u, measured with the transducers in the scanning valves, to the actual pressures at the model surface p_i with the use of the transfer function of the tubing system. This procedure is indicated schematically in figure 5.1c: the vector p_i is obtained from the vector p_u by a counter-clockwise rotation θ and a reduction in magnitude with a factor α. The values of the amplification α and the phase lag θ of the tubing system follow from the transfer function, as is indicated in figure 5.1b. As a next step (Fig. 5.1c), the vector p_i is decomposed in a real and an imaginary component relative to the motion of the model, which usually is measured by means of accelerometers or displacement pick-ups.

In this procedure, the accurate determination of the transfer functions of tube-transducer systems under the actual conditions in the wind tunnel is extremely important. For this reason, considerable attention was paid at NLR to the study of the dynamic behaviour of thin circular tubes connected with small instrument volumes.

5.2 THEORETICAL MODEL FOR THE DYNAMIC RESPONSE OF TUBE-TRANSDUCER SYSTEMS

In order to aid in the design of optimal tube-transducer systems, a theoretical model was developed to calculate their dynamic response characteristics (Refs. 22 and 72). This theoretical model deals with N tubes and N volumes connected in series (Fig. 5.2). Across the entrance of the system, the flow has a mean velocity U, while the pressure comprises a sinusoidal variation p_i, induced by the model oscillation. For the present purpose, one is interested in the ratio between the pressure perturbation in volume $V_{v,j}$ and the pressure variation p_i. In general, this ratio is a complex number, because it describes both magnitude and phase angle relative to the input pressure.

The special case of a single system (Fig. 5.3a) can easily be derived. Further, the model offers the possibility to consider a system with

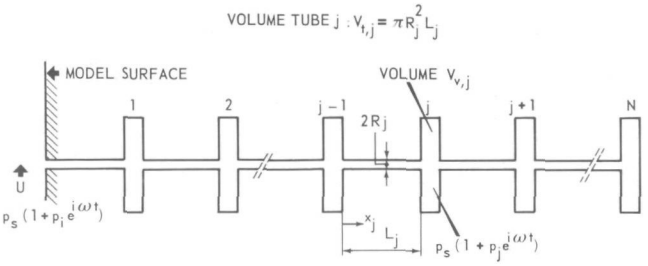

Fig. 5.2 Series connection of tubes and transducers.

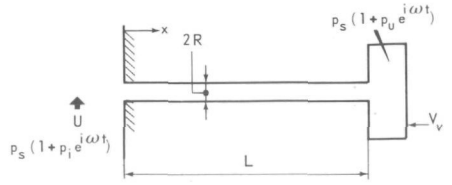

Fig. 5.3a Single pressure-measuring system.

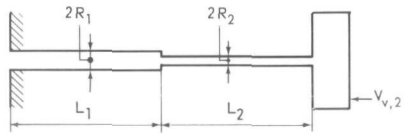

Fig. 5.3b Tube with discontinuity in tube radius.

one or more discontinuities in tube diameter (Fig. 5.3b), a situation which often occurs in practice.

Originally the model was derived for the system in still air (Ref. 22). Afterwards, when it became apparent that the main flow across the tube entrance had a significant influence on the dynamic response, the model was extended to take also this effect into account (Ref. 72).

5.2.1 The propagation of pressure waves through cylindrical tubes

To arrive at the dynamic response formulae for tube-transducer systems (for the details of the derivation, reference is made to Appendix B), first the sinusoidal motion of a fluid column in a rigid tube with circular cross section has to be considered. This motion is governed by the following basic equations:

- the Navier-Stokes equations (axi-symmetrical),
- the equation of continuity,
- the equation of state, and
- the energy equation that gives the balance between thermal and kinetic energies;

together five equations for the same number of un-

known quantities: the velocity perturbations in axial and radial direction and the perturbations in density, temperature and pressure.

As shown in Appendix B, the solution that suffices for the present application is the so-called "low-reduced-frequency solution", which for the pressure perturbation, p, inside the tube reads:

$$p = \left[A \exp\{\Gamma(\omega x/a_o)\} + B \exp\{-\Gamma(\omega x/a_o)\} \right] e^{i\omega t} , \tag{5.1}$$

with

$$\Gamma = \left[J_o(i^{3/2}s) \,/\, J_2(i^{3/2}s) \right]^{\frac{1}{2}} (\gamma/n)^{\frac{1}{2}} , \tag{5.1a}$$

$$n = \left[1 + \frac{\gamma-1}{\gamma} J_2(i^{3/2}\sigma s) \,/\, J_o(i^{3/2}\sigma s) \right]^{-1} , \tag{5.1b}$$

$$s = R\,(\rho_s \omega/\mu)^{\frac{1}{2}} . \tag{5.1c}$$

Here J_o and J_2 are Bessel functions of first kind of zero and second order, respectively.
In the expression (5.1)-(5.1c), x denotes the coordinate in axial direction of the tube, a_o the velocity of sound, γ the ratio of specific heats, σ the square root of the Prandtl number, R the tube radius, ρ_s the mean density and μ the viscosity. As σ and γ can be considered as constants for a given gas, the main parameter for the propagation of the pressure perturbations through the tubes is the so-called shear wave number s, defined in (5.1c). This number is a measure for the shearing effects along the tube wall.

5.2.2 Solution for complete tube-transducer systems

The solution (5.1) contains two constants, A and B, which can be determined by specifying the boundary conditions at both ends of the tube. For the general tube-transducer system (Fig. 5.2), the following boundary conditions have been introduced: at the entrance of tube j the pressure perturbation equals the pressure perturbation in the preceding volume $V_{v,j-1}$, which in its turn equals the pressure perturbation at the end of tube j-1. Furthermore, for each volume $V_{v,j}$ the increase in mass at each moment has to be equal to the difference in

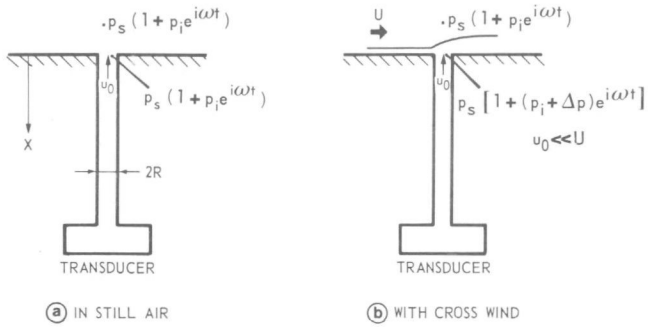

Fig. 5.4 Boundary conditions at the entrance of the tube-transducer system.

mass leaving tube j and the mass entering tube j+1. In order to obtain a relation between the pressure perturbation and density perturbation inside the volumes, it has also been assumed that there the thermodynamic process takes place polytropically, with a polytropic constant n_v to be specified.

A separate condition has to be prescribed at the entrance of the first tube (j = 1). In still air, this boundary condition is dictated by the fact that the pressure equals the value p_i imposed upon the system (Fig. 5.4a):

$$x_1 = 0 , \qquad p = p_i . \tag{5.2}$$

This implies that there is no restriction for the oscillatory flow velocity u_o in the tube entrance, so that air is free to move in and out of the tube opening. In case an airflow blows across the tube entrance, however, the air leaving the tube has to displace the main flow, which locally leads to an additional oscillatory pressure at the tube entrance (Fig. 5.4b). This means that, if an oscillatory perturbation p_i exists in the main flow, the boundary condition at the tube entrance (5.2) has to be modified into:

$$x_1 = 0 , \qquad p = p_i + \Delta p . \tag{5.3}$$

As argued in Appendix B, a logical assumption for this extra pressure perturbation is

$$\Delta p = C \rho_s u_o U , \tag{5.4}$$

with C being still an unknown constant and U the

velocity of the airflow across the entrance opening.

By application of the afore-mentioned boundary conditions, a recursion formula has been derived for the general tube-transducer system of figure 5.2, which relates the sinusoidal pressure perturbation in volume $V_{v,j}$ to the sinusoidal pressure perturbation in the preceding volume j-1 and the next volume j+1 (formulae B.47 and B.51 of Appendix B).

For a simple system that consists of one tube and one transducer (Fig. 5.3a), the resulting formula for the dynamic response in still air becomes:

$$\left\{p_u/p_i\right\}_{U=0} = \left[\cosh\left(\frac{\omega L}{a_o}\Gamma\right) + (V_v/V_t)(n/n_v)\left(\frac{\omega L}{a_o}\Gamma\right)\sinh\left(\frac{\omega L}{a_o}\Gamma\right)\right]^{-1}, \quad (5.5)$$

while the following formula is obtained for the situation with a cross flow across the entrance:

$$p_u/p_i = \left[\left\{p_u/p_i\right\}_{U=0}^{-1} + C\,(U/a_o)(i\gamma/n\Gamma) \times \left\{\sinh\left(\frac{\omega L}{a_o}\Gamma\right) - (V_v/V_t)(n/n_v)\left(\frac{\omega L}{a_o}\Gamma\right)\cosh\left(\frac{\omega L}{a_o}\Gamma\right)\right\}\right]^{-1}. \quad (5.6)$$

A closer examination of (5.5) and (5.6) reveals that the dynamic response of a simple tube-transducer system depends on the following parameters:

- Γ , the propagation constant. As follows from (5.1a), Γ only depends on the shear wave number $s = R(\rho_s\omega/\mu)^{\frac{1}{2}}$. In practice, this means that the propagation is determined by the internal tube radius R, the mean density in the tube ρ_s (which is directly related to the mean steady pressure and the mean temperature), the frequency ω and the viscosity μ;
- $\omega L/a_o$, the ratio between the tube length and the wave length a_o/ω;
- V_v/V_t , the ratio between the transducer volume and the volume of the tube;
- U , the velocity of the airflow across the entrance opening;
- n , a factor given in (5.1b), which - as explained in Appendix B - can be interpreted as the polytropic constant for the thermodynamic process inside the tube;
- n_v , the polytropic constant for the transducer volume V_v, for which a value has to be chosen.

5.3 THE DYNAMIC CHARACTERISTICS OF TUBE-TRANSDUCER SYSTEMS

5.3.1 The dynamic response in still air

The transfer function of tube-transducer systems in still air for a single system can be calculated with formula (5.5) and for systems involving more than one volume and connecting tubes with formula (B.47) of Appendix B. Some examples that are characteristic for the agreement normally obtained between calculated and measured response characteristics are shown in figure 5.5. Note that in the example of figure 5.5a, like in organ pipes, resonance peaks occur where the dynam-

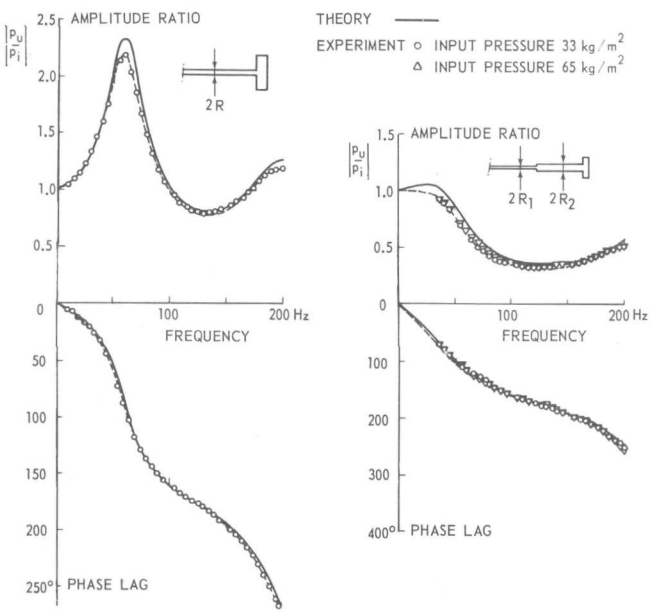

(a) SINGLE TUBE - TRANSDUCER SYSTEM
R = 0.795 mm
L = 1000 mm
V_v = 285 mm³
n_v = 1.4
T_s = 24° C
p_s = 10500 kg/m²

(b) DOUBLE TUBE - TRANSDUCER SYSTEM
R_1 = 0.525 mm R_2 = 0.790 mm
L_1 = 500 mm L_2 = 500 mm
V_v = 285 mm³
n_v = 1.4
T_s = 24° C
p_s = 10500 kg/m²

Fig. 5.5 Experimental and theoretical transfer functions of tube-transducer systems in still air.

ic response shows a maximum. The example of figure 5.5b, which deals with a system with a discontinuity in tube radius, is damped more heavily and does not exhibit these pronounced resonance peaks. In the latter example, two values of the input pressure are used, thereby demonstrating that the system behaves linear.

For geometrically identical tubes - as normally applied in the wind-tunnel models - and for a given frequency ω, the transfer function only depends on the following quantities: ρ_s, μ, a_o and n, which for normal air are completely determined by the value of the mean steady pressure p_s and the mean temperature T_s. The influence of these two parameters is shown in figure 5.6, which indicates that a variation in mean temperature (Fig. 5.6a) of 30 °C does not have much effect, whereas the mean pressure has a considerable influence (Fig. 5.6b). The latter effect is of importance, because in high-speed wind-tunnel tests there are considerable differences in local airspeed over the airfoil, which results in a considerable difference in the mean steady pressure in the various tubes. For instance, in an atmospheric wind tunnel, a change in local Mach number between 0.5 and 1.0 results in pressure changes from 0.84 to 0.53 ata.

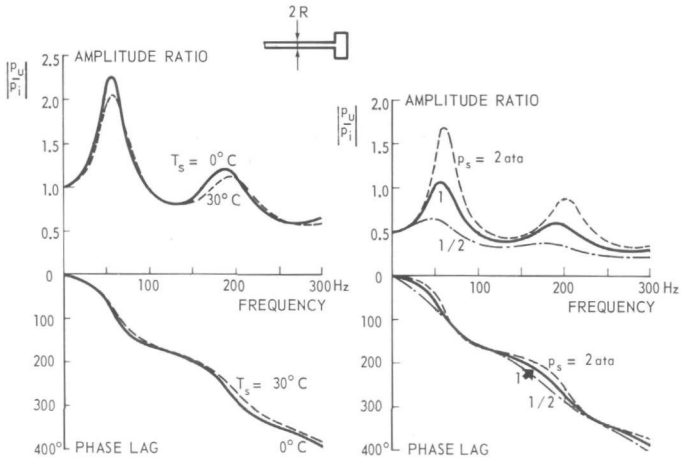

ⓐ INFLUENCE OF MEAN TEMPERATURE

R = 0.75 mm
L = 1000 mm
V_v = 300 mm^3
n_v = 1.4
p_s = 1 ata

ⓑ INFLUENCE OF MEAN PRESSURE

R = 0.75 mm
L = 1000 mm
V_v = 300 mm^3
n_v = 1.4
T_s = 15° C

Fig. 5.6 Calculated transfer functions of a tube-transducer system in still air, showing the influence of mean temperature and mean steady pressure.

5.3.2 Influence of the airflow

In the preliminary tests at NLR on oscillating wind-tunnel models in high-speed flow, it was not recognized that the main flow across the entrance of the pressure tubes was an important parameter, and for the data reduction of these tests use was made of the transfer functions determined in still air for the correct values of frequency and steady pressures. Afterwards, when serious doubts arose against the test results, the influence of the main flow was investigated in an extensive experimental program on a two-dimensional airfoil with oscillating flap (for details, see reference 72). These tests revealed the considerable influence that the main flow may have on the dynamic characteristics of the tubing system. This is illustrated in figure 5.7, which shows the transfer functions for zero and nonzero flow velocity for two different tube lengths. It was also experienced that a very satisfactory agreement between theory and experiment can be achieved for a wide range of Mach numbers and frequencies when the constant C appearing in formula (5.6) is taken equal to 0.9.

In addition, the results of the experiments showed that the chordwise location of the pressure orifices on a wind-tunnel model does not affect the transfer function, while additional pairs of pressure tubes and transducers mounted in the side wall of the wind tunnel (underneath a relatively thick boundary layer) also give the same results. This justifies the conclusion that the boundary layer does not have a significant effect, at least as long as the flow remains attached.

5.3.3 Verificaton in a joint ONERA-NLR investigation

The measuring technique in which use is made of pressure tubes has been verified in a program of unsteady pressure measurements on an oscillating model of a swept wing, jointly performed by ONERA (Office National d'Etudes et des Recherches Aérospatiales) and NLR. During these tests, two different techniques to measure unsteady pressures were

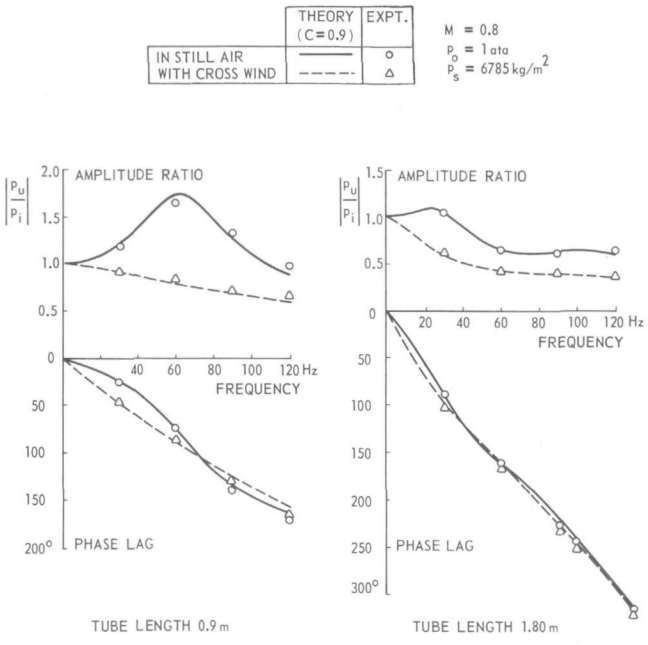

Fig. 5.7 Calculated and measured transfer functions of tube-transducer systems at the same static pressure p_s with and without cross wind (M = 0.8).

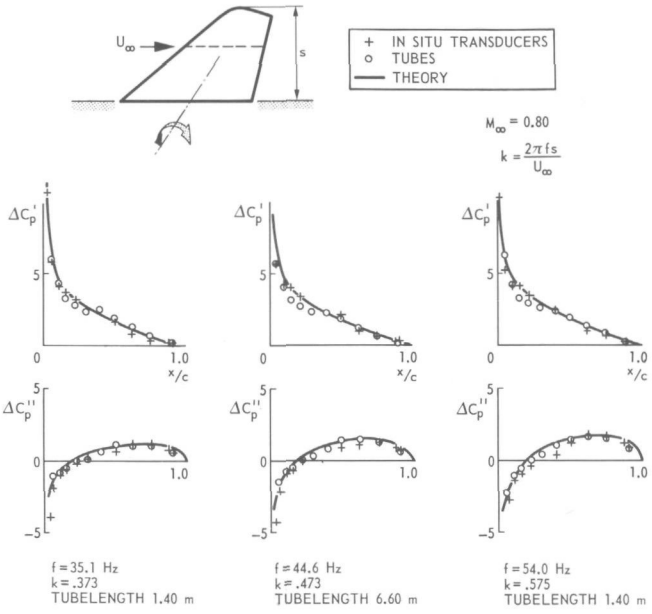

Fig. 5.8 Comparisons between unsteady pressure distributions measured with in situ transducers and via tubes (M_∞= 0.80) on a model of a swept wing performing oscillations in pitch (Ref. 39) (Note difference in tube lengths).

used simultaneously, namely in situ transducers (ONERA) and the system of pressure tubes and scanning valves (NLR). The tests were performed in the High-Speed Tunnel (HST) of NLR; both parties used their own data-registration system and data-reduction procedures. In the data reduction of NLR, the effect of the main flow on the transfer functions of the tube system was determined theoretically. (For details of this investigation, performed under the auspices of AGARD, reference is made to reference 39.)

The final results of both measuring methods agree well for all test conditions and for widely different tube lengths (see examples in figure 5.8), which justifies the conclusion that either technique gives satisfactory results if applied carefully.

As an additional check on the pressure measurements with the tubes, the overall unsteady aerodynamic moments on the wing model as obtained by integration of the unsteady pressure distribution were compared with the aerodynamic moments obtained from decay tests of the complete model. The results, given in figure 5.9, agree satisfactorily, which further increased the confidence in the NLR technique for unsteady pressure measurements.

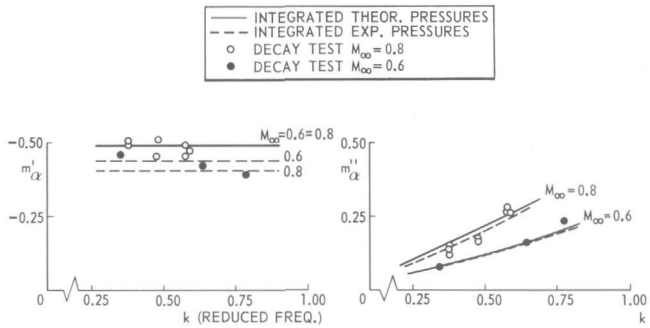

Fig. 5.9 Comparison between overall moments directly measured and moments from integrated pressures (Ref. 39).

5.4 PRACTICAL APPLICATION IN WIND-TUNNEL TESTS

5.4.1 Choice and calibration of tube-transducer systems

To make an optimum choice for the dimensions of the tube system for given model size and test conditions (Mach number and frequency), a computer program is used for the calculation of the dynamic response of tube-transducer systems, which is based on equations (B.47) and (B.51) of Appendix B.

Apart from the obvious demand that the pressure signals are not attenuated too much by the tube, other criteria that are applied are that at

the test frequencies the effect of the mean steady pressure remains small, and that these frequencies do not coincide with resonance frequencies of the tube-transducer system. The latter requirement is imposed, because experience has learned that nonlinearities start to occur first around the resonance peaks. Further, the theoretically predicted transfer functions are very useful to support the still-air and "in-wind" calibrations of the tubes during the actual wind-tunnel program.

In order to keep the data reduction as simple as possible, the still-air transfer functions are made identical by choosing the same length and diameter for all tubes. These transfer functions are checked by performing calibrations with a test set-up as sketched in figure 5.10. The orifice at the entrance is covered by a small cap, in which a sinusoidal pressure variation is generated with variable frequency and variable mean steady pressure. The oscillatory pressure at the entrance is measured directly with the reference transducer in the cap. At the exit both the mean steady and the oscillatory pressure are determined with the transducer in the scanning valve.

During a high-speed wind-tunnel test, the local Mach number at the entrance of the various tubes will in general be different, which implies that the pressure transfer of the tubes will also be different. Since, however, for each tube the local mean steady pressure (and, thus, the local Mach number) is measured simultaneously with the unsteady pressure, it is relatively easy to determine the transfer of each individual tube, provided that their common transfer function as a function of Mach number is known. In principle, this transfer function can be determined both

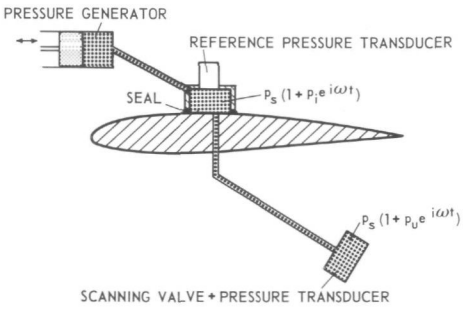

Fig. 5.10 Test set-up for still-air calibrations.

theoretically and experimentally. In practice it has proven to work satisfactorily when the calibration of a limited number of tubes is performed during the wind-tunnel experiments. For this purpose, a small number of miniature transducers is mounted in the model, which are distributed over the airfoil in such a way that considerable differences in local Mach number can be expected. Each of the miniature transducers is positioned close to the entrance of a pressure tube (reference tubes). During the wind-tunnel tests, a direct calibration of the reference tubes is obtained by a comparison of their output with the pressures measured simultaneously with their corresponding miniature transducers. By collecting the data for the reference tubes and by plotting them as a function of the mean steady pressure (or its equivalent local Mach number) the calibration curve can be made. Some examples of calibrations obtained in this way and applied in the data reduction of the present investigations are shown in figure 5.11.

5.4.2 Measuring equipment and data reduction

For the steady and unsteady pressure measurements, a semi-automatic data-acquisition system (DYDRA) is used, which is designed especially for this purpose (Ref. 95). The most salient operations are:

- generation of a 0.1 Hz to 10 kHz signal with constant amplitude for model excitation;
- computation of the first Fourier component of the signals from the pressure transducers, accelerometers and other pick-ups;
- measurement of the direct-current (DC) values of these signals.

The system features a very flexible control for channel selection and subscanner operation, and includes a self-test facility to ascertain system integrity before a test run. A block diagram of the equipment is shown in figure 5.12.

A normal test run proceeds as follows: at a given test condition (Mach number, mean incidence, or mean flap angle), the model is forced into a sinusoidal motion at the desired frequency and am-

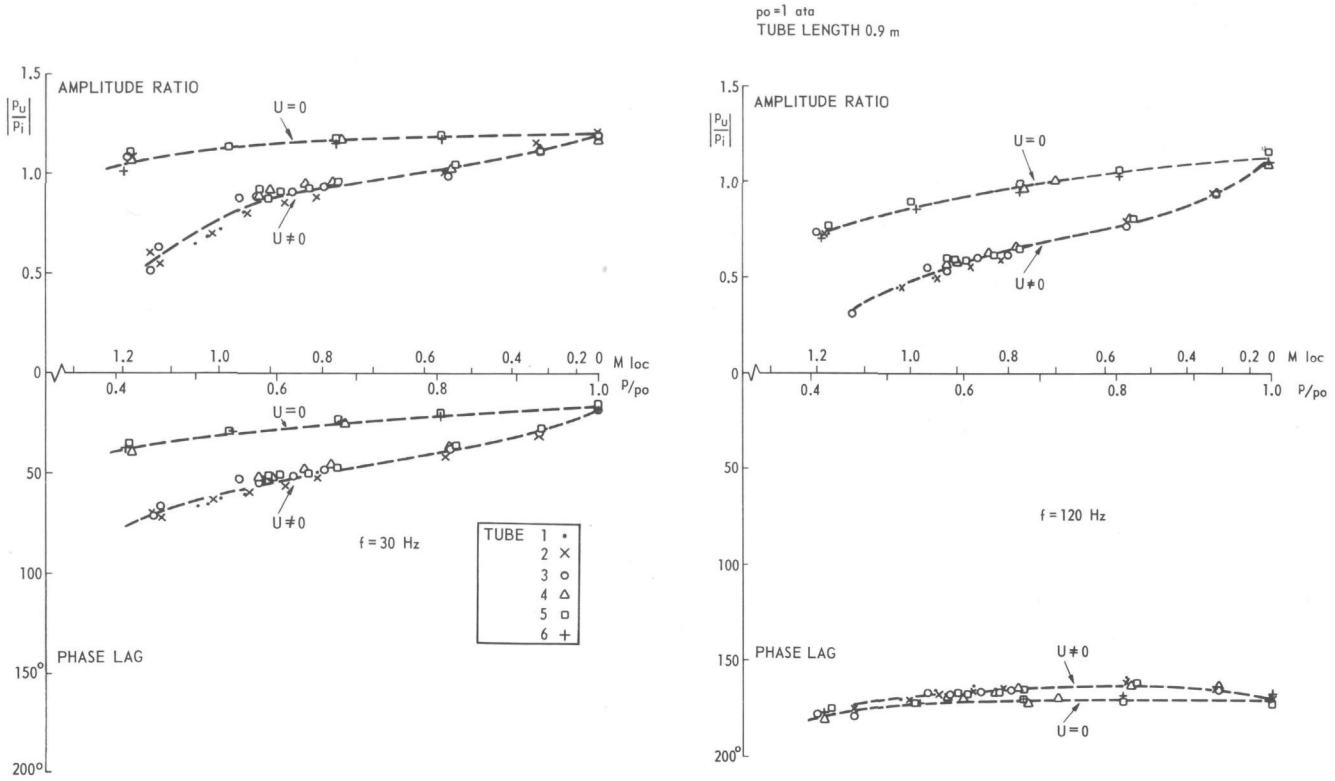

Fig. 5.11 *Examples of measured transfer functions in still air and in flowing air.*

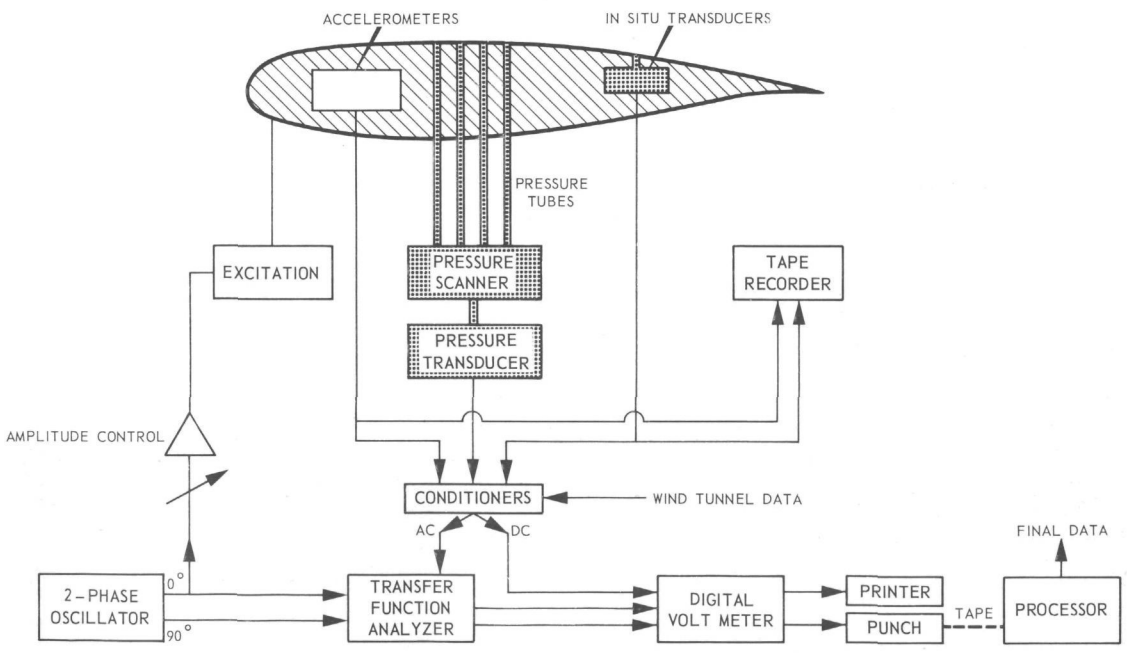

Fig. 5.12 Block diagram of measuring equipment.

plitude of oscillation. Then, the signals of the pressure transducers, accelerometers and displacement pick-ups are fed into the data-acquisition system, one after another, and are decomposed into a steady part and the real and imaginary part of the first Fourier component. These data are stored on punched tape and reduced afterwards by a computer to the actual values of interest. From the signals of the accelerometers the motion of the model is determined,and the signals of the pressure transducers serve to determine the mean steady and unsteady pressure distributions.

To perform the data reduction of the unsteady pressures measured in the scanning valve, first the transfer function of the tubes as a function of mean steady pressure has to be determined. As described in the preceding section, this calibration is obtained from the pressures measured with the in situ transducers and their respective reference tubes. Next, the transfer functions of each tube can be determined by use of its measured local pressure. Finally, the unsteady pressures measured at the end of the tubes are translated to the actual pressures at the model surface according to the procedure as sketched in figure 5.1. The result consists of a mean steady pressure distribution and an unsteady pressure distribution for a unit amplitude (for the definitions,see Appendix A).

The procedure described above provides only the first Fourier component of the unsteady pressures; however, to gain additional information about the higher harmonics, the electric output of both the in situ pressure transducers and the accelerometers are recorded directly on a magnetic tape.

6 WIND - TUNNEL MODELS AND TEST SET-UP

6.1 NACA 64A006 AIRFOIL WITH FLAP

The model investigated first has an NACA 64A006 airfoil section and is fitted with a trailing-edge flap of 25 per cent of the chord. The maximum thickness of this symmetrical airfoil (for contour data, see table 1) is 6 per cent and is located at about 28 per cent of the chord. The total length of the chord is 18 cm. The gap between the nose circle of the flap and the main surface is kept as small as possible and measures about 0.1 mm. The main surface of the model is made of steel and the flap of Dural. During the tests, the model was mounted horizontally in the test section of the NLR Pilottunnel (Fig. 6.1), where it was clamped between the perspex windows in the tunnel side walls. The hinge axis was extended through the windows and supported by bearings. At both sides of the wind tunnel, an electrodynamic exciter was placed, enabling flap excitation by means of a lever system. The mean flap angle could be varied easily by giving a prerotation to the hinge axis.

Because the electrodynamic exciters were not able to withstand a large mean steady load, it was necessary to add a spring system of sufficient stiffness to keep the mean position of the oscillating flap constant during the tests. On the other hand, the springs could not be too stiff, which would make excitation impossible. To fulfil these requirements, a spring system was built of which

TABLE 1

Coordinates of NACA 64A006 airfoil

x (% c)	z (% c)	x (% c)	z (% c)
0	0	40	2.999
0.5	0.485	45	2.945
0.75	0.585	50	2.825
1.25	0.739	55	2.653
2.5	1.016	60	2.438
5.0	1.399	65	2.188
7.5	1.684	70	1.907
10	1.919	75	1.602
15	2.283	80	1.285
20	2.557	85	0.967
25	2.757	90	0.649
30	2.896	95	0.331
35	2.977	100	0.013

L.E. radius: 0.246 % c

T.E. radius: 0.014 % c

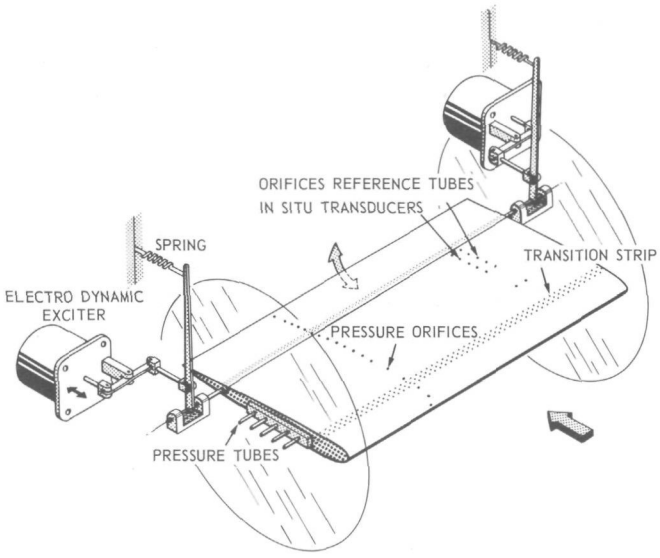

Fig. 6.1 Schematic view of test set-up of the NACA 64A006 airfoil with flap.

the stiffness could be adjusted in such a way that the resonance frequency of the flap-spring combination could be "matched" with the desired test frequency. In practice this worked reasonably well, be it that it could not be avoided completely that the mean flap angle varied somewhat with Mach number.

Both the upper and the lower surface of the measuring section of the model were provided with 19 pressure orifices and tubes (Figs. 6.2 and 6.3). To determine the transfer functions of the tubes during the tests, six small pressure transducers (manufactured by Kulite) were placed inside the model, together with six tubes having the same geometry as the tubes in the measuring section.

To determine the motion of the flap, two accelerometers (x_1, x_2) and two capacitive displacement pick-ups were used. The capacitive pick-ups served also to measure the mean position of the flap. In addition, two accelerometers were placed in the main surface, close to the measuring section, to detect unwanted oscillations of this part of the model. A scheme of the instrumentation of the model is shown in figure 6.2.

To obtain a turbulent boundary layer with a fixed transition point, a 2.5 mm wide strip of carborundum grains was placed at 10 per cent of the chord on both the upper and the lower surface.

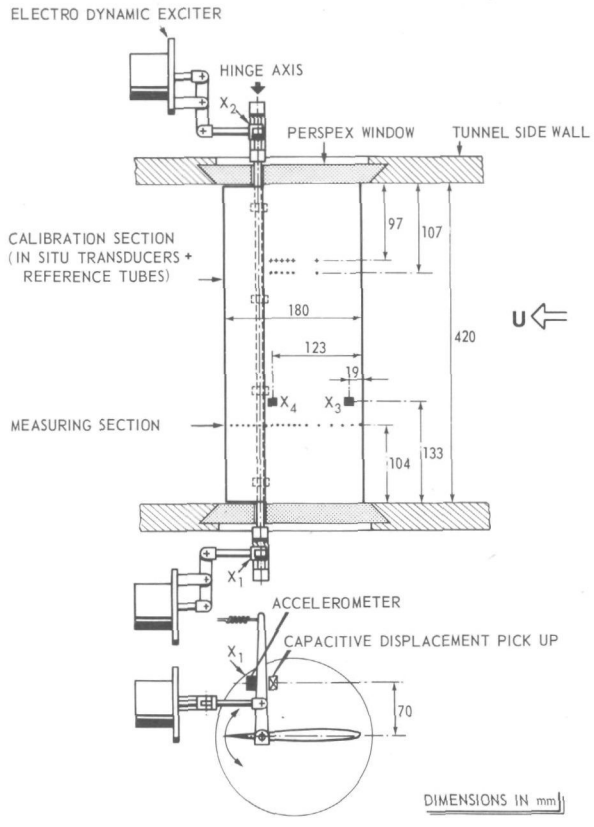

Fig. 6.2 Test set-up and instrumentation of the NACA 64A006 airfoil with flap.

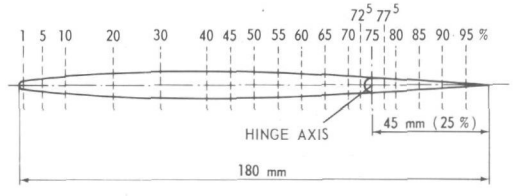

MEASURING SECTION (BOTH UPPER AND LOWER SURFACE)			
No. 1	x/c = .01	No. 11	x/c = .65
2	.05	12	.70
3	.10	13	.725
4	.20	14	.75
5	.30	15	.775
6	.40	16	.80
7	.45	17	.85
8	.50	18	.90
9	.55	19	.95
10	.60		

CALIBRATION SECTION (UPPER SURFACE ONLY)	
No. 1	x/c = .30
2	.50
3	.55
4	.60
5	.65
6	.70

Fig. 6.3 Location of pressure orifices on the NACA 64A006 airfoil with flap.

6.2 NLR 7301 AIRFOIL

The second model under consideration has an NLR 7301 airfoil section, which is designed for

shock-free flow and has a maximum thickness of 16.5 per cent of the chord (for geometric data, see table 2). The model has a chord of 18 cm and can perform pitching oscillations about an axis at 40 % of the chord. The model, made of Dural, spanned horizontally the test section of the Pilot-tunnel (Figs. 6.4 and 6.5).

TABLE 2

Coordinates of NLR 7301*

Upper surface		Lower surface	
x (% c)	z(% c)	x(% c)	z (% c)
0	-.0004		
.0033	.0196	.0018	-.0134
.0124	.0369	.0079	-.0247
.0207	.0454	.0180	-.0340
.0299	.0511	.0370	-.0437
.0397	.0554	.0650	-.0525
.0499	.0590	.1000	-.0598
.0600	.0618	.1300	-.0643
.0748	.0651	.1649	-.0685
.0998	.0697	.2000	-.0718
.1300	.0741	.2499	-.0750
.1649	.0781	.2998	-.0767
.1995	.0813	.3499	-.0770
.2498	.0847	.3999	-.0760
.2998	.0869	.4497	-.0733
.3497	.0881	.4998	-.0684
.3993	.0883	.5496	-.0613
.4492	.0876	.5996	-.0526
.4996	.0860	.6393	-.0447
.5493	.0832	.6791	-.0361
.5993	.0792	.7193	-.0273
.6493	.0736	.7597	-.0185
.6993	.0661	.7994	-.0104
.7494	.0573	.8377	-.0039
.7982	.0475	.8785	.0013
.8385	.0388	.9188	.0043
.8786	.0297	.9487	.0047
.9184	.0207	.9781	.0037
.9479	.0140		
.9784	.0074		
1.0000	.0030		

* for a more detailed description, see reference 78.

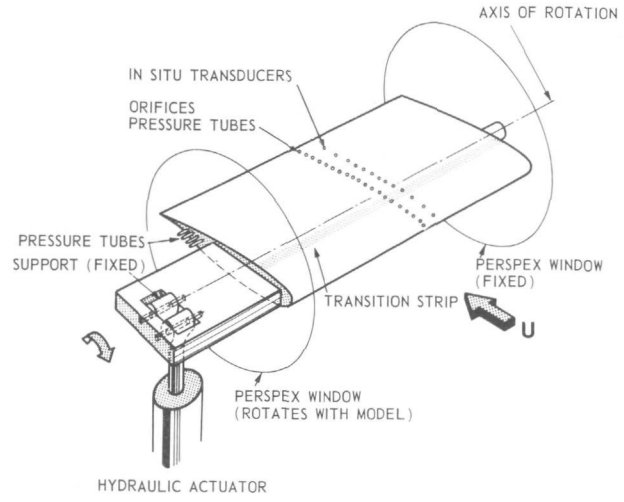

Fig. 6.4 Schematic view of test set-up of the NLR 7301 airfoil.

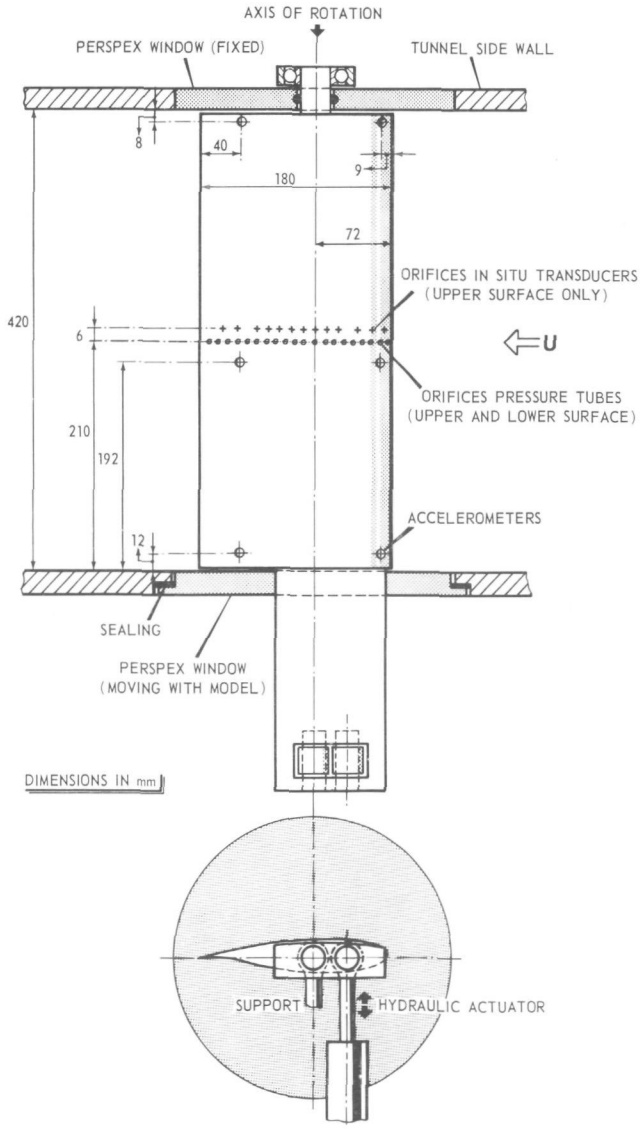

Fig. 6.5 Test set-up and instrumentation of the NLR 7301 airfoil.

The mounting of the model differed from the system mentioned in the preceding section. This time, use was made of a hydraulic actuator that was able to supply simultaneously a large time-dependent force as well as a considerable steady force. This steady force was necessary, since the model carried, in the majority of the test conditions (like the shock-free design condition), a considerable mean steady airload, which could not be withstood by a spring system that at the same time had to produce the relatively low resonance frequencies required for the model excitation with the electrodynamic exciters. An additional advantage of hydraulic excitation was that the test frequencies could be varied freely, because it was no longer necessary to match the desired test frequency with a resonance frequency of a model-spring system. Moreover, the mean incidence of the model could be varied easily by changing the mean position of the hydraulic actuator.

To keep the mounting as simple as possible, the model was excited at one side, while the opposite side was supported by a bearing just outside the tunnel wall (Fig. 6.5). To avoid a complicated sealing between model and window, the window closest to the actuator was attached to the model and followed its motion. In addition, a clear view on the model for optical flow studies was provided. For further details of the hydraulic excitation system, reference is made to Poestkoke (Ref. 96).

Both the upper and the lower surface of the NLR 7301 model were provided with 20 pressure orifices (Figs. 6.5 and 6.6), connected with two

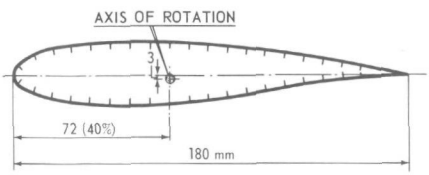

PRESSURE ORIFICES TUBING SYSTEM (BOTH UPPER AND LOWER SURFACE)			
No. 1	x/c = .01	No. 11	x/c = .50
2	.05	12	.55
3	.10	13	.60
4	.15	14	.65
5	.20	15	.70
6	.25	16	.75
7	.30	17	.80
8	.35	18	.85
9	.40	19	.90
10	.45	20	.95

IN SITU TRANSDUCERS (UPPER SURFACE ONLY)			
No. 1	x/c = .04	No. 11	x/c = .70
2	.10	12	.80
3	.19	13	.88
4	.28		
5	.34		
6	.40		
7	.46		
8	.52		
9	.58		
10	.64		

Fig. 6.6 Location of pressure orifices of the NLR 7301 airfoil.

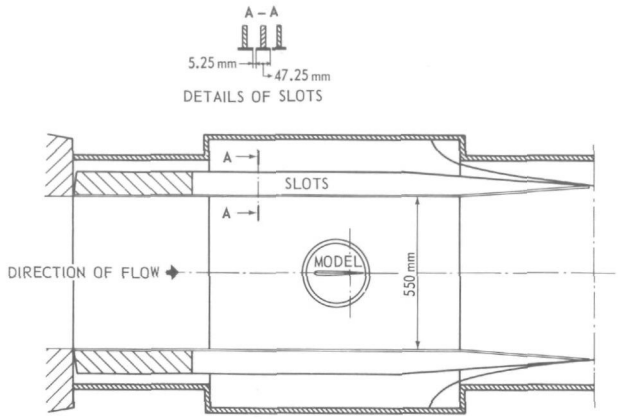

Fig. 6.7 Transonic test section of the Pilottunnel.

scanning valves outside the wind tunnel via pressure tubes. In addition, 13 miniature transducers were built in. This number, larger than necessary for the dynamic calibration of the pressure tubes, created the possibility to record the actual time histories (containing the higher harmonics) of the chordwise pressure distribution along the upper surface.
Further, to determine the motion of the model, 6 accelerometers were used, located in three spanwise stations (see figure 6.5).

The main part of the wind-tunnel tests was performed with a transition strip of carborundum grains, located at both the upper and the lower surface at 30 per cent of the chord.

6.3 WIND TUNNEL

The tests have been performed in the Pilottunnel of NLR, which is an atmospheric, closed-circuit wind tunnel for Mach numbers up to about 1. The dimensions of the test section are 0.55 x 0.42 m (Fig. 6.7). The upper and the lower surface of the test section are fitted with longitudinal slotted walls. The open-area ratio of the walls is 0.1, and there is no connection between the plenum chambers of floor and bottom. Further details of the Pilottunnel are given in reference 97.

6.4 OPTICAL FLOW STUDIES

The periodical shock-wave motions on both oscillating models have been determined in two

different ways. First, shadowgraph pictures were taken by means of a stroboscopic light source triggered by an electrical signal from a displacement pick-up in the model. By means of an adjustable phase shift in the electric circuit between the accelerometer and the light source, the oscillating model with its instantaneous shock pattern could be photographed in every position desired. The second way of registration was obtained by taking high-speed films of the time histories of the flow (with a film speed up to 4000 frames per second).

7 TEST PROGRAM

7.1 NACA 64A006 AIRFOIL WITH FLAP

The tests on the NACA 64A006 airfoil with oscillating flap covered the Mach number range from 0.5 to 1.0 and the frequencies were 30 and 120 Hz. For a few cases, tests were performed also at 10, 20 and 90 Hz. The maximum value of the reduced frequency achieved during the tests varied from 0.39 at M_∞ = 0.5 to 0.21 at M_∞ = 1.0. The results for the limiting case of zero frequency have been derived from an extensive series of steady tests.

As it was the intention to study symmetrical as well as nonsymmetrical flow conditions, the model was tested at incidences of 0, -2 and -4 degrees, and mean flap angles of -3, 0 and +3 degrees, respectively.

Due to the mechanical properties of the model, the maximum frequency of the flap was limited to 120 Hz and the amplitude of oscillation to about 1 degree. For mean incidences of the model of -2 and -4 degrees, the maximum Mach number was reduced to about 0.94, due to lack of power of the wind tunnel. A survey of the test program is given in table 3.

In chapters 8 and 9 a substantial part of the test results will be used to analyze the features encountered in high-subsonic and transonic flows. For the detailed test data, i.e. a collection of tables with steady and unsteady pressure coefficients, the reader is referred to references 98 - 100.

TABLE 3

Test program for the NACA 64A006 airfoil with flap

TEST CONDITION	FREQ. (Hz)	MACH NUMBER .50	.75	.775	.80	.825	.85	.875	.90	.92	.94	.96	.98	1.00
α_o= 0° δ_o= 0°	0	x	x		x	x	x	x	x	x	x	x	x	
	10	x				x	x	x	x			x		
	20	x						x						
	30	x			x	x	x	x	x			x		
	90	x				x	x	x	x			x		
	120	x	x	x	x	x	x	x	x	x	x	x	x	x
α_o= 0° δ_o= 3°	0	x	x		x	x	x	x	x	x	x	x	x	x
	30	x				x	x	x		x				
	120	x	x	x	x	x	x	x		x	x	x		
α_o= -2° δ_o= 0°	0	x	x		x	x	x	x	x	x	x	x		
	30	x				x	x	x	x					
	120	x	x	x	x	x	x	x	x	x	x			
α_o= -2° δ_o= 3°	0	x	x	x	x	x	x	x	x	x	x	x		
	30	x				x	x	x	x					
	120	x	x	x	x	x	x	x	x					
α_o= -2° δ_o= -3°	0	x	x	x	x	x	x	x	x	x	x	x		
	30	x				x	x	x						
	120	x	x	x	x	x	x	x						
α_o= -4° δ_o= 0°	0	x	x	x	x	x	x	x	x	x				
	10	x					x							
	30	x				x	x							
	120	x	x	x	x	x	x	x	x	x				

AMPLITUDE OF OSCILLATION : δ = 1 DEGREE

7.2 NLR 7301 AIRFOIL

The tests on the NLR 7301 airfoil that could perform pitching oscillations around an axis at 40 per cent of the chord covered the Mach number range between 0.5 and 0.8. The maximum test frequency was 80 Hz, which corresponds to a reduced frequency that varied from 0.26 at M_∞ = 0.5 to 0.17 at M_∞ = 0.8.

The combinations of mean incidence and free-stream Mach number for which tests were performed were selected in such a way that the C_ℓ-M diagram of the airfoil (Fig. 3.11) was covered reasonably well, so that a good overall picture of the unsteady aerodynamic characteristics could be obtained (table 4a). In addition, four characteristic conditions of Mach number and mean incidence were selected, for which extra test runs were conducted to explore the influence of amplitude and frequency of oscillation (table 4b).

TABLE 4

Test program for the NLR 7301 airfoil

a BASIC PROGRAM : AMPLITUDE OF OSCILLATION : $\Delta\alpha$ = 0.5 DEGREE
FREQUENCIES : 0 , 10 AND 80 Hz
TRANSITION STRIP AT x/c = 0.3

INCIDENCE	MACH NUMBER										
	.5	.6	.65	.675	.70	.725	.74	.75	.76	.775	.80
α_o = 0°	x				x			x			
0.85	x	x	x	x	x	x	x	x	x	x	x
1.50	x				x			x			
3.00	x	x	x	x	x	x		x			

b INFLUENCE OF AMPLITUDE AND FREQUENCY TRANSITION STRIP AT x/c = .3

INCIDENCE	AMPLITUDE $\Delta\alpha$	FREQ.	MACH NUMBER		
			.5	.7	.75
α_o =0.85°	0.1;0.25;0.75;1.0;1.5	10 ; 80 Hz	x	x	x
3.00	0.1;0.25;0.75;1.0	10 ; 80		x	
0.85°	0.5 ; 1.0°	10;30;60;80 Hz	x	x	x
3.00	0.5 ; 1.0°	10;30;60;80		x	

c ADDITIONAL TESTS WITH NATURAL TRANSITION

INCIDENCE	AMPLITUDE $\Delta\alpha$	FREQ.	MACH NUMBER		
			.5	.7	.75
α_o =0.85°	0.5 ; 1.0	10 Hz	x	x	x
	0.5 ; 0.75	80	x	x	x
3.00	0.5 ; 1.0	10		x	
	0.5 ; 0.75	80		x	
0.85	0.5	30 ; 60	x		x

The main program was performed with a transition strip, and a limited number of tests was repeated with natural transition (table 4c).

The results of the experiments on the NLR 7301 airfoil will be analyzed in chapter 10. The tables containing the detailed test data have been collected in a separate data report (Ref. 101).

PART III ANALYSIS OF RESULTS

8 THE INTERACTION BETWEEN THE STEADY AND UNSTEADY FLOW FIELD

8.1 INTRODUCTORY REMARKS

As argued in section 4.1, one of the main aspects to be considered in an analysis of the experimental results should be the interaction between the steady and unsteady flow field. This implies that emphasis should be placed upon the effects of airfoil shape, Mach number, mean incidence, and mean flap angle on the unsteady airloads and upon the development of these effects with frequency.

In order to get a clear view of the various effects as observed in the present tests, the following presentation is chosen. First the results of the NACA 64A006 airfoil with flap will be described. These results have the advantage that the unsteady pressure distributions exhibit a large pressure peak at the leading edge of the flap which, for a qualitative discussion, can be interpreted as a point disturbance. This behaviour makes the results well-suited for physical interpretations. Further, the optical flow studies on this airfoil revealed some interesting periodical shock-wave motions, which will be analyzed in a separate chapter (chapter 9).

In chapter 10, an analysis will be given of the results for the supercritical NLR 7301 airfoil. Here attention will be paid to results for oscillations around the shock-free design condition as well as to results for some typical off-design conditions. For both the NACA 64A006 and the NLR 7301 airfoil, the effects of Mach number, mean incidence, mean flap angle, and reduced frequency will be considered.

To emphasize the dynamic effects in the unsteady flow, in many cases the corresponding "quasi-steady" pressure distributions are considered first, i.e. the "unsteady" pressure distributions that occur when the oscillations are infinitely slow. These quasi-steady pressure distributions can be derived easily from a sequence of steady pressure measurements. Further, the test results will be compared with the predictions of "thin-airfoil theory", in which an infinitely thin wing in a uniform main flow is considered. The comparisons with thin-airfoil theory appear to be very useful to identify the typical effects associated with the high-subsonic and transonic flow regime.

8.2 THE INFLUENCE OF MACH NUMBER ON THE AIRLOADS OF THE NACA 64A006 AIRFOIL WITH FLAP

8.2.1 Steady pressure distributions

The chordwise distribution of the steady pressures along the airfoil with undeflected flap is given in figure 8.1 for several values of the free-stream Mach number. The critical Mach number is between 0.825 and 0.85. At the latter Mach number, a weak shock wave appears at about 45 per cent of the chord. When the Mach number is increased further, this shock grows in strength and is displaced in downstream direction. At about $M_\infty \approx 0.92$ the shock reaches the hinge line, and slightly beyond this Mach number the flow downstream of the shock wave separates from the airfoil.

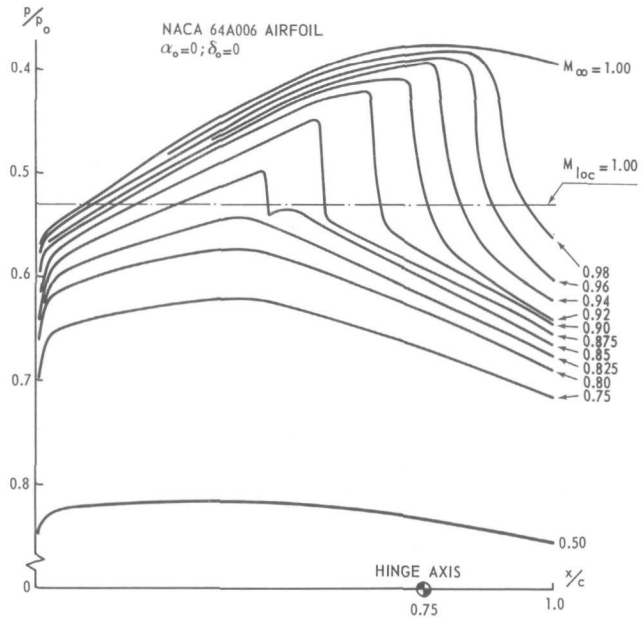

Fig. 8.1 Chordwise pressure distribution as a function of free-stream Mach number.

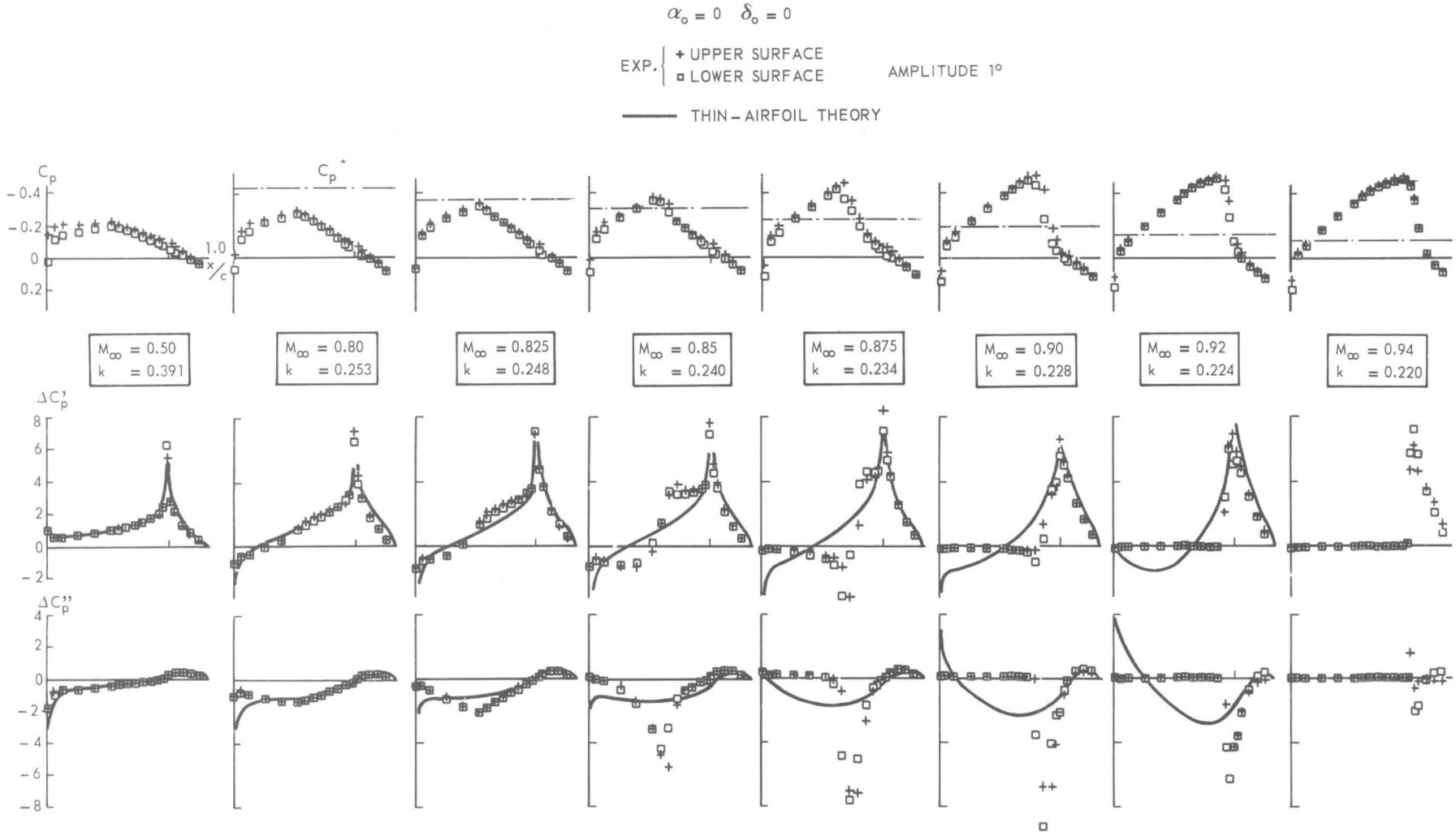

Fig. 8.2 Development of mean steady and unsteady pressure distributions with Mach number (f = 120 Hz).

8.2.2 Unsteady pressure distributions

The unsteady pressure distributions for a flap oscillation with a frequency of 120 Hz and an amplitude of 1 degree are collected in figure 8.2. This figure contains the mean steady pressure distributions and the unsteady pressure distributions, the latter in terms of the real and the imaginary part. The mean steady pressure distributions correspond reasonably well with the steady pressure distributions of figure 8.1, obtained on the non-oscillating model. The unsteady pressures at the lower surface are displayed with a minus sign, to facilitate the comparison between the upper and the lower surface. Since we are dealing with zero incidence and zero mean flap angle, the mean flow is symmetric. Therefore, the unsteady pressures on the upper and the lower surface are almost equal in magnitude, but differ 180 degrees in phase angle.

At the lowest Mach number, a good agreement exists between the measured unsteady data and the results of thin-airfoil theory. This agreement becomes worse with increasing Mach number and, as soon as the flow becomes supercritical, the agreement is good only in the subsonic part of the flow downstream of the shock wave. Above a free-stream Mach number of about 0.875, the measured unsteady pressures in front of the shock wave decrease strongly, and at $M_\infty = 0.94$ they are zero ahead of the hinge axis.

The influence of the Mach number on the unsteady pressure distributions can be considered in a somewhat different way with the help of figures 8.3-8.8, which contain the measured and theoretical unsteady pressure distributions in terms of magnitude and phase angle, together with the corresponding steady and quasi-steady pressure distributions.

The first figure in this series (Fig. 8.3) represents a typical low-speed example. Figure 8.3a shows the steady pressure distributions on the upper surface of the airfoil for three flap angles, namely -1.5, 0 and 1.5 degrees, respectively. From these steady pressure distributions, the quasi-steady pressure

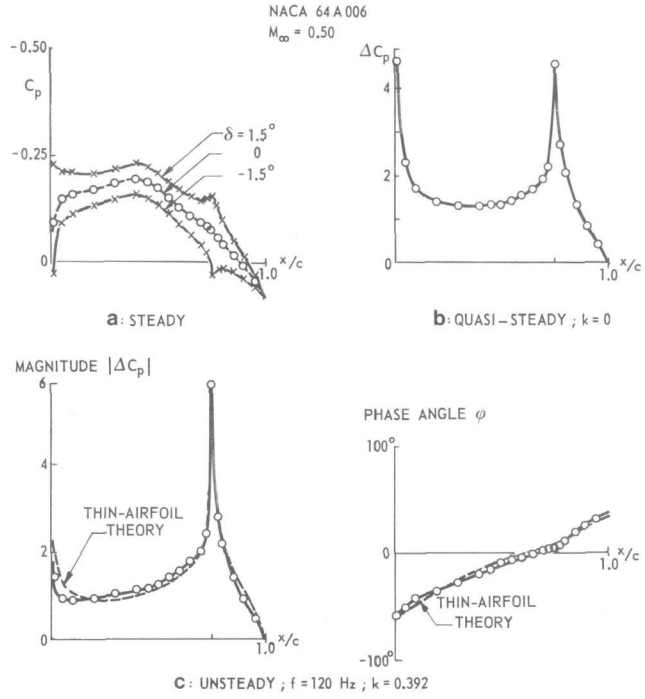

Fig. 8.3 Steady, quasi-steady and unsteady pressure distributions in low-subsonic flow.

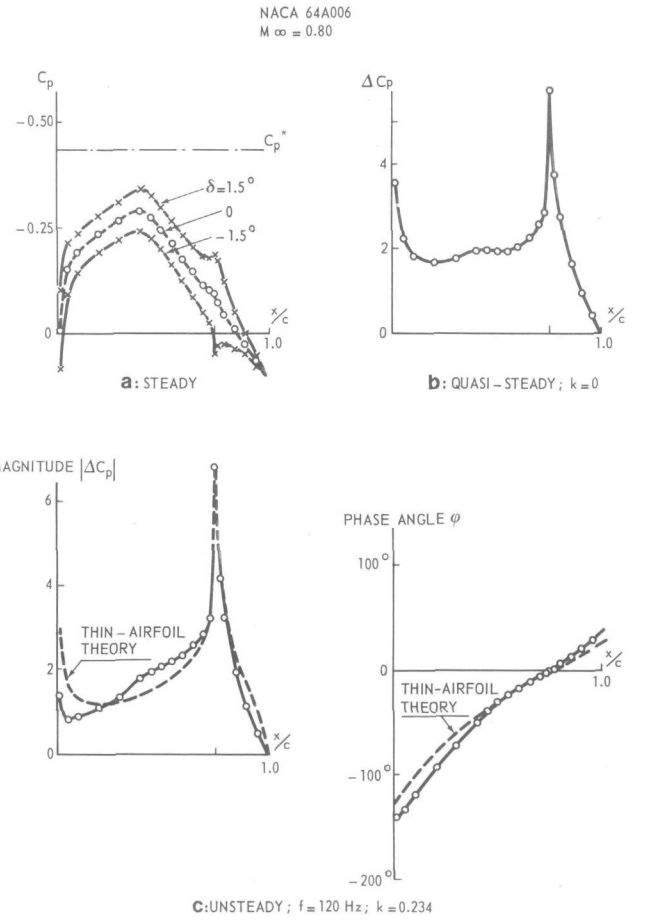

Fig. 8.4 Steady, quasi-steady and unsteady pressure distributions in subsonic flow.

$$\Delta C_p = \frac{C_p(\delta_o - \Delta\delta) - C_p(\delta_o + \Delta\delta)}{2\,\Delta\delta}$$

is determined and the resulting chordwise distribution is shown in figure 8.3b.
As mentioned before, this quasi-steady pressure distribution can be interpreted as the unsteady pressure distribution for zero frequency. In figure 8.3c, the unsteady pressure distribution for a frequency of 120 Hz and an amplitude of about 1 degree is presented. The magnitude of the unsteady distribution very much resembles the quasi-steady distribution, because both show the characteristic peaks at the leading edge of the airfoil and at the hinge axis at 75 per cent of the chord. For the unsteady example, also the result of thin-airfoil theory is given. At this low speed, the agreement with the experimental magnitude and phase distribution is satisfactory.

Results for the same configuration in high-subsonic flow are shown in figure 8.4. Around the 50 per cent chord point, a bulge starts to occur in the magnitude of the measured distribution of both the quasi-steady and unsteady pressures, which is not predicted by thin-airfoil theory. The phase curve also is predicted less satisfactorily by theory than in the preceding low-speed case. A characteristic feature is that the calculated phase lag on the front part of the airfoil is consistently smaller than the measured value. These discrepancies between thin-airfoil theory and experiment become more pronounced in the example of figure 8.5, where the free-stream Mach number is increased further and the flow is almost critical.

Some characteristic results for a transonic flow with normal shock waves are given in figures 8.6 - 8.8. It is clear, from the pressure distribu-

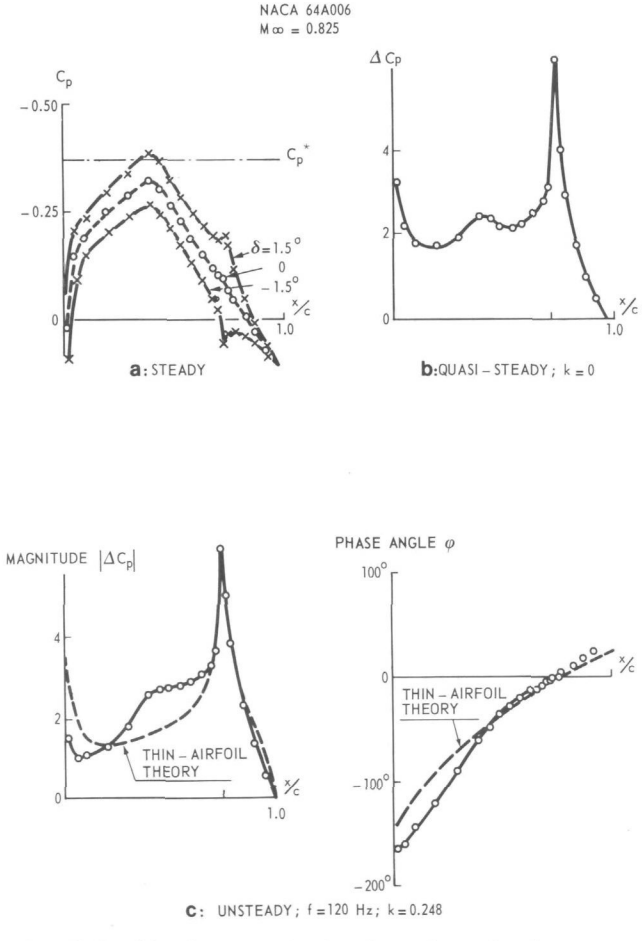

Fig. 8.5 Steady, quasi-steady and unsteady pressure distributions in high-subsonic flow.

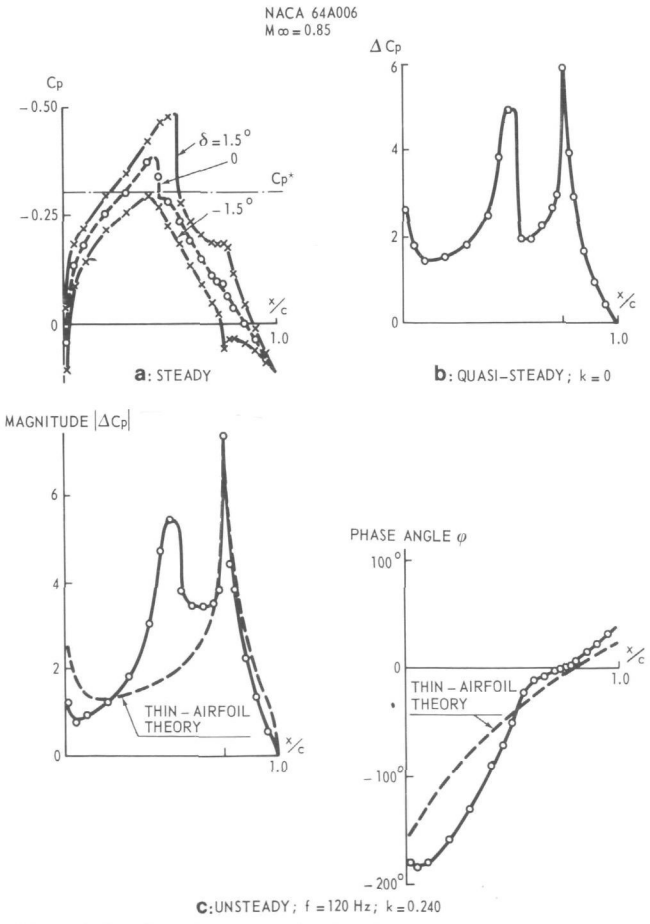

Fig. 8.6 Steady, quasi-steady and unsteady pressure distributions in slightly supercritical flow.

tions in these figures, that a change in flap angle is followed by a shift in shock position, which leads to a high peak in the magnitude of the quasi-steady and unsteady pressures. This peak gives a significant contribution to the overall unsteady lift and moment, which of course cannot be found with thin-airfoil theory. Another observation is that the pressure perturbations in front of the shock wave are smaller than those predicted by theory, and that the measured phase curves show a sharp change in gradient in the region of the shock wave. This effect will be discussed in more detail in section 8.3. When the free-stream Mach number is increased further, the shock strength and the size of the supersonic region become so large that perturbations generated by the flap are no longer felt ahead of the shock wave (compare figures 8.6 - 8.8).

At about $M_\infty = 0.92$, the shock reaches the hinge axis and pressure perturbations generated by the flap are felt only on the flap itself. At still higher Mach numbers, the flow pattern becomes much more complicated. Then a lambda shock and a Prandtl-Meyer expansion alternately occur on either side of the flap (see figure 3.6), while in addition the flow becomes separated. An example of the pressure distributions measured in such a complicated flow pattern at near-sonic free-stream conditions is shown in figure 8.9.

8.2.3 Unsteady aerodynamic coefficients

Examples of the development with Mach number of the overall force and moment coefficients for quasi-steady and unsteady flow are shown in

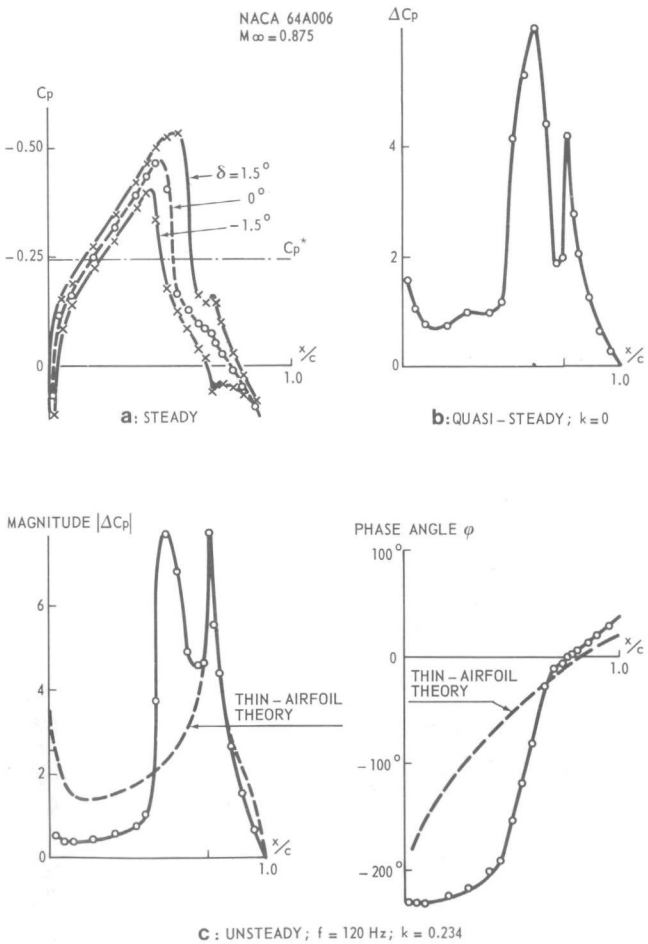

Fig. 8.7 Steady, quasi-steady and unsteady pressure distributions in transonic flow.

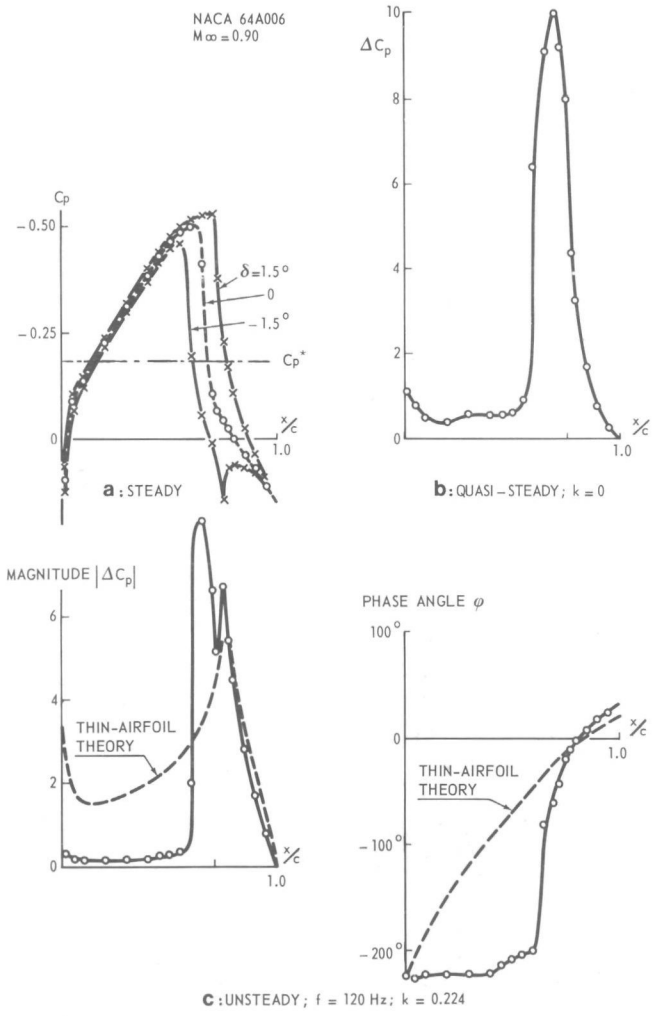

Fig. 8.8 Steady, quasi-steady and unsteady pressure distributions in transonic flow.

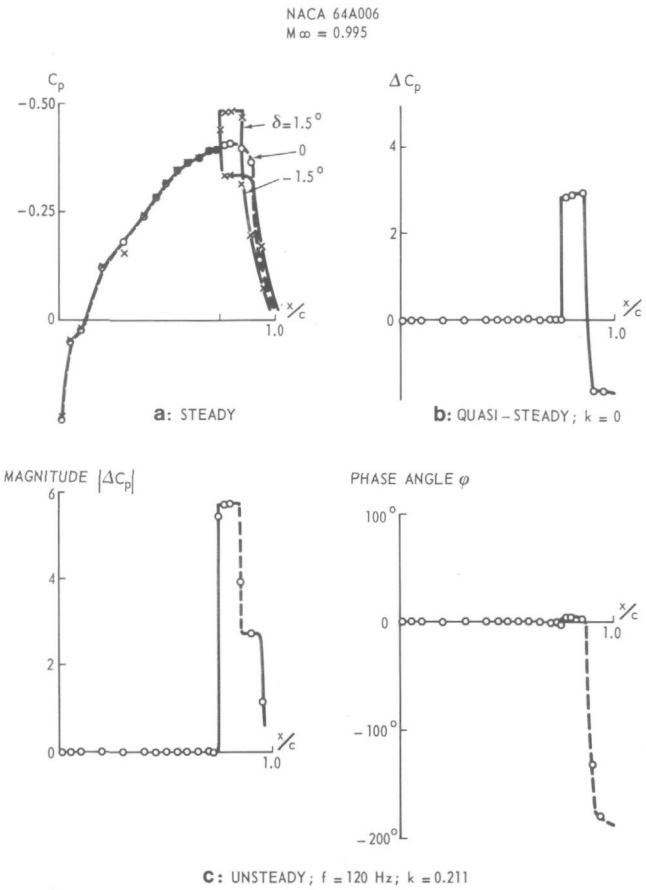

Fig. 8.9 Steady, quasi-steady and unsteady pressure distributions in near-sonic flow.

figures 8.10 and 8.11. As might be expected from the pressure distributions in the transonic regime, the coefficients vary strongly with Mach number. The sharp decrease of the normal-force coefficient, k_c, and the moment coefficient, m_c, occurring after the appearance of a shock wave ($M_\infty \approx 0.85$), can be correlated with the drop observed in the magnitude of the pressure perturbations ahead of the shock wave. The hinge-moment coefficient n_c falls off after the shock wave has passed the hinge axis, which leads to the more complicated flow pattern on the flap and shock-induced separation.

The theoretical curves in figures 8.10 and 8.11 again are based on thin-airfoil theory. When the theoretical curves are compared with the experimental data, it appears that the trend with Mach number is predicted reasonably well, especially for the unsteady-flow case (Fig. 8.11). A difference is that the maximum value of the magnitude of the calculated moment coefficient (Fig. 8.11) occurs at a somewhat higher Mach number than the experimental peak values. This is not surprising, because a closer look at figure 8.2 learns that the measured pressure distribution for $M_\infty = 0.825$ fits better with the calculation for $M_\infty = 0.875$ than the calculation for $M_\infty = 0.825$ does. Evidently, at least for subcritical flows, a better theoretical prediction is obtained if the calculations are performed for a Mach number averaged over the airfoil surface instead of for the free-stream Mach number.

An uncertainty is the contribution of interference from the tunnel walls in the measured results. Unfortunately, a reliable method to determine the corrections for the presence of slotted tunnel walls in unsteady-flow tests is still lacking. Corrections can only be indicated for zero frequency (Fig. 8.10), for which case it appears that the effect of the tunnel walls is responsible for at least a part of the differences

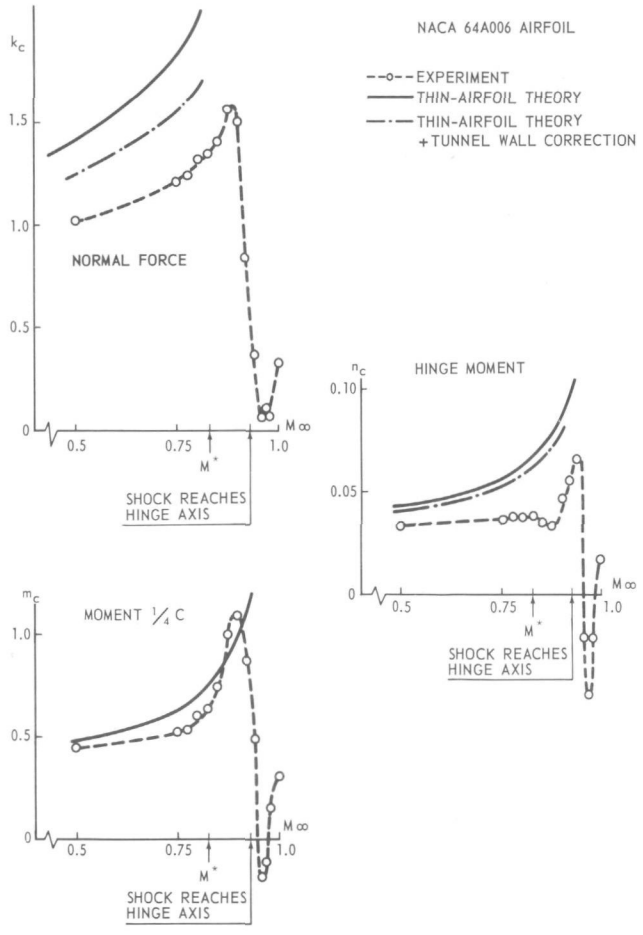

Fig. 8.10 Quasi-steady aerodynamic coefficients as a function of Mach number.

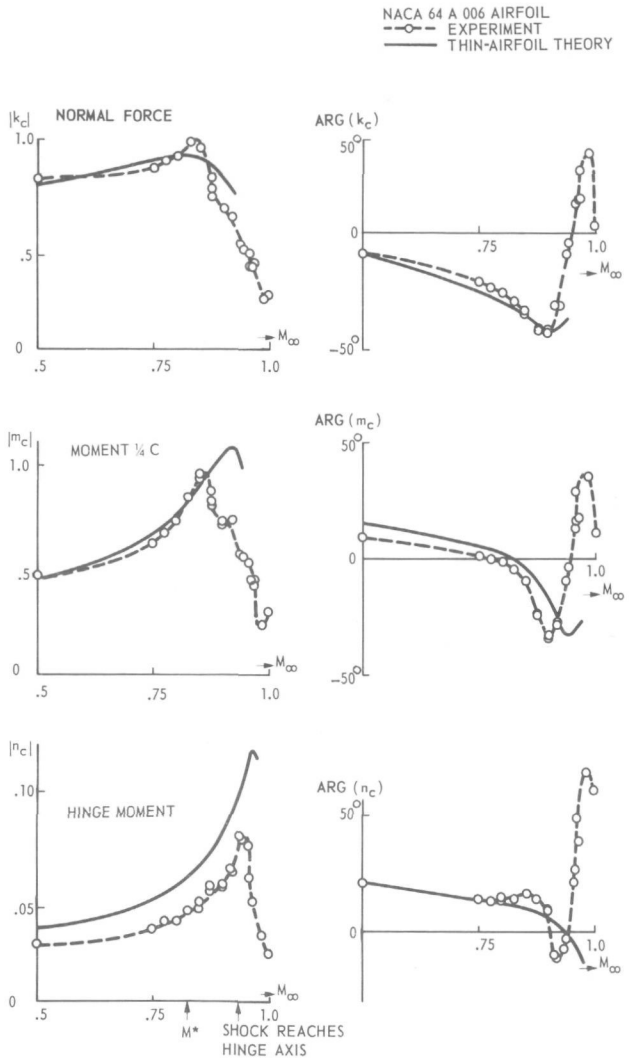

Fig. 8.11 Unsteady aerodynamic coefficients as a function of Mach number (f=120 Hz).

between the calculated and the measured results, in particular for the normal-force coefficients. For a more detailed account of the effect of wall interference, reference is made to part IV of this thesis.

8.3 GRAPHICAL EXPERIMENT

The mechanism of the interaction between the steady and unsteady flow fields for the airfoil with oscillating flap can be explained very well by means of a graphical experiment. For this purpose, the airfoil is schematized to an airfoil with a pulsating pressure disturbance located at the hinge axis. From this disturbance, acoustic waves are going out and propagate into the surrounding non-uniform air flow.

Under these circumstances, a picture of the acoustic wave pattern can be obtained with the well-known construction of Huygens. With this method, the time history of a wave front generated at a certain point can be constructed rather easily, because the local propagation speed of the wave front is equal to the vector sum of the local speed of sound taken normal to the wave front and the local flow velocity (Fig. 8.12). Earlier, Spee (Ref. 20) successfully applied the method to investigate some aspects of shock-free flow around airfoils.

In the following examples for the velocity distribution close to the airfoil surface, use is made of the velocities measured along the airfoil contour, while the velocity distribution in the outer field is estimated. For simplicity, reflected waves from the tunnel walls have been neglected.

Figure 8.13a shows the position of the wave fronts after equal time intervals Δt, plotted for two different Mach numbers. The part of the figure above the airfoil depicts the time histories of the wave fronts in the actual flow field. Below the airfoil, the same wave fronts are shown, but now for a steady uniform flow field, in which the local Mach number everywhere is equal to the free-stream Mach number. The corresponding travel-

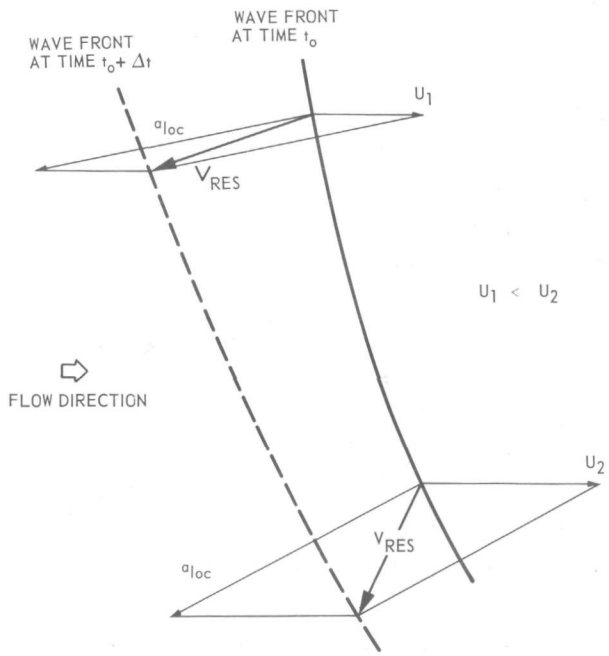

Fig. 8.12 Upstream propagation of a wave-front element in a non-uniform flow.

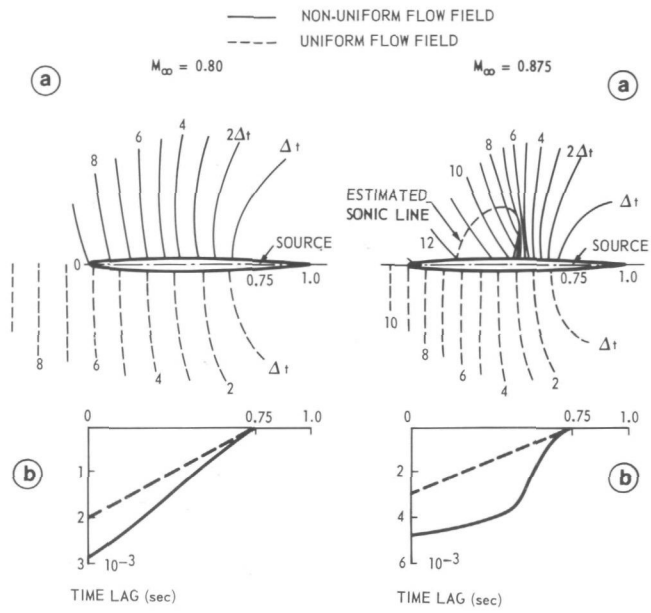

Fig. 8.13 Upstream propagation of wave fronts generated by a source at the hinge axis.
a: Wave propagation.
b: Time lag derived from wave pattern.

ling times (time lags) are given in the diagrams of figure 8.13b.

At M_∞ = 0.8, where the flow is subcritical, the wave fronts encounter more "head wind" in the actual flow than in the uniform case, as can be concluded from the closer spacing of the fronts and from the time lag curves. Moreover, the velocity gradients normal to the chord in the actual flow cause a forward inclination of the wave fronts. When it is recognized that the spacing of the wave fronts is a measure for the intensity of the local pressure perturbation gradient, while the time lag is a measure for the phase shift, it becomes clear that the high-subsonic effects observed in figures 8.4c and 8.5c (bulge in magnitude distribution and shift in phase curve on the front part of the airfoil) can be attributed mainly to the influence of the non-uniform steady flow field.

At M_∞ = 0.875, when in the actual flow field a supersonic region is present terminated by a shock wave (Fig. 8.13), the afore-mentioned inclination of the wave fronts is essential for enabling the waves to penetrate the supersonic region. The graphical experiment for this Mach number shows that, in the actual flow field, the parts of the upstream-moving wave fronts close to the airfoil surface merge into the shock, but the upper parts bend around the top of the shock and penetrate the supersonic region. This is reflected in the time lag curve by a sudden steepening. Since the energy content of the wave fronts penetrating the supersonic region has decreased, due to the longer distance they have travelled around the top of the shock, only small pressures can be built up in front of the shock wave. These findings correlate very well with the effects observed in the wind-tunnel results presented in figure 8.7c, i.e. relatively low pressures in front of the shock, a sudden steepening of the phase curve, and a pressure peak at the shock position. The main contribution to the latter peak should, of course, be attributed to the oscillatory displacement of the shock waves, which is not included in this simple graphical experiment.

At higher Mach numbers, both the strength and the length of the shock are increased, which leads to a continued decrease in amplitude of the pressures measured in front of the shock wave (compare figures 8.7 and 8.8).

The considerations on the moving wave fronts in high-subsonic flow are illustrated in figure 8.14 by shadowgraph pictures. The upstream-travelling wave fronts, which were made visible with the help of a spark exposure (exposure time 10^{-6} sec), are generated by a vortex street, shedding from the sharp edges at the rear of an airfoil from which the trailing-edge flap was removed for this purpose. The receding motion of the wave fronts is smallest near the surface at maximum profile thickness. In the spark exposure of figure 8.15, the motion of wave fronts in a transonic flow is shown. This picture demonstrates how the upstream-travelling wave fronts coalesce at the foot of the shock and how the upper parts penetrate the supersonic region.

8.4 THE INFLUENCE OF INCIDENCE AND MEAN FLAP ANGLE

8.4.1 Unsteady pressure distributions

In order to investigate the influence of incidence and mean flap angle, a number of tests

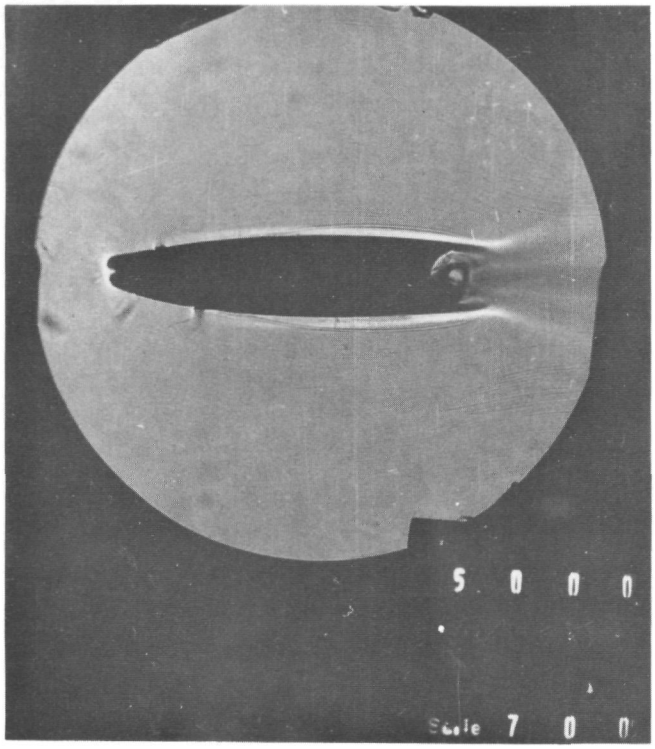

a CONTINUOUS LIGHT

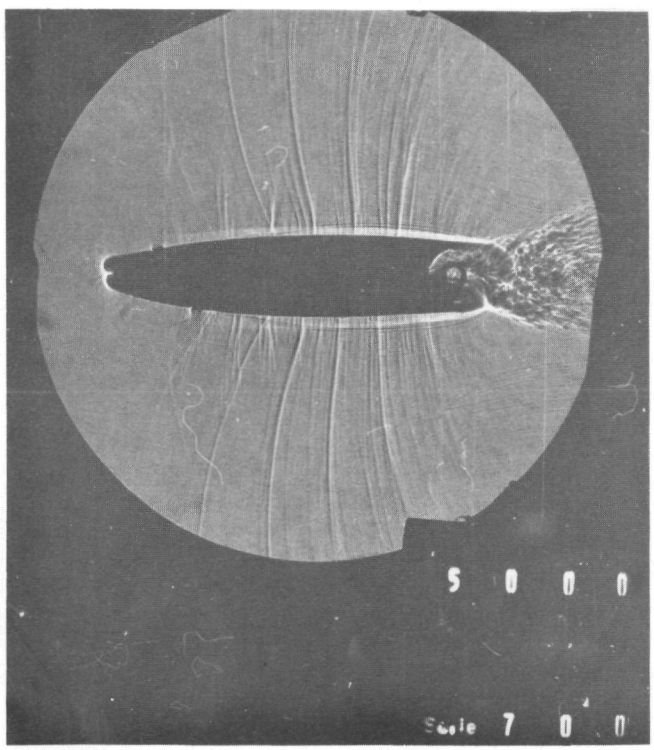

b SPARK EXPOSURE (10^{-6} SEC.)

Fig. 8.14 Shadowgraph pictures in high-subsonic flow.

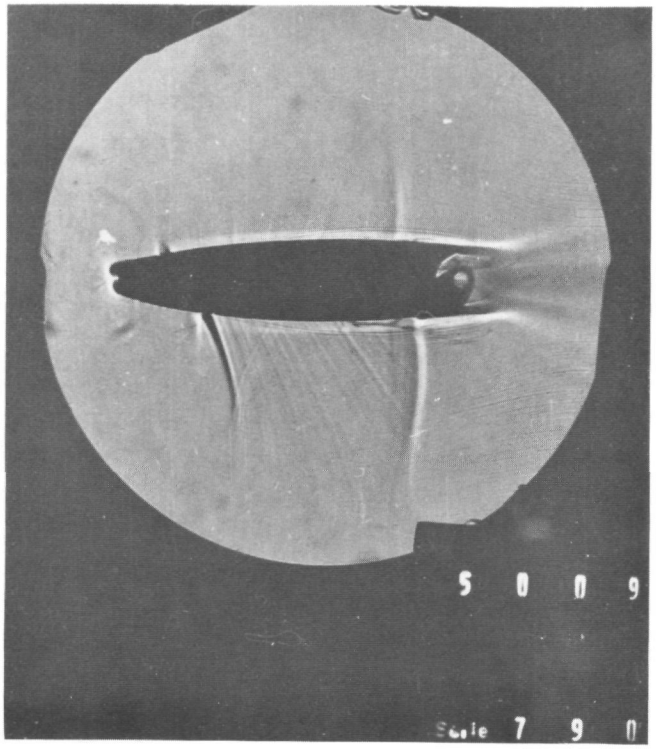

a CONTINUOUS LIGHT

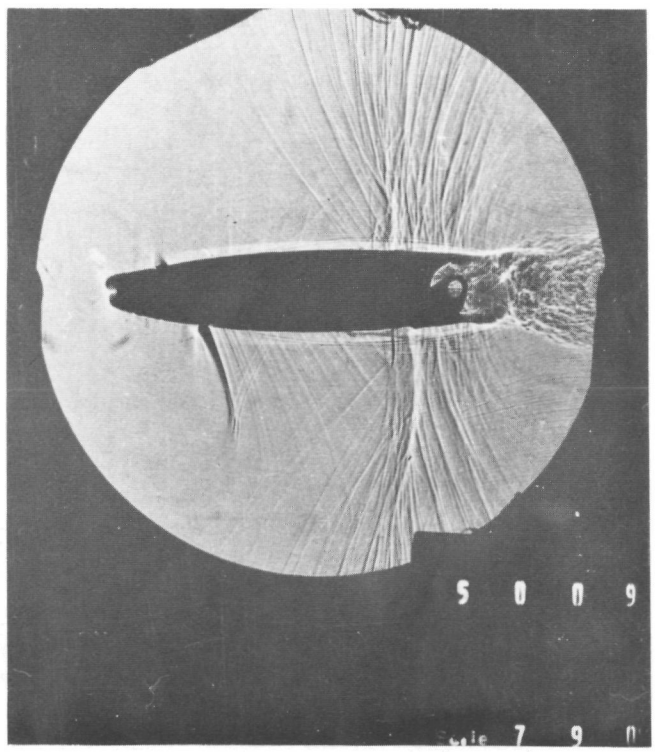

b SPARK EXPOSURE (10^{-6} SEC.)

Fig. 8.15 Shadowgraph pictures in transonic flow.

were conducted in which an incidence was given to the steady main surface or in which the mean angle around which the flap was oscillating was varied. Some characteristic results of these tests are collected in figures 8.16 and 8.17. The unsteady pressures measured at the lower surface are again plotted with a minus sign.

Figure 8.16 shows the effect that a small mean flap angle already has on the development of the mean steady and unsteady pressure distributions with Mach number. As can be observed from the mean steady pressure distributions, deflecting the flap leads to an increase in velocity along the upper surface of the airfoil and to a decrease in velocity along the lower surface. At the lowest Mach number, $M_\infty = 0.5$, the differences in velocity between the upper and the lower surface are not sufficient to create significant differences between the unsteady pressure distributions at both sides. At a free-stream Mach number of about 0.75, however, the differences in mean steady flow along the upper and the lower surface give rise to small differences in the corresponding unsteady distributions. These differences become larger when the free-stream Mach number is increased further, and they become particularly pronounced from about $M_\infty = 0.83$, when at the upper surface a supersonic region appears, terminated by an oscillating shock wave, while the lower surface remains subcritical.

A similar development of the unsteady pressure distributions with Mach number can be seen in figure 8.17, for an incidence of -2 degrees, while the flap oscillates around zero mean flap position with an amplitude of 1 degree. At about $M_\infty = 0.75$, the flow along the upper surface becomes supercritical, and the first signs of a (weak) shock can be noticed in the mean steady and unsteady pressure distributions near the leading edge. With further increase in Mach number, the shock wave becomes stronger and its effect on the unsteady pressure distribution along the upper surface becomes more pronounced.

The mean steady and unsteady pressure distributions in the two examples given above show that at high-subsonic and transonic speeds the unsteady pressure distributions are no longer anti-symmetrical, as a consequence of the differences in steady flow field. This implies that in the calculation of unsteady pressure distributions it is not possible anymore to use the anti-symmetry of the problem with respect to the chord.

An interesting point, which may be of importance when calculation methods are developed, is that for practical applications the interactions between the steady and unsteady flow fields at the upper surface and at the lower surface take place independently of one another. This is illustrated in figure 8.18, which shows a comparison of the measured result for a mean flap angle of 3 degrees with results for zero mean flap angle at a lower and at a higher Mach number. For 3 degrees of mean flap angle, both the mean steady and the unsteady pressure distribution at the upper surface are almost the same as those obtained for zero mean flap angle at the higher Mach number, whereas the mean steady and unsteady pressure distribution at the lower surface are very similar to those obtained for zero flap angle at the lower Mach number. Evidently, the unsteady pressure distributions at the upper and the lower surface are determined mainly by their respective steady flow field, independent of the steady flow field at the other surface.

8.4.2 Unsteady aerodynamic coefficients

From the preceding discussion on the effect of incidence and mean flap angle on the unsteady pressure distributions, it may be expected that the overall coefficients will be sensitive to these parameters also. This is shown in figures 8.19 - 8.21, which give the unsteady aerodynamic coefficients for a frequency of 120 Hz and various values of the incidence and the mean flap angle. Up to $M_\infty = 0.75$, the effect of incidence or flap angle is negligible. Deviations occur, in particular in the normal force and moment about the quarter-chord point, as soon as the flow becomes transonic. It appears that, due to a non-zero mean incidence or mean flap angle, the transonic effects, like the sharp decrease in magnitude in both the normal-force coefficient (Fig. 8.19) and the moment coefficient (Fig. 8.20), shift to a lower value of the free-stream Mach number.

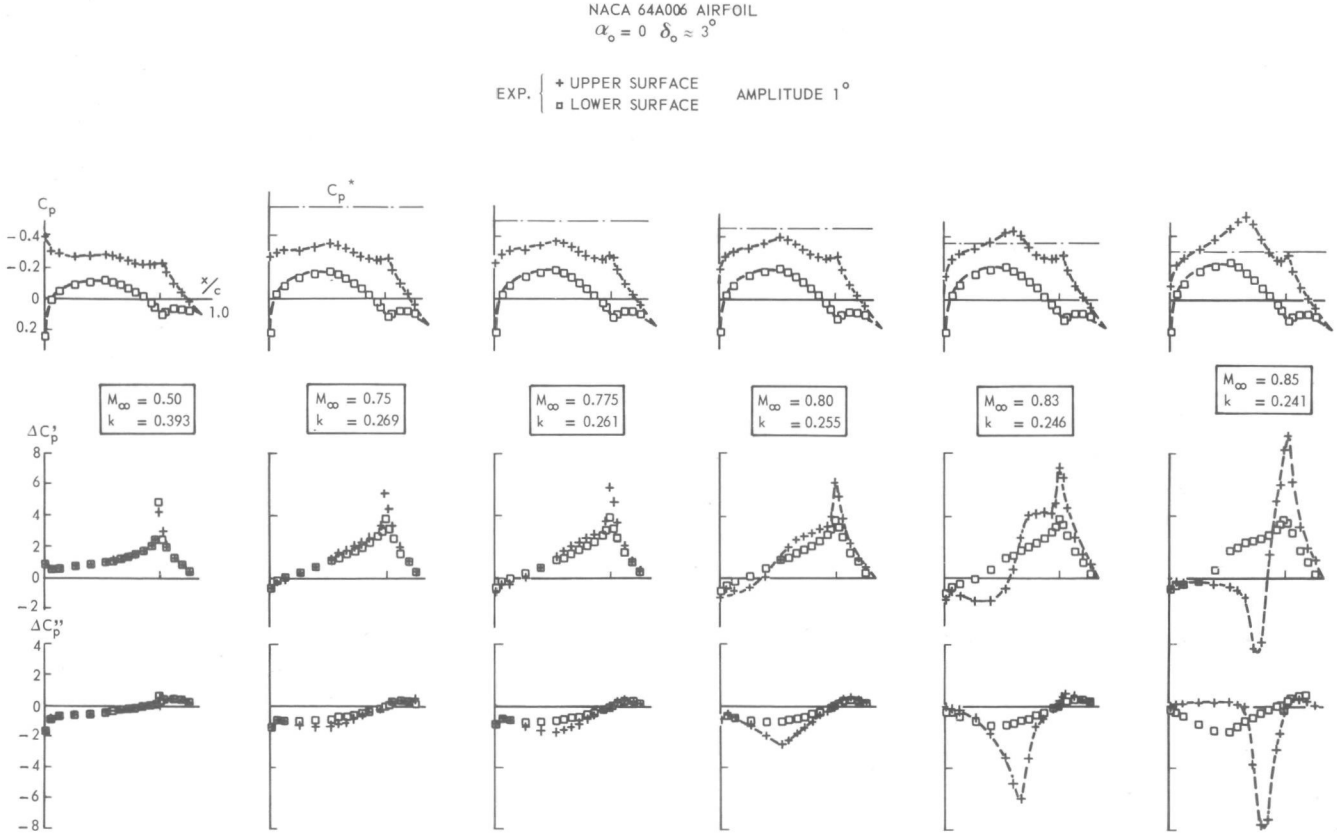

Fig. 8.16 Mean steady and unsteady pressure distributions for zero incidence and a mean flap angle of 3 degrees (f = 120 Hz).

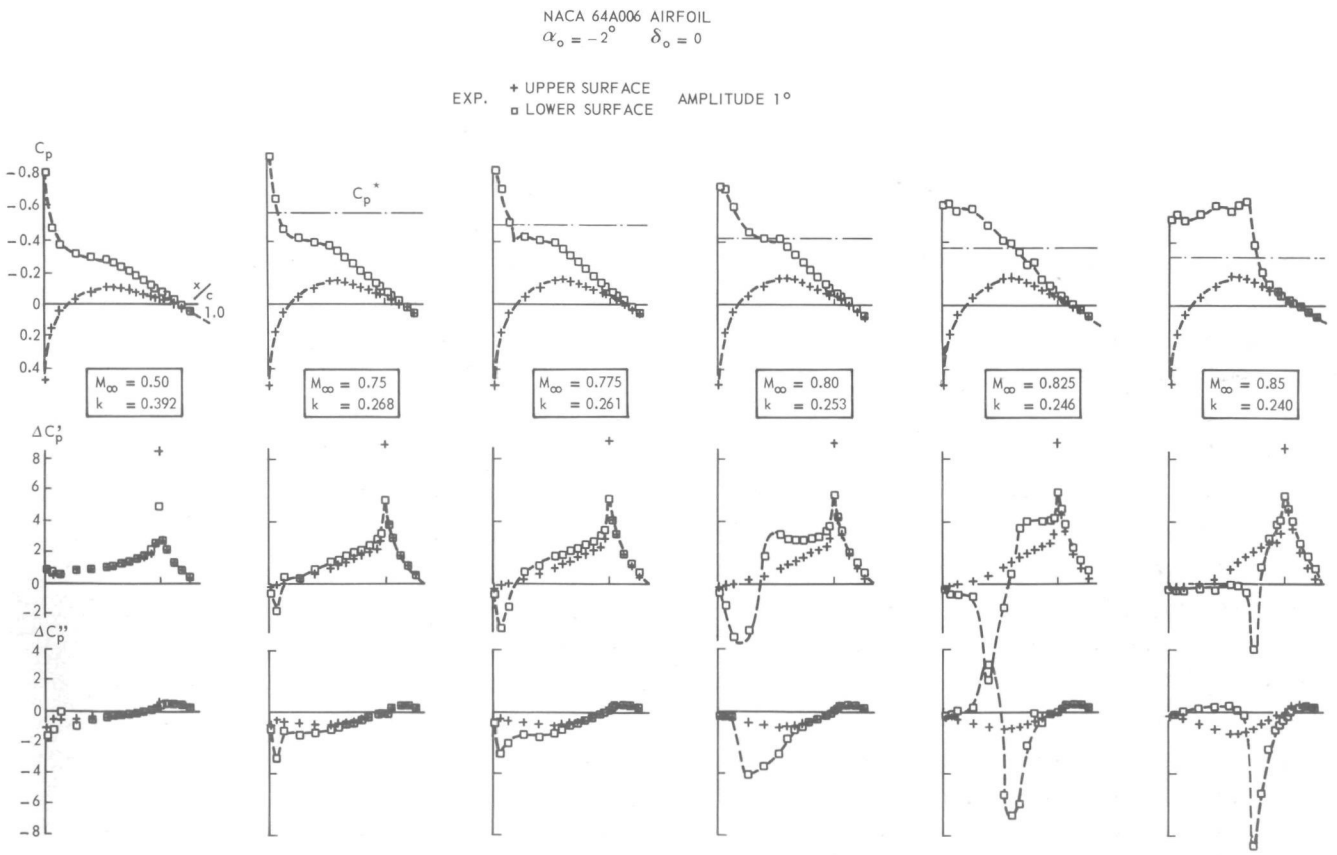

Fig. 8.17 Mean steady and unsteady pressure distributions for an incidence of minus 2 degrees and zero mean flap angle (f = 120 Hz).

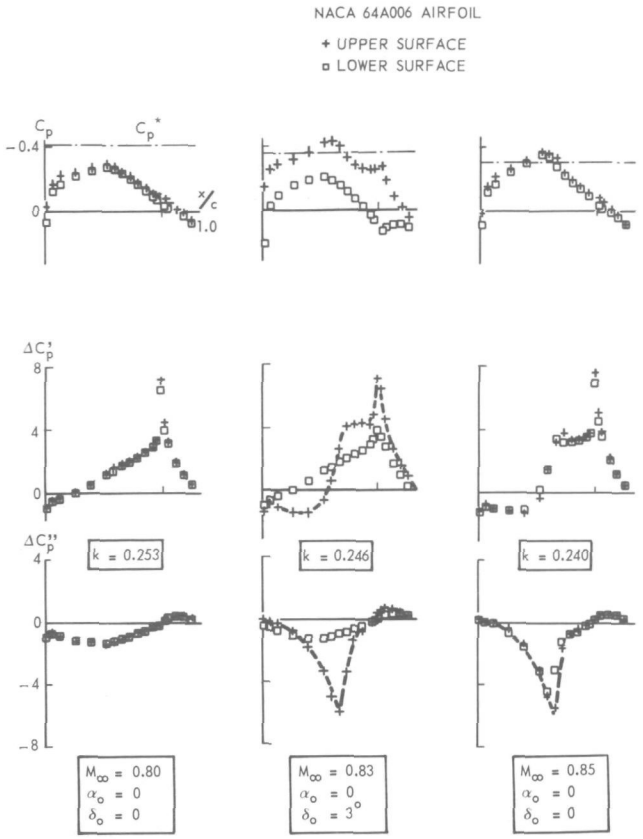

Fig. 8.18 Mean steady and unsteady pressure distributions showing the influence of mean flap angle and Mach number (f = 120 Hz).

The hinge moment is less sensitive to changes in incidence and flap angle, at least as long as the flow remains attached (Fig. 8.21). This is not surprising, since the Mach number at which the flap becomes supercritical is much higher than the Mach number at which shock waves occur on the main wing.

8.5 THE INFLUENCE OF FREQUENCY

8.5.1 Unsteady pressure distributions

As discussed in section 2.1 (see figure 2.1), the reduced frequency $k = \omega\ell/U_\infty$ is an important parameter, because it is a measure for the unsteadiness of the flow. The effect of this parameter on the unsteady pressure distributions of the airfoil with oscillating flap is shown in figures 8.22 - 8.24 for various Mach numbers. At low speed (Fig. 8.22), the measured pressure distributions develop with frequency in the same way as predicted by thin-airfoil theory, and in general a good agreement exists between theory and experiment, which improves slightly with frequency.

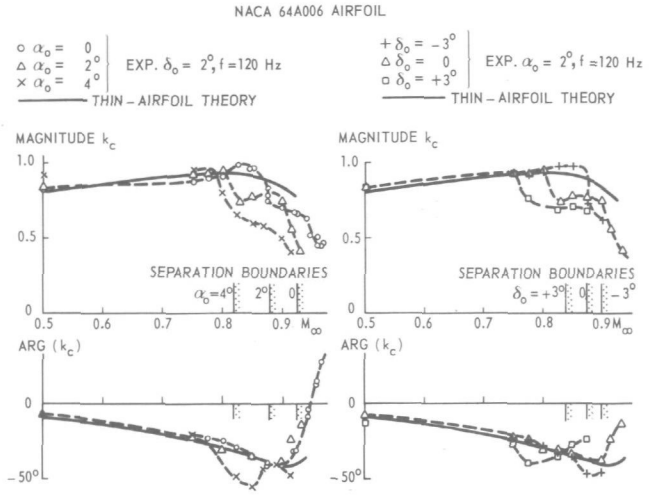

Fig. 8.19 Effect of incidence and mean flap angle on the normal-force coefficient.

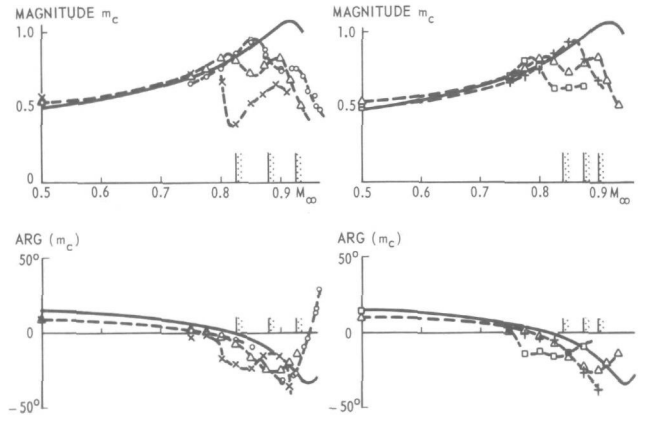

Fig. 8.20 Effect of incidence and mean flap angle on the moment coefficient about quarter chord.

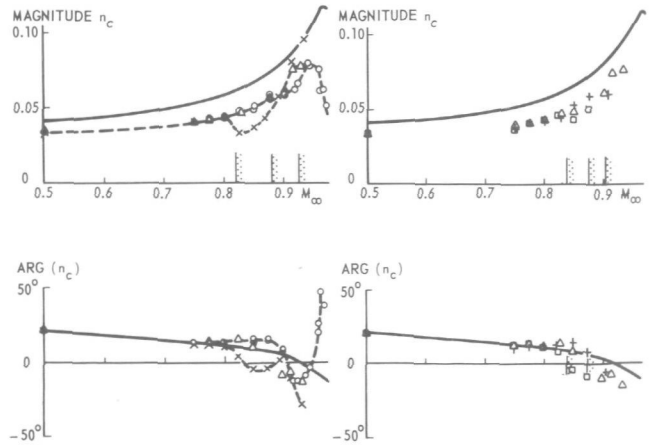

Fig. 8.21 Effect of incidence and mean flap angle on the hinge-moment coefficient.

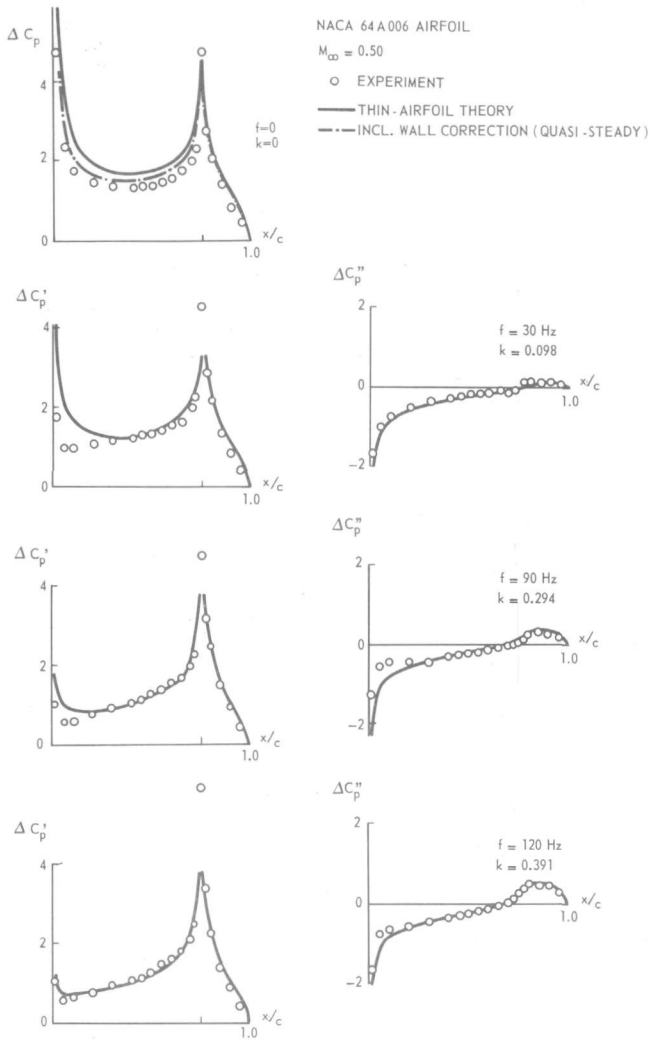

Fig. 8.22 Development of unsteady pressure distributions with frequency at low speed.

As shown in figure 8.22, a substantial part of the differences between theory and experiment for the limiting case of zero frequency can be attributed to interference of the tunnel walls. For closed tunnel walls, De Jager (Ref. 102) showed that for unsteady flow the interference effects are larger than for quasi-steady flow with a maximum for reduced frequencies between 0.1 and 0.3. For higher frequencies, the interference effect on the unsteady airloads diminishes rapidly and becomes negligible. At present it is not known whether a similar effect may be expected in a wind tunnel with slotted roof and bottom as applied in the present investigation, since an adequate theory for this case is not yet available.

The influence of the reduced frequency on the unsteady pressure distributions in slightly supercritical flow is shown in figure 8.23, while in figure 8.24 an example with a relatively strong shock wave is presented. In both figures the contribution of the oscillating shock wave can easily be recognized. Since the phase lag of the shock motion with respect to the motion of the flap increases with frequency, the large peak induced by the shock wave in the real part becomes smaller with frequency, whereas the peak in the imaginary

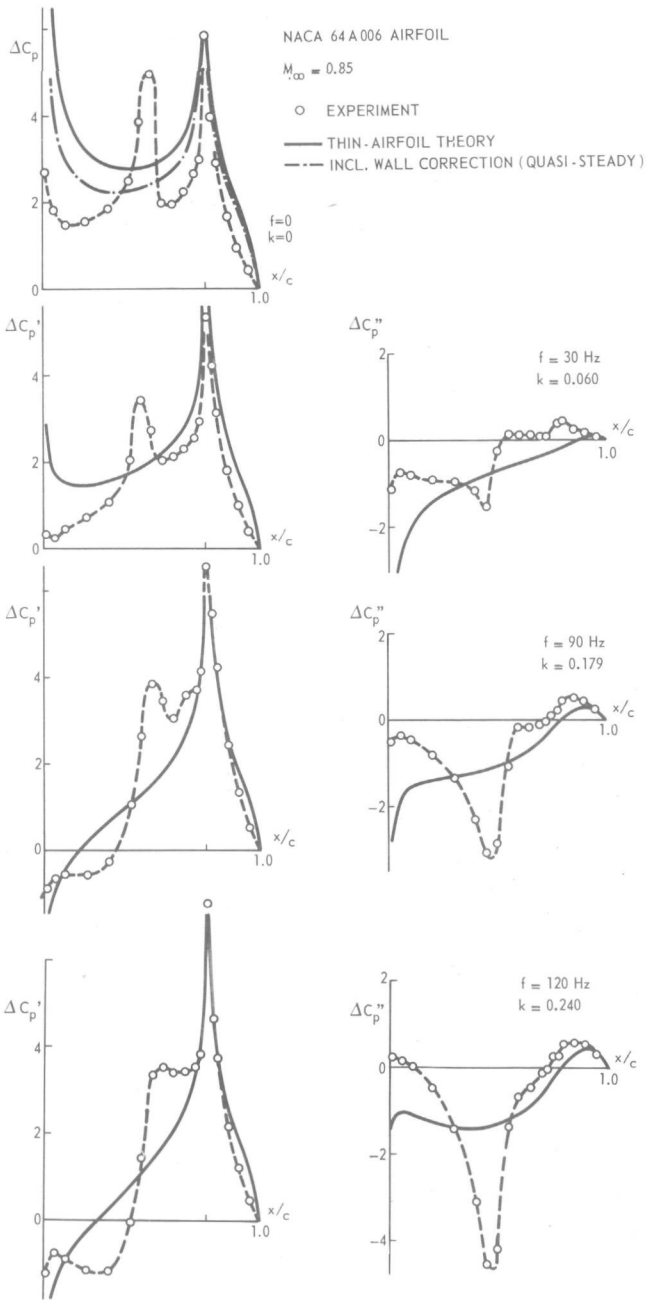

Fig. 8.23 Development of unsteady pressure distributions with frequency in slightly supercritical flow.

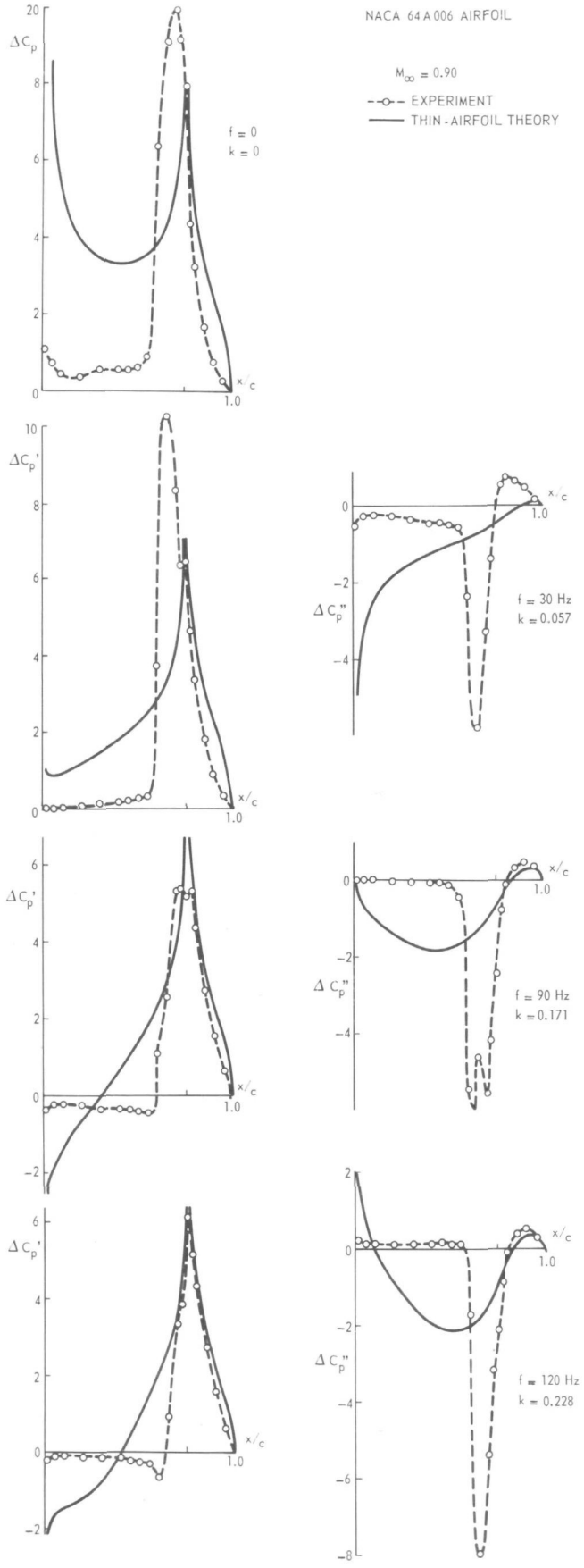

Fig. 8.24 Development of unsteady pressure distributions with frequency in transonic flow.

part increases.

When the supersonic region is sufficiently large and is terminated by a relatively strong shock wave, the pressure peak resulting from the shock motion forms a dominant contribution to the overall aerodynamic loading (Fig. 8.24). As thin-airfoil theory does not include this effect, it is evident that there exists a considerable discrepancy between the theoretical and experimental pressure distributions. On the flap, which remains subcritical, theory and experiment show about the same agreement as in the subsonic case. With respect to the contribution of the oscillating shock wave, it finally can be noted that the magnitude of the pressure distribution (Fig. 8.25) seems to indicate that the shock wave moves over a shorter trajectory when the frequency is increased. This will be confirmed by the considerations on the periodical shock wave motions, given in chapter 9.

8.5.2 Unsteady aerodynamic coefficients

In the preceding section, it was shown that at subsonic speed the agreement between the mea-

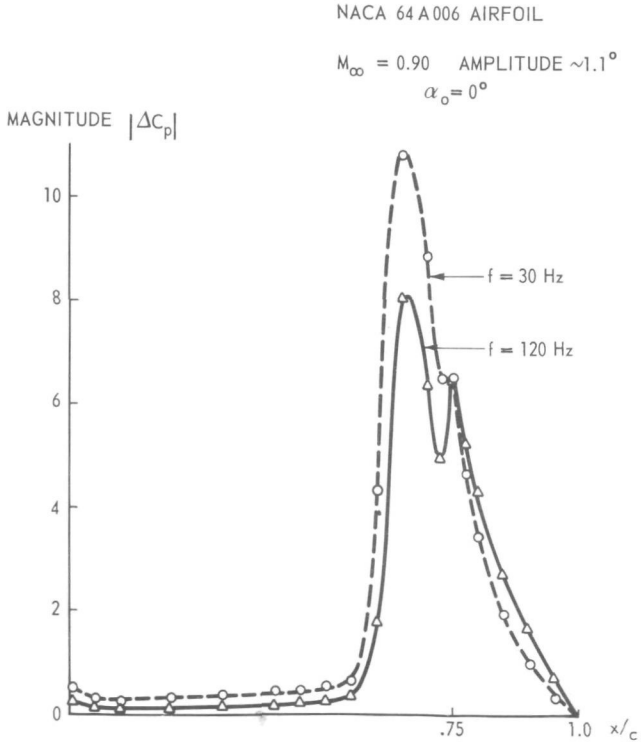

Fig. 8.25 Influence of frequency on magnitude distribution.

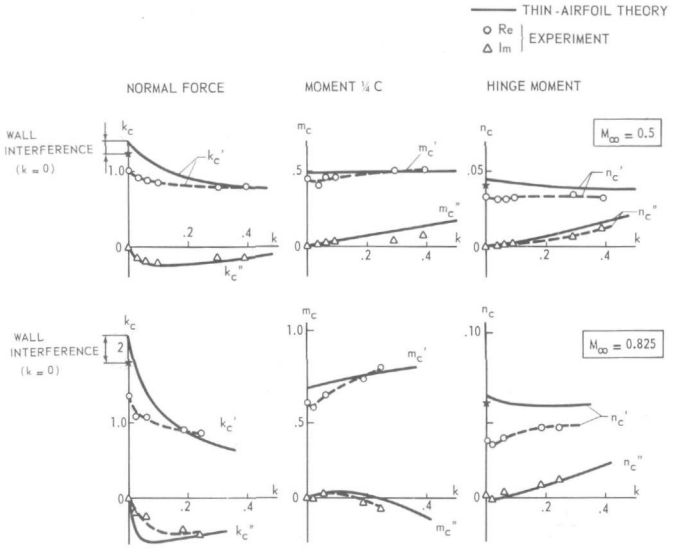

Fig. 8.26 Unsteady aerodynamic coefficients as a function of reduced frequency in subcritical flow.

sured unsteady pressure distributions and those calculated with thin-airfoil theory improves with increasing frequency. This is reflected also in the overall aerodynamic coefficients (Fig. 8.26), which all three show the same tendency.

In supercritical flow (Fig. 8.27), the measured normal-force coefficients also seem to show a better agreement with theory when the frequency increases. This happens, however, only by coincidence, as may be concluded for instance from a closer look at figure 8.24. In the theory, an increase in frequency leads at high Mach numbers to rapid changes in phase angle on the front part of the airfoil, and, as a result, the real part of the calculated pressures upstream of the hinge axis changes sign, which results in about zero net force at the higher frequencies. The real parts of the measured pressures do not produce a net force either, for a quite different reason. Here the presence of the shock wave prevents the pressure perturbations generated by the oscillating flap from reaching the front part of the airfoil. The agreement for the imaginary part of the normal force is only due to the fact that the integral over the imaginary part of the pressure peak generated by the oscillating shock wave has about the same value as the integral over the imaginary part of the calculated pressure distribution.

The fact that the nature of the calculated and the measured pressure distributions is quite different shows up in the deviations between the theoretical and the experimental moment coefficients. These deviations become larger with increasing Mach number as a consequence of the rearward shift of the mean position of the shock wave and its associated pressure peak.

Finally, the hinge moment shows a tendency to agree better with theory as the frequency is increased. This improvement, which was mentioned already in the preceding section, is indeed the result of the better agreement between the calculated and the measured pressure distribution over the chord of the flap.

When the findings with respect to the influence of frequency are summarized, it can be concluded that, at subcritical speed, a tendency

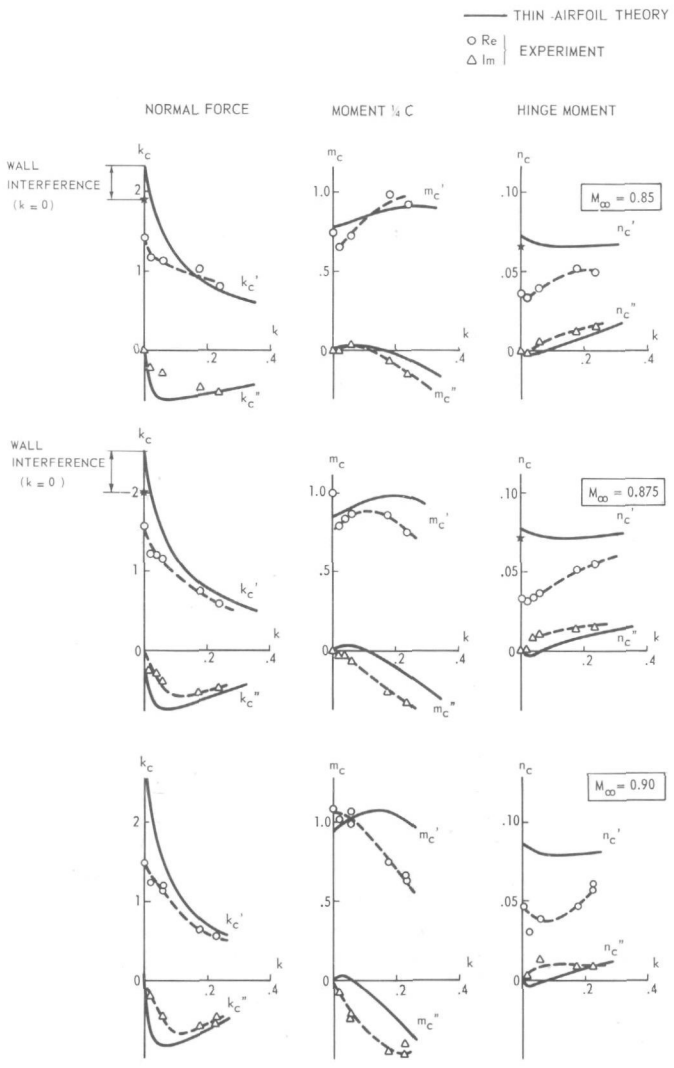

Fig. 8.27 Unsteady aerodynamic coefficients as a function of reduced frequency in transonic flow.

exists towards an improved agreement between measured and calculated data with increasing frequency. A decisive answer to the question whether this improvement can be ascribed to a decrease in tunnel-wall interference at the higher frequencies cannot be given at present.

In transonic flow, the nature of the measured unsteady pressure distributions is quite different from the theoretical predictions as a result of the presence of shock waves. At very high frequencies this may change, since then, as will be shown in the next chapter, the amplitude of the periodical shock motion and, thus, its contribution to the unsteady airloads will become very small.

9 ON THE PERIODICAL MOTION OF SHOCK WAVES

9.1 INTRODUCTORY REMARKS

In the preceding chapter, it was noted that the periodical motion of shock waves on oscillating airfoils gives rise to considerable contributions to the unsteady airloads. It is, therefore, of prime interest to understand the mechanism of unsteady shock-wave motions and to identify the governing parameters. Moreover, a good physical insight will be of help in the theoretical modelling of unsteady transonic flows.

In the literature, experimental investigations on the behaviour of shock waves on oscillating airfoils are relatively scarce, and they are directed mainly to the control-surface buzz problem, which occurs under separated flow conditions (Refs. 60, 62, 63, 103-108). For this reason it was decided to complement the pressure measurements on the airfoil with oscillating flap with optical flow studies in which the accompanying motions of the shock waves could be determined. In this chapter, some typical examples of the observed shock-wave motions are discussed. It will be shown that three different types of motion can be distinguished for a normal shock. All three can be explained very satisfactorily by the unsteady shock relations derived for a simplified model of the flow field.

9.2 SHOCK STRENGTH AND SHOCK POSITION IN STEADY FLOW

The steady pressure distributions of interest for the present discussions and the corresponding shock-wave patterns are shown in figures 9.1 and 9.2, respectively. The flow

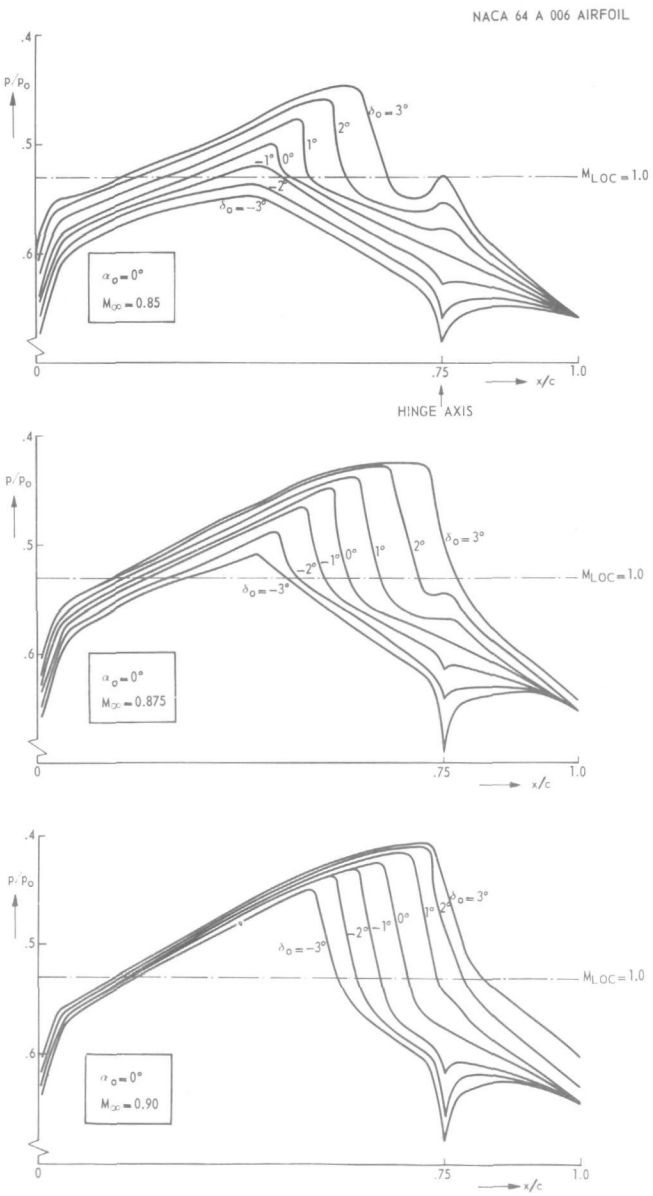

Fig. 9.1 Steady pressure distributions on the upper surface for zero incidence and various flap deflections.

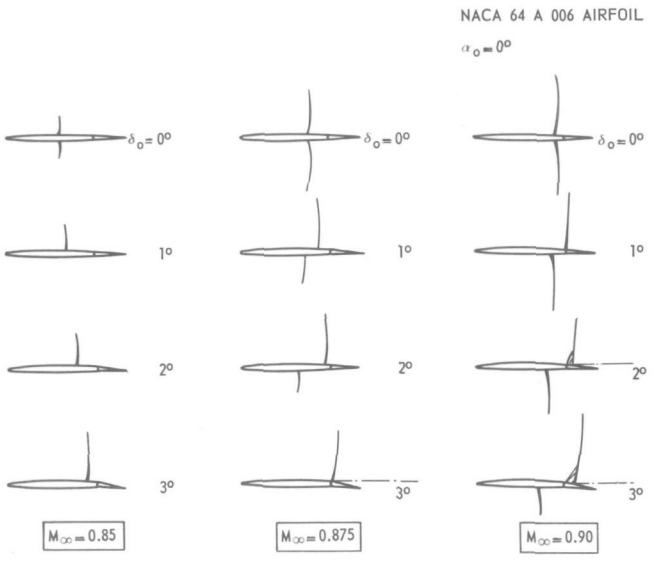

Fig. 9.2 *Steady shock patterns for zero incidence and various flap deflections.*

pattern on the airfoil shows a development with flap angle and Mach number, as is usual for conventional airfoils. A steady shock appears as soon as the maximum local Mach number reaches a value of about 1.05, and shock-induced separation occurs when just ahead of the shock wave the local Mach number is increased up to about 1.3.

From figure 9.1 it follows that, at M_∞ = 0.85 and zero flap angle, weak shock waves are present on both the upper and the lower surface of the airfoil at about 45 per cent of the chord. When the flap is deflected downward, the speed along the upper surface is increased and the shock is displaced downstream while both the shock strength and the size of the supersonic region are increased. At the same time, the flow speed along the lower surface is reduced and the development of the flow pattern is reversed: the size of the supersonic region decreases and the shock wave becomes weaker. Beyond a certain flap deflection, the lower surface becomes completely subcritical. A development similar to the one described above can be observed also at M_∞ = 0.875 and M_∞ = 0.90, but here larger flap deflections are required to suppress the shock wave at the lower surface.

In an inviscid flow, the strength of a normal shock wave, which is the pressure ratio across the shock, is determined by the Rankine-Hugoniot relation:

$$p_2/p_1 = 1 + \frac{2\gamma}{\gamma+1}\,(M_1^2 - 1)\,, \qquad (9.1a)$$

where the indices 1 and 2 refer to the positions just ahead and just behind the shock wave, respectively. As a consequence, however, of the presence of the boundary layer, the shock strengths measured on airfoils are consistently less than those predicted by this relation. This is demonstrated in figure 9.3, in which the shock strengths determined from the present steady pressure measurements are compared with the shock strength according to (9.1a) and with the shock strengths determined from other investigations (Ref. 14). The measured shock strengths follow the trend of the theoretical curve reasonably well until M_1 is about 1.3. Beyond this Mach number, the experimental shock strengths tend to decrease, which is caused by the afore-mentioned shock-induced

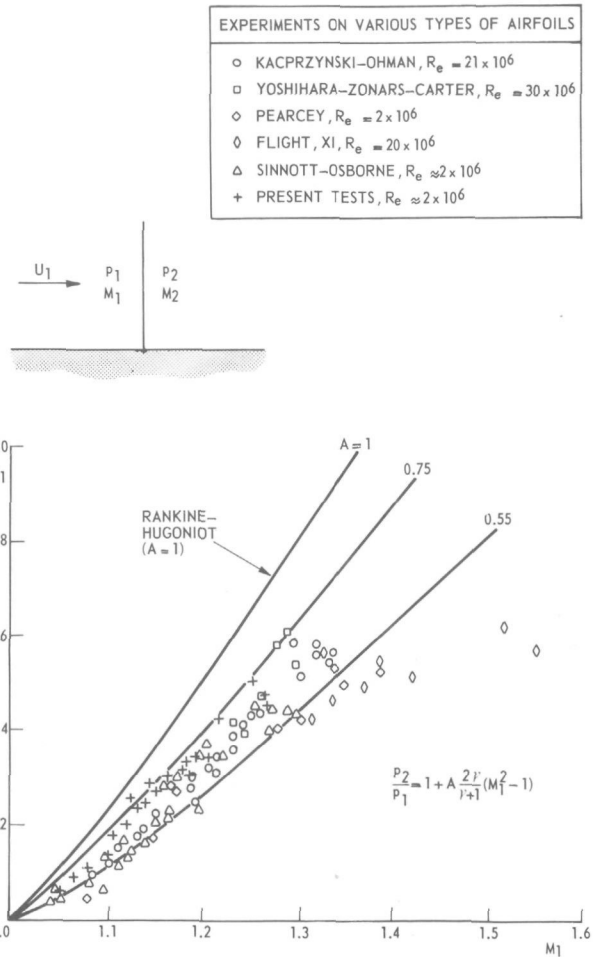

Fig. 9.3 **Pressure ratio across the shock wave (partly reproduced from Ref. 14).**

separation. As shown in figure 9.3, a reasonable approximation of the experimental shock strengths ($M_1 < 1.3$) is obtained by the slightly modified normal shock relation:

$$p_2/p_1 = 1 + A \frac{2\gamma}{\gamma+1} (M_1^2 - 1) , \qquad (9.1b)$$

where the constant A has a value between 0.55 and 0.75, instead of 1 as in the original expression (9.1a).

An important result of the steady tests is given in figure 9.4, which contains the steady shock position and the shock strength as a function of flap angle. From these results, the quasi-steady shock-wave motions can be determined, which serve as a basis for the interpretation of the results of the dynamic tests.

As long as the flow remains attached, there exists an almost linear relationship between shock position and flap angle (Fig. 9.4a), which implies that an infinitely slow sinusoidal flap displacement will result in an almost pure sinusoidal excursion of the shock wave. Figure 9.4b illustrates that the change in shock position is accompanied by a change in shock strength: the strength increases when the shock is displaced downstream, and decreases by an upstream displacement of the shock wave. In the case that the pressure ratio p_2/p_1 across the shock wave is reduced until about 1.0, the shock wave vanishes. In the examples shown, this happens on the upper surface at $M_\infty = 0.85$ for a flap angle of about -0.5 degrees, and at $M_\infty = 0.875$ for a flap angle of about -3 degrees (see also figure 9.2).

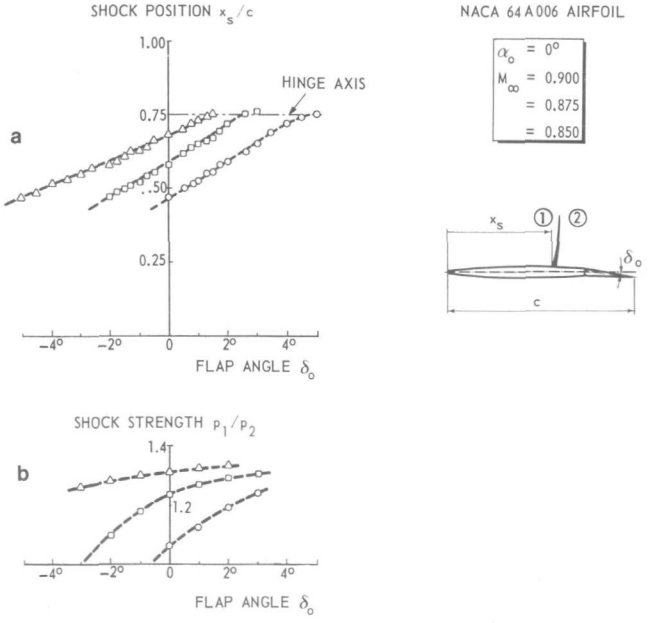

Fig. 9.4 Shock position and shock strength on the upper surface as function of flap angle.

9.3 TYPES OF SHOCK-WAVE MOTION OBSERVED IN UNSTEADY FLOW

As described in section 6.4, the time histories of the shock-wave motions were recorded in two independent ways, namely by means of shadowgraph pictures and by means of high-speed films. An analysis of the time histories for the tests at 120 Hz and an amplitude of 1 degree reveals the existence of three different types of shock-wave motion. These occur for zero incidence of the main surface and zero mean flap angle at values of M_∞ of 0.90, 0.875, and 0.85, respectively. As shown in figures 9.5, and 9.6, the following types can be distinguished:

type A: sinusoidal shock-wave motion

For the highest Mach number ($M_\infty = 0.90$), an almost sinusoidal motion is observed (Figs. 9.5a and 9.6a), which resembles more or less the shock-wave motion described by Lambourne (Ref. 105) and Nakamura (Ref. 62). As shown in figure 9.5a, the shock-wave motion at 120 Hz has a phase shift with respect to the sinusoidal flap motion and the quasi-steady shock-wave motion. Moreover, the changes in thickness and size of the shock waves as observed in the original high-speed film also indicate a phase shift between shock strength and shock position, in such a way that the shock wave reaches its maximum strength during its upstream motion and its minimum strength during the downstream motion. These phase shifts between the shock-wave motion and flap motion on the one hand and between shock-wave motion and shock strength on the other hand are absent in the quasi-steady case, and they thus have to be attributed to the dynamic character of the phenomenon (see section 9.4.2).

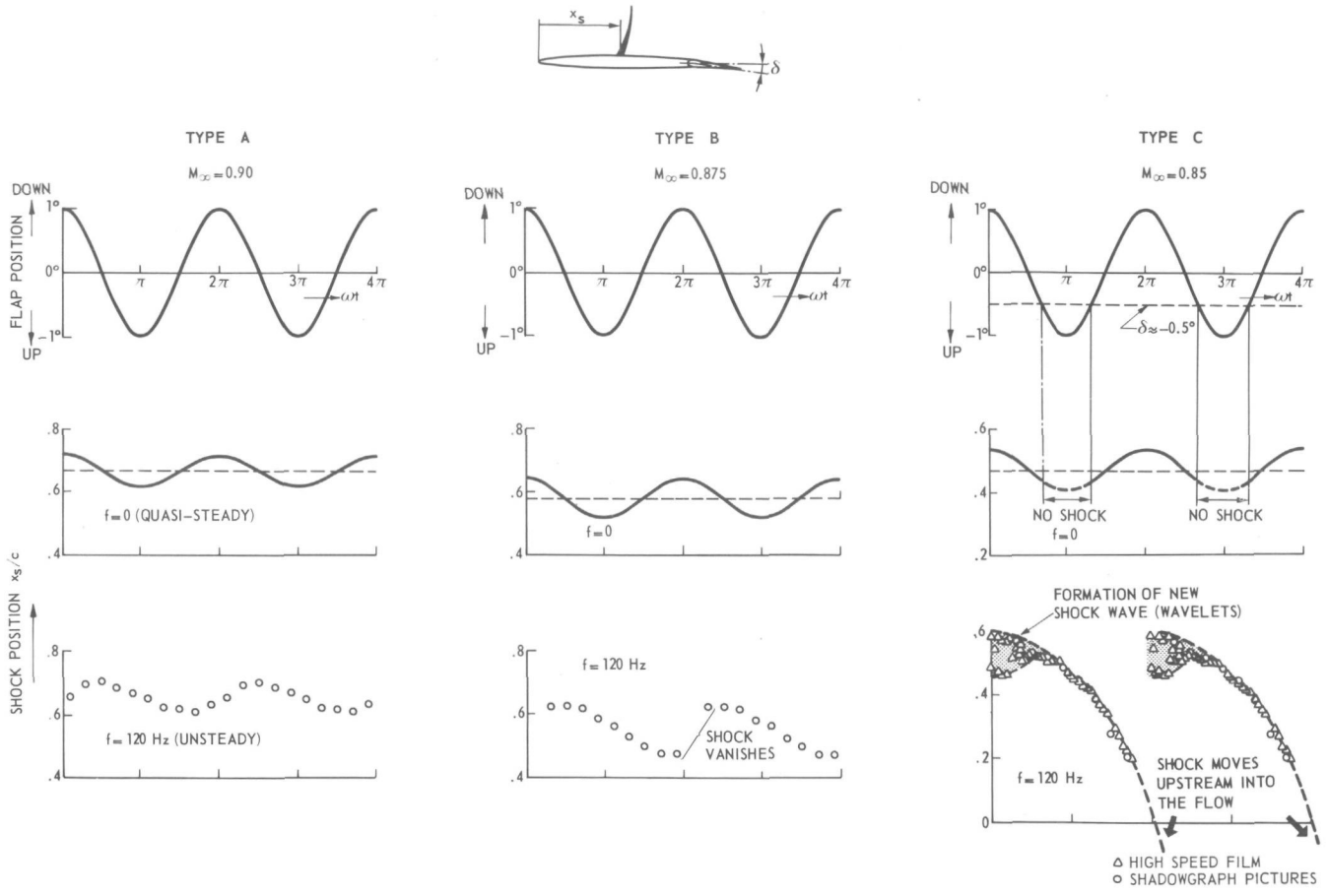

Fig. 9.5 Observed types of periodical shock-wave motion on the upper surface.

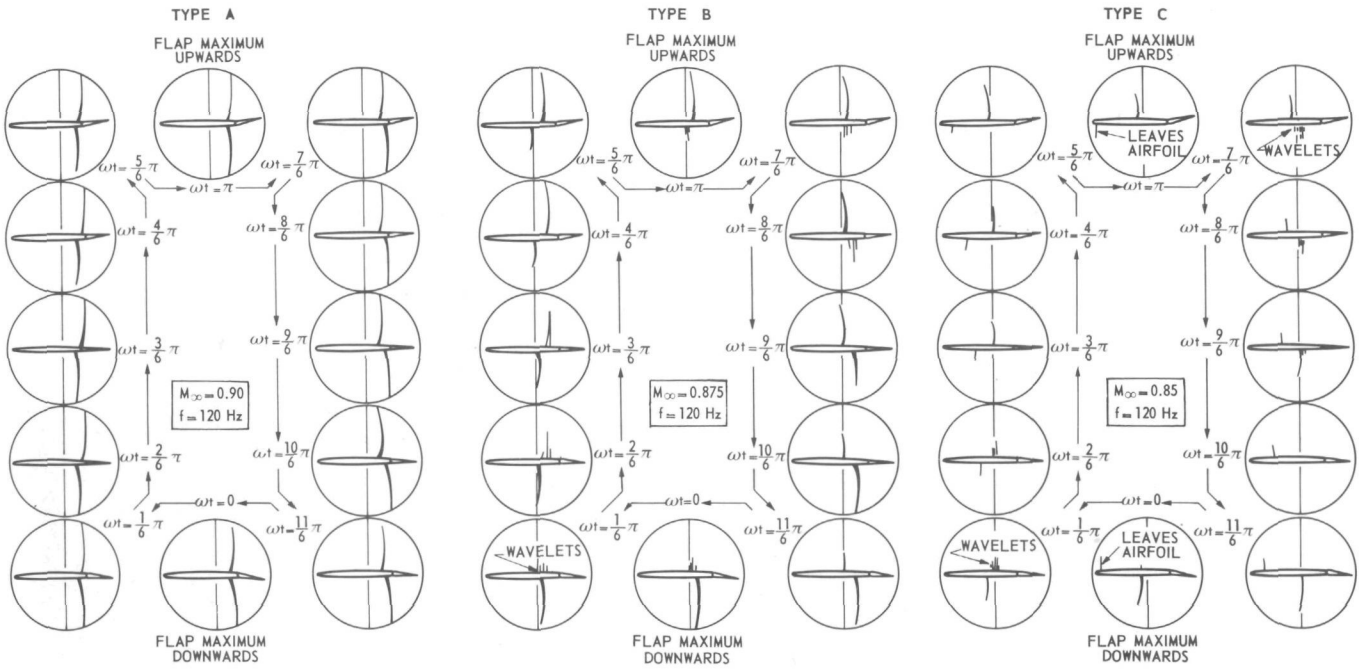

Fig. 9.6 Time histories of the periodical shock-wave motions.

type B: interrupted shock-wave motion

The second type of periodical shock-wave motion, observed at a somewhat lower free-stream Mach number ($M_\infty \approx 0.875$), is characterized by the disappearance of the shock wave in the dynamic case during a part of its backward motion (Fig. 9.5b). In the same way as for type A, the shock wave reaches its maximum strength during the upstream motion, as can be noticed clearly from the size of the shock waves in the successive pictures of figure 9.6b.

type C: upstream-propagated shock waves

At $M_\infty = 0.85$, where the flow is just supercritical, a third type of periodical shock-wave motion is observed (Figs. 9.5c and 9.6c), which differs completely from the preceding types. At 120 Hz a shock wave is formed on the upper surface of the airfoil at the moment the flap has just passed its maximum deflection downwards. This shock wave moves upstream while increasing in strength. Then the shock wave weakens again, but continues its upstream motion, leaves the airfoil from the leading edge, and propagates upstream into the oncoming flow as a (weak) free shock wave. This phenomenon is repeated periodically and alternates between the upper and lower surface (Fig. 9.6c). It is noted here that in the quasi-steady case the shock wave vanishes during a part of the cycle (Fig. 9.5c, f = 0). As will be shown later, this is essential for the occurrence of a type-C unsteady shock-wave motion.

9.4 INTRODUCTION OF AN ANALYTICAL MODEL

9.4.1 Relation between shock position and shock strength

To understand the physics behind the observed types of shock-wave motions, it is sufficient to consider the instantaneous shock strength of a shock wave which oscillates sinusoidally with prescribed amplitude and frequency in a given (steady) flow field. For simplicity, the following flow model is introduced (Fig. 9.7c).

(1) The flow with a normal shock wave is considered to be one-dimensional, i.e. pressure gradients in a direction normal to the flow are neglected.

(2) Upstream of the normal shock wave, a known pressure distribution with gradients in streamwise direction exists, which does not change when the shock wave is displaced over a small distance. In other words, if the shock wave is displaced over a distance Δx, the pressure upstream of the shock wave is assumed to follow a known p_1-locus.

The first assumption is reasonable when the flow around thin airfoils is described, but may be less satisfactory for thick airfoils, where in general large pressure gradients normal to the surface occur.

The second assumption is no real restriction in the quasi-steady case, because then the p_1-locus can be obtained from the steady pressure distributions (Figs. 9.7a,b). For the oscillatory case, however, it is necessary to assume that the pressure just in front of the shock wave changes in the same way as in quasi-steady flow. Other-

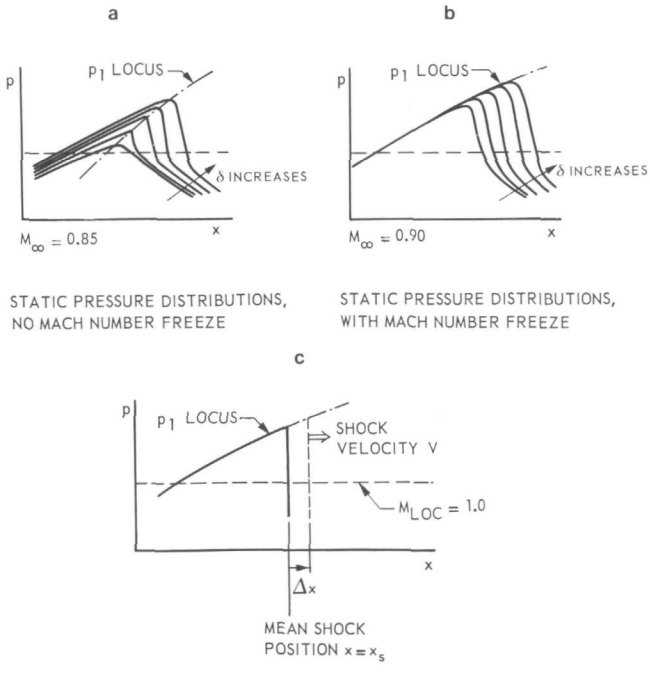

Fig. 9.7 Schematization for analytical flow model.

wise, also the time-dependent relations between flap position and the pressure perturbations just up- and downstream of the shock wave have to be included. This means that for unsteady flow this simple flow model is fully justified only in the case of a so-called "Mach number freeze" (Fig. 9.7b): the phenomenon that the pressure distribution upstream of the shock wave does not change any longer with Mach number or flap angle.

In the simplified flow field, the instantaneous shock strength $\bar{p}_2/\bar{p}_1$ across a shock wave which oscillates sinusoidally with a small amplitude x_o and frequency ω can be expressed as (see Appendix C):

$$\frac{\bar{p}_2}{\bar{p}_1} = \left\{\frac{p_2}{p_1}\right\}_{x=x_s} + \frac{4\gamma M_1}{\gamma+1}\left\{\frac{\partial M_1}{\partial x} - \frac{i\omega}{a_1}\right\} x_o\, e^{i\omega t}. \quad (9.2)$$

The quantities M_1, $\partial M_1/\partial x$ and a_1 refer to the conditions just upstream of the shock wave in its steady mean position ($x = x_s$). The first term of the right-hand side of equation (9.2) denotes the strength of the shock in its steady mean position and can be calculated with equation (9.1a). The second part denotes the change in shock strength due to the oscillatory motion $x_o e^{i\omega t}$. In this part, two effects can be distinguished. The term containing $\partial M_1/\partial x$ accounts for the change in shock strength caused by the change in shock position (displacement effect), an effect which exists already in the quasi-steady case ($\omega = 0$). The term with $i\omega$ represents the change in shock strength due to the velocity of the shock wave relative to the airfoil (dynamic effect).

The advantage of the present model over the unsteady shock-wave models presented earlier by Coupry and Piazolli (Ref. 109), Eckhaus (Ref. 110), and Landahl (Ref. 24) is that the Mach number upstream of the shock wave is not constant, which makes it valid for low frequencies as well as for the quasi-steady flow case. Moreover, the presence of a streamwise gradient in Mach number is essential to explain all three types of shock-wave motions, as will be demonstrated in the next section.

9.4.2 Application of the analytical model

For the present airfoil, relation (9.2) was used to calculate the variation in shock strength that corresponds to an assumed sinusoidal motion of the shock wave. The amplitudes of the shock-wave motion were taken to be about equal to the amplitudes observed during the wind-tunnel tests, and the quantities $p_1(x_s)$, M_1 and $\partial M_1/\partial x$ were determined from the measured steady pressure distributions (Fig. 9.1). To obtain agreement with the steady tests, the shock strength in the mean position was calculated with equation (9.1b), in which a factor A of 0.7 is used. To obtain agreement for the quasi-steady results, the same factor has also been used for the displacement effect. Since any better knowledge was lacking, no reduction was applied to the term accounting for the dynamic effects.

The result for $M_\infty = 0.90$ is given in figure 9.8a. In the quasi-steady case ($f = 0$), a sinusoidal shock-wave motion generates a sinusoidal variation in shock strength, which is in phase with the shock-wave displacement. In the unsteady case ($f = 120$ Hz), the dynamic effect gives rise to two important changes: a phase shift and an amplification of the variation in shock strength. The maximum shock strength is reached about 64 degrees after the shock wave has passed its most backward position, whereas the minimum strength is reached during its downstream motion. For the given amplitude of the shock-wave motion, the shock strength remains always larger than 1.0, which means that a shock wave is present during the complete cycle. These results are in agreement with the experimental observations for the shock-wave motion of type A, as discussed in section 9.3.

The calculated results for $M_\infty = 0.875$ are plotted in figure 9.8b. Again a quasi-steady shock-wave motion results in an in-phase variation in shock strength. For $f = 120$ Hz, however, the dynamic effect increases the variation in shock strength in such a way that during a part of the cycle ($1.17\,\pi < \omega t < 1.43\,\pi$) the pressure ratio $\bar{p}_2/\bar{p}_1$ is lower than 1.0. This means that the shock

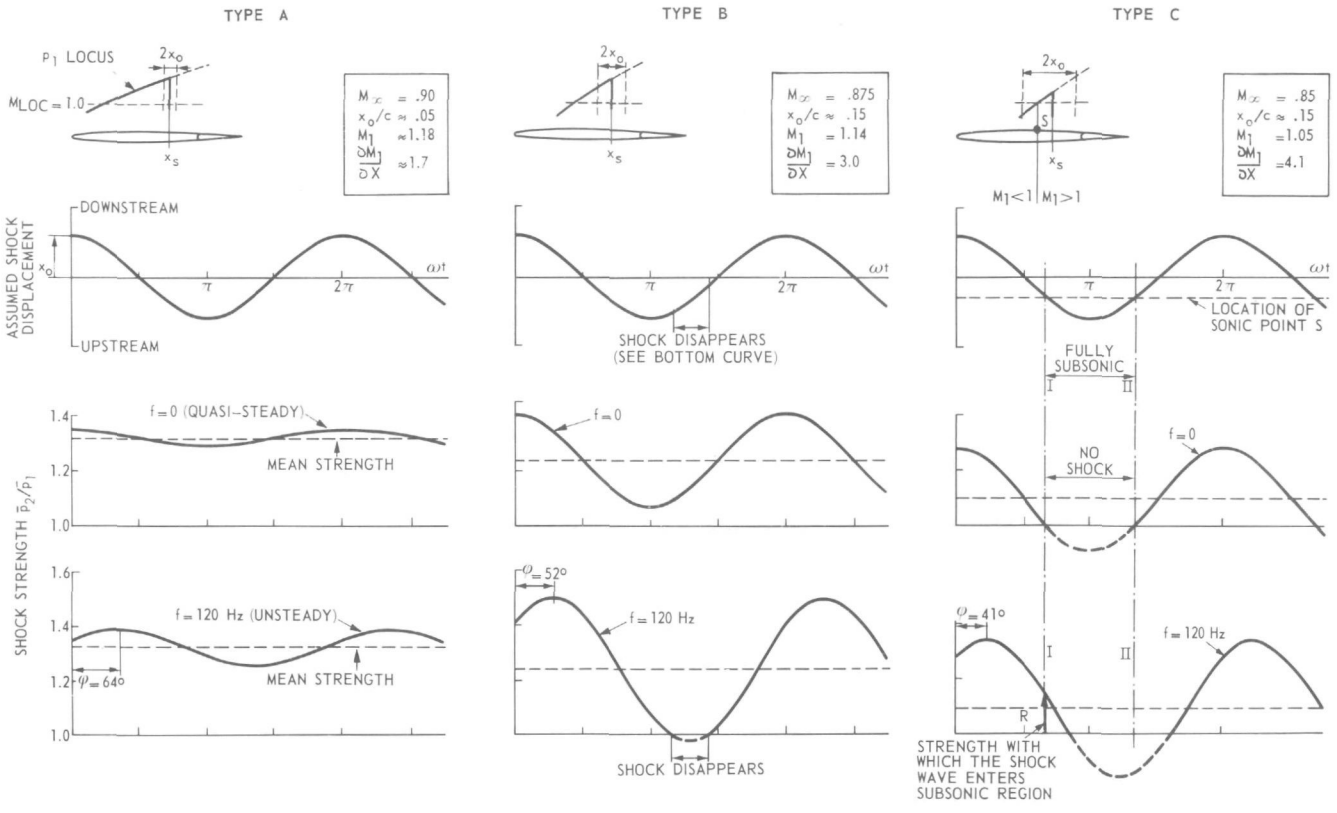

Fig. 9.8 Explanation of different types of shock-wave motion.

wave vanishes during that part of the cycle. This result is typical for type B, and it is in qualitative agreement with the experiments.

Finally, the shock-wave motion of type C can be understood with the help of the calculated results for $M_\infty = 0.85$, presented in figure 9.8c. The amplitude of the assumed shock-wave motion in the given flow field is so large that, during a part of the cycle ($0.67\,\pi < \omega t < 1.33\,\pi$), the "shock" is located upstream of the sonic point S. For quasi-steady motion, the shock strength $\bar{p}_2/\bar{p}_1$ is always smaller than 1.0 during the part of the cycle mentioned, or, in other words, no shock wave is present then. This is in accordance with the experiments.

The periodical shock strength as calculated for 120 Hz is given in the bottom curve of figure 9.8c. The phase shift and amplification resulting from the dynamic effect lead to a drastic change in the situation. Now the upstream-moving shock wave enters the subsonic region upstream of the sonic point S with a certain residual strength R. This means that a similar situation is created as for a shock wave generated by a local explosion: the shock wave entering the subsonic region continues its upstream motion as a free shock wave with a speed of propagation nearly equal to the difference between the local velocity of sound and the local flow velocity. From figure 9.8c it follows also that a new shock wave is formed on the airfoil, when the shock wave is on its way to its maximum downstream position. So the calculated results confirm the results of the present tests also for the type-C shock-wave motion.

When the results are summarized, it can be stated that the three examples discussed above demonstrate the adequacy of the analytical model. A closer look at equation (9.2) also reveals that it is not strictly necessary that these three types will occur at different Mach numbers as happened in these cases. In principle, all three types may occur at the same free-stream Mach number, but then for different amplitudes or frequencies.

9.5 ADDITIONAL REMARKS

9.5.1 Some properties of the unsteady shock relations

For the simplified flow model of figure 9.7, the relation between the sinusoidal pressure perturbation Δp_2 behind the shock wave and the shock-wave motion, as derived in Appendix C, reads:

$$\frac{\Delta p_2}{p_1(x_s)} \simeq \frac{2\gamma M_1}{\gamma+1}\left[\left\{\frac{3+\gamma-2M_1^2}{2+(\gamma-1)M_1^2}\right\}\frac{\partial M_1}{\partial x}-\frac{2i\omega}{a_1}\right]x_o e^{i\omega t}. \qquad (9.3)$$

This relation says that an oscillatory pressure perturbation behind the shock wave creates an oscillatory motion of the shock wave with such an amplitude that the Rankine-Hugoniot relations are satisfied instantaneously. From (9.3) it follows that in general a phase shift different from 90 degrees may occur between shock-wave displacement and pressure perturbation. This phase shift is determined by the frequency, the Mach number, and the gradient in Mach number just ahead of the shock wave.

The phase shift becomes exactly 90 degrees when $\partial M_1/\partial x = 0$, for which case the following expression applies:

$$\frac{\Delta p_2}{p_1(x_s)} \simeq -i\,\frac{4\gamma M_1\omega}{(\gamma+1)a_1}\,x_o\,e^{i\omega t}. \qquad (9.4)$$

This expression corresponds with formulae given by Eckhaus (Ref. 110) and Lambourne (Ref. 105), derived for a flow model with a constant Mach number ahead of the shock wave. The expression was given also by Fiszdon (Ref. 111). A higher-order approximation of the relation between shock-wave motion and pressure perturbation was produced by Dvořák (Ref. 112). A weak point of these models is that they fail for low frequency and in the quasi-steady case ($\omega = 0$), since then, as follows from (9.4), infinitely large shock amplitudes are required to compensate for any pressure perturbation Δp_2.

As far as the behaviour at high frequencies is concerned, it can be concluded from both (9.3) and (9.4) that, for a given pressure perturbation Δp_2, the amplitude of the shock-wave motion decreases with increasing frequency. In other words, high-frequency pressure perturbations cause smaller amplitudes of the resulting shock-wave motion than low-frequency perturbations do

A particular property of the quasi-steady case is revealed by the quasi-steady part of equation (9.3):

$$\frac{\Delta p_2}{p_1(x_s)} \simeq \frac{2\gamma M_1}{\gamma+1}\left[\frac{3+\gamma-2M_1^2}{2+(\gamma-1)M_1^2}\right]\frac{\partial M_1}{\partial x}x_o. \qquad (9.5)$$

The right-hand side of this equation becomes zero for $M_1 = \sqrt{\frac{1}{2}(\gamma+3)} = 1.483$, $(\partial M_1/\partial x \neq 0)$. Above this Mach number, the expression changes sign. This behaviour results from two counter-acting effects, which occur when the Mach number ahead of the shock wave is increased: the static pressure ahead of the shock wave decreases, but at the same time the pressure ratio across the shock wave increases. Evidently, above $M_1 = 1.483$ the first effect predominates, which means that for a given initial stagnation pressure the maximum absolute static pressure behind a normal shock wave is obtained at $M_1 = 1.483$. Laitone (Refs. 113, 114) also observed this effect and argued that this Mach number corresponds to the limit velocity that can exist on a two-dimensional airfoil just ahead of a normal shock terminating a local supersonic region. This seems to be confirmed in practice, since, to the author's knowledge, values of the local Mach number higher than about 1.5 just upstream of a normal shock wave never have been observed in experiments on two-dimensional airfoils.

Actually, equation (9.5), with the linearization in its derivation, is not valid for Mach numbers close to 1.483, but the result seems to indicate that, in the case that the Mach number just upstream of the shock wave approaches this value, quasi-steady pressure perturbations behind the shock wave will result in relatively large shock-wave displacements.

9.5.2 Possible use of the shock-wave model

The unsteady shock-wave model presented here was introduced primarily to understand the physics behind the different types of periodical shock-wave motion. For this purpose, the model was kept as simple as possible. For further use, one may think of application in unsteady transonic-flow theories, in which the unsteady shock relations are introduced explicitly ("shock-fitting"). As such, the present model is an improvement if compared with the shock models (constant Mach number ahead of the shock) of references 24, 109, and 110. The model has, however, the disadvantage that in the oscillatory case the pressure ahead of the shock wave is assumed to vary in the same way as in the quasi-steady case. When the model is used in a "shock-fitting" procedure, it is advisable to refine the model in this respect and to include the time-dependent variation in pressure (or Mach number) upstream of the shock wave. In its present form, expression (9.3) may be of use in qualitative studies on the "willingness" of a shock wave to move in reaction upon pressure fluctuations downstream of the shock, such as generated by flap oscillations, flow separation (buffet) or by noise sources. As mentioned before, parameters of interest then are the magnitude and frequency of the pressure perturbations and the Mach-number distribution upstream of the shock wave.

10 THE UNSTEADY AERODYNAMIC CHARACTERISTICS OF THE "SHOCK-FREE" NLR 7301 AIRFOIL

10.1 INTRODUCTORY REMARKS

The results in the preceding chapters concern a conventional-type airfoil. As mentioned in chapter 1, however, nowadays there is a considerable interest in the unsteady aerodynamic characteristics of so-called supercritical airfoils. Therefore, as a next step in the NLR program on unsteady transonic aerodynamics, a wind-tunnel investigation was performed on the 16.5 per cent thick NLR 7301 airfoil, designed for "shock-free" flow under prescribed conditions (Fig. 10.1). On a two-dimensional model of this airfoil that could perform pitching oscillations about an axis at 40 per cent of the chord (for details see section 6.2), steady and unsteady pressure distributions were determined. In addition, time histories of the shock wave motions were recorded.

In the following sections, the main unsteady aerodynamic characteristics of the NLR 7301 airfoil are discussed for three different flow conditions, which can be characterized as follows (see figure 10.2):

I: fully subsonic flow

II: transonic flow with shock wave. In this domain two examples will be discussed, namely

II-1: slightly supercritical flow on the upper surface, and

II-2: flow with a well-developed shock wave

III: "shock-free" flow.

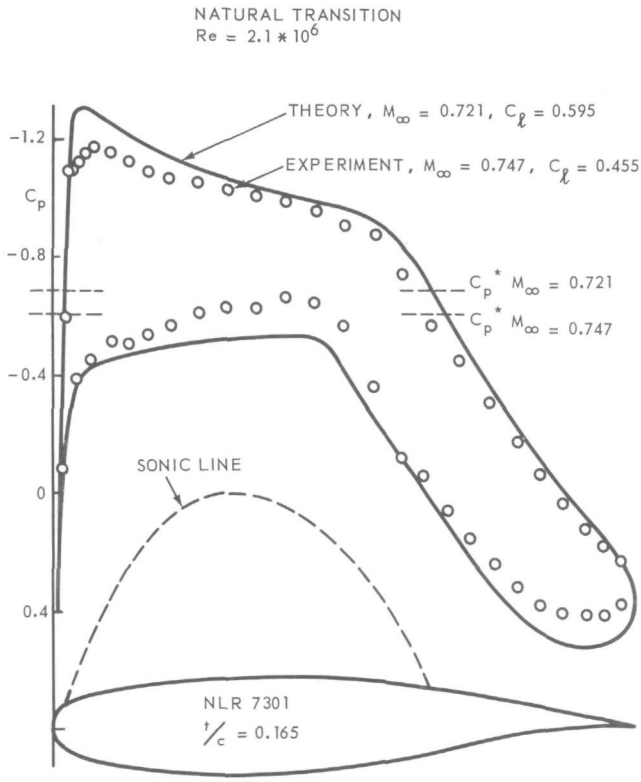

Fig. 10.1 Theoretical and experimental "shock-free" pressure distributions of the NLR 7301 airfoil (reproduced from Ref. 73).

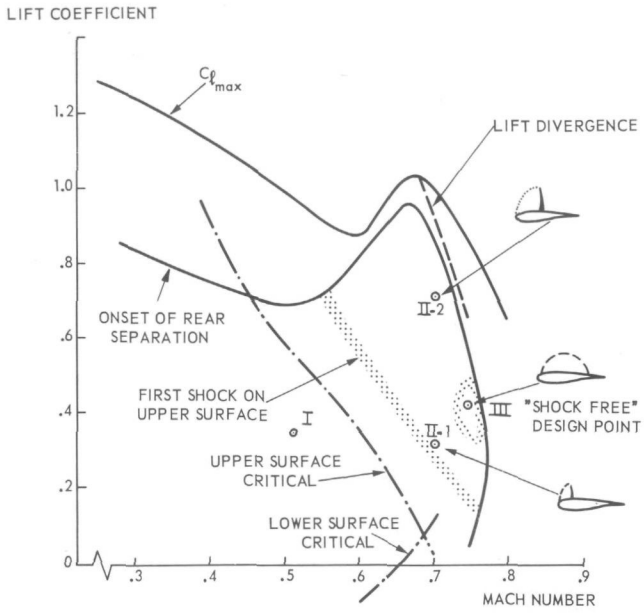

Fig. 10.2 C_ℓ-M_∞ plane for the NLR 7301 airfoil.

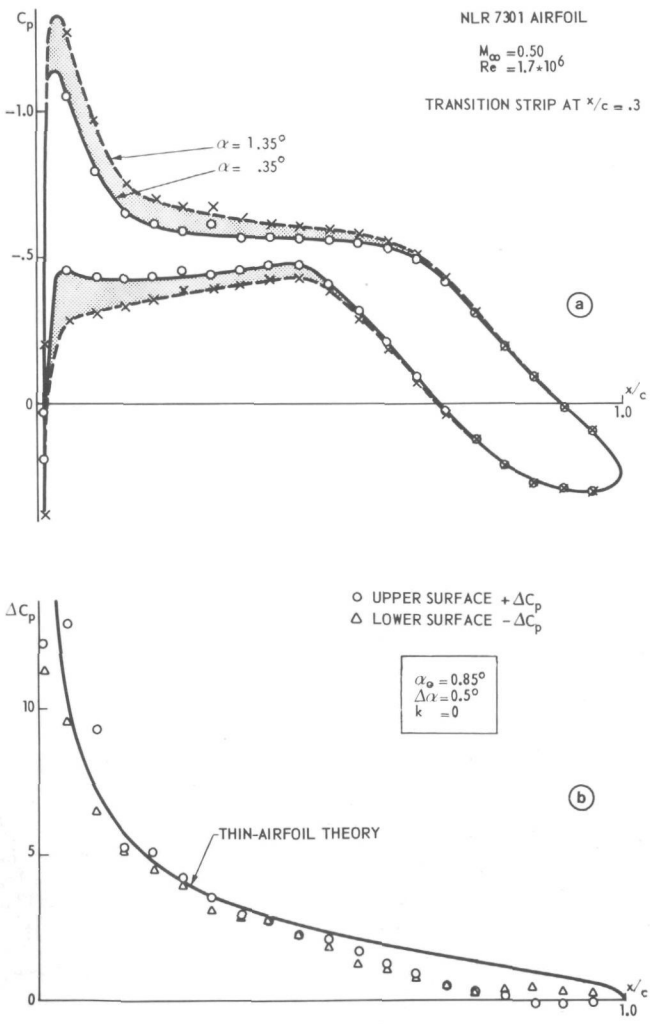

Fig. 10.3 Steady and quasi-steady pressure distributions at subsonic speed (condition I).

It will turn out that the pressure distribution for conditions I and II show essentially the same features as those observed for the conventional airfoil with flap, while for condition III some new aspects appear.

10.2 UNSTEADY PRESSURE DISTRIBUTIONS

10.2.1 Fully subsonic flow (condition I)

The steady pressure distributions measured in subsonic flow (condition I) for two values of the angle of attack are shown in figure 10.3a, while the corresponding quasi-steady pressure coefficients, defined as

$$\Delta C_p = \frac{C_p(\alpha-\Delta\alpha) - C_p(\alpha+\Delta\alpha)}{2\Delta\alpha} \quad , \qquad (10.1)$$

are given in figure 10.3b. In order to facilitate the comparison between the upper and the lower surface, the quasi-steady pressures on the lower surface are plotted again with a reversed sign. The agreement between the measured quasi-steady data and the prediction of thin-airfoil theory is reasonable. Deviations can be seen over the rear part of the airfoil, where the measured values are below the calculated curve, and near the leading edge, where the pressures measured on the upper surface are larger than those predicted

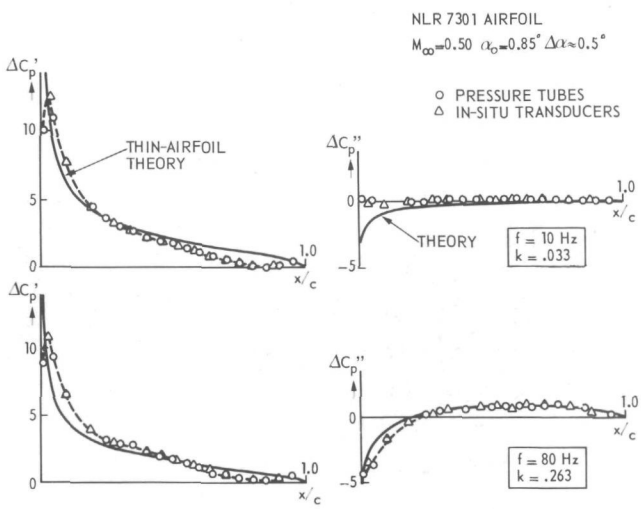

Fig. 10.4 Unsteady pressure distributions on the upper surface at subsonic speed (condition I).

by the theory and also larger than the values measured on the lower surface. As will be discussed later (chapter 13), these differences have to be attributed to the combined effect of airfoil thickness (plus incidence) and the boundary layer. The first effect dominates on the front part of the airfoil, while the boundary-layer effect is more pronounced on the rear part.

A comparison between the unsteady pressures measured on the upper surface of the oscillating airfoil and the corresponding results of thin-airfoil theory (Fig. 10.4) shows differences similar to those observed in the quasi-steady case. In general, the agreement between theory and experiment is reasonable and is of the same order as that observed earlier for the airfoil with flap. Further, as could be expected, there is a very satisfactory agreement between the unsteady pressures measured directly with the in-situ transducers and the pressures obtained via the pressure tubes.

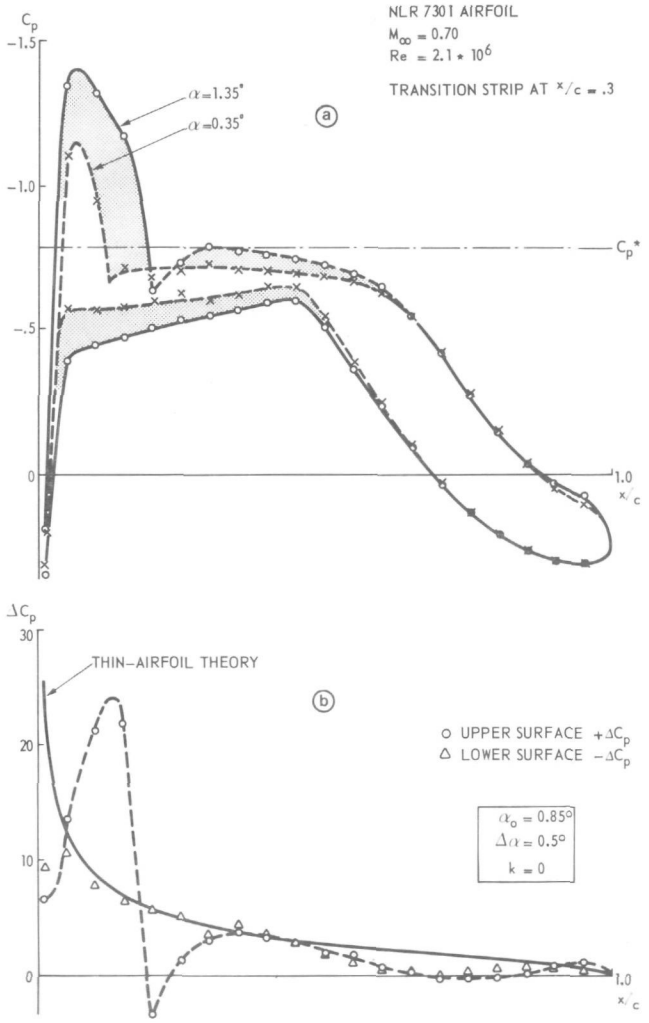

Fig. 10.5 Steady and quasi-steady pressure distributions in slightly supercritical flow (condition II-1).

10.2.2 Transonic flow with shock wave (condition II)

The next two examples concern oscillations of the airfoil around the off-design conditions II-1 and II-2 (Fig. 10.2). These conditions are typical for "classical" transonic flows, in which a supersonic region terminated by a normal shock wave occurs. Both cases deal with a free-stream Mach number of 0.7, but with a different incidence of the airfoil. For condition II-1, the mean incidence is 0.85 degrees and the flow along the upper surface is slightly supercritical with a weak shock wave. For condition II-2, in which the incidence is 3 degrees, the upper surface carries a well-developed supersonic region, terminated by a relatively strong shock wave.

Condition II-1: slightly supercritical flow

The steady pressure distributions measured for two incidences close to condition II-1 (Fig. 10.5a) show the appearance of a weak shock wave

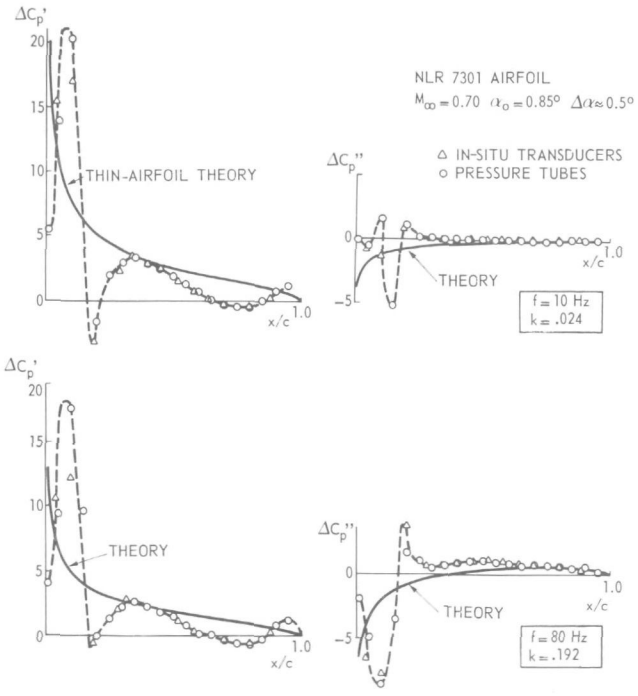

Fig. 10.6 Unsteady pressure distributions on the upper surface at slightly supercritical speed (condition II-1).

Bibliotheek TU Delft

Magazijnslip/*Picking slip*

Ik wil dit document graag verlengen/*I would like to renew this loan.*

in te vullen door de Bibliotheek TU Delft/*to be completed bij the Delft University of Technology Library*

☐ verlengd tot/*renewed until :*

☐ niet verlengbaar, a.u.b. retour/*renewal not possible, please return the document*

☐ opmerkingen/*other* :

Briefkaart

FRANKEREN
ALS
BRIEFKAART

Aan de Bibliotheek van de
Technische Universiteit Delft
Postbus 98
2600 MG DELFT

Geleend op/*Date of issue*: Terugbezorgd op/*Returned on*:

14 25 29 08 1997

Uiterlijk terugbezorgen op/*Date due*:

26 09 1997 Paraaf/*Initials:*

Documentgegevens/*Received on loan*:

Tijdeman, Hendrik
INVESTIGATIONS OF THE TRANSONIC FLOW AROUND OSCILL

1371022 CBmg bkuitln 298294

Gebruikersgegevens/*Borrower* :

59241 Prananta, B.B.----------
Fac. L&R
Kluyverweg 1
2629 HS Delft
RAS baknr. 14

11811563 ja

on the upper surface of the airfoil, which shifts in downstream direction to about 20 per cent of the chord as the incidence is increased from 0.35 to 1.35 degrees. In the quasi-steady pressure distribution on the upper surface (Fig. 10.5b), this shift in shock position causes a pressure peak on the front part of the airfoil, which is of the same type as that observed earlier on the airfoil with flap (section 8.2.2). The lower surface of the airfoil remains subsonic, and the quasi-steady pressure distribution along this side is predicted reasonably well with thin-airfoil theory. This confirms the observations for the airfoil with flap (section 8.4.1) that the unsteady pressure distributions at the upper and the lower surface are determined primarily by their respective steady flow fields, independent of the steady flow at the other surface.

Unsteady pressure distributions for condition II-1 are given in figure 10.6 for 10 and 80 Hz, respectively. Since the results for the lower surface behave as usual in subsonic flow, they have been omitted. The pressure distributions of figure 10.6 show about the same characteristics as those in quasi-steady flow, and one recognizes easily the pressure peak on the front part of the airfoil, which is caused by periodical shock-wave motion.

Condition II-2: flow with a well-developed shock wave

As the next example of an unsteady transonic flow with shock wave, oscillations of the airfoil about condition II-2 (Fig. 10.2) will be considered. In this condition, the upper surface carries a supersonic region that extends to about 50 per cent of the chord and is terminated by a rather strong shock wave. As shown in figure 10.7a, a change in incidence of 1 degree results in a shift of the steady shock position of about 10 per cent of the chord. The flow along the lower surface remains subcritical.

From the corresponding quasi-steady pressure distributions (Fig. 10.7b), it can be deduced that along the upper surface the pressure is dominated by the effect of the shock displacement

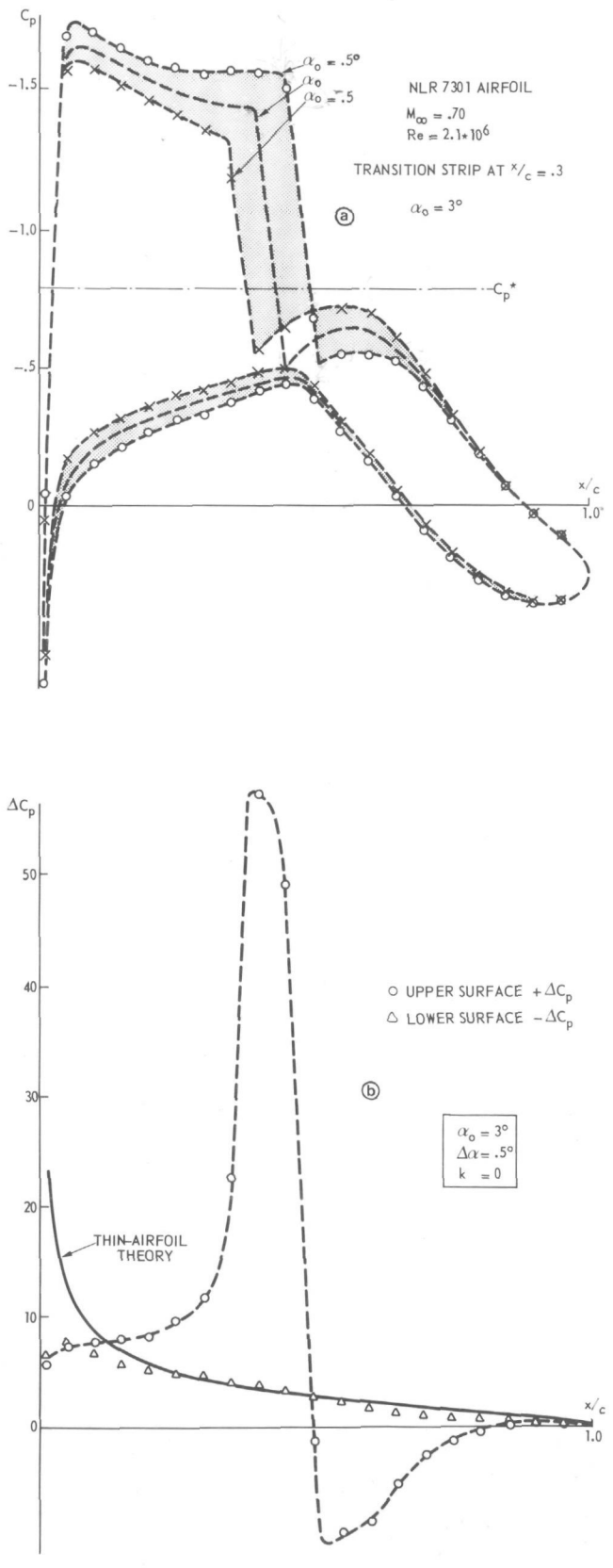

Fig. 10.7 Steady and quasi-steady pressure distributions in a transonic flow with well-developed shock wave (condition II-2).

Similar to the NACA 64A006 airfoil (Figs. 8.7 and 8.8), a high-pressure peak is generated, which of course cannot be predicted by thin-airfoil theory. As before, the quasi-steady pressure distribution on the subsonic lower surface is predicted reasonably well.

Pressure distributions on the upper surface for the unsteady case are presented in figure 10.8, for three different frequencies. These results also show the dominant effect of the pressure peak due to the moving shock wave. It is noted that this pressure peak shifts from the real part of the pressure distribution to the imaginary part with increasing frequency. This is caused by the increased phase lag of the periodical shock motion relative to the motion of the airfoil, a phenomenon that was observed earlier for the airfoil with flap (see figures 8.23 and 8.24), and that will be discussed in some more detail in section 10.4.

Further, by representing the unsteady pressure distributions in terms of magnitude and phase angle (Fig. 10.9), it can be shown that the width and the height of the pressure peak associated with the shock wave decrease as the frequency is increased. This is caused by the decrease of the amplitude of the shock motion with increasing frequency. Concerning the phase curves in figure 10.9, it can be noted that the measurements show a jump of about 180 degrees just downstream of the mean position of the shock wave. This jump is present already in quasi-steady flow and, thus, is not a dynamic effect.

From the comparisons of the measured pressure distributions with the distributions calculated with thin-airfoil theory (Figs. 10.8 and 10.9), it is evident that, as far as the upper surface is concerned, this theory is not applicable.

10.2.3 The "shock-free" design condition (condition III)

Of special interest is the unsteady behaviour of the airfoil in its "shock-free" design condition (condition III of figure 10.2). In the discussion of the results for this specific condition, preference is given to the data obtained with natural transition, since the flow in this condition is found to be influenced inconveniently by the presence of the transition strip (a discussion on the effect of the transition strip will be given in section 10.5).

As shown in figure 10.10a, a variation in incidence of 0.5 degrees about the design point leads to a considerable change in the steady pressure distribution along the upper surface, in particular in the supersonic region, which ranges from about 3 per cent to 65 per cent of the chord. Furthermore, variations of 0.5 degree appear to be sufficient to generate a shock wave at about 65 per cent of the chord. At the lower surface, the steady pressure distribution changes regularly. Noteworthy is that here the velocity becomes slightly supercritical, but still without shock formation

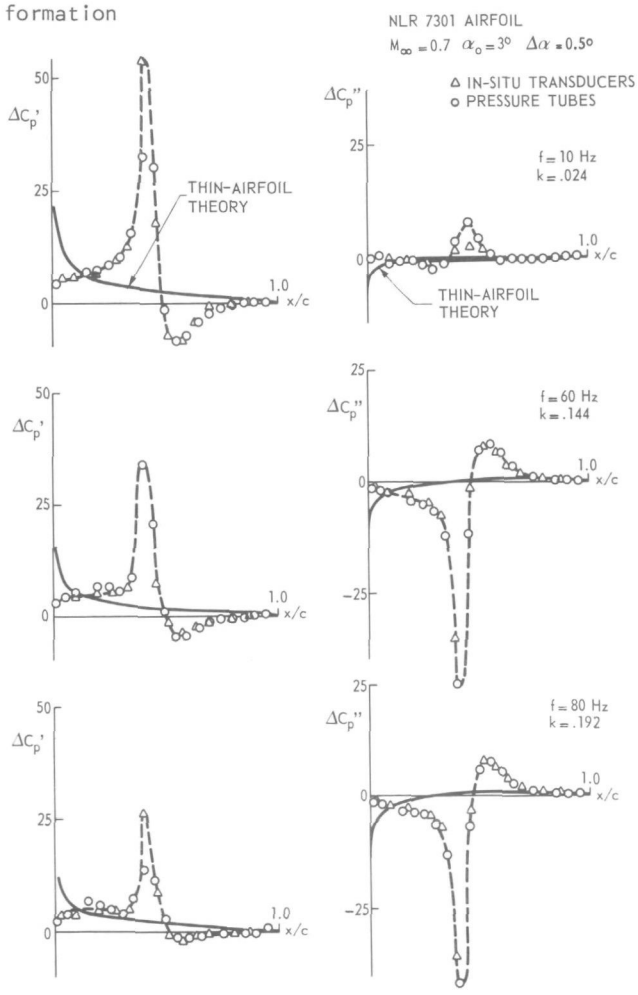

Fig. 10.8 Development of the unsteady pressure distributions on the upper surface with frequency in transonic flow with shock wave (condition II-2).

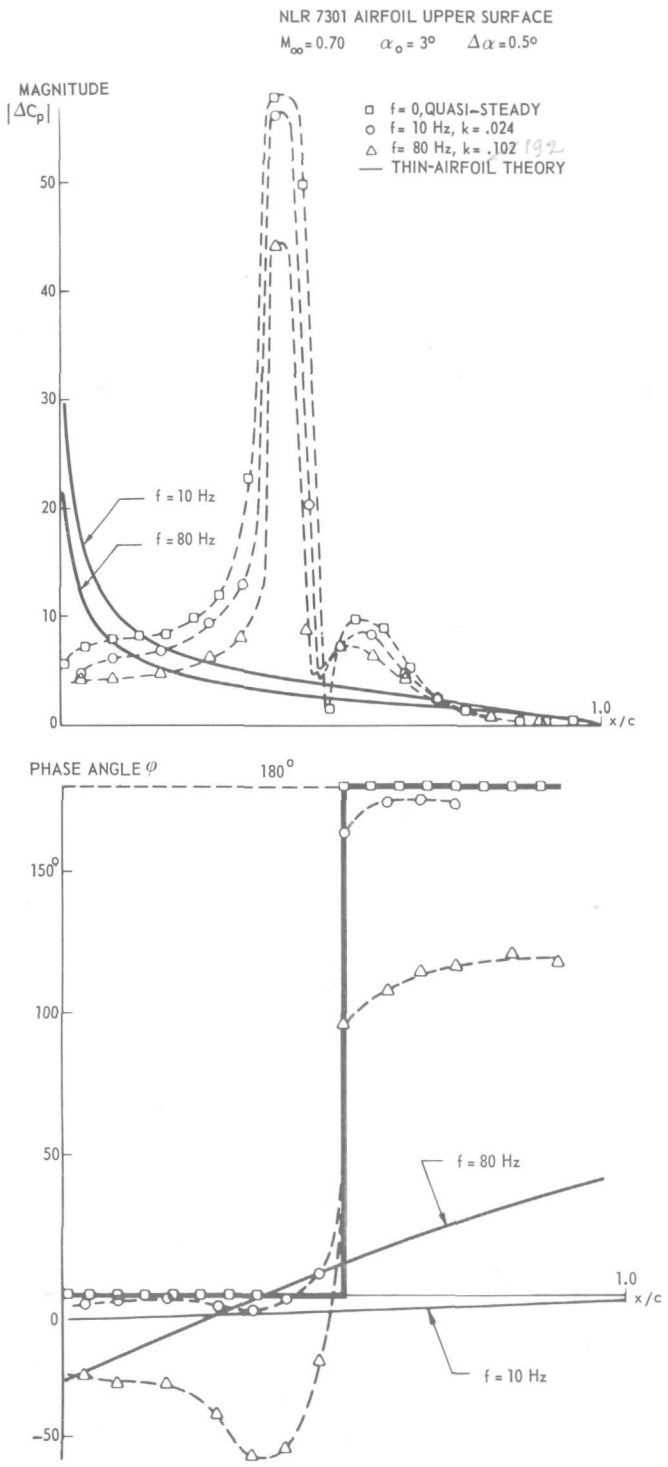

Fig. 10.9 Effect of shock wave on the unsteady pressure distributions (condition II-2).

The changes in steady pressure distribution result in a quasi-steady distribution as given in figure 10.10b. A wide bulge occurs on the upper surface, which is caused by the above-mentioned change in pressure distribution in the supersonic region. Probably this wide bulge is characteristic for the present type of "shock-free airfoil, with its relatively blunt nose and its extensive region of supersonic flow.

When the quasi-steady distribution obtained from the measurements is compared with the curve determined with thin-airfoil theory, it appears that for the upper surface the prediction is completely useless. For the lower surface, where the flow is only slightly supercritical, the difference between theory and experiment is considerably smaller. Here a small bulge in the measured data between 20 and 50 per cent of the chord is found, which is similar to the one observed on the airfoil with flap, and which also occurred when the flow locally became slightly supercritical (see for instance figure 8.5).

A series of fully unsteady pressure distributions along the upper surface in terms of magnitude and phase angle is given in figure 10.11. The magnitude curves clearly exhibit the large contributions associated with the changes in the shape of the pressure distribution in the supersonic region on the front part of the airfoil. In addition, a small peak occurs at about 65 per cent of the chord, which is caused by the periodical formation of a weak shock wave in this region (see figure 10.12). With increasing frequency the bulge on the front part decreases, and the unsteady pressure distribution shows a tendency to change in a direction towards the pressure distributions found for flow condition II-2. The phase curves in figure 10.11 behave very regularly over the first 60 per cent of the chord. Then a jump in phase angle of about 180 degrees occurs, which is due to the presence of the shock wave.

Finally, a comparison of the measured unsteady pressure distributions with thin-airfoil theory confirms what could be concluded already on the basis of the quasi-steady data: one has to apply other prediction methods for these types of mixed flows.

10.3. UNSTEADY AERODYNAMIC COEFFICIENTS

The unsteady aerodynamic coefficients obtained by chordwise integration of the measured

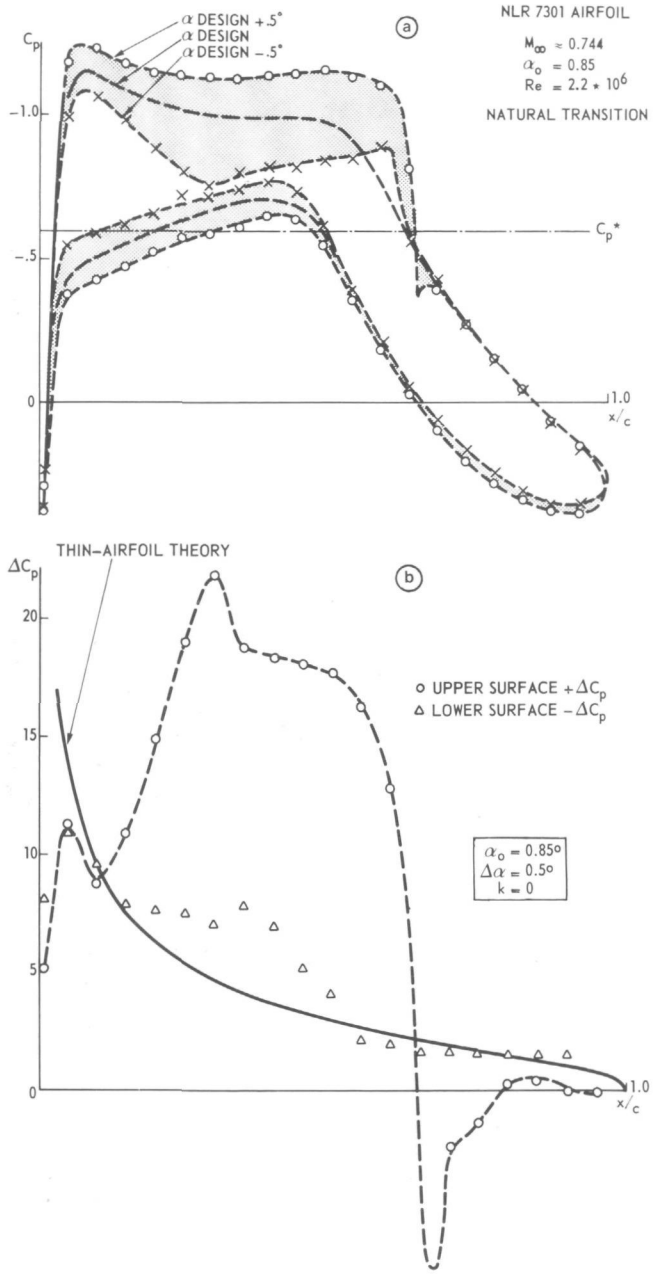

Fig. 10.10 Steady and quasi-steady pressure distributions about the design point (condition III).

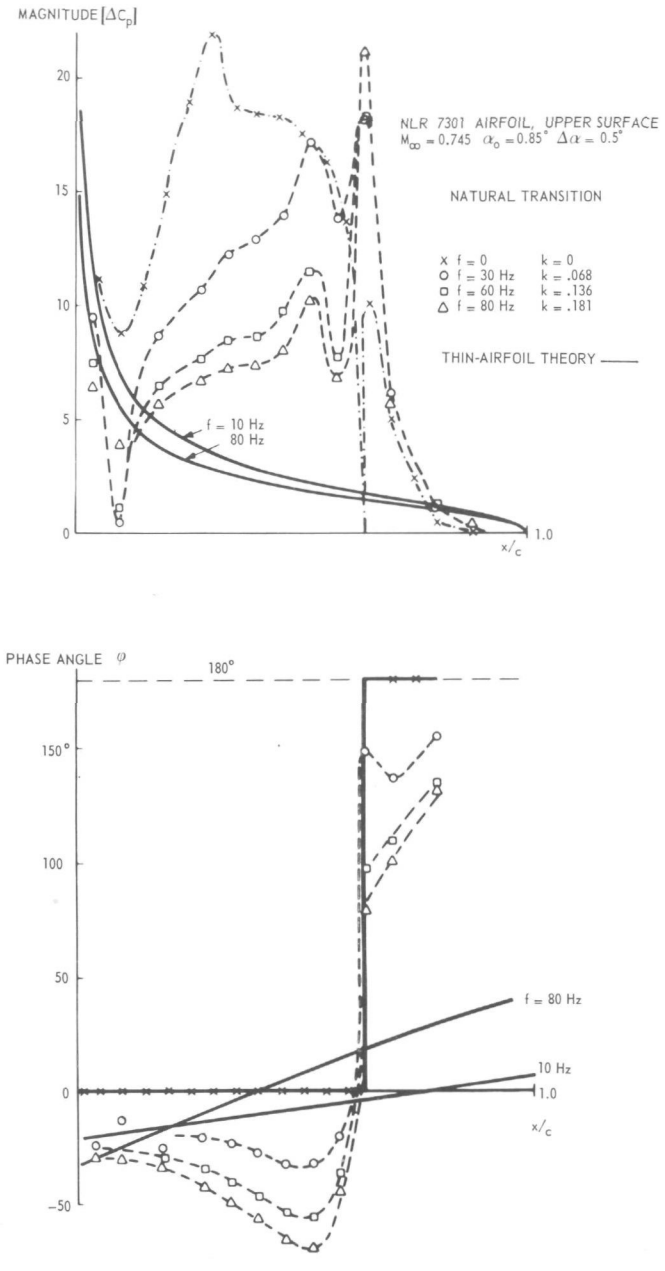

Fig. 10.11 Unsteady pressure distributions for the "shock-free" design point (condition III).

unsteady pressure distributions are collected as functions of the reduced frequency in figures 10.13 - 10.16, for the characteristic flow conditions I, II-1, II-2, and III, respectively. For reference purposes, the results according to thin-airfoil theory are given as well.

The agreement between the theoretical and experimental pressure distributions for the subsonic flow condition I (see section 10.2.1) is reflected in the curves of figure 10.13. The largest deviations occur in the real part of both the normal-force coefficient and the moment coefficient. Further, as far as the normal force is concerned, the agreement between theory and experiment improves with increasing frequency. This phenomenon was observed earlier in the results of the airfoil with flap (section 8.5.2).

For the slightly supercritical flow condition II-1 (Fig. 10.14), the differences between theory and experiment are of the same order as in subsonic flow, in spite of the larger differences in pressure distribution (Fig. 10.6). This happens

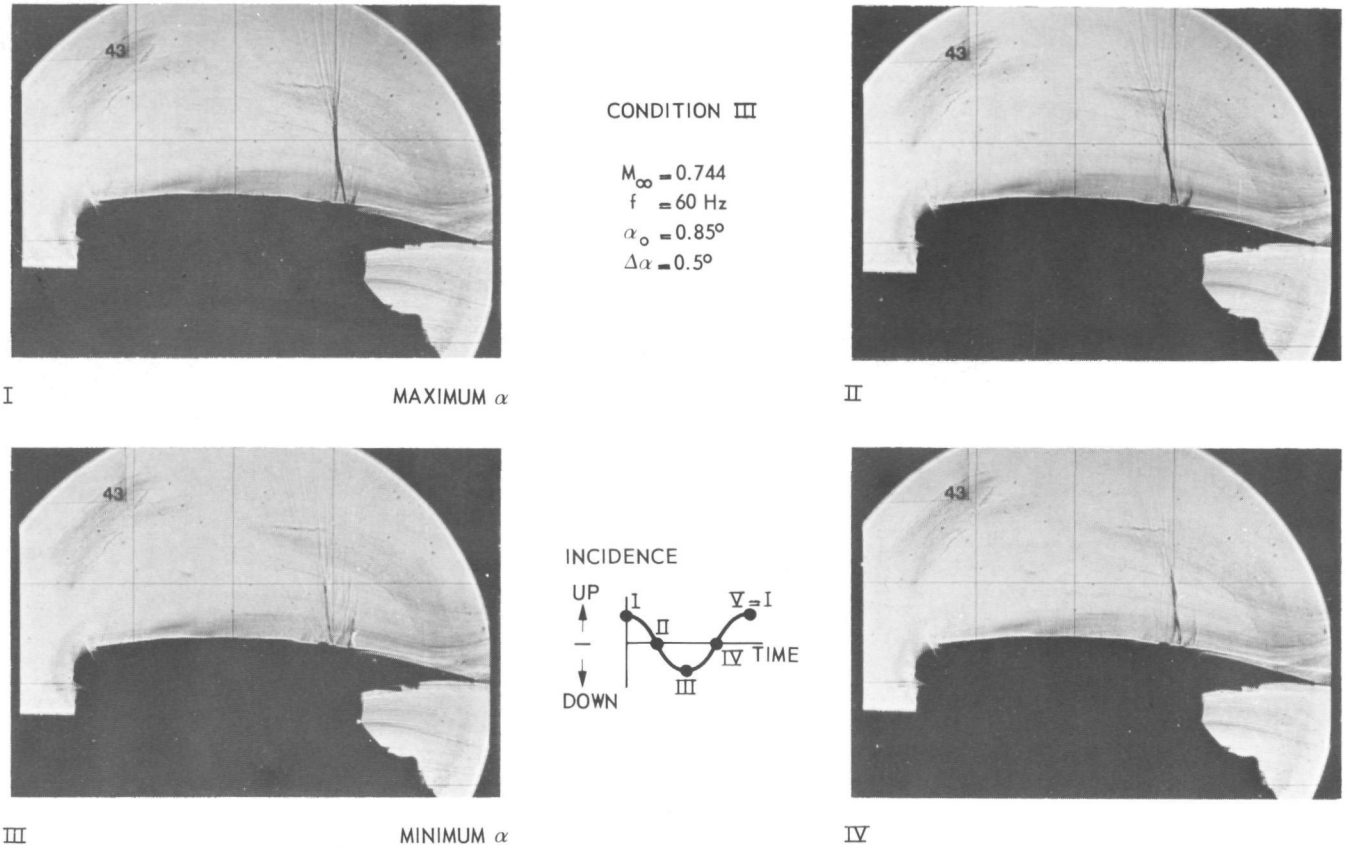

Fig. 10.12 Time history of the periodical shock-wave motion (condition III).

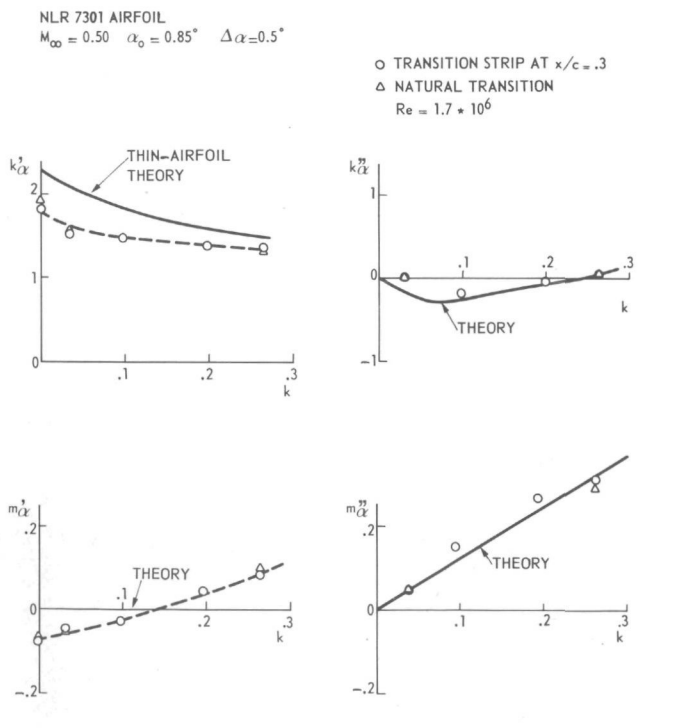

Fig. 10.13 Unsteady normal-force and moment coefficients as a function of frequency in subsonic flow (condition I).

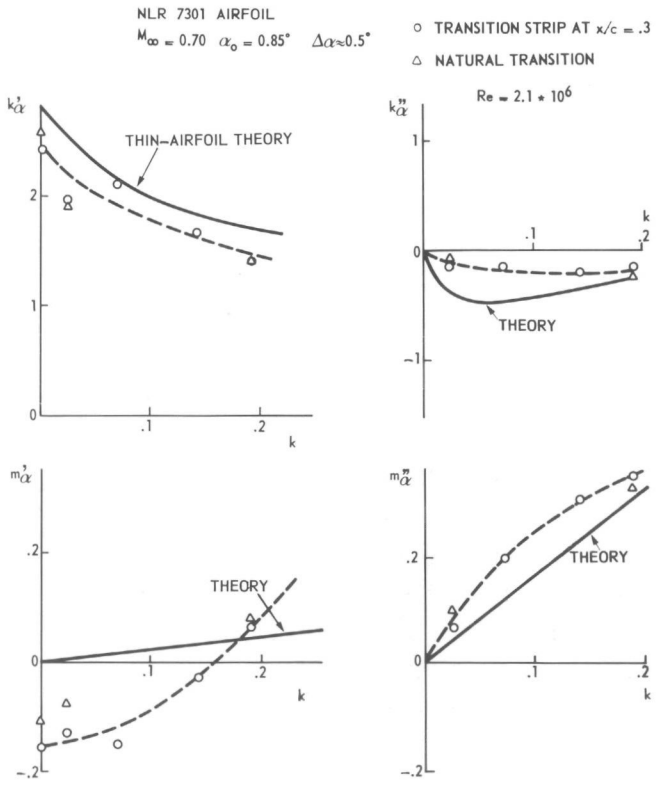

Fig. 10.14 Unsteady normal-force and moment coefficients as a function of frequency in slightly supercritical flow (condition II-1).

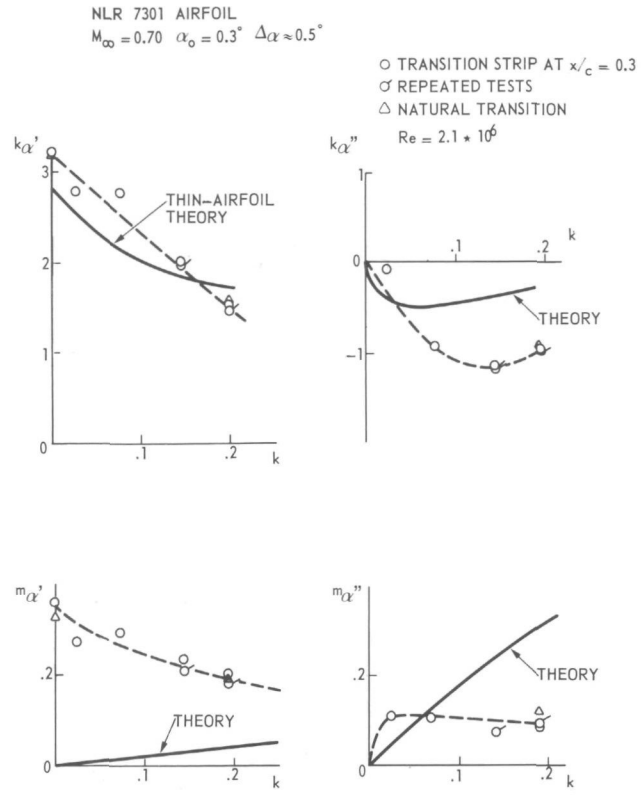

Fig. 10.15 Unsteady normal-force and moment coefficients as a function of frequency in transonic flow with a well-developed shock wave (condition II-2).

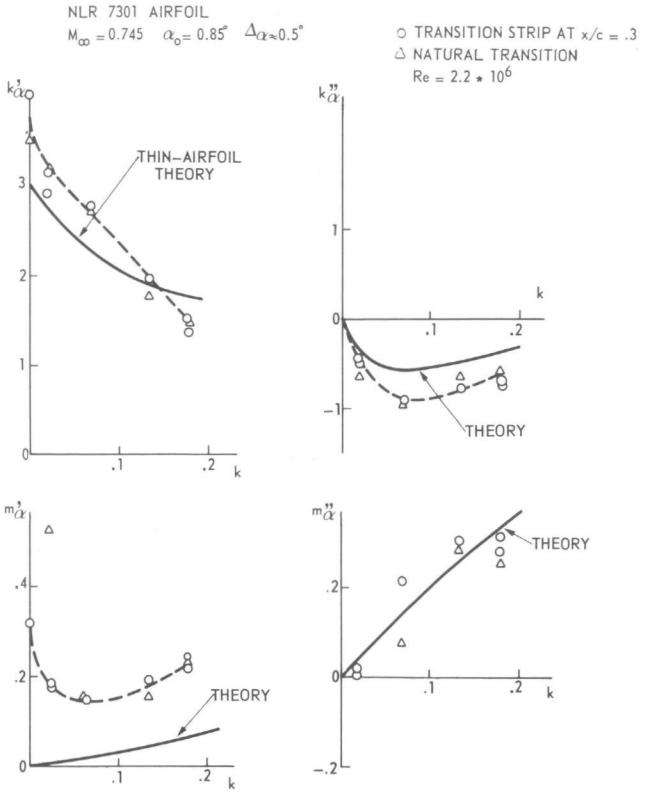

Fig. 10.16 Unsteady normal-force and moment coefficients as a function of frequency for the "shock-free" design point (condition III).

because the pressure peak generated by the (weak) shock wave on the front part of the airfoil provides about the same contribution to the normal force as the theoretical suction peak near the leading edge. Moreover, due to its chordwise location, the pressure peak associated with the shock wave hardly influences the moment about the quarter-chord point.

For the condition with a well-developed shock wave near midchord (condition II-2), the differences between theory and experiment are considerably larger than in the preceding two examples (see figure 10.15). This is true also for the unsteady aerodynamic coefficients in the "shock-free" design condition (Fig. 10.16). A comparison of figures 10.15 and 10.16 learns that the deviations from thin-airfoil theory for the design condition are of the same order of magnitude as for the "classical" transonic flow condition II-2.

The experimental results of condition 11-2 (Fig. 10.15) can be explained with the idealization shown in figure 10.17. The contribution of the moving shock wave as estimated from the measured pressure distributions is indicated separately. Without this contribution, the curves closely follow theory, except for a shift in m_α, which is due to the rearward location of the pressure peak relative to the quarter-chord point. This location, $\Delta x/c$, can be derived from

$$\Delta x/c = \tfrac{1}{2}\, \Delta m_\alpha / k_\alpha \ ,$$

and amounts to roughly 5 per cent of the chord. Adding the moving shock causes an increase of k_α' and m_α' at low frequencies. This effect shifts to k_α'' and m_α'' at the higher frequencies, which is correlated with the shift of the pressure peak due to the shock from the real part to the imaginary part of the pressure distribution, as was shown in figure 10.8.

10.4 REMARKS ON THE MOTION OF THE SHOCK WAVE

With the help of optical flow studies, additional information was obtained about the

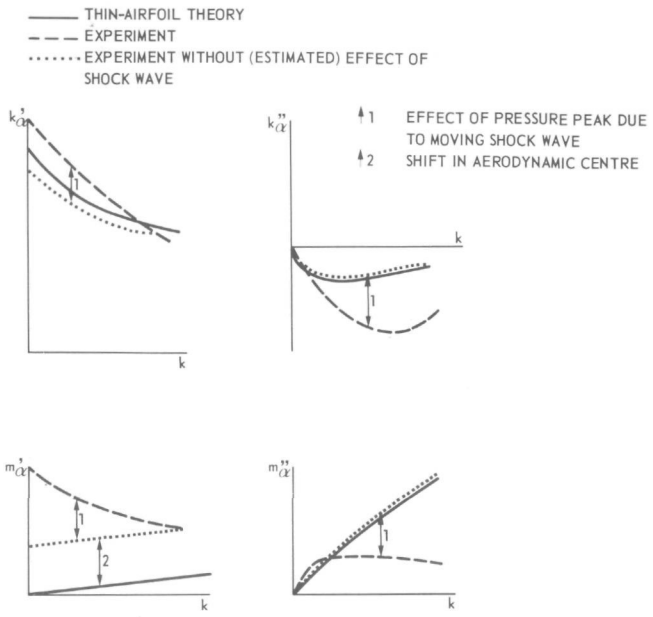

Fig. 10.17 Qualitative explanation of the effect of the oscillating shock wave on the unsteady aerodynamic coefficients.

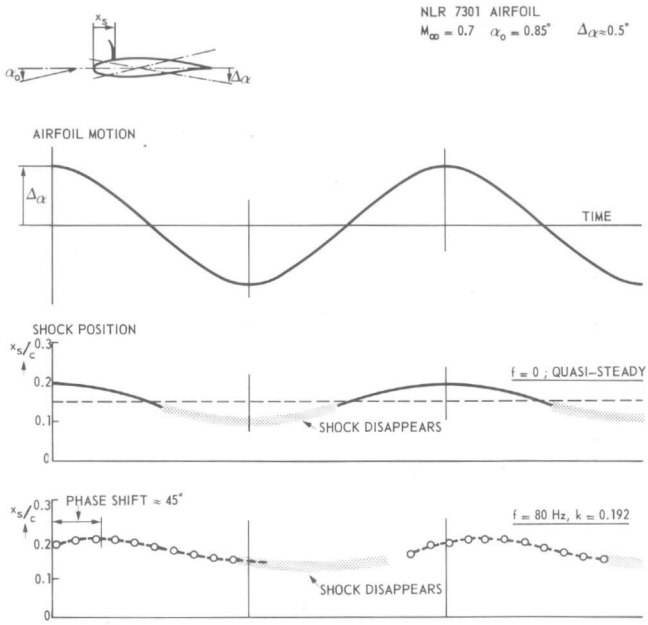

Fig. 10.18 Periodical shock-wave motion in slightly supercritical flow (condition II-1).

periodical motion of the shock wave in conditions II-1 and II-2. Figure 10.18 gives some results for the slightly supercritical condition II-1. In both the quasi-steady and the unsteady case, the shock wave vanishes during a part of the cycle. In the unsteady case, the trajectory along which this happens is shifted to that part of the motion where the shock moves in downstream direction. Evidently, this is caused by the dynamic effect of the shock motion on the strength of the shock, which results in an increase in shock strength during the upstream motion and a decrease in strength during the downstream motion. The unsteady shock motion of figure 10.18 is of type B, described in chapter 9. The flow conditions are such, however, that for higher frequencies and larger amplitudes of the airfoil motion shock-wave motions of type C (upstream-propagating waves) can be expected.

From the time histories of the shock displacement for the transonic-flow condition II-2 (Figs. 10.19 and 10.20), it follows that in this condition the shock wave performs almost sinusoidal motions, similar to the type-A motion in chapter 9. As shown in figure 10.19, the amplitude of the shock motion is almost proportional to the amplitude of oscillation of the airfoil. From the

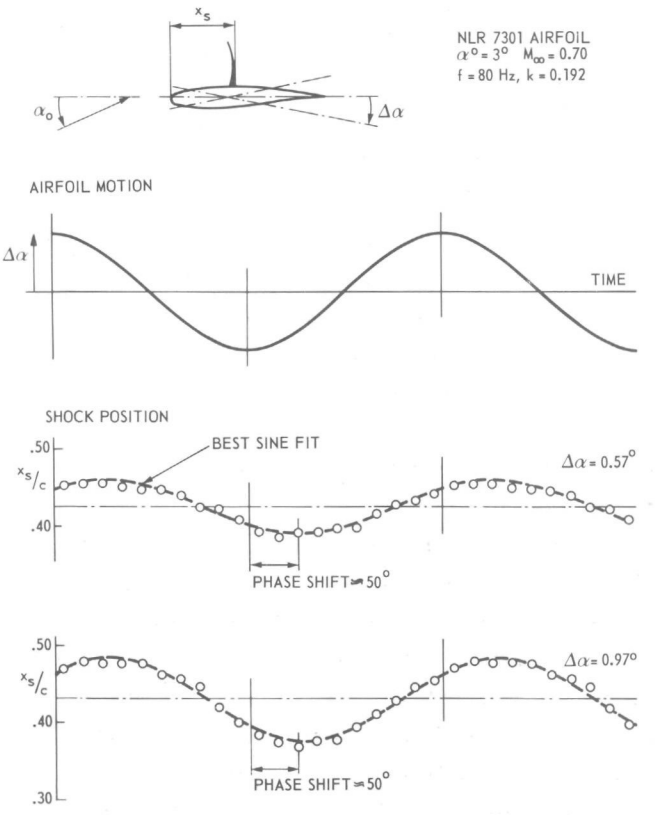

Fig. 10.19 Influence of the amplitude of the airfoil oscillation on shock-wave motion (condition II-2).

results in figure 10.20, which gives the shock trajectories for different frequencies, it can be observed that the phase lag of the shock motion relative to the airfoil motion increases with fre-

quency, while the amplitude of the motion decreases. The latter corresponds very well with the observation mentioned earlier concerning the contribution of the moving shock wave to the unsteady pressure distribution (see figures 10.8 and 10.9).

A closer examination of the phase lag of the shock motion relative to the airfoil motion (Fig. 10.21) learns that an almost linear relationship is found between frequency and phase lag. In other words, there is a constant time lag between the motion of the airfoil and the shock-wave motion. This corresponds with the result of Erickson and Stephenson (Ref. 103), who observed a fixed relation between the phase lag of the shock motion and the time required for a pressure impulse to travel from the trailing edge to the shock wave. This travelling time indeed seems to be a logical parameter for an airfoil with a large supersonic region terminated by a shock wave, because it is the time period after which major changes in flow condition, namely changes in flow direction at the trailing edge (Kutta condition), can be felt by the shock wave (Fig. 10.22).

The time required by a signal to travel from the trailing edge to the shock wave is

$$\Delta t = -\int_{x=c}^{x_s} \frac{dx}{(1 - M_{loc})\, a_{loc}}, \qquad (10.2)$$

with M_{loc} being the local Mach number and a_{loc} the local velocity of sound. Due to the gradient in Mach number normal to the airfoil surface, the acoustic waves propagate along paths away from the airfoil. Therefore, the propagation speed in upstream direction will be some average between the value of $(1-M_{loc})a_{loc}$ near the airfoil surface and the free-stream value. To account for this effect, the following value of the local Mach number is introduced:

$$M_{loc} = R\left[M_{loc}(\text{at the surface}) - M_\infty\right] + M_\infty, \qquad (10.3)$$

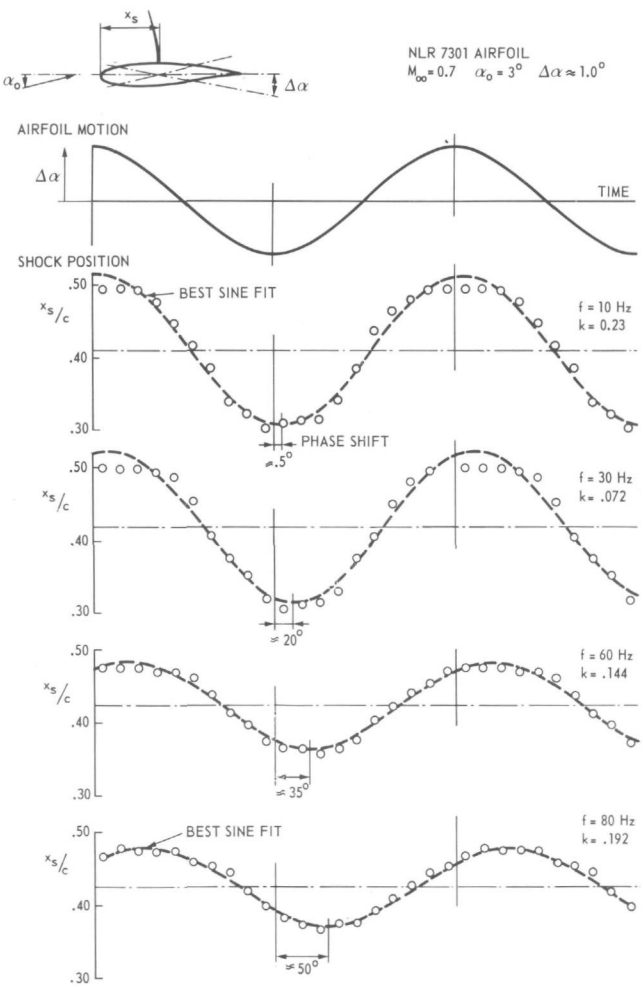

Fig. 10.20 Periodical shock-wave motion for various frequencies (condition II-2).

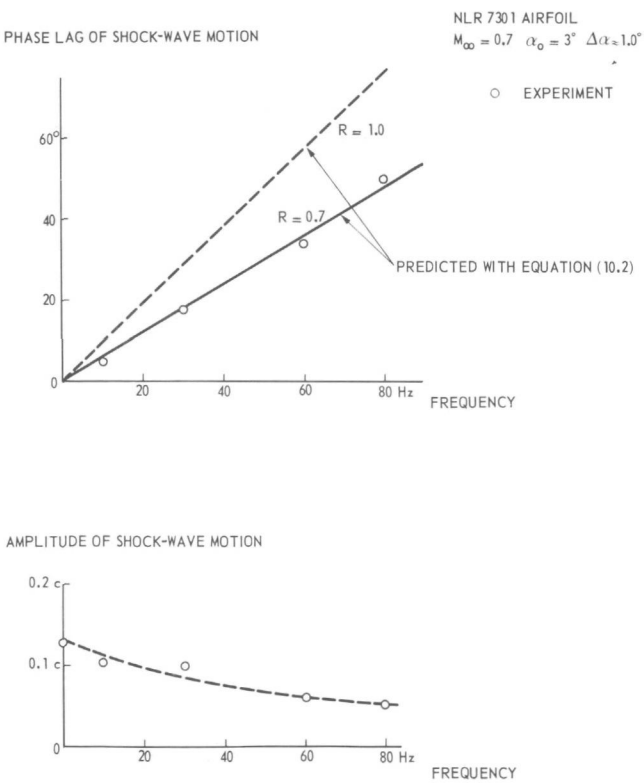

Fig. 10.21 Effect of frequency on the amplitude and phase lag of the periodical shock-wave motion (condition II-2).

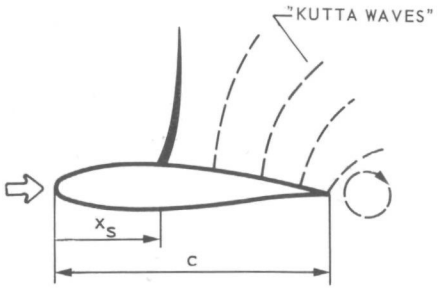

Fig. 10.22 The propagation of information from the trailing edge to the shock wave.

where R denotes a relaxation factor, which has a value between 0 and 1.0.
For R ≃ 0.7, an excellent agreement is obtained between the travelling time of the "Kutta waves" and the corresponding phase lag of the motion, as is demonstrated in figure 10.21.

10.5 THE INFLUENCE OF THE TRANSITION STRIP

The present investigations were conducted in a small atmospheric wind tunnel and, as a consequence, only relatively small values of the Reynolds number could be attained (about 2.2×10^6, to be compared with 30 to 50×10^6 for full-scale flight). In practice this means that in the wind tunnel the transition of the boundary layer from laminar to turbulent takes place far more downstream than in free flight. Moreover, the location of the transition point may be very sensitive to changes in the free-stream Mach number or incidence. This might have led to two unwanted effects, one caused by the periodically shifting transition point (see, for instance, reference 115), and the other by the interaction of a shock wave with a laminar rather than with a turbulent boundary layer. As discussed in section 3.4 (Fig. 3.8), the latter leads to a lambda-type shock wave, which is not present in free flight.

To avoid these effects, it was decided to force transition artificially by means of a roughness strip. This created, however, a dilemma about the chordwise position of the strip, especially since the question about an adequate simulation of high-Reynolds-number effects on rear-loaded airfoils by means of artificial transition is still quite open and forms a source of constant concern to the steady aerodynamicists. The final choice for the location of the transition strip at 30 per cent of the chord was made for three reasons:

- to suppress the large chordwise shift in transition point at the upper surface of the airfoil, which had been observed (Ref. 73) at the design Mach number for incidence between -1 and +1 degree (Fig. 10.23a).
- to avoid at the lower surface a boundary layer that remains laminar to about 60 per cent of the chord (Fig. 10.23b), and
- to be consistent with the previous steady wind-tunnel investigations on the NLR 7301 airfoil.

The effect of the transition strip was checked by repeating a small part of the unsteady

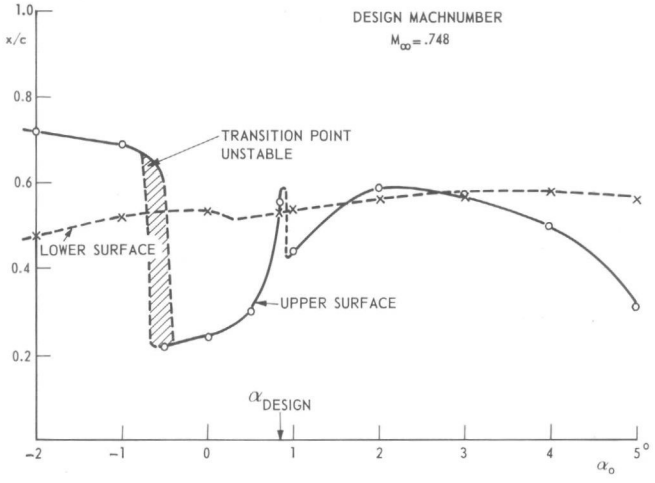

a Variation in transition point with incidence at the design Mach number.

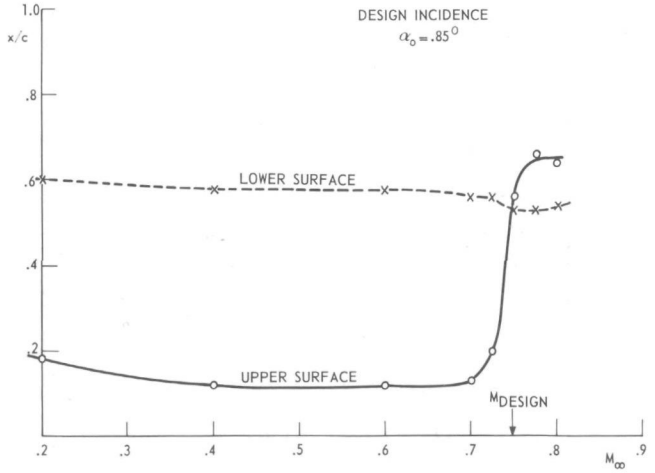

b Variation in transition point with Mach number at the design incidence.

Fig. 10.23 Location of natural transition point (from Ref. 73).

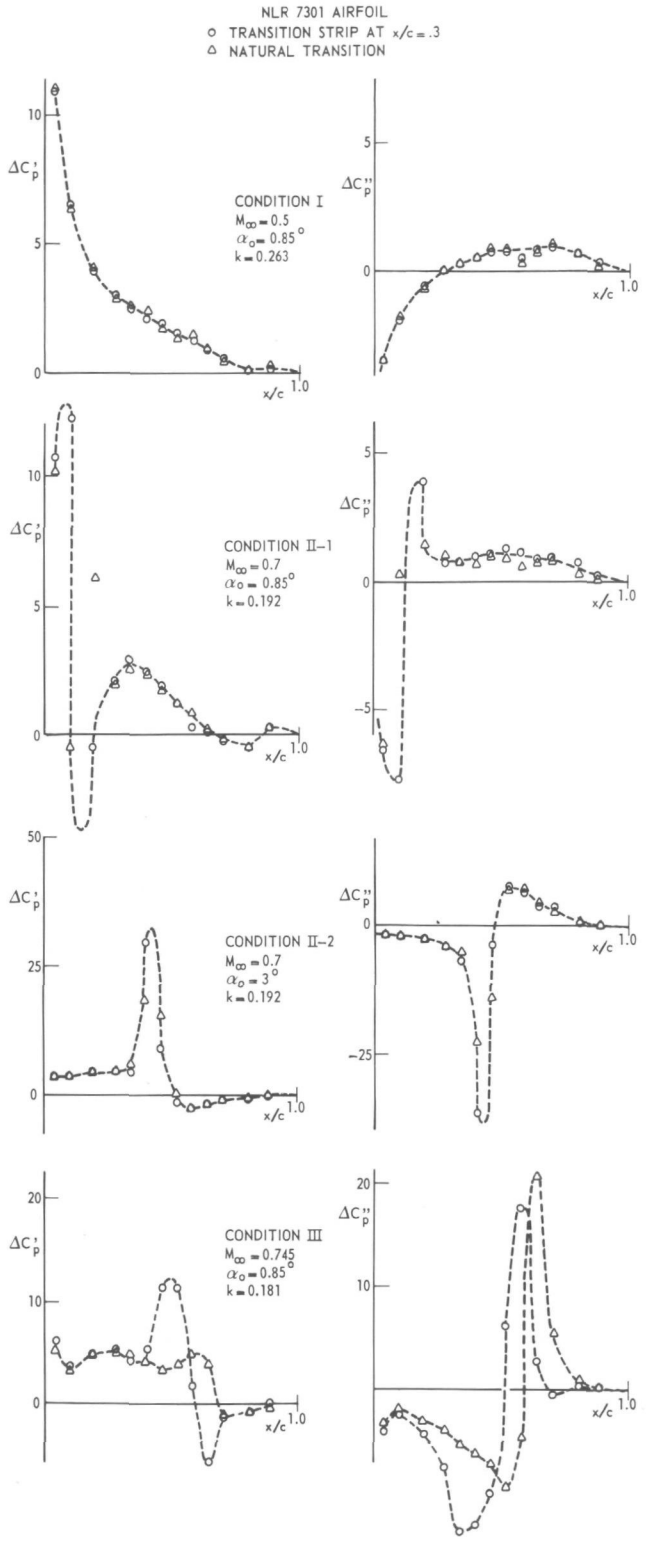

Fig. 10.24 Effect of transition strip on the unsteady pressure distributions (f = 80 Hz, $\Delta\alpha \approx 0.5^{o}$).

tests with natural transition. The results of these additional tests can be summarized as follows (see figure 10.24): At low subsonic speed (condition I), the effect of the strip on the unsteady pressure distributions and the corresponding unsteady aerodynamic coefficients (Fig. 10.13) is negligible. Also for the "classical" transonic flow conditions II-1 and II-2, the effects are very small. This is not surprising, since, as far as the upper surface is concerned, the natural transition in condition II-1 takes place upstream of the location of the transition strip (Fig. 10.23b), while for condition II-2 natural transition occurs at about the same location as the strip.

In contrast herewith, the flow in the design condition appears to be very sensitive to the presence of the transition strip (Figs. 10.24 and 10.25). The addition of the strip causes a drastic increase in unsteady pressures between 30 and 60 per cent of the chord, while the weak shock wave is shifted to a more upstream position. This latter effect can be inferred very well from the location of the "180 degrees" jump in the phase curves of figure 10.25. The differences are caused by the oblique compression wave, which emanates from the transition strip and is reflected as an expansion wave from the sonic line (see figure 10.26). When the airfoil oscillates, the location of the oblique compression wave AB and the sonic line change periodically. As a result, the location of the points where the successive expansion waves impinge on the airfoil also changes periodically. This leads to the complicated flow patterns shown in the shadowgraph pictures of figure 10.27. A comparison of these pictures with the ones for natural transition (Fig. 10.12) clearly shows that the disturbance of the flow field by the transition strip is an improper element in the delicate condition of "shock-free" flow. In the analysis of the results for the "shock-free" design condition (section 10.2.3), preference therefore was given to the data obtained during the wind-tunnel tests with natural transition, be it at the cost of an unknown effect caused by possible large changes in location of the transition point.

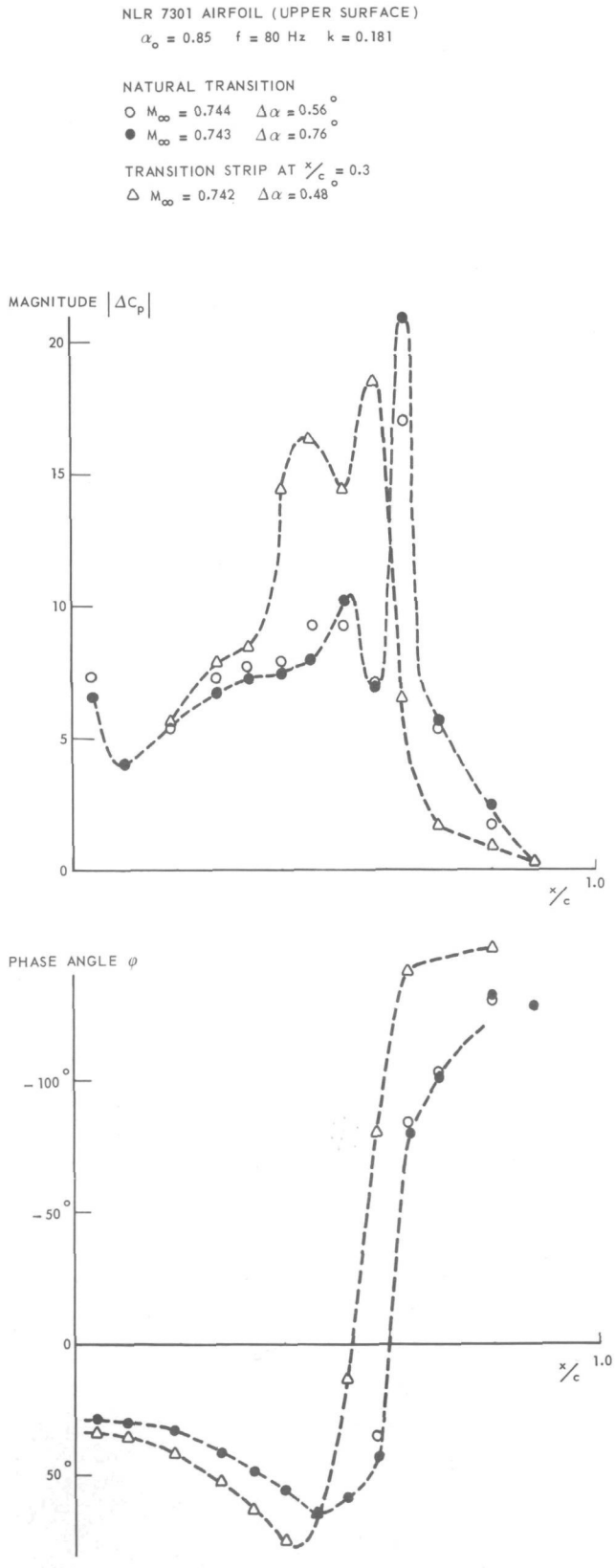

Fig. 10.25 Influence of transition strip on the unsteady pressure distribution for oscillations around the design point (condition III).

10.6 SOME ADDITIONAL EFFECTS

10.6.1 The effect of Mach number

The influence of the free-stream Mach number on the unsteady normal-force coefficient is illustrated in figure 10.28. It appears that for the design incidence, $\alpha_o = 0.85^o$, at low frequency (Fig. 10.28a) a high peak is found in the magnitude of k_α, which coincides with the design Mach number. At higher frequencies (Fig. 10.28b), this peak decreases considerably, which is in accordance with the development of the unsteady pressure distributions shown previously (Fig. 10.11).
The normal-force coefficient for an incidence of 3 degrees also shows a peak value, but now at a lower Mach number, at which a relatively strong oscillating shock wave is present. An increase in frequency, leading to a decrease in the amplitude of the shock motion, has less effect on the peak value of the normal force in this case than in the "shock-free" flow condition.
Finally, it can be observed from figure 10.28 that, at least at low frequency, the transonic effects on the unsteady airload of the airfoil in its design condition are of the same order of magnitude as those occurring in the "classical" transonic flow conditions with shock wave for $\alpha_o = 3^o$.

10.6.2 The effect of the amplitude of oscillation

In relation to the possibility of linearization, it is an important question whether a linear relationship exists between the amplitude of the airfoil motion and the resulting unsteady aerodynamic loading. For this reason, a number of additional tests was performed, in which the amplitude of the model oscillation was varied. Because in this respect the possibilities of the test set-up were limited, only amplitudes up to 1 degree could be realized.
The results of these additional tests (as an example, the data for the maximum frequency of 80 Hz are summarized in table 5) show no system-

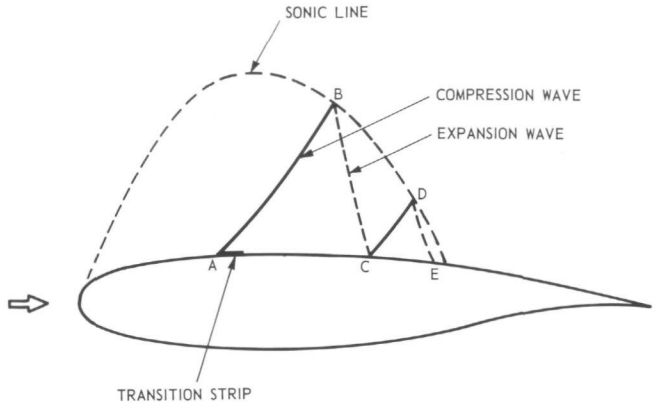

Fig. 10.26 Sketch showing effect of transition strip (condition III).

atic changes, which can be interpreted as a consistent effect of amplitude. Only small variations in the overall coefficients are found, which fall completely within the accuracy of the tests, to be estimated at about 5 to 10 per cent in magnitude and 3 to 6 degrees in phase angle.

10.7 CONCLUDING REMARKS

When the outcome of the analysis of the test data of the NLR 7301 airfoil is summarized, it can be concluded that the results for high-subsonic and transonic flow with normal shock waves confirm very well the findings of the experiment on the NACA 64A006 airfoil with flap. In high-subsonic flow, a reasonable agreement with the results of thin-airfoil theory exists. For transonic flow with a shock wave, the periodical motion of the shock gives rise to high local loads, which determine the overall unsteady airloads to a large extent. The contribution of the oscillating shock wave to the loading diminishes as the frequency is increased, which is the result of the decrease in amplitude of the shock motion. It can, thus, be expected that for very high frequencies the motion of the shock wave will become less important for the unsteady airloads. For the present airfoil, however, this will happen at frequencies well above the range of practical interest for flutter investigations.

A new feature is observed for oscillations of the airfoil about its "shock-free" design condition. Then the unsteady pressure distribution is

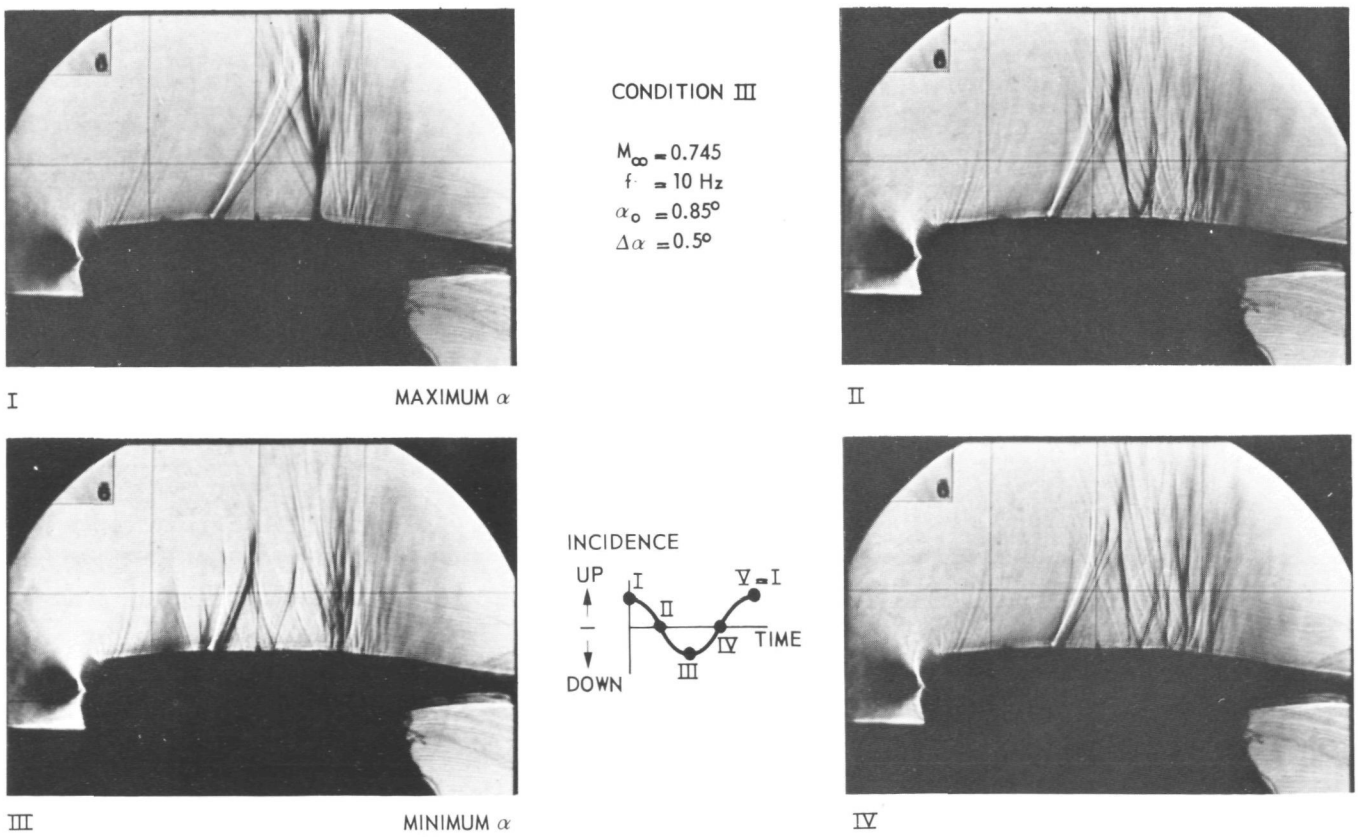

Fig. 10.27 Time history of the periodical shock-wave motion showing effect of transition strip (condition III).

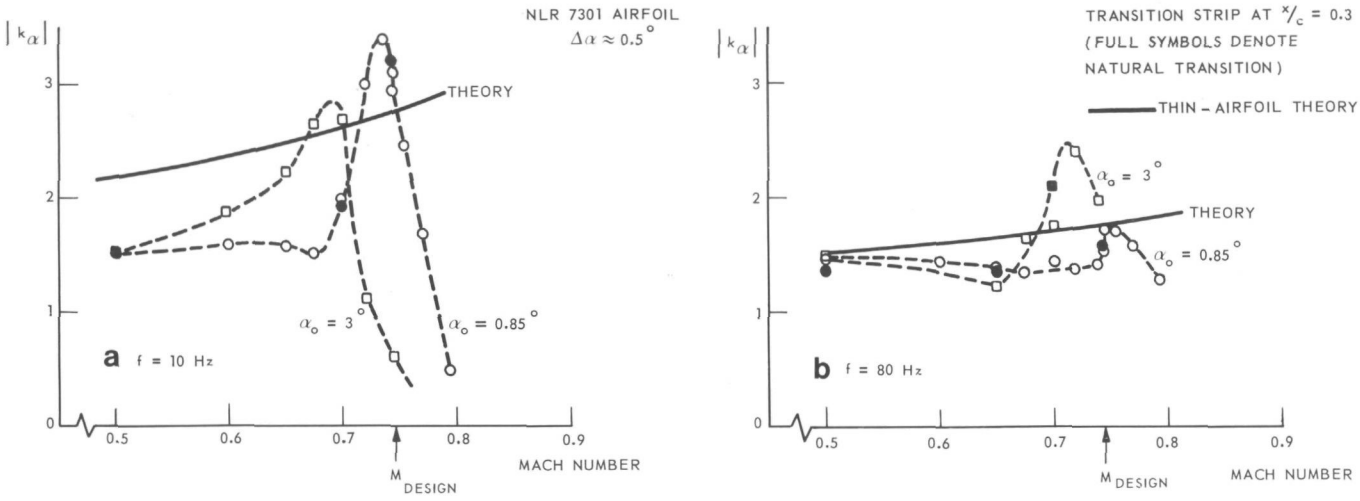

Fig. 10.28 Influence of Mach number on the magnitude of the normal-force coefficient.

TABLE 5

Effect of amplitude of oscillation on the unsteady aerodynamic coefficients

M_∞	α_o	$\Delta\alpha$	k	$\lvert k_\alpha \rvert$	$\arg(k_\alpha)$	$\lvert m_\alpha \rvert$	$\arg(m_\alpha)$	
0.5	0.85°	.44°	.263	1.36	0.4°	.32	73°	Condition I
		.55		1.36	2.1	.33	75	
		.76		1.45	4.7	.36	76	
		.77		1.35	2.0	.32	76	
		.94		1.37	2.5	.33	78	
0.7	0.85°	.25°	.192	1.62	-5.9°	.39	78°	Condition II-1
		.60		1.43	-6.7	.36	80	
		.70		1.52	-4.3	.40	84	
		.87		1.54	-2.2	.43	82	
0.7	3°	.55°	.192	1.83	-32.7°	.23	23°	Condition II-2
		.58		1.76	-33,7	.21	27	
		.70		1.86	-34.7	.23	21	
		.83		1.72	-33.9	.22	21	
0.745	0.85°	.27°	.181	1.64	-28.4°	.35	59°	Condition III
		.48		1.54	-27.4	.35	52	
		.52		1.70	-26.1	.40	52	
		.69		1.68	-26.9	.37	51	NLR 7301 airfoil
		1.13		1.46	-31.3	.24	57	Frequency: 80 Hz
0.745	0.85°	.56°	.181	1.56	-22.9°	.33	55°	Condition III
		.61		1.61	-21.3	.35	47	(Natural transition)
		.76		1.66	-23.9	.35	43	

dominated by the large changes occurring in the supersonic region on the front part of the airfoil. The resulting unsteady airloads are, at least at low frequency, of the same order of magnitude as those observed for "classical" transonic flows with a well-developed shock wave.

11 SOME CONSIDERATIONS ON A LINEARIZED TREATMENT OF UNSTEADY TRANSONIC FLOWS

11.1 INTRODUCTORY REMARKS

As outlined in chapter 4, it is an important question to what extent the linear relationship between the unsteady aerodynamic loads and the airfoil motion holds. This question is of interest, not only with respect to the development of methods to calculate the aerodynamic loads, but also for the application of the aerodynamic data in aeroelastic calculations, since calculation methods for the solution of nonlinear equations of motion on a routine basis are not well developed. In this chapter it is attempted to assess the possibility of linearization in a practical sense. For this purpose it is supposed that linearization of the unsteady airloads about a given mean position of an airfoil is justified as long as small, but still practical changes in incidence or flap angle (say in the order of 0.5 and 1 degree, respectively) around this mean position give rise to linearly developing changes in the flow field. In this respect it is also of interest which procedure has to be followed to select a minimum number of suitable mean steady flow conditions.

When considering the linearity of transonic flows, one can think of the following flow conditions in which linearity may be violated:

- flow conditions with an oscillating shock wave,
- flow conditons, like the "shock-free" design condition, in which a small change in incidence is followed by a rather abrupt change of the flow pattern.

In the subsequent sections, these conditions will be considered in some more detail. The considerations will be mainly based on the quasi-steady behaviour of the airfoils used in the present investigation. A quasi-steady analysis seems justified, since it may be expected that nonlinear effects will be largest in the quasi-steady case and at low frequencies. This expectation is based on the observation that in the transonic small-perturbation equation (eq. 2.15 of chapter 2), rewritten for sinusoidal perturbations as:

$$\left[1 - M_\infty^2 - M_\infty^2 \left[(\gamma+1)/U_\infty\right] \Phi_x\right] \Phi_{xx} + \Phi_{yy} + \\ - 2ikM_\infty^2 \Phi_x + k^2 M_\infty^2 \Phi = 0, \qquad (11.1)$$

the terms containing the reduced frequency k are linear in Φ. This suggests that with increasing k the linear part of the equation becomes more dominating, while for low frequency and quasi-steady flow (k = 0) the nonlinear term is more important. Of course, an important question is also whether or not the decrease of the nonlinear character happens monotonously with frequency. No definite conclusion in this respect can be drawn from the present experiments.

11.2 FLOW CONDITIONS WITH AN OSCILLATING SHOCK WAVE

11.2.1 Local effects of a shock wave

The local effects introduced by a shock wave can be illustrated conveniently with diagrams in which the steady pressures at constant chordwise stations are plotted as a function of incidence (or flap angle). Diagrams of this type, which clearly show the difference between a subsonic flow and a transonic flow with shock wave, are given in figures 11.1 and 11.2, respectively.

In subsonic flow (Fig. 11.1), the curves of the local-pressure coefficient vary almost linearly with incidence, which implies that their slopes $dC_p/d\alpha$ and, thus, the quasi-steady pressures are constant and independent of the actual value of the incidence. So it can be concluded that, at least as long as the flow remains attached, linearization is no problem in this flow regime. This observation is confirmed in unsteady flow, where the actual recordings of the pressures felt by the in-situ Kulite transducers in the oscillating model show almost sinusoidally varying signals (see figure 2.2). Also the summed signals, representing the unsteady lift and moment, behave linearly.

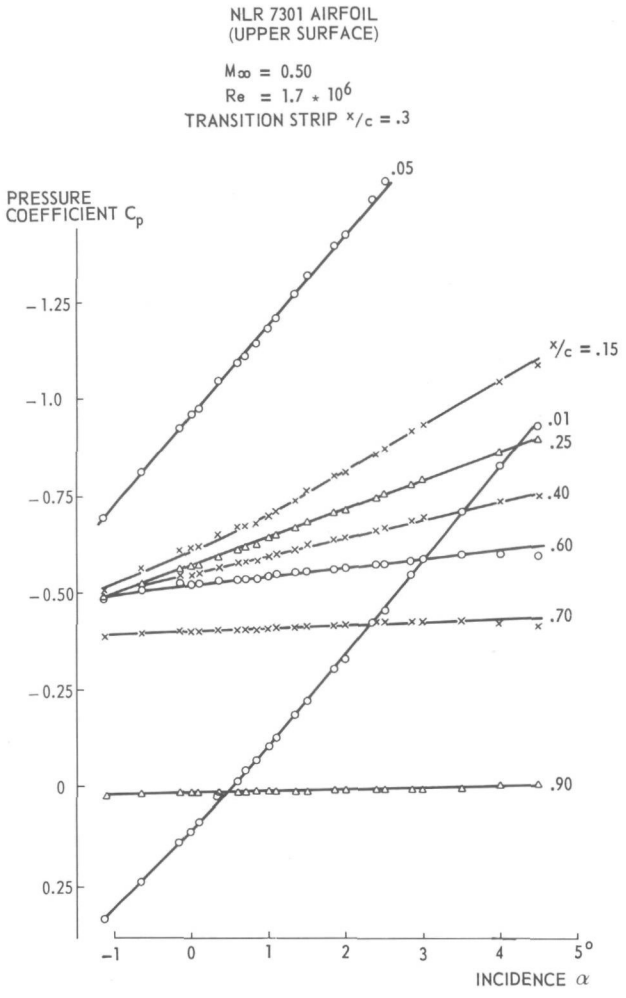

Fig. 11.1 Steady pressures at constant chordwise positions as a function of incidence in subsonic flow.

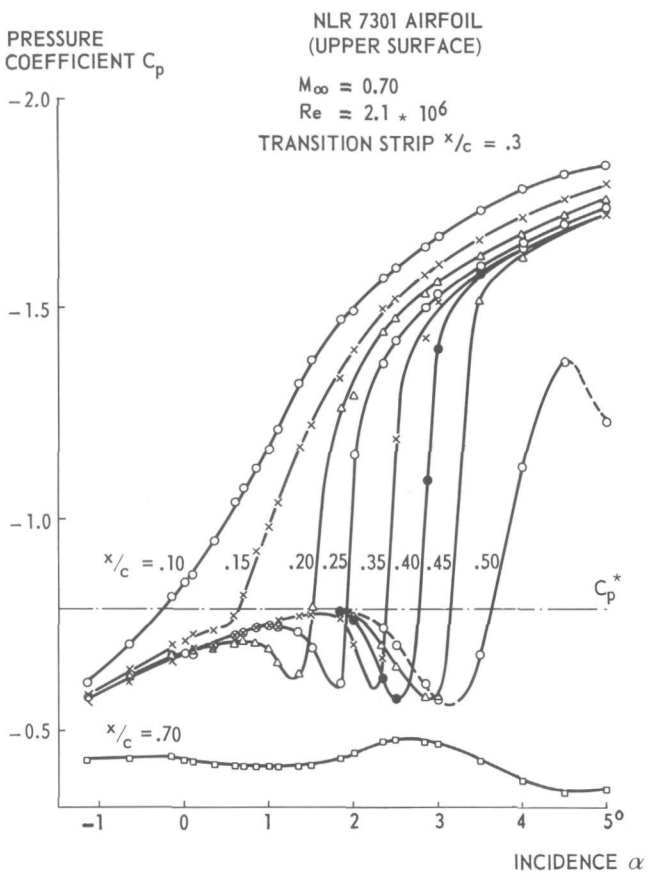

Fig. 11.2 Steady pressures at constant chordwise positions as a function of incidence in a transonic flow with shock wave.

The diagram for the transonic flow condition with a shock (Fig. 11.2) shows that the passage of the shock wave across a fixed point on the airfoil surface gives rise to a sudden jump in the curves of the local pressure against incidence. As indicated schematically in figure 11.3, this implies that a quasi-steady, sinusoidal variation in incidence results no longer in a sinusoidal pressure perturbation, but in a pressure variation exhibiting periodical jumps at the instant the shock wave passes.

Quasi-steady pressures for a mean incidence of 3 degrees and an amplitude of 0.5 degrees have been derived from figure 11.2. They are plotted as a function of time in figure 11.4. The passage of the shock wave is felt only in a local region between 35 and 50 per cent of the chord. In spite of the strong nonlinearity of the pressures in

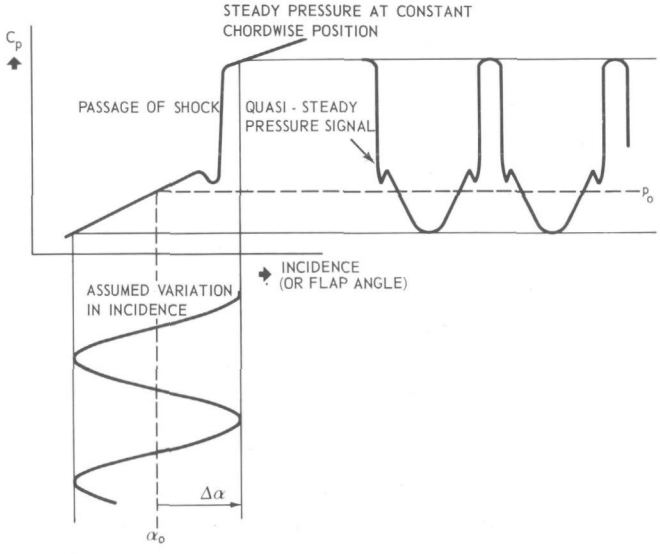

Fig. 11.3 Determination of quasi-steady pressure signals (transonic flow with shock wave).

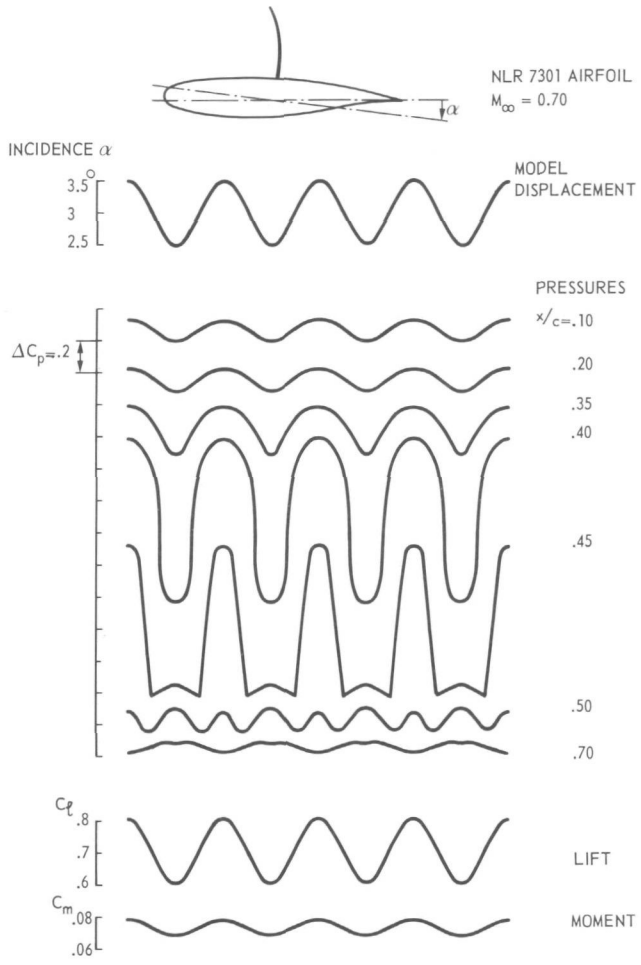

Fig. 11.4 Histograms of pressures and overall coefficients for a quasi-steady pitch motion.

this region, the corresponding overall lift and moment vary almost sinusoidally. Evidently, the nonlinearities introduced by the shock wave have only a local effect and do not influence the overall loads.

From the time histories of the pressure signals for the oscillating model (see figure 2.4), it becomes apparent that this conclusion remains valid for unsteady flow. The unsteady pressure signals show similar characteristics as the quasi-steady histograms, and also the unsteady lift varies almost sinusoidally. The overall moment shows irregularities, but its amplitude is very small and has been strongly amplified. From these results it can be concluded that in the present example the overall unsteady aerodynamic coefficients behave linearly for amplitudes of oscillation up to about at least 0.5 degrees, in spite of the presence of an oscillating shock wave.

11.2.2 Contribution of a shock wave to the overall aerodynamic loads

The phenomenon that the oscillating shock wave leads to an almost linear contribution to the overall unsteady airloads can be made plausible as follows. In flow patterns with a well-developed shock wave, the shock motion is observed to take place almost sinusoidally, and the amplitude of the shock motion appears to be almost proportional to the amplitude of the sinusoidal motion of the airfoil (see figures 10.19 and 10.20). This makes it possible to introduce the schematic model of figure 11.5, in which the change in pressure at a fixed point A is considered as generated by a sinusoidal shock-wave motion of amplitude x_o. As follows from the considerations in chapter 9, the local shock strength when the shock passes a point A located within the shock trajectory can be written as:

$$\left(p_2 - p_1\right)_{x_A} = \left(p_2 - p_1\right)_{x_s} + \Delta p(\omega, M_1, \partial M_1/\partial x)\; x_o e^{i\omega t} \; . \tag{11.2}$$

Here Δp denotes the variation in shock strength

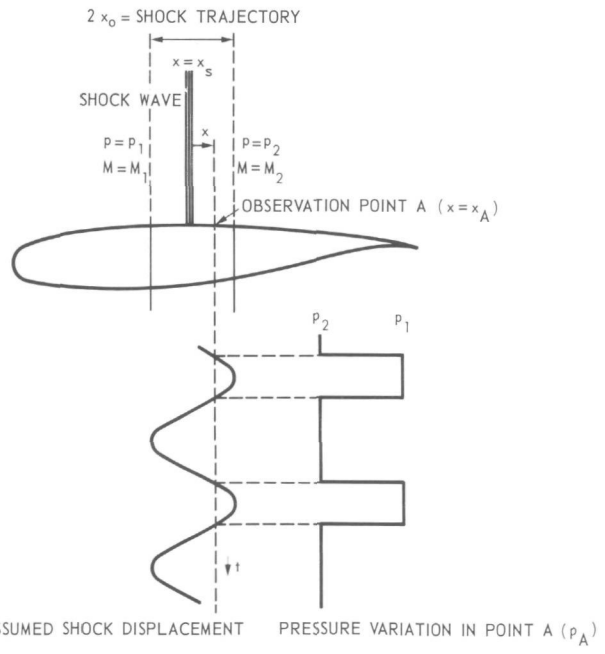

Fig. 11.5 Contribution of a periodical moving shock wave to the pressure signal in a fixed observation point.

during the shock-wave motion. For strong shock waves and small amplitude motions, the last term in the above expression can be discarded relative to $(p_2-p_1)_{x_s}$.

When the local pressure in point A is described as a function of time, a block-type signal occurs (see figure 11.5), of which the Fourier decomposition yields:

$$p(x_A) = \left[p_2(x_s) - \left(p_2 - p_1\right)_{x_s} \frac{1}{\pi} \arccos\{x_A/x_o\}\right] +$$

$$-\left(p_2 - p_1\right)_{x_s} \left[\frac{2}{\pi} \sin\{\arccos\{x_A/x_o\}\} \cos\omega t + \right.$$

$$+ \frac{1}{\pi} \sin\{2 \arccos\{x_A/x_o\}\} \cos 2\omega t +$$

$$+ \frac{3}{2\pi} \sin\{3 \arccos\{x_A/x_o\}\} \cos 3\omega t +$$

$$\left. + - - - - \right] \quad , \qquad (11.3)$$

where $|x_A| \leq x_o$.

The corresponding distributions of the first Fourier components along the trajectory of the shock motion are shown in figure 11.6. The distribution of the mean value illustrates that the pressure jump as occurring in steady flow

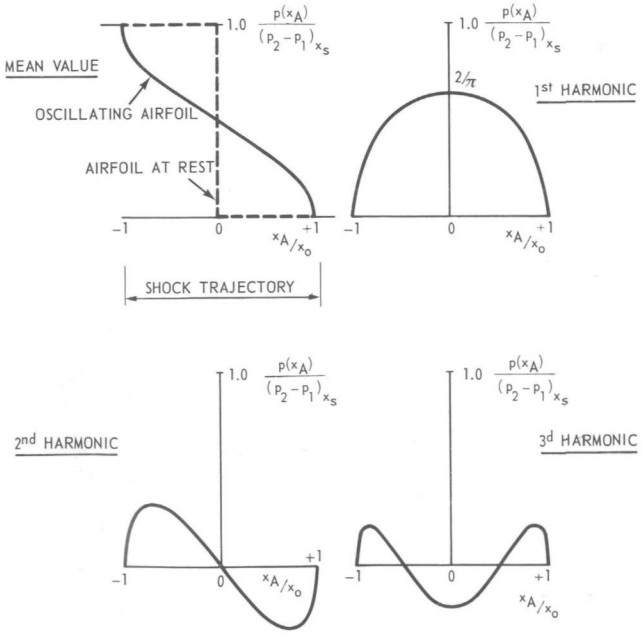

Fig. 11.6 Distribution of the first four Fourier components of the unsteady airload due to an oscillatory shock-wave motion.

is spread out over the shock trajectory as a consequence of the oscillatory motion of the shock wave. The distribution of the Fourier component with the same frequency as the airfoil motion has a maximum value of $2/\pi$ times the steady pressure jump $(p_2-p_1)_{x_s}$. Integration of the various components over the shock trajectory, to obtain the contributions to the overall lift and moment, learns that the lift contains only a contribution of the fundamental frequency. The moment contains, however, also a term like

$$\left(p_2 - p_1\right)_{x_s} x_o^2 \cos 2\omega t \quad .$$

Thus, it can be expected that the effects of the second harmonic first show up in the unsteady moment and not in the lift.

From the considerations given above, it also follows that measuring the first Fourier component of the pressure signals, as is done in the present tests via the tubing system, gives after chordwise integration a correct value of the unsteady lift. As far as the moment is concerned, the second harmonic of order x_o^2 cannot be distinguished.

11.3 SPECIAL FLOW CONDITIONS

In the present investigation it was found that flow conditions in which a small change in incidence (or flap angle) is followed by a rather abrupt change in a substantial part of the flow field can be traced easily by considering the behaviour of the steady aerodynamic coefficients. In particular the behaviour of the moment coefficient appears to be an excellent indicator for linearity, as will be illustrated with some examples.

11.3.1 "Shock-free" flow

Figure 11.7 shows the steady-lift and moment coefficient of the NLR 7301 airfoil as a function of incidence in the neighbourhood of the

"shock-free" design condition. Besides the measured data, this figure also contains the theoretical curves calculated with the finite-difference method of Bauer, Korn, and Garabedian (Ref. 116), who include the effect of thickness and incidence but not the viscous effects.

It appears that the rather abrupt change in the pressure distribution around the design condition is reflected in the calculated moment curve by a nonlinear behaviour between 0 and 2 degrees of incidence. In contrast herewith, the calculated lift curve shows that, for inviscid theory, a linear relation is found between lift and incidence. In other words, nonlinearities in the flow pattern do not show up in the quasi-steady lift coefficients. Evidently, the aerodynamic moment is much more sensitive to the details of the pressure distribution than the overall lift.

In a qualitative sense one can say that, until flow separation occurs, the steady aerodynamic coefficients as measured with a transition strip show about the same characteristics as those predicted by the theory. The data obtained with natural transition show a much deeper local dip, especially in the moment curve, which has to be attributed to a large extent to the rapid variation in the location of the transition point (see figure 10.23). Quantitatively, there is a large discrepancy between the theoretical and the experimental results of figure 11.7. This discrepancy should be attributed to the effect of the boundary layer, which in the transonic regime is very important. (A more detailed discussion of these differences is given in chapter 13.)

It is of interest to note that the slope of the moment curves (Fig. 11.7) becomes negative in a small range of incidences near the "shock-free" flow condition. In principle, this phenomenon may cause a self-exciting oscillation of limited amplitude. Whether this occurs in reality will largely depend on the elastic and inertia properties of the specific structure under consideration. Therefore, no conclusion can be inferred from this without a proper (nonlinear) calculation of the aeroelastic characteristics of this structure. Another uncertainty in this respect is whether the negative slope in the measured moment curve remains present for full-scale values of the Reynolds number.

From the observations of the quasi-steady aerodynamic coefficients, it can be concluded that a nonlinear behaviour of the aerodynamic moment can be expected for the particular condition of "shock-free" flow. For unsteady flow, this behaviour is confirmed by the time histories of the local pressures and the corresponding aerodynamic loads recorded while the airfoil was oscillating (Fig. 11.8). These recordings indeed show that

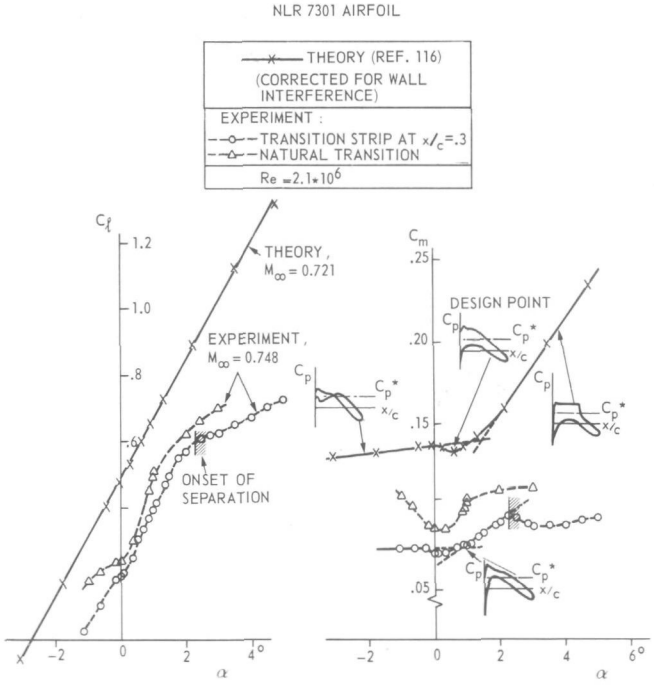

Fig. 11.7 Steady lift and moment coefficients as a function of incidence at the design Mach number.

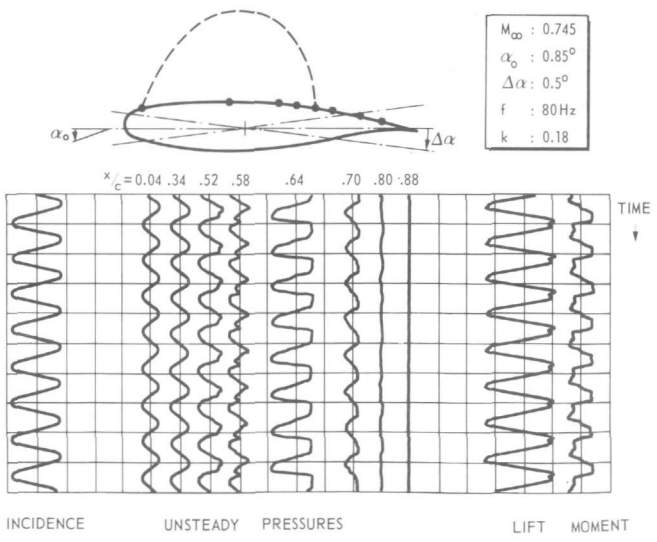

Fig. 11.8 Unsteady pressure signals for the NLR 7301 airfoil oscillating around its design condition.

the pressures are nonlinear over a substantial section of the chord. Also the overall moment exhibits a nonlinear behaviour, while the resulting lift is less influenced.

11.3.2 Flow with a double shock

A second example of a nonlinearity can be traced from the behaviour of the aerodynamic coefficients for the NLR 7301 airfoil at $M_\infty = 0.7$ (Fig. 11.9). Again it appears that in theory a linear relationship exists between lift and incidence, independent of the details of the flow or the presence of shock waves. The calculated aerodynamic moment shows a relatively strong change in slope in a small range of incidences between 2 and 3 degrees. This rapid change in slope is associated with a drastic change in flow pattern; at $\alpha \approx 2.5$ degrees, a flow pattern with even two shock waves behind each other occurs. Outside this range, linearization over practical ranges of incidence variations (say in the order of 0.5 degrees) seems to be possible again.

The measured data in figure 11.9 follow the trends predicted by the inviscid theory in a qualitative sense. Quantitatively, there are large deviations again, resulting from viscous effects (see also chapter 13). The bulge in the measured lift curve between -0.5 and 2.5 degrees of incidence is caused (as shown in reference 117) by a shift in the transition point of the boundary layer. In this range the shock wave is located upstream of the transition strip at 30 per cent of the chord, which causes transition ahead of this strip.

The results in figure 11.9 show that for practical purposes linearization is possible, with the exception of a small range that can be determined from the behaviour of the moment curve.

11.3.3 Flow around an airfoil with flap

The final example of a special flow condition for which linearization is not justified concerns an airfoil with flap. This condition occurs when a well-developed supersonic region

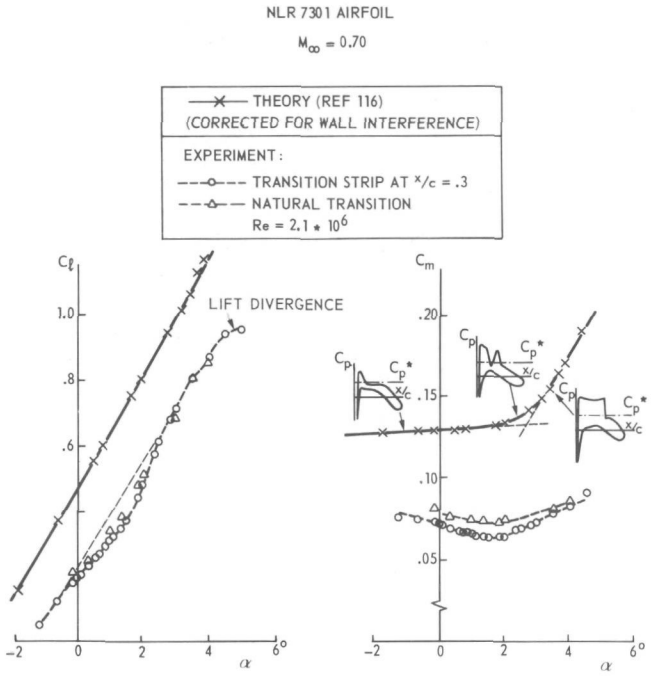

Fig. 11.9 Steady lift and moment coefficients as a function of incidence in transonic flow.

extends over a part of the flap. Then the change in airfoil contour at the leading edge of the flap leads to widely different flow patterns occurring during one cycle of oscillation (Fig. 11.10). A fan of expansion waves is formed at one side, terminated by a normal shock wave, while simultaneously at the other side a lambda shock is generated. The flow pattern is complicated further by a flow separation near the trailing edge. The

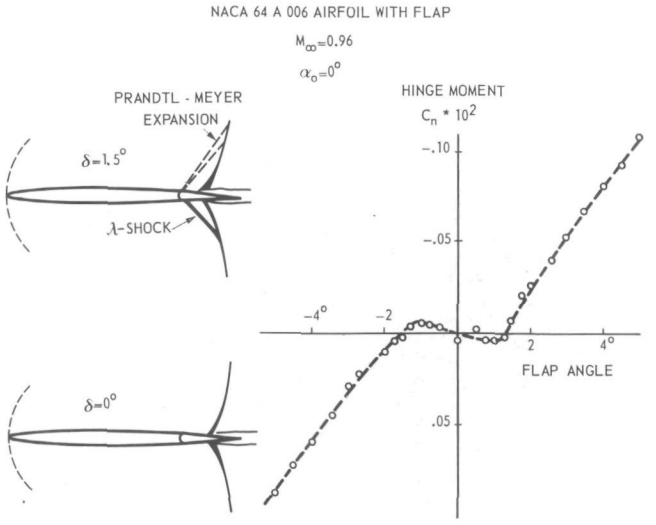

Fig. 11.10 Special flow condition for an airfoil with flap, which shows a strongly nonlinear behaviour.

steady hinge moment as a function of flap angle, shown also in figure 11.10, reveals that the slope of the hinge moment is negative for flap angles between +1 and -1 degrees. This behaviour of the hinge moment is one of the conditions for which in practice self-exciting oscillations of limited amplitude of control surfaces (so-called aileron buzz) have been encountered.

11.4 CONCLUDING REMARKS

The considerations on the possibility of linearization in quasi-steady flow indicate that the normal force allows a linearized treatment around a given mean position of the airfoil, at least as long as the flow remains attached and other severe viscosity effects are absent. The moment, being more sensitive to the details of the pressure distribution, shows an essential nonlinear character in only relatively small ranges of incidence or flap angle. Beyond these ranges, linearization around a few suitably chosen mean positions of the airfoil is possible. This contrasts with the subsonic and supersonic flow regimes, where the unsteady-flow problem can be treated independently of the mean position.

In order to select the mean positions in transonic flow and in order to locate the nonlinear ranges, use can be made of measured or calculated steady aerodynamic coefficients. In this respect, the calculation method for steady transonic flow of Bauer, Korn, and Garabedian (Ref. 116) and its extended version, which includes the effect of the boundary layer (Ref. 118), can form a useful tool. It may be expected that the conclusions for quasi-steady flow can be extended to unsteady flow. For a definite answer, however, further insight is needed in the way in which the nonlinear regions change with frequency.

In the considerations given above, the aeroelastician was assumed not to be interested in the detailed nonlinear behaviour of the pressures, as for instance introduced by shock-wave oscillations. One may, however, think of problems (such as panel flutter) in which one is interested primarily in the local behaviour of the pressures. Here the linear behaviour of the overall coefficients described above is of no avail.

PART IV THE CURRENT STATUS OF UNSTEADY FLOW THEORY AND EVALUATION OF SOME NEW METHODS FOR UNSTEADY TRANSONIC FLOW

12 REVIEW OF CALCULATION METHODS FOR TWO - DIMENSIONAL UNSTEADY FLOW

12.1 CLASSIFICATION OF THE VARIOUS METHODS

During the last few years, quite a number of calculation methods for high-subsonic and transonic flow have been developed, which take into account the interaction between the steady and the unsteady flow fields and - if shock waves are present - also the effect of the periodic shock-wave motion. A summary of these new methods is given in table 6, while the equations forming the basis of the various methods are collected in figure 12.1. This figure shows the equations obtained in successive stages of approximation of the full Navier-Stokes equations. For completeness, also the corresponding equations for steady flow are given.

Solving the full Navier-Stokes equations, together with suitable turbulence models, is certainly the most accurate way of solving a fluid-flow problem, but also the most complicated one. Recently, the first successful computations for steady transonic flow, based on these equations, were reported by Deywert et al. (Refs. 146-148). Their computations required an enormous amount of computer time (up to 10 hours on a CDC 7600 computer!), which indicates that calculations of this type are still far from routine application. Similar attempts for unsteady flow are just beginning to be explored (Ref. 149).

The most advanced calculation methods now available for unsteady flows (Magnus and Yoshihara, Refs. 119, 120; Beam and Warming, Ref. 122; Laval, Ref. 123; and Lerat and Sidès, Ref. 124) are based on the Euler equations (12.1), which follow from

TABLE 6

Review of calculation methods for 2-D high subsonic and transonic flow

	EQUATIONS SOLVED	AUTHOR(S)	YEAR	REF.	METHOD OF SOLUTION	REMARKS
METHODS FOR TRANSONIC FLOW WITH SHOCK WAVES	NAVIER – STOKES EQS.					NOT YET EXISTING
	EULER EQS.	◦ MAGNUS & YOSHIHARA	1974	119,120	FINITE DIFFERENCES	THE METHOD IS EXTENDED TO INCORPORATE VISCOUS EFFECTS (REF. 121)
		◦ BEAM & WARMING	1974	122	FINITE DIFFERENCES	–
		◦ LAVAL	1975	123	FINITE DIFFERENCES	–
		◦ LERAT & SIDÈS	1977	124	FINITE DIFFERENCES	–
	FULL POTENTIAL EQ.	◦ ISOGAI	1977	125	FINITE DIFFERENCES	–
	TRANSONIC SMALL-PERTURBATION EQ.	◦ BALLHAUS & LOMAX	1974	126	FINITE DIFFERENCES	–
		◦ BALLHAUS & STEGER	1975	127	FINITE DIFFERENCES	LOW-FREQUENCY APPROX.
		◦ KRUPP & COLE	1976	128	FINITE DIFFERENCES	LOW-FREQUENCY APPROX.
		◦ CHAN & CHEN	1977	129	FINITE ELEMENTS	–
	LINEARIZED TRANSONIC SMALL-PERTURBATION EQ.	◦ EHLERS	1973	130	FINITE DIFFERENCES	–
		◦ TRACI, FARR & ALBANO	1975	131	FINITE DIFFERENCES	LOW-FREQUENCY APPROX.
		◦ CHAN & BRASHEAR	1975	132	FINITE ELEMENTS	–
METHODS FOR NEAR SONIC FLOW ($M_\infty \approx 1$) WITHOUT SHOCK WAVES	LINEARIZED TRANSONIC SMALL-PERTURBATION EQ.	◦ STAHARA & SPREITER	1973	133	LOCAL LINEARIZATION	–
		◦ ISOGAI	1974	134,135	LOCAL LINEARIZATION	–
		◦ KIMBLE & WU	1974	136	LOCAL LINEARIZATION	–
		◦ DOWELL & PARK	1975	137,138	LOCAL LINEARIZATION	–
METHODS FOR HIGH SUBSONIC FLOW ($M_\infty \leq M^*$)	LINEARIZED TRANSONIC SMALL-PERTURBATION EQ.	◦ ZWAAN	1968	139	INTEGRAL METHOD	–
		◦ NIXON	1974	140,141	INTEGRAL METHOD	–
		◦ ISOGAI	1976	142	INTEGRAL METHOD	–
	EQ. FOR SUBSONIC LINEAR LIFTING-SURFACE THEORY	◦ TIJDEMAN & ZWAAN, ROOS	1974	143,144	INTEGRAL METHOD	LOCAL MACH NUMBER CORRECTION
		◦ GIESING, KALMAN, RODDEN	1976	145	INTEGRAL METHOD	LOCAL MACH NUMBER CORRECTION

DECREASING DEGREE OF APPROXIMATION

COMPLETE

NAVIER-STOKES EQUATIONS

NO VISCOSITY

EULER EQUATIONS:

$$\frac{\partial}{\partial t}\begin{Bmatrix}\rho\\ \rho U\\ \rho V\\ e\end{Bmatrix} + \frac{\partial}{\partial x}\begin{Bmatrix}\rho U\\ \rho U^2+p\\ \rho UV\\ U(e+p)\end{Bmatrix} + \frac{\partial}{\partial y}\begin{Bmatrix}\rho U\\ \rho UV\\ \rho V^2+p\\ V(e+p)\end{Bmatrix} = 0$$

with $e = (\gamma-1)^{-1} p + \frac{1}{2}\rho (U^2+V^2)$ (12.1)

$\frac{\partial V}{\partial x} - \frac{\partial U}{\partial y} = 0$

$p\rho^{-\gamma} = \text{constant}$

$\rightarrow$ $U = U_\infty + \Phi_x$, $V = \Phi_y$

IRROTATIONAL; ISENTROPIC

FULL POTENTIAL EQUATION:

$$(a^2-U^2)\Phi_{xx} + (a^2-\Phi_y^2)\Phi_{yy} - 2U\Phi_y\Phi_{xy} - 2U\Phi_{xt} - 2\Phi_y\Phi_{yt} - \Phi_{tt} = 0$$

with $a^2 = a_\infty^2 - (\gamma-1)\left[U_\infty\Phi_x + \Phi_t + \frac{1}{2}(\Phi_x^2+\Phi_y^2)\right]$ (12.2)

small perturbations $\rightarrow$

SMALL THICKNESS, INCIDENCE AND AMPLITUDE

TRANSONIC SMALL-PERTURBATION (TSP) EQUATION:

$$(1 - M_\infty^2 - M_\infty^2 \frac{\gamma+1}{U_\infty}\Phi_x)\Phi_{xx} + \Phi_{yy} - 2\frac{M_\infty^2}{U_\infty}\Phi_{xt} - \frac{M_\infty^2}{U_\infty^2}\Phi_{tt} = 0$$ (12.3)

non-uniform steady flow + small unsteady perturbations $\rightarrow$

$\Phi = \Phi_o + \phi e^{i\omega t}$

$k = \frac{\omega \ell}{U_\infty}$; $\ell = 1$

AMPLITUDE << THICKNESS AND INCIDENCE

LINEARIZED TRANSONIC SMALL-PERTURBATION EQUATION:

$$(1 - M_\infty^2 - M_\infty^2 \frac{\gamma+1}{U_\infty}\Phi_{ox})\phi_{xx} + \phi_{yy} - 2ikM_\infty^2\phi_x + k^2M_\infty^2\phi - (\gamma+1)\frac{M_\infty^2}{U_\infty}\Phi_{oxx}\phi_x = 0$$ (12.4)

HIGH FREQUENCY: $k >> |1-M_\infty|$

CLASSICAL TRANSONIC EQUATION:

$$\phi_{yy} - 2ikM_\infty^2\phi_x + k^2M_\infty^2\phi = 0$$ (12.5)

$M_\infty << 1$ or $M_\infty >> 1$

EQUATION FOR SUBSONIC AND SUPERSONIC LINEAR LIFTING-SURFACE THEORY:

$$(1-M_\infty^2)\phi_{xx} + \phi_{yy} - 2ikM_\infty^2\phi_x + k^2M_\infty^2\phi = 0$$ (12.6)

Fig. 12.1 Basic equations of the various calculation methods for two-dimensional flow

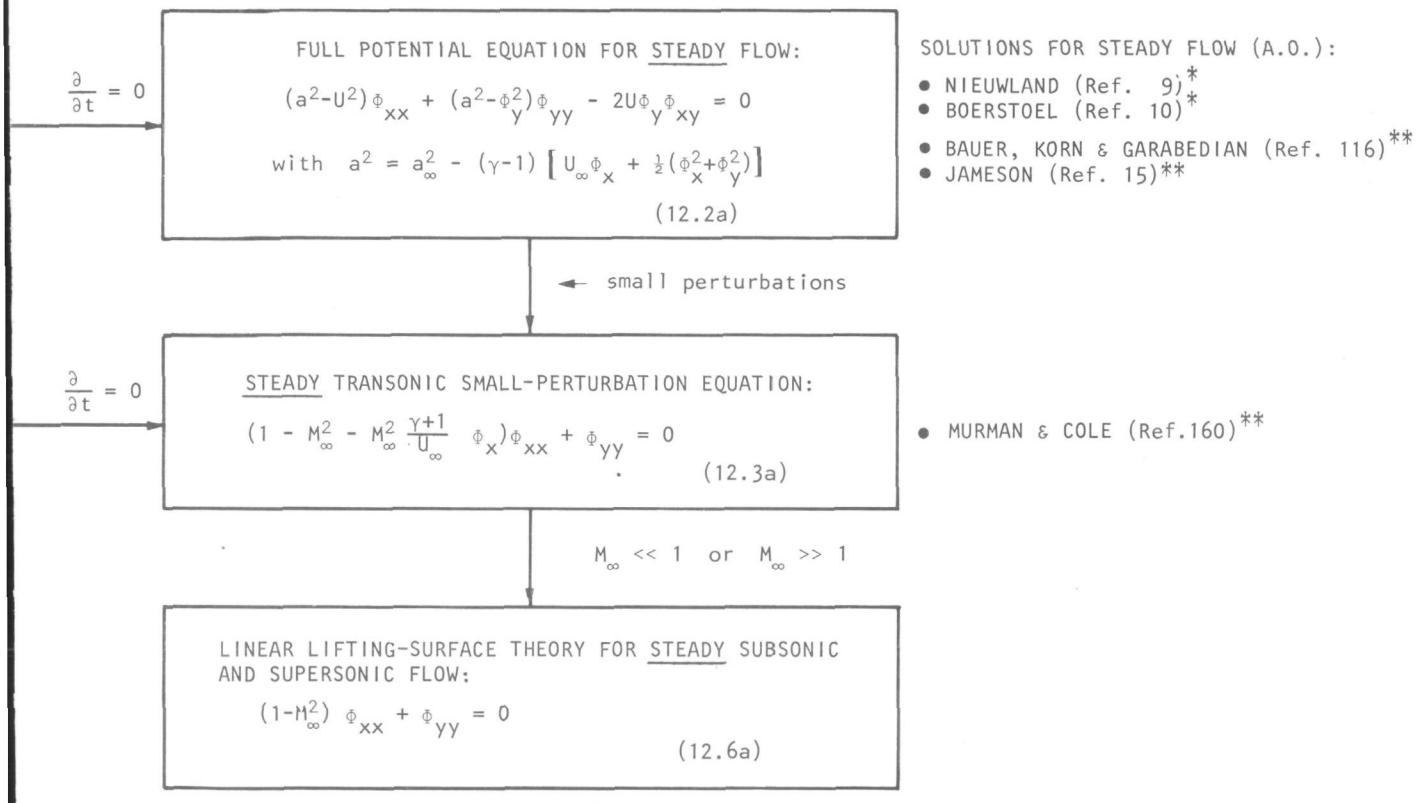

* via hodograph transform

** finite-difference methods

the Navier-Stokes equations by assuming the flow to be inviscid. This implies that the effect of the boundary layer is not included, which may lead to a change in effective airfoil contour and, thus, to a change in circulation, shock strength, and shock position. This drawback is removed to a certain extent in an engineering type of procedure described by Magnus and Yoshihara (Ref. 121), who included the displacement effect of the boundary layer in an approximative way.

A further simplification of the unsteady-flow equations is obtained if one assumes the flow to be isentropic and irrotational. This has the advantage that the flow problem can be described by a potential equation with only one unknown. A serious drawback, however, is that the shock strength included inherently in the potential theory is no longer correct. As pointed out by Van der Vooren and Slooff (Ref. 150), in potential flow the velocity (or pressure) jump across a normal shock wave is larger than that derived from the Rankine-Hugoniot relations (see figure 12.2). The difference increases with Mach number and, as a consequence, potential theory is limited to weak and moderately strong shock waves, for which the upstream Mach number remains less than about 1.3.

So far, only one method is reported in which the full potential equation (12.2) is solved (Isogai, Ref. 125). In the other methods, use is made of more simplified versions of this equation. Ballhaus and his colleagues (Refs. 126, 127), Krupp and Cole (Ref. 128), and Chan and Chen (Ref. 130) developed methods to solve the transonic small-perturbation equation (12.3), which is based on the additional assumption that the steady and the unsteady perturbations of the flow field remain small. These methods are therefore limited to thin airfoils and small amplitudes of oscillation. In addition, the description of the flow is less accurate near locations where the flow has to adjust itself to abrupt changes in surface slopes, such as the leading edge of the airfoil or the leading edge of a deflected flap.

As indicated in figure 12.1 (and discussed earlier in section 2.2.3), the transonic small-perturbation equation can be linearized by considering the unsteady flow field as a small perturbation superimposed upon a non-uniform mean steady flow field. The resulting linear equation (12.4) possesses spatially varying coefficients, which depend on the velocity distribution of the mean steady flow field. This steady flow field has to be known either from steady computations or from experiment. This implies that the effect of shock waves can be included only, if the shocks do exist already in the steady flow field. From the methods based on the linearized transonic small-perturbation equation (Refs. 130-142), only those of Ehlers (Ref. 130), Traci, Farr and Albano (Ref. 131), and Chan and Brashear (Ref. 132) are able to take the effect of shock waves into account. The other methods are limited to near-sonic flows without shock waves or to subcritical flows (see table 6).

As a final step in the successive stages of approximation, the potential equation (12.4) can be reduced to the classical transonic-flow equation (12.5), applied by Landahl (Ref. 24), or to equation (12.6), used in linearized lifting-surface theory. The latter theory, together with a semi-empirical correction for the effect of the mean steady flow field, is used in the last two methods, given in table 6 (Refs. 143-145). The methods based on the classical transonic-flow equation (12.5) are not considered here, since they are only applicable in the case of reduced frequencies, which normally are too high for practical applications in aeroelastic problems.

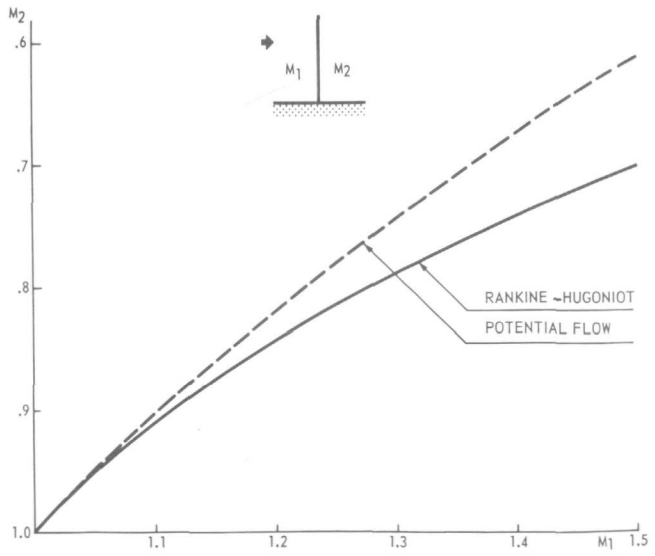

Fig. 12.2 Relation between the Mach number upstream and downstream of a normal shock wave (from Ref. 150).

In the subsequent sections of this chapter, the various calculation methods are briefly described. This description is preceded by an outline of linearized subsonic lifting-surface theory, which is in widespread use for aeroelastic investigations and forms an important basis of comparison for the results of the present investigation. Moreover, this theory is used in the semi-empirical method for high-subsonic flow developed at NLR and described in section 12.3.

12.2 LINEARIZED SUBSONIC LIFTING-SURFACE THEORY

12.2.1 The integral equation relating downwash and load distribution

The essence of the majority of the methods used in subsonic lifting-surface theory is that the sinusoidally oscillating thin airfoil is represented by a sheet of pressure doublets, with their axes normal to the flow (Fig. 12.3). In this way, the potential equation can be transformed into an integral equation relating the known downwash distribution, w, at the airfoil surface (assumed at y = 0) to the unknown load distribution ΔC_p. For two-dimensional flow, this equation reads:

$$w(x)/U_\infty = \frac{1}{8\pi} \oint_0^1 K(x_o;k,M_\infty)\ \Delta C_p(\xi)\ d\xi \ , \qquad (12.7)$$

with $x_o = x - \xi$.

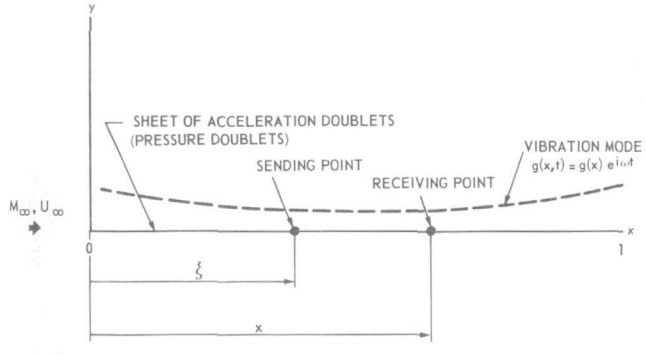

Fig. 12.3 Representation of an oscillating airfoil in linearized subsonic lifting-surface theory.

The complicated Kernel function $K(x_o;k,M_\infty)$ (for more details, see references 25, 27, 151, 152) can be interpreted in a physical sense as an aerodynamic influence function, giving the downwash induced in point x due to a pressure jump of unit strength in point ξ. This influence function depends on the reduced frequency, k, the free-stream Mach number, M_∞, and the distance between the sending and receiving point, x_o. The downwash, w(x), is determined by the requirement that at each instant the flow is tangential to the surface of the oscillating airfoil. If the airfoil oscillation is described by

$$g(x,t) = g(x)\ e^{i\omega t} \ , \qquad (12.8)$$

the tangency condition yields:

$$w(x)/U_\infty = \partial g(x)/\partial x + ik\ g(x) \ , \qquad (12.9)$$

where k is the reduced frequency, based on a reference length $\ell = 1$.

In the literature, several methods have been published to solve the integral equation (12.7), the main difference between the various methods being the way in which the numerical integrations are performed. In the context of the present review, the Kernel-function method and the Doublet-Lattice method, nowadays being the most popular methods, will be briefly described. For details of the other methods, reference is made to the well-known textbooks on aeroelasticity (Refs. 25, 27, 151, 152).

12.2.2 The Kernel-function method

In the Kernel-function method, it is assumed that the unknown pressure distribution appearing in the integral equation (12.7) can be described by a series of preselected loading functions:

$$\Delta C_p(x) = \sum_{j=0}^{N} a_j\ H_j(x) \ . \qquad (12.10)$$

The functions $H_j(x)$ are chosen in such a way that

each function satisfies the edge conditions known for the load distribution on a flat plate, i.e. the root singularity at the leading edge and the Kutta condition at the trailing edge (see the example in figure 12.4). In the case of a flap, other loading functions have to be added to take care of the singular behaviour of the load distribution at the leading edge of the flap.

As a next step, (12.10) is substituted in (12.7), and the integrals

$$K_{ij} = \oint_0^1 H_j(\xi) K(x_i - \xi; k, M_\infty)\, d\xi \qquad (12.11)$$

are evaluated for a set of N suitably chosen points x_i, the so-called collocation points. By prescribing the downwash w_i in the N collocation points, according to (12.9), a set of N simultaneous algebraic equations is obtained, which has to be solved for the unknown coefficients a_j:

$$w_i/U_\infty = \sum_j K_{ij}(k, M_\infty)\, a_j \,. \qquad (12.12)$$

The most laborious part of the method is the proper evaluation of the integrals K_{ij} (12.11), which can be interpreted as the downwash in point x_i due to a chordwise load distribution $H_j(x)$.

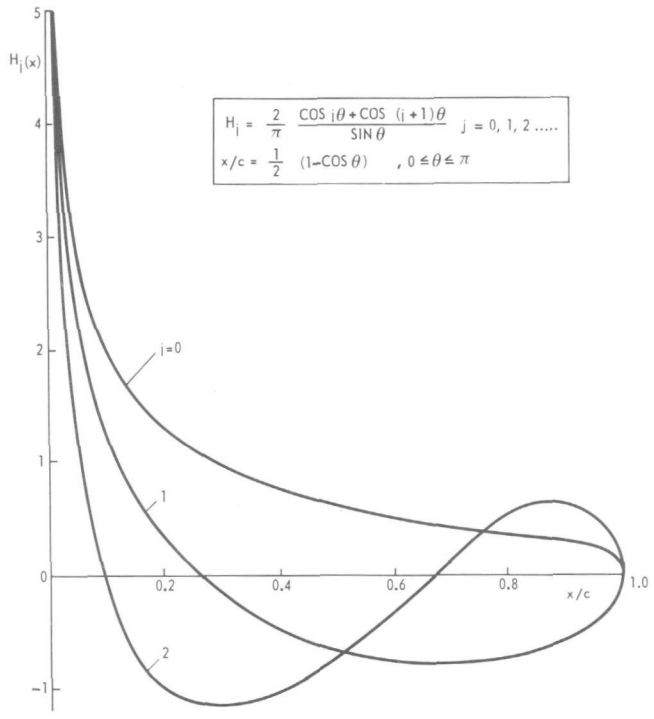

Fig. 12.4 Example of pressure loading functions used in the Kernel-function method.

12.2.3 The Doublet-Lattice method

In the Doublet-Lattice method, developed originally by Albano and Rodden (Ref. 153), the integral equation (12.7) is discretized by dividing the airfoil into a large number of elements. At the quarter-chord point of each element, a pressure doublet of yet unknown strength is placed, while at the three-quarter-chord point of each element a control point is chosen. By equalizing for each control point the downwash introduced by all doublets to the downwash according to (12.9), the following set of algebraic equations is obtained:

$$w_i/U_\infty = \sum_j D_{ij}(k, M_\infty)\, \Delta C_{p,j} \,, \qquad (12.13)$$

where D_{ij} is the aerodynamic influence coefficient, representing the downwash in the control point of element i due to a doublet of unit strength at the quarter-chord point of element j. From (12.13) the strength of the doublets and, hence, of the pressure coefficients $\Delta C_{p,j}$ can be computed.

An important difference between the Kernel-function method and the Doublet-Lattice method is that the aerodynamic influence coefficients in the first method involve complete chordwise pressure loading functions, whereas in the second method a point-to-point relation is used. This local relationship makes the Doublet-Lattice method well-suited for the introduction of semi-empirical effects, such as the effect of local Mach number, to be discussed in the next section.

12.3 METHODS FOR HIGH-SUBSONIC FLOW

12.3.1 Local-Mach-number corrections in linearized lifting-surface theory

A relatively simple procedure to introduce

the effect of the non-uniformity of the steady flow field in an approximative way has been developed at NLR (Tijdeman and Zwaan, Ref. 143; Roos, Ref. 144). Inspired by the graphical experiments described in section 8.3, the idea was conceived to consider the doublets in linearized lifting-surface theory as elements emitting waves that induce the downwash in the control points. Then the effect of the non-uniform main flow can be introduced by making the influence coefficients, D_{ij}, of equation (12.13) functions of the local Mach number between the sending point and the receiving point. For simplicity, D_{ij} is made a function of M_{ij}, which is the local Mach number averaged between point i and point j. Accordingly, relation (12.13) becomes:

$$w_i/U_\infty = \sum_j D_{ij}(k_{ij},M_{ij})\ \Delta C_{p,j} \ , \qquad (12.13a)$$

in which

$$M_{ij} = R\ \{M_{ij}(\text{at the surface}) - M_\infty\} + M_\infty , \qquad (12.13b)$$

and

$$k_{ij} = kM_\infty/M_{ij} \ . \qquad (12.13c)$$

The constant, R, in (12.13b) is a relaxation factor ($0 < R < 1.0$) that is introduced to take care of the fact that the waves propagate along the surface of the airfoil as well as along paths at a certain distance away from the airfoil surface (see figure 8.13). This implies that the average "head wind" of the upstream-propagating waves is somewhere between the velocity at the airfoil surface and the free-stream velocity. Relation (12.13c) indicates that the reduced frequency varies locally with Mach number.

For practical applications, the values of M_{ij} can be determined from either experimental or theoretical steady pressure distributions. It was found at NLR that satisfactory results are obtained if the relaxation factor R is set equal to 0.7 (Roos, Ref. 144). This value agrees with the relaxation factor that, for the same reason, was used in section 10.4 for the explanation of the phase shift between the shock-wave motion and the pitching motion of the NLR 7301 airfoil.

Apart from the semi-empirical correction of the influence coefficients, also a local-Mach-number effect is introduced in the boundary condition, by changing (12.9) into

$$w_i/U_\infty = \{M_i/M_\infty\}\ \{\partial g(x_i)/\partial x\} + ik\ g(x_i) \ , \qquad (12.14)$$

where M_i denotes the local Mach number in the control point i. This local correction of the boundary condition was applied earlier by Ashley and Rowe (Ref. 154) and by Rowe, Winther and Redman (Ref. 155), without further corrections, however, of the aerodynamic influence functions.

Recently, Giesing, Kalman and Rodden (Ref. 145) reported a modification of the NLR approach. The basic idea of their method is to transform the distance between the sending and the receiving point, depending on the time required by the pressure signals to travel that distance.

12.3.2 Methods based on the linearized transonic small-perturbation equation

Calculation methods for unsteady high-subsonic flow, based on the linearized transonic small-perturbation equation (12.4), were developed by Zwaan (Ref. 139), Nixon (Refs. 140, 141), and Isogai (Ref. 142). Zwaan introduced the additional assumption that the local Mach number of the steady flow field only depends on the x-coordinate. By applying the matched-asymptotic-expansions technique, he obtained a solution for an airfoil with oscillating flap in high-subsonic and low-supersonic flow. Nixon and Isogai also solved equation (12.4) in an approximative way. Their methods should be considered as an extension of the well-known integral-equation methods for steady flow, as initiated by Oswatitsch (Ref. 156) and extended, among others, by Nixon and Hancock (Ref. 157).

The results obtained by all three authors demonstrate that in inviscid high-subsonic flow the thickness of an airfoil may have a considerable effect on the unsteady airloads. Nixon, for

instance, shows that the aerodynamic coefficients k_c and m_c (with the exception of the control-surface coefficient n_c) for an NACA 0012 airfoil with a trailing-edge flap of 40 per cent of the chord are 15 to 35 per cent larger than the corresponding linear values. The differences are largest for low values of the reduced frequency.

12.4 METHODS FOR NEAR-SONIC FLOW WITHOUT SHOCK WAVES

For Mach numbers near unity, the effect of airfoil thickness has been taken into account in the methods of Stahara and Spreiter (Ref. 133), Isogai (Refs. 134, 135), Kimble and Wu (Ref. 136), Dowell and Park (Refs. 137, 138). In all four methods, the linearized transonic small-perturbation equation (12.4) is solved by employing a concept analogous to the local linearization method developed for steady flow about twenty years ago by Spreiter and Alksne (Ref. 158).

For the unsteady case, calculated results are presented for a number of oscillating parabolic- and circular-arc airfoils with several thickness ratios. The examples clearly indicate that for low reduced frequencies ($k \approx 0.1$) thickness has an important influence, while for high reduced frequencies (k larger than 1) the results converge to the results that can be obtained with the linear transonic theory based on the classical, transonic equation (12.5). This latter behaviour could be expected already on the basis of the analysis given by Landahl (Ref. 24).

12.5 METHODS FOR TRANSONIC FLOW WITH SHOCK WAVES

12.5.1 General remarks

With the exception of the methods of Chan and Chen (Ref. 129) and Chan and Brashear (Ref. 132), all calculation methods developed recently for unsteady transonic flow with shock waves make use of a finite-difference technique for the solution of the unsteady-flow equations (see table 6). They can be considered as extensions of the well-established finite-difference methods for steady transonic flow (Refs. 11-15, 118, 159-161).

Concerning the finite-difference methods for steady flow, two different approaches can be distinguished: time-progressing methods (Ref. 159) and relaxation methods (Refs. 14, 116, 118, 160, 161). In the former approach, the time-dependent equations are used and the desired steady-flow condition is obtained asymptotically with a proper finite-difference procedure marching in time. The second approach is based on the steady-flow equations and the corresponding finite-difference analogue is solved by a relaxation process. As far as computer time is concerned, the latter methods are much more efficient than the time-progressing methods.

For the finite-difference methods for unsteady flow, also a choice can be made between time-progressing methods and relaxation methods. This choice depends largely on the type of unsteady equations considered. As pointed out by Beam and Warming (Ref. 122), time-progressing methods probably are most efficient for the non-linear time-dependent equations, i.e. the Euler equations, the full potential equation, and the transonic small-perturbation equation. For these equations, relaxation methods are less efficient since, in the unsteady case, one more dimension (time) is required than in steady flow. For the linearized transonic small-perturbation equation (small unsteady perturbations, superimposed upon a non-uniform main flow), the choice is less evident. According to Beam and Warming, relaxation schemes appear most promising if stationary sinusoidal motions are considered, whereas time-progressing methods seem to be better suited for the so-called indicial-function approach. In the latter approach, which is valid only for linear systems, a step change is imposed in the normal velocity component on the airfoil, which corresponds to the desired mode of vibration. The resulting aerodynamic response (indicial function) is computed as a function of time, and the required airloads for sinusoidal oscillations are

obtained by a Fourier transform of the indicial response.

12.5.2 Methods based on the Euler equations

As indicated in table 6, a number of methods have been produced that are based on the Euler equations. Beam and Warming (Ref. 122) considered small perturbations in a non-uniform steady flow and solved the corresponding unsteady Euler equations with a time-progressing method. They demonstrated the applicability of the indicial-function approach for a flat plate in compressible flow and showed further an example of a biconvex airfoil oscillating in pitch in transonic flow.

Magnus and Yoshihara solved the Euler equations without further assumptions concerning frequency or amplitude of oscillation. The boundary conditions are imposed along a contour coincident with the mean position of the airfoil surface. In reference 120, detailed unsteady pressure distributions are published for the NACA 64A410 airfoil performing oscillations in pitch around its midchord point. Similar results for the NACA 64A006 airfoil with flap were given in references 121 and 162. For the latter airfoil, also an approximative method was introduced to take the displacement effect of the boundary layer into account. All computations started with the steady-flow solution and were continued until a complete cycle of the periodic flow was obtained. This is a time-consuming process, in particular at low reduced frequency, where the shock wave exhibits large excursions. The first result given in reference 120 took about 7 hours on a CDC 7600 computer. After refinement of the computer program, this could be reduced to about 2 hours. It should be noted, however, that it was not intended to develop a method for routine use, but rather to generate some solutions that might reveal the nature of the flow or serve as test cases for more approximative but faster methods.

An approach very similar to that of Magnus and Yoshihara is followed by Laval. In reference 123 he presents an example of an oscillating biconvex airfoil with a periodically moving shock wave.

The complete Euler equations were solved also by Lerat and Sidès (Ref. 124). They used a time-dependent mapping technique, which has the advantage that the boundary conditions can be imposed on the airfoil contour in its actual position, rather than on some mean position. Lerat and Sidès presented unsteady pressure distributions on an NACA 0012 airfoil oscillating in pitch. The reduced frequency of this example is very high, and as a result the shock wave remains in an almost stationary position.

12.5.3 Methods based on the potential equation

Solutions of the full potential equation were reported by Isogai (Ref. 125), who used a time-progressing finite-difference technique and applied the tangential-flow condition on the airfoil contour in its mean position. Isogai presented numerical results for the NACA 64A006 airfoil with flap and for a supercritical airfoil developed by Bauer et al. (Ref. 118), which performs oscillations in pitch around its "shock-free" design condition. The latter examples show that the nonlinear behaviour of the airfoil in its design condition diminishes with increasing frequency.

The solution of the unsteady-transonic-flow problem as given by Ballhaus and Lomax (Ref. 126) is based on the transonic small-perturbation equation. In addition, they considered the low-frequency version of this equation, in which the term Φ_{tt} is put equal to zero. Computed results were given for impulsively started airfoils. Later on, the low-frequency method was extended to the lifting case (Ref. 163), and the efficiency of the method was increased considerably by the implementation of a very efficient algorithm developed by Ballhaus and Steger (Ref. 127) to solve the finite-difference equations.
In references 163 and 164, some results are shown for sinusoidally oscillating airfoils. In the second reference, a comparison is made between

results obtained with the small-perturbation equation in the low-frequency limit and results from the procedure of Magnus and Yoshihara, both applied to the pitching NACA 64A410 airfoil. The agreement is not very satisfactory, the main deficiency being the improper capture of the shock wave in the small-perturbation method. It must be noted, however, that the amplitudes of oscillation as applied in this comparative study were 2 degrees, which in transonic flow certainly cannot be considered as a small perturbation. Moreover, during a large part of a cycle of oscillation the Mach number just upstream of the shock wave on the NACA 64A410 example is larger than 1.3, which seriously violates the assumptions of potential flow (see section 12.1).

Ballhaus and Goorjian (Refs. 165, 166) published calculated results for the thinner NACA 64A006 airfoil with flap. Also for this airfoil comparisons were made with results of the method of Magnus and Yoshihara, and this time a much better agreement was achieved (see also chapter 13). In this respect, it is of interest to know that on a CDC 7600 computer the method of Ballhaus required 8 seconds per cycle of oscillation, whereas the procedure of Magnus and Yoshihara required 1500 seconds per cycle.

Recently, the method of Ballhaus et al. was extended with a "shock-fitting" procedure (Yu, Seebass and Ballhaus; Ref. 167), which means that the unsteady-shock relations are fed explicitly into the calculation process. This procedure increases further the efficiency of the original method, in which the shock wave evolves automatically as a part of the numerical solution.

Also Krupp and Cole (Ref. 128) formulated a finite-difference method for the low-reduced-frequency version of the transonic small-perturbation equation. They produced an interesting example of a plunging NACA 0012 airfoil, which shows a moving shock wave that disappears during a part of the cycle (type-B shock motion).

To conclude the description of finite-difference methods based on the transonic small-perturbation equation, also the work of Caradonna and Isom (Refs. 168, 169), should be mentioned. Although they derived and solved the small-perturbation equation appropriate for a helicopter rotor in forward flight, they gave also results of two-dimensional computations, showing a type-C shock-wave motion (Ref. 169). They obtained their solutions with a finite-difference scheme, which is an extension of the technique of Murman and Cole (Ref. 160) for steady flow.

As mentioned previously, a simplification of the transonic small-perturbation equation is obtained if the unsteady flow is considered as a small perturbation upon a known non-uniform steady flow field (Fig. 12.1). A finite-difference solution of the linearized small-perturbation equation was given by Ehlers (Ref. 130). Traci, Farr and Albano (Ref. 131) presented a method for the solution of a low-reduced-frequency approximation of the equation. In both methods, a relaxation technique is applied that is very similar to the one developed by Murman and Cole (Ref. 160). Both Ehlers and Traci et al. presented unsteady pressure distributions for an airfoil with oscillating flap.

A quite different approach to the solution of the transonic small-perturbation equation and the linearized version of it was followed by Chan and Chen (Ref. 129) and Chan and Brashear (Ref. 132), who used a finite-element method. Here the flow field is divided into a large number of small subregions (triangles, for instance). The velocity potential in each subregion is approximated by piecewise polynomials, and the polynomial coefficients in the various subregions are determined by a minimization procedure. An advantage of the method is the easy way of tayloring the airfoil contour and the shape of the shock wave. According to references 129 and 130, this method offers also the promise of a vast reduction in computation times and, therefore, certainly deserves further attention.

12.6 ROLE OF THE NLR RESULTS

From the review in the preceding sections, it is apparent that in the past few years con-

siderable progress is achieved in the computation of two-dimensional unsteady transonic flow. The investigations performed at NLR were just in time to support this development. The detailed experimental results for the NACA 64A006 airfoil, published previously in references 99, 100, and 170, were used as the basis for comparison in the majority of the theoretical and the semi-empirical methods developed recently. Calculated results for this configuration were published by Zwaan (NLR, Ref. 139), Roos (NLR, Ref. 144), Ehlers et al. (Boeing, Refs. 130, 171), Magnus and Yoshihara (General Dynamics, Refs. 121, 162), Chan et al. (Lockheed, Refs. 129, 132), Giesing, Kalman and Rodden (Douglas, Ref. 145), Ballhaus and Goorjian (NASA Ames, Refs. 165, 166), Isogai (National Aerospace Laboratory, Tokyo, Refs. 125, 141) and Traci, Farr and Albano (developed for the Air Force Flight Dynamics Laboratory, Ref. 131).

For the present author, this situation with its stimulating contacts created the opportunity to make a first evaluation of the capabilities of the new generation of calculation methods for unsteady flow (see chapter 13). At this moment the evaluation is limited to a conventional-type airfoil. In the near future, however, a further evaluation can be performed for the supercritical NLR 7301 airfoil, of which recently the first experimental results were released (Refs. 172, 173). Meanwhile, both the NACA 64A006 airfoil with flap and the NLR 7301 airfoil have been selected by the Structures and Materials Panel of AGARD as standard airfoils for the evaluation of theoretical methods for unsteady transonic flow.

13 EVALUATION OF SOME NEW CALCULATION METHODS FOR UNSTEADY TRANSONIC FLOW

13.1 INTRODUCTORY REMARKS

In this chapter, some of the new calculation methods for unsteady flow will be evaluated by comparing a number of results of calculations and measurements. Prior to these comparisons, however, a few remarks should be made concerning some possible sources of discrepancies. First, it is noted that the various theories may produce different results because different flow equations are involved (see figure 12.1). It is evident that decreasing the degree of approximation of the Navier-Stokes equations may result in less accurate results. The assumption of potential flow, for instance, leads to less accurate shock relations, while an additional assumption of small perturbations gives rise to less reliable results near the leading and trailing edge of the airfoil. As far as this last problem is concerned, serious difficulties can be foreseen for thick blunt-nosed airfoils, like the NLR 7301.

Another and often more important discrepancy between results of calculations, even if they are based on the same equations, occurs if so-called non-conservative finite-difference schemes are used. Only if the flow equations and the corresponding finite-difference schemes are brought in conservation form, the conservation of mass is assured across discontinuities (i.e. shock waves) in the flow field. In the absence of these discontinuities, the choice between conservative or non-conservative differencing is irrelevant, but, in order to obtain the correct value of the pressure jump across the shock wave, the conservative form is imperative. (For further details on this subject, see references 14 and 174.)

To illustrate the discrepancies that may be caused by the afore-mentioned sources, figure 13.1 shows a number of steady pressure distributions on the NACA 64A006 airfoil, calculated with different methods. The result of Magnus and Yoshihara (Ref. 121) can be considered as the most accurate solution of the inviscid-flow problem. The solution of the full potential equation (Bauer et al., Ref. 118) agrees very well with the one of Magnus and Yoshihara, at least if a conservative finite-difference scheme is used. Application of a non-conservative scheme leads to a weaker shock wave at a position too far upstream. Finally, the steady part of the solution of Traci et al. (Ref.

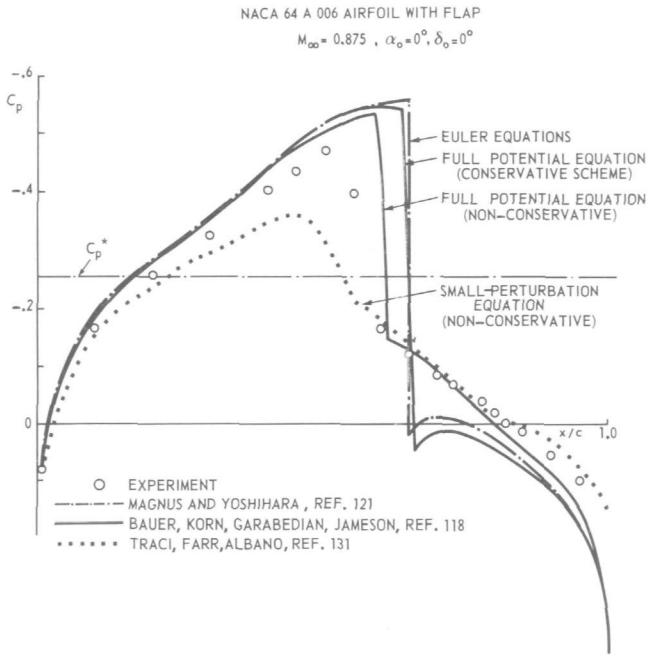

Fig. 13.1 Comparison of the steady-flow fields as predicted by a number of finite-difference methods.

131), which is based on a non-conservative treatment of the small-perturbation equation, deviates considerably from the other ones.

It is inevitable that discrepancies in the steady flow field as shown in figure 13.1 also show up in the unsteady results. It is, therefore, advisable to compare not only the unsteady results, but also the corresponding results of the calculations for the airfoil at rest.

A major source of discrepancy between theory and experiment is that all calculation methods developed so far for unsteady transonic flow deal with inviscid flow and thus neglect the boundary layer (except for a recent attempt in reference 121). Moreover, the experimental data are contaminated by tunnel-wall interference.

To gain some insight into the influence of the boundary layer, the discussion of the unsteady results is preceded by a consideration of quasi-steady results for both the NACA 64A006 and the NLR 7301 airfoil. Considering the quasi-steady case first has the great advantage that for the comparative calculations use can be made of the existing routine method for steady flow, which includes a procedure to take the boundary layer into account (Ref. 118). In addition, for the steady wind-tunnel tests a reasonable estimate can be given of the amount of interference with the slotted tunnel walls, a situation which has not yet been achieved for the unsteady measurements.

13.2 COMPARISONS BETWEEN THEORY AND EXPERIMENT IN STEADY AND QUASI-STEADY FLOW

13.2.1 Correction for tunnel-wall interference

To determine the amount of wall interference in the steady wind-tunnel tests, it was assumed that the main effect of the tunnel walls is a change in effective incidence, which for the NLR Pilottunnel can be taken as (Ref. 175):

$$\Delta\alpha = C\, C_\ell \text{ (degrees)}, \qquad (13.1)$$

where C_ℓ is the steady lift coefficient, and C a coefficient that varies with the free-stream Mach number (Fig. 13.2).

In the following examples, the quasi-steady results as obtained from the measurements are presented both with and without correction for the tunnel walls. The uncorrected values are given also, because they are consistent with the fully unsteady results, on which no tunnel-wall correction could be applied.

The comparative calculations for the symmetrical NACA 64A006 airfoil are performed for zero mean incidence and zero mean flap position, while the calculations for the lifting NLR 7301 airfoil concern a mean incidence, α_c, which in-

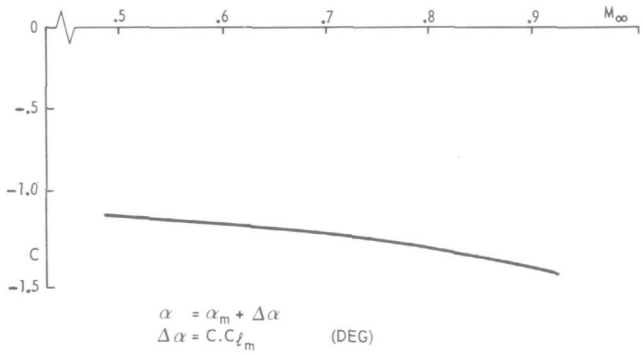

Fig. 13.2 Wall-interference correction for the NLR Pilottunnel.

cludes the correction for wall interference. No further correction is applied on the variations in flap angle or incidence around the respective mean conditions, which are necessary to determine the theoretical quasi-steady results.

13.2.2 Subsonic flow

The first comparison concerns the measured and calculated subsonic pressure distributions for the NACA 64A006 airfoil (Fig. 13.3). The steady pressure distributions on the airfoil with deflected flap (Fig. 13.3a) clearly indicate that a large part of the difference between the results of potential theory and experiment can be attributed to the presence of the boundary layer. From the corresponding quasi-steady pressure distributions (Fig. 13.3b), it can be concluded that, compared with thin-airfoil theory, the inclusion of thickness increases the pressure ahead of the hinge axis, whereas the pressures on the flap show a slight decrease. Further, the addition of the boundary layer has a significant effect, which compensates to a large extent the contribution due to thickness.

The effect of the boundary layer is also significant for the 16.5 per cent thick NLR 7301 airfoil (Fig. 13.4a). The quasi-steady results given in figure 13.4b demonstrate that the deviations of the test results from thin-airfoil theory are due to the combined effects of thickness, incidence, and viscosity. The effect of thickness and incidence dominates on the front part of the airfoil, and the effect of the boundary layer is more important towards the rear (see also the discussion in section 10.2.1). Further it can be noted that the presence of the tunnel walls has a large influence on both the NACA 64A006 and the NLR 7301 airfoil.

13.2.3 Transonic flow with shock wave

In transonic flow, the presence of the boundary layer leads to a considerable change in shock position and shock strength. As a consequence, its effect on the steady and quasi-steady aerodynamic loading is even larger than in subsonic flow. This is demonstrated for the NACA 64A006 airfoil in figure 13.5, and for the NLR 7301 airfoil in figure 13.6. Both figures show a considerable improvement in the theoretical prediction if thickness and boundary-layer effects are taken into account simultaneously.

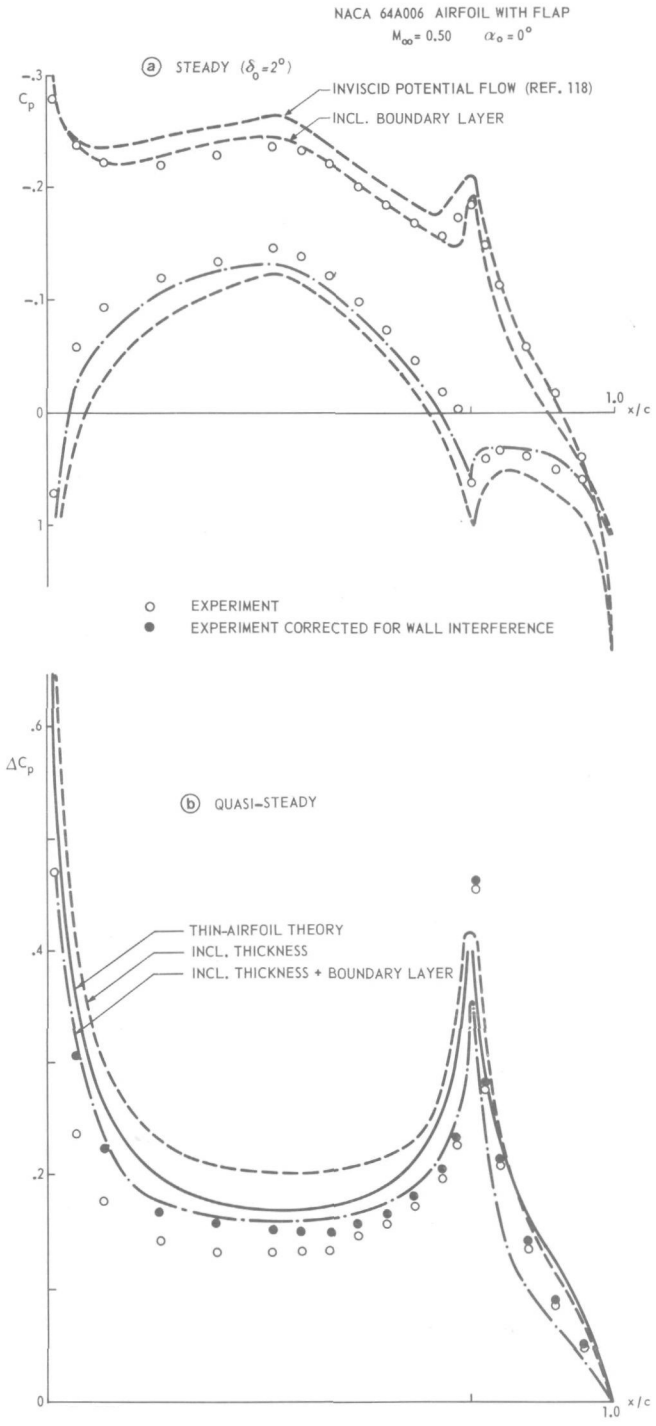

Fig. 13.3 Effect of thickness and boundary layer on the steady and quasi-steady pressure distribution in subsonic flow.

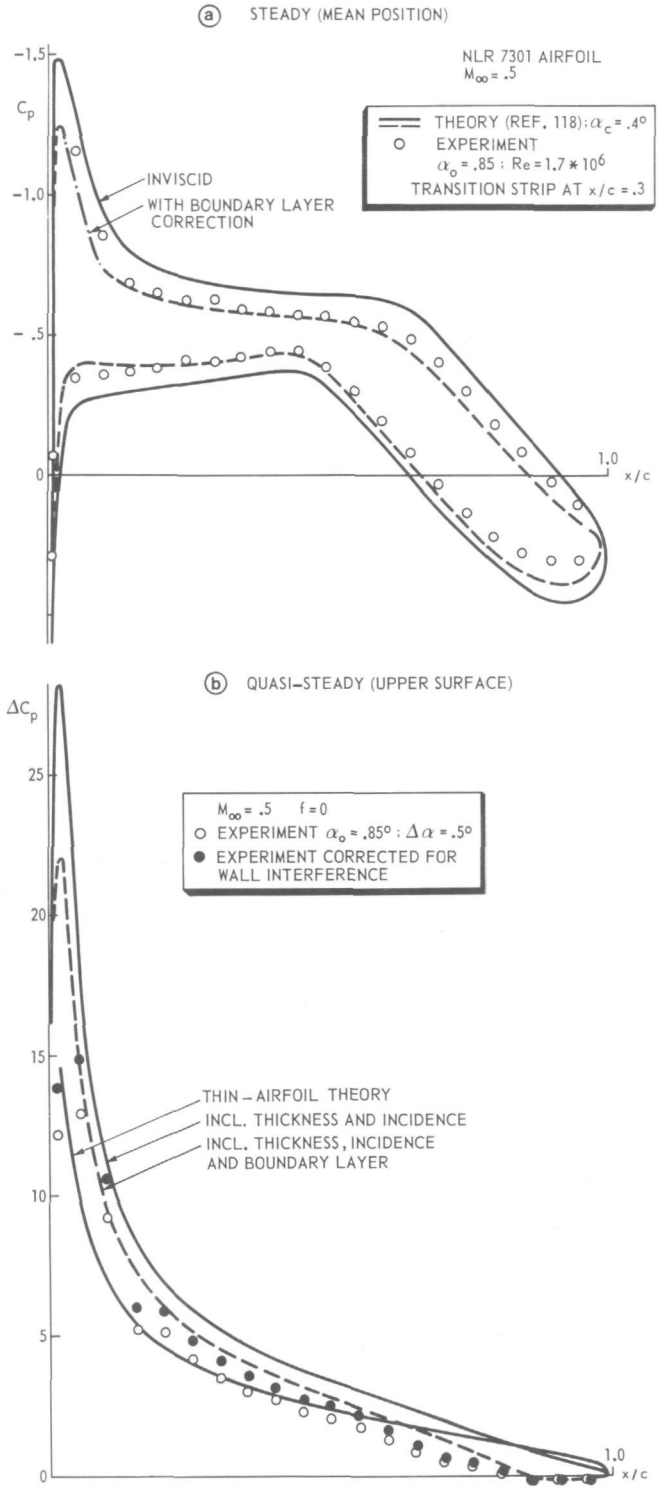

Fig. 13.4 Effect of thickness, incidence and boundary layer on the steady and quasi-steady pressure distribution in subsonic flow (condition I).

The fact that for the NACA 64A006 airfoil with flap the effect of thickness is fully compensated by the effect of the boundary layer is illustrated also by the overall coefficients, collected in table 7. This table shows, for instance, that at $M_\infty = 0.85$ the inclusion of wing thickness increases the normal-force coefficient, k_c, as obtained with thin-airfoil theory, with about 55 per cent, whereas the boundary layer is responsible for a decrease of about 70 per cent. The interference with the tunnel walls contributes for roughly 20 per cent. After the various corrections, the agreement between theory and experiment is improved considerably.

The aerodynamic coefficients for the NLR 7301 airfoil at $M_\infty = 0.7$ (table 8) reveal that also for this case thickness and incidence provide

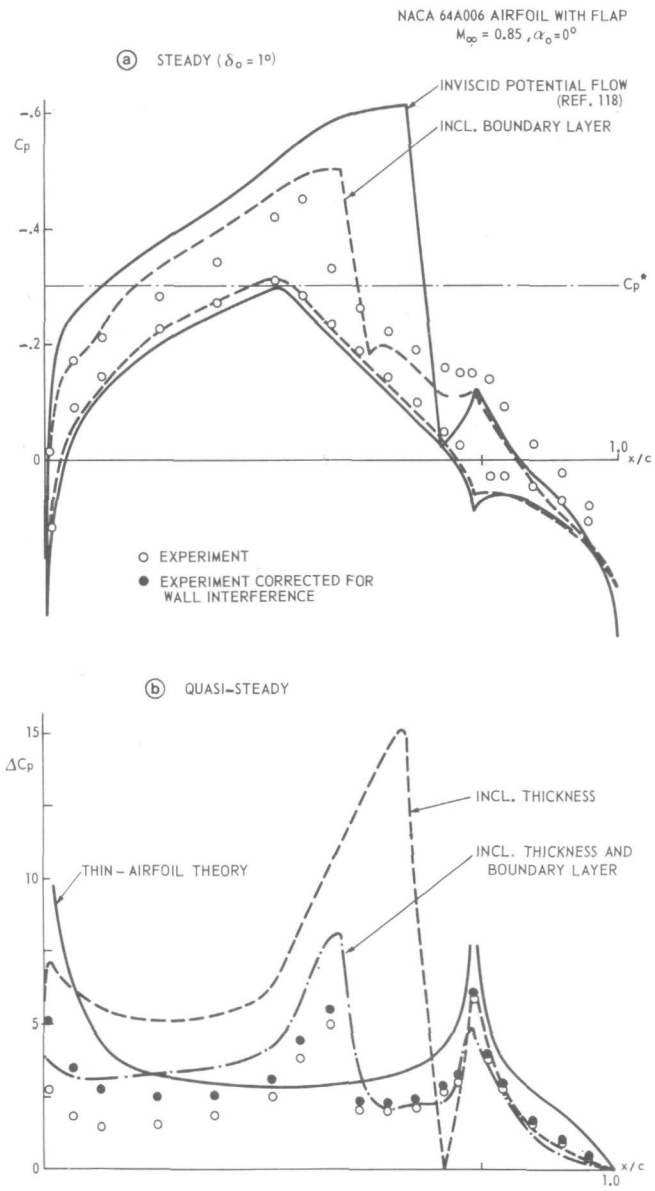

Fig. 13.5 Effect of thickness and boundary layer on the steady and quasi-steady pressure distribution in transonic flow.

an increase of the thin-airfoil value of the normal-force coefficient, k_α, of more than 50 per cent. Accounting for the boundary layer leads to a decrease of about 35 per cent, as follows from both values obtained with the non-conservative calculation scheme. The conservative scheme, which guarantees the best numerical solution, did not converge for inviscid flow, so this value is not included. The last two columns show that in the present tests the tunnel walls are responsible for a correction of about 30 per cent. At $M_\infty = 0.5$, the effects mentioned above are less than at transonic speed, but still significant.

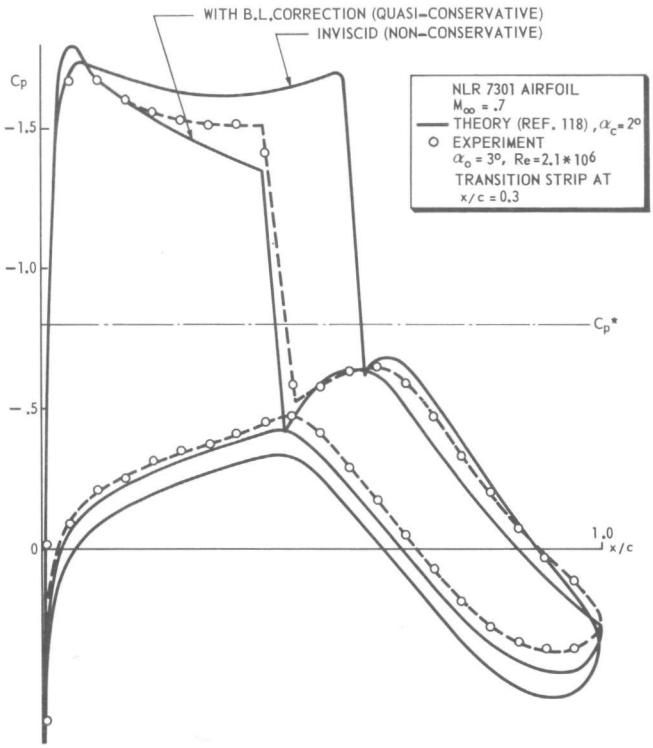

Fig. 13.6a Steady pressure distribution in the mean position (condition II-1).

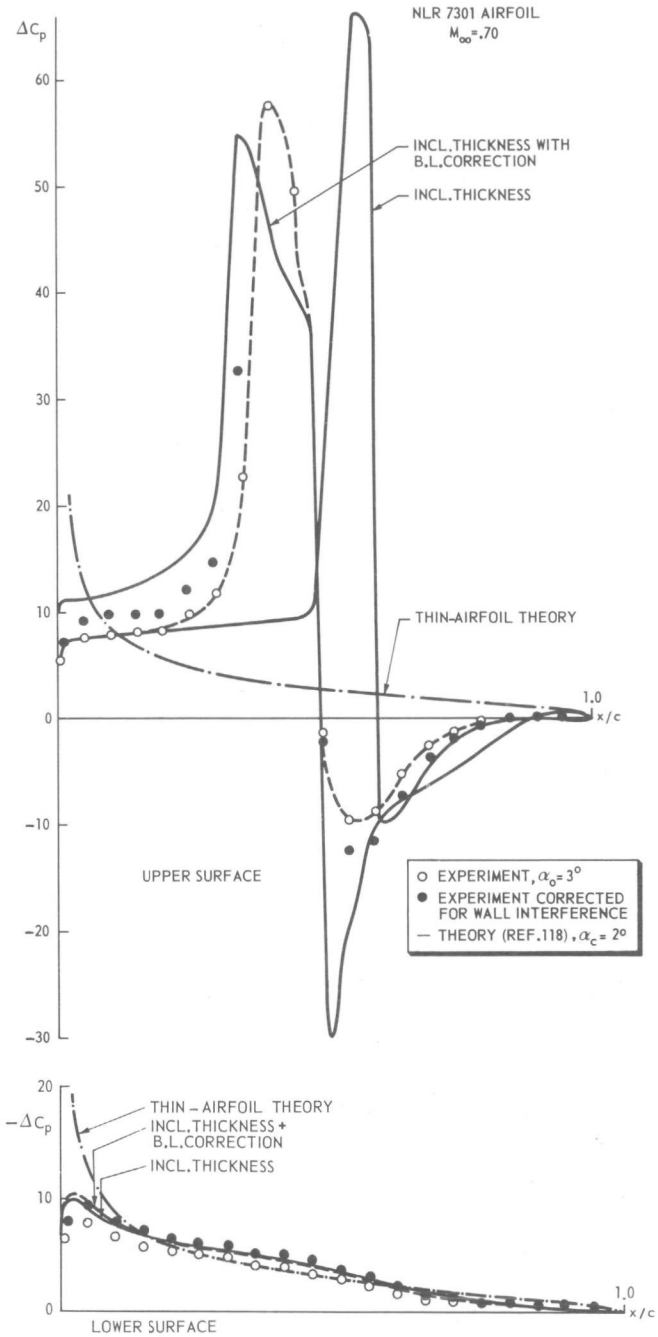

Fig. 13.6b Quasi-steady pressure distribution in transonic flow (condition II-1).

TABLE 7

Quasi-steady aerodynamic coefficients (NACA 64A006 airfoil with flap)

	Thin-airfoil theory		Theory of Ref. 118*				Experiment			
			Incl. thickness		Incl. thickness + bound. layer		Incl. tunnel-wall correction		Uncorrected	
M_∞	k_c	m_c	k_c	m_c	k_c	m_c	k_c	m_c	k_c	m_c
0.8	2.03	0.69	2.44	0.80	1.88	0.65	1.66	0.61	1.32	0.61
0.85	2.31	0.79	3.61	1.29	1.94	0.60	1.82	0.75	1.41	0.75

* with conservative finite-difference scheme

TABLE 8

Quasi-steady aerodynamic coefficients (NLR 7301 airfoil)

		Thin-airfoil theory		Theory of Ref. 118						Experiment			
				Incl. thickness		Incl. thickness + bound. layer		Incl. thickness + bound. layer		Incl. tunnel-wall correction		Uncorrected	
M_∞	α_o	k_α	m_α	k_α	m_α	k_α	m_α	k_α	m_α	k_α	m_α	k_α	m_α
0.5	0.85°	2.31	0	2.73	0.04	2.53	-0.04	2.53	-0.04	2.55	-0.10	2.18	-0.09
0.7	3.00°	2.80	0	4.24	0.11	3.21	0.00	3.92	-0.22	4.10	-0.44	3.20	-0.34
				Non-conservative F-D scheme		Non-conservative F-D scheme		Conservative F-D scheme					

F-D = Finite Difference

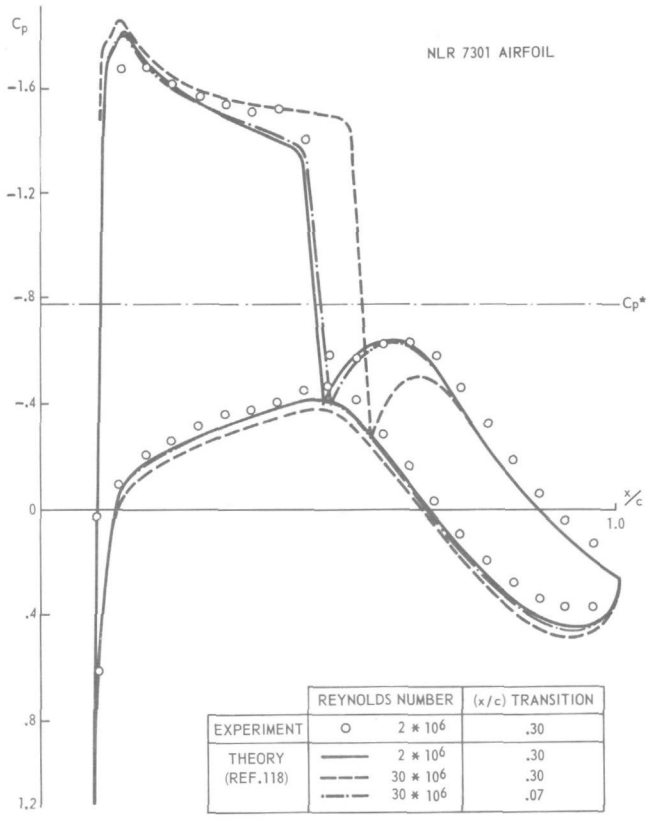

Fig. 13.7 Influence of Reynolds number and location of transition point on the steady pressure distribution (condition II-2).

The experiments and calculations given above deal with a relatively low Reynolds number (about 2 million), while for full-scale aircraft one is interested in much higher values of this parameter (20 - 40 million). It may be expected, however, that at high Reynolds numbers the influence of the boundary layer remains of the same order of magnitude as shown here (see figure 13.7, contributed by Kooi, Ref. 176). The reason for this is that increasing the Reynolds number produces two counteracting effects. One effect is the decrease of the boundary-layer thickness, which changes the pressure distribution in the direction of inviscid theory. The other is that the transition point, in which the boundary layer changes from laminar to turbulent, shifts towards the leading edge. This results in a thickening of the boundary layer, which counteracts the first effect.

From the examples discussed so far, it can be concluded that inviscid-flow theories that include a proper representation of thickness and incidence produce in a qualitative sense correct characteristics of the pressure distributions. Representation of the boundary layer is, however, essential to obtain quantitative agreement between theory and experiment.

13.2.4 "Shock-free" flow

To conclude the evaluation of the capability of advanced theories on the basis of quasi-steady flow, the "shock-free"-flow condition of the NLR 7301 airfoil will be considered. For this purpose, a comparison is made between results from calculations with the method of Bauer, Korn and Garabedian (Ref. 116) for the theoretical "shock-free" design condition, and experimental results for the condition at which "shock-free"

flow is obtained in the wind tunnel. In this way the fact that the experimental design condition (i.e. Mach number and incidence) differs from the inviscid theoretical design condition can be discarded, which assures that both theory and experiment deal with the carefully balanced condition of "shock-free" flow.

The steady pressure distributions computed for incidences at and around the design condition (Fig. 13.8a) exhibit the same characteristic changes in shape in the supersonic region at the upper surface as those observed in the measurements (Fig. 10.10). The lower surface behaves very regularly.

The comparison between the corresponding quasi-steady pressure distributions given in figure 13.8b shows a considerable improvement over thin-airfoil theory. The typical character of the distribution along the upper surface is predicted reasonably well, and also the prediction for the lower surface is improved. This justifies the expectation that methods based on inviscid theory are able to predict, at least qualitatively, the main characteristics of the unsteady flow for oscillations aroung the "shock-free" design condition. It has to be noted, however, that this conclusion is based on comparisons with solutions of the full potential equation. Whether similar improvements can be achieved with small-perturbation theories is questionable.

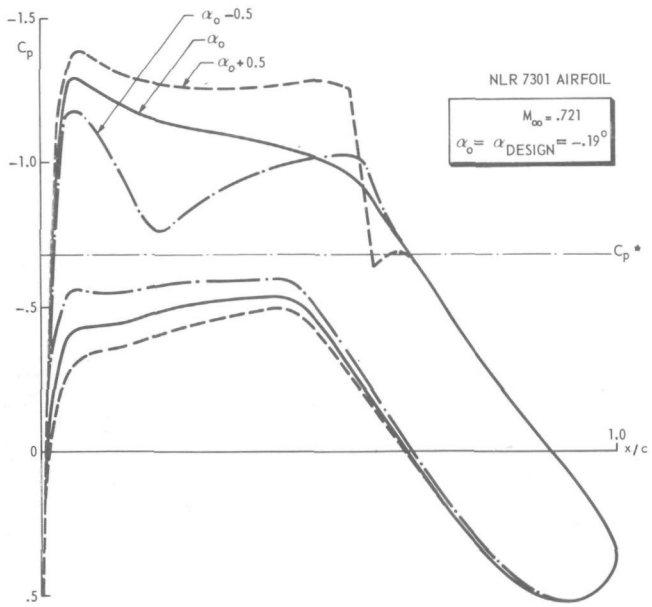

Fig. 13.8a Calculated steady pressure distributions at and about the theoretical "shock-free" design condition.

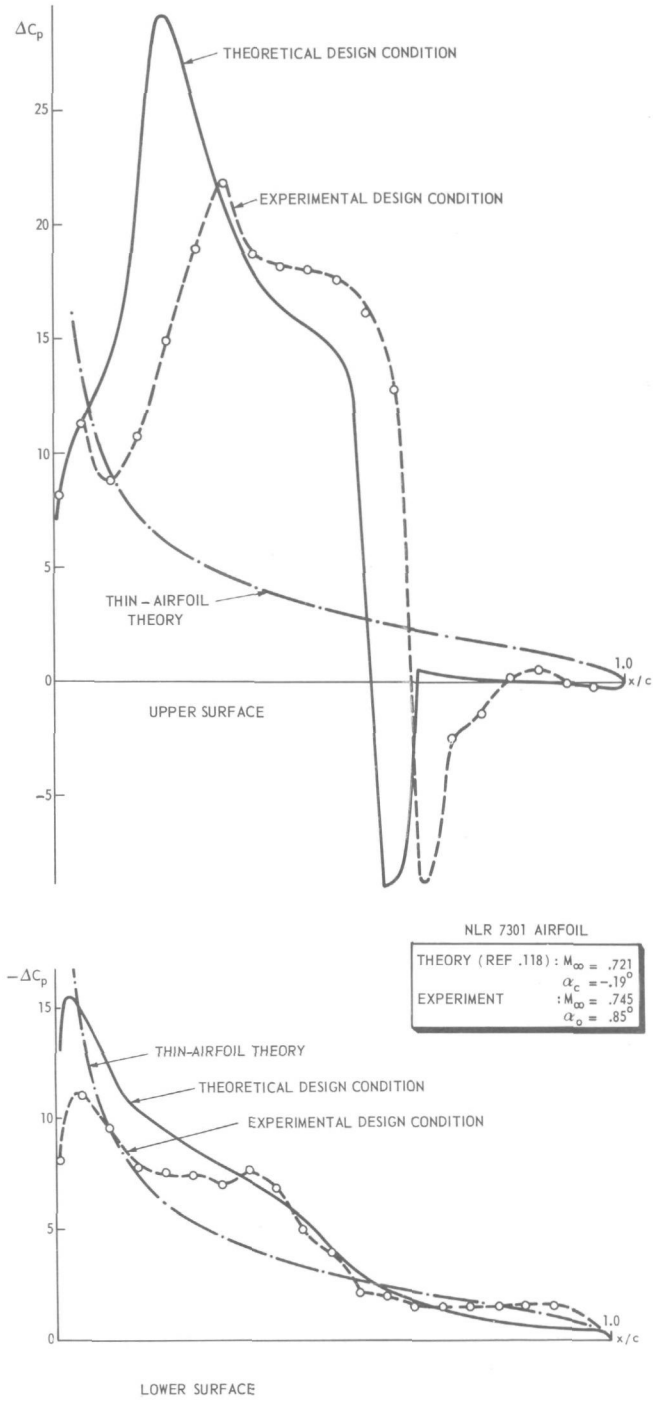

Fig. 13.8b Quasi-steady pressure distributions for the theoretical and experimental "shock-free" design condition (condition III).

13.3 COMPARISONS BETWEEN THEORY AND EXPERIMENT IN UNSTEADY FLOW

13.3.1 Pressure distributions

As mentioned before, the comparison between theory and experiment for fully unsteady flow has

to be limited to the NACA 64A006 airfoil with flap, since, at the moment of writing, this airfoil is the only one for which results both from measurements and from calculations are available. The comparisons are limited to inviscid-flow theories; no corrections are applied for wall interference.

(a) Pressure distributions in high-subsonic flow

In figure 13.9, some comparisons are shown for high-subsonic flow. For the sake of completeness, also the quasi-steady results (f = 0), obtained with the method of reference 118, are added.

A comparison between the chordwise magnitude distributions for 30 Hz calculated with thin-airfoil theory, by Ehlers and by Roos, shows that in front of the hinge axis the more advanced theories are less accurate in predicting the measurements than thin-airfoil theory. On the flap, a slight improvement can be noticed. This corresponds very well with the observed differences in quasi-steady flow (section 13.2.2).

The theoretical magnitude distributions obtained by the different authors for 120 Hz are still far from unanimous. The results of Chan and Brashear look somewhat suspicious, since their magnitude distribution on the front part of the airfoil is consistently less than that predicted by thin-airfoil theory, which conflicts with what should happen physically. (As shown in reference 132, this difference exists already for quasi-steady flow.) With respect to the phase curves in figure 13.9 it can be observed that, compared with thin-airfoil theory, the phase curves upstream of the hinge axis have changed in a direction that could be expected from the graphical experiment shown in figure 8.13. It is not understood why for 30 Hz the phase curve calculated by Ehlers does not behave in the same sense.

A comparison between experiment, the two calculation methods for high-subsonic flow developed at NLR, and the high-subsonic method of Isogai (Ref. 142), given in figure 13.10, illustrates that the relatively simple Doublet-Lattice method with local-Mach-number correction gives

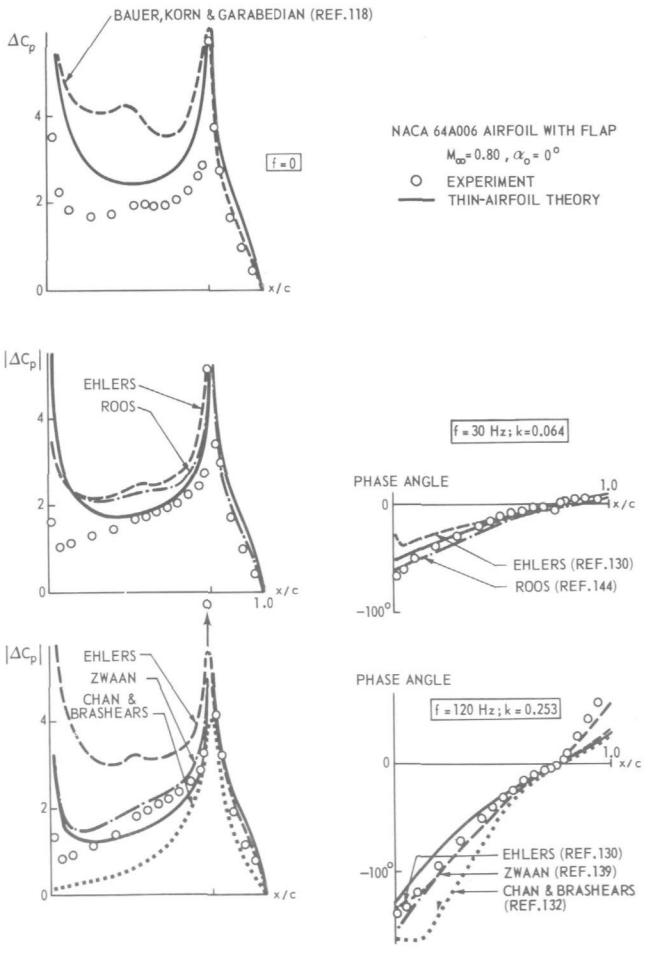

Fig. 13.9 Comparison between calculated and measured unsteady pressure distributions in high-subsonic flow.

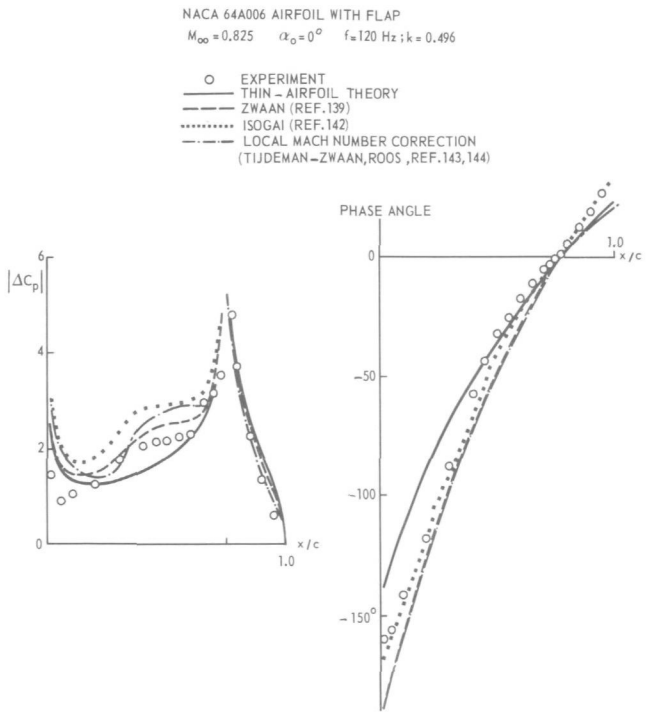

Fig. 13.10 Comparison between calculated and measured unsteady pressure distributions in high-subsonic flow.

about the same results as the methods of Zwaan (Ref. 139) and Isogai. Similar results have been reported by Giesing, Kalman and Rodden (Ref. 145), who followed a closely related approach.

(b) Pressure distribution in transonic flow

The results in figure 13.11 for the slightly supercritical flow condition at $M_\infty = 0.85$ are taken from Ehlers (Ref. 130), Ballhaus and Goorjian (Refs. 165, 166), and Isogai (Ref. 125). As can be observed, the deviations between theory and experiment are of the same order of magnitude as those in quasi-steady flow. Compared with thin-airfoil theory, there is a drastic improvement in a qualitative sense, especially the peak in the magnitude distribution that occurs near the mean shock position is predicted very well. Also the character of the phase curves is improved, in particular in front of the hinge axis, where the typical steepening effect confirms the observations from the graphical experiment (Fig. 8.13). In quantitative sense there is still a large discrepancy between theory and experiment, which - as was argued in the preceding section for quasi-steady flow (see figure 13.5) - should be attributed mainly to the effects of the boundary layer and the tunnel walls.

Similar remarks as those made for the examples of figure 13.11 apply to the comparisons in figure 13.12, which deal with a transonic flow with a well-developed shock wave. The discrepancies between the results of the different theoretical methods can to a large extent be attributed to the differences that do exist already in the corresponding steady-flow field, which were shown in figure 13.1: The steady-flow field of Magnus and Yoshihara, for instance, gives a stronger shock wave at a more rearward position than the small-perturbation method. Thus it is not surprising that in their results the high peak in the unsteady pressure distribution generated by the shock wave (Fig. 13.12) is higher and located more downstream than in the other calculations. Moreover, the increased shock strength makes it more difficult for the pressure perturbations generated by the oscillating flap to travel around the top of the shock wave, which results in a lower pressure level upstream of the shock wave.

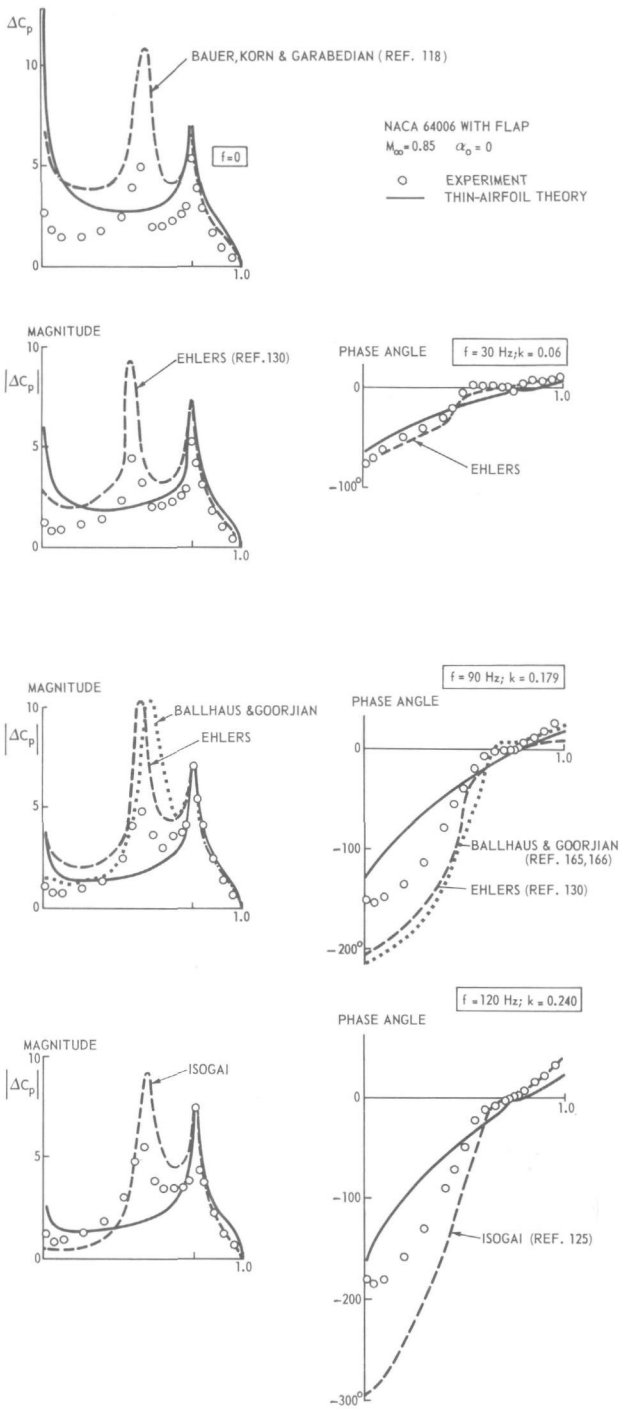

Fig. 13.11 Comparison between calculated and measured unsteady pressure distributions in slightly supercritical flow.

13.3.2 Aerodynamic coefficients

As far as the resulting overall unsteady forces and moments are concerned, Traci, Farr and Albano (Ref. 131) are the only ones who considered the behaviour of the coefficients as a function of

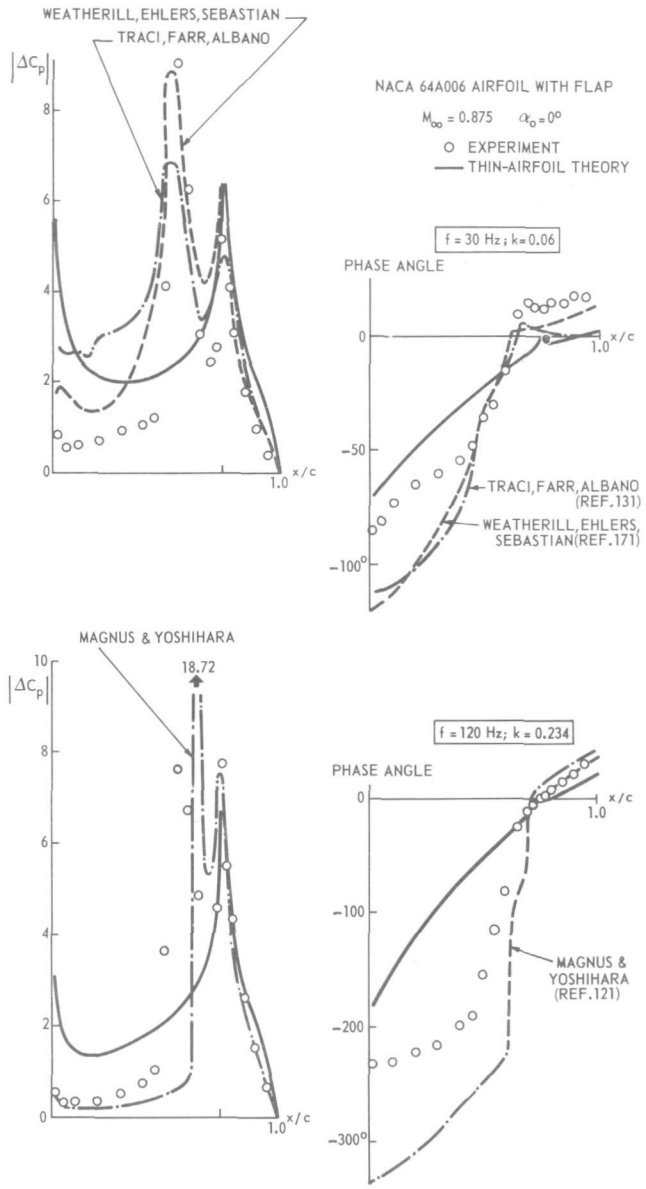

Fig. 13.12 Comparison of calculated and measured unsteady pressure distributions in transonic flow.

frequency and Mach number in a systematic way. Their result for the normal-force coefficient is shown in figure 13.13. The theoretical curve coincides with the results of linear lifting-surface theory for subsonic and supersonic flow for $M_\infty \ll 1$ and $M_\infty \gg 1$, respectively. There is a qualitative agreement with the test results, but in quantitative sense there is a large discrepancy, which is of the same order as that observed for quasi-steady flow (table 7).

In reference 121, Magnus and Yoshihara show an example of the time histories of the normal force, moment, and hinge moment for the airfoil with flap. These curves, reproduced in figure 13.14, reveal that the aerodynamic coefficients behave almost sinusoidal, despite the large nonlinearities in the local pressures near the oscillating shock wave. Similar experiences have been reported by Magnus and Yoshihara (Ref. 120) for a pitching NACA 64A410 airfoil, by Laval (Ref. 123), and by Krupp and Cole (Ref. 128), who all three observed an almost linear behaviour of the overall aerodynamic loads, in spite of the presence of an oscillating shock wave. These findings are in good agreement with the conclusions drawn in chapter 11 about the possibilities of linearization in unsteady transonic flow.

13.3.3 Shock-wave motions

The unsteady pressure distributions calculated by Ehlers et al. (Refs. 130, 171) and Traci et al. (Ref. 131) for transonic flow show the high pressure peaks associated with the presence of shock waves (Figs. 13.11 and 13.12). No information is obtained, however, about the shock-wave motion itself, because the effect of the velocity of the shock wave relative to the airfoil, which is essential for the type of shock motion, is not automatically included in methods based on the

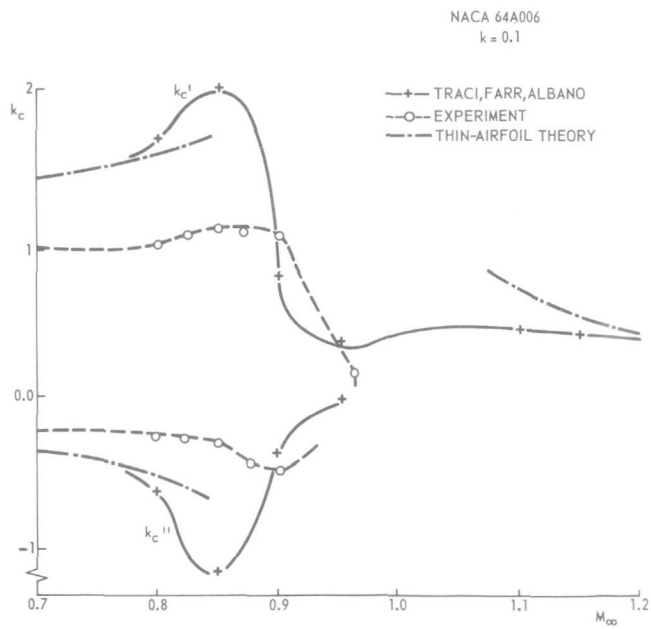

Fig. 13.13 Unsteady normal-force coefficient as a function of Mach number (reproduced from Ref. 131).

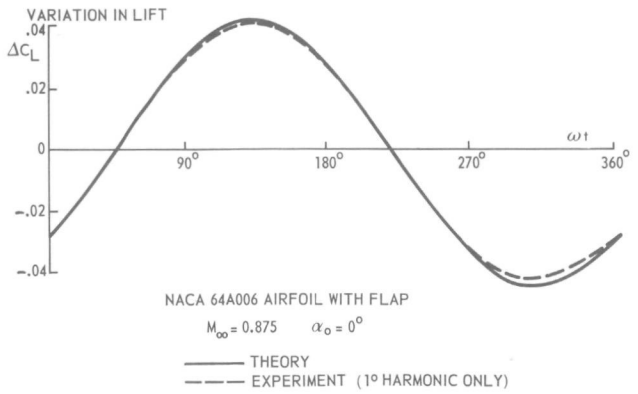

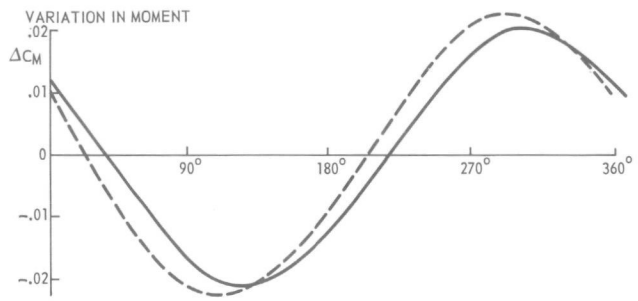

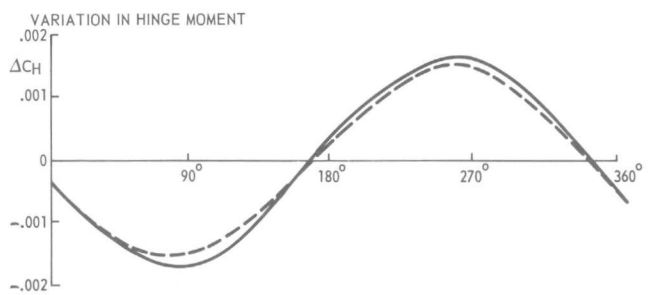

Fig. 13.14 Time histories of the unsteady airloads as calculated by Magnus and Yoshihara (Ref. 121).

linearized transonic small-perturbation equation. This problem can be solved by a shock-fitting procedure, for which purpose an additional relation must be fulfilled at the mean shock position. This additional relation can be derived by matching a small-perturbation expansion of the nonlinear potential equation with the unsteady shock relations for an oscillating shock wave. In principle, this idea was employed already in the studies of Coupry and Piazolli (Ref. 109), Eckhaus (Ref. 110), and Landahl (Ref. 24). Recent work along these lines is reported by Hafez, Rizk and Murman (Ref. 177).

In contrast herewith, the methods based on the nonlinear equations in which no distinction is made between steady and unsteady flow are able to predict the details of the periodical shock-wave excursions without additional measures. This is illustrated with the results of some calculations, which exhibit the different types of shock-wave motion described in chapter 9.

Figure 13.15 contains the instantaneous pressure distributions computed by Magnus and Yoshihara (Ref. 121) for the airfoil with flap at $M_\infty = 0.875$. It is evident that the shock motion is of type A, i.e. the shock moves almost sinusoidal and remains present during the complete cycle of oscillation.

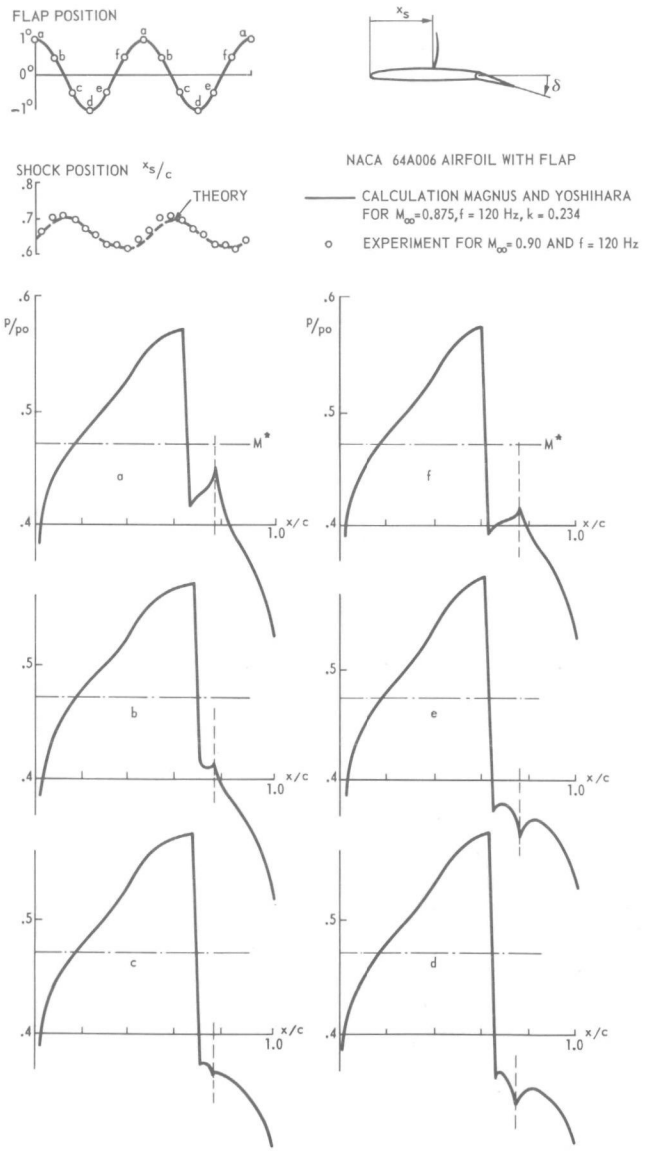

Fig. 13.15 Calculated instantaneous pressure distributions at the upper surface showing type-A shock motion (reproduced from Ref. 121).

A good agreement is obtained between the shock trajectory calculated for $M_\infty = 0.875$ and the measured trajectory for $M_\infty = 0.90$. The small shift in free-stream Mach number agrees very well with the fact that the calculated steady pressure distribution at $M_\infty = 0.875$ upstream of the shock wave shows a systematic deviation from the measured pressures (see figure 13.1), which corresponds to a shift in Mach number of about 0.02. The suggestion (Refs. 121 and 162) that this small deficiency may be caused by some wall-interference effects seems plausible, at least for a part. Comparative calculations with the method of Bauer et al. (Ref. 118), however, show that the presence of the boundary layer upstream of the shock wave, which is neglected in the calculations of references 121 and 162, is responsible for the major part of the observed shift in local Mach number upstream of the shock wave.

Ballhaus and Goorjian (Refs. 165, 166) succeeded in reproducing all three types of shock-wave motion. Their results for type-B and type-C motion are shown in figures 13.16 and 13.17, respectively. Since the calculations deal with a frequency of 90 Hz, whereas the corresponding tests were performed at 120 Hz, no direct comparison between the calculated and the measured shock trajectories can be made.

A closer look at the subsequent instantaneous pressure distributions of figure 13.16 reveals that the shock vanishes during a part of the cycle, although the local flow remains supersonic. In figure 13.16 a comparison is made also between the results of Ballhaus and Goorjian and the results of Magnus and Yoshihara. It appears that, for this thin airfoil and its relatively small amplitude of oscillation, a satisfactory agreement is obtained.

From figure 13.17, which shows a type-C shock-wave motion, it can be observed that a shock wave is formed at some time between a and b, which strengthens and propagates upstream. Between c and d the embedded supersonic region is completely eliminated and, although the flow is entirely subsonic, the shock wave continues to propagate upstream, as shown at times g, h, and i. At time j, the shock has disappeared, probably dissipated by numerical viscosity.

Finally, a more illustrative example of a type-C shock-wave motion (calculated by Ballhaus and Steger, Ref. 127) is shown in figure 13.18 for a pulsating parabolic-arc airfoil. This airfoil thickens during the first 15 chord lengths of airfoil travel and becomes flat again during the subsequent 15 chord lengths. During the thickening part of the motion (Fig. 13.18a), a shock wave forms and propagates downstream, reaching its maximum downstream location at t = 18.25 chord lengths of travel. As the airfoil becomes thinner, the shock wave reverses direction and propagates off the front of the airfoil (Fig. 13.18b).

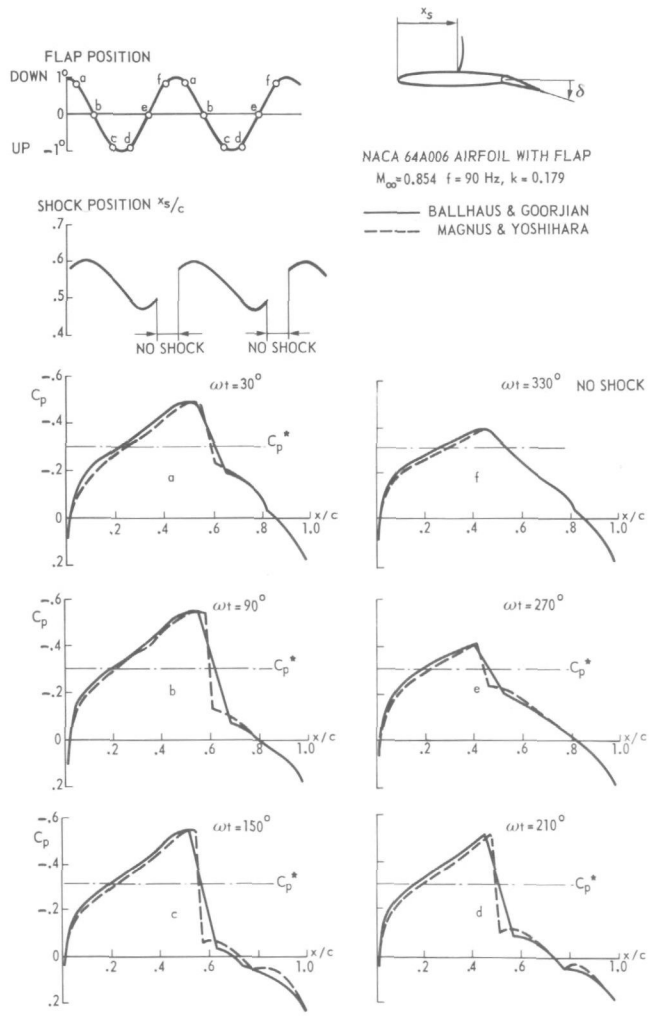

Fig. 13.16 Calculated instantaneous pressure distributions at the upper surface, showing type-B shock motion (reproduced from Ref. 165).

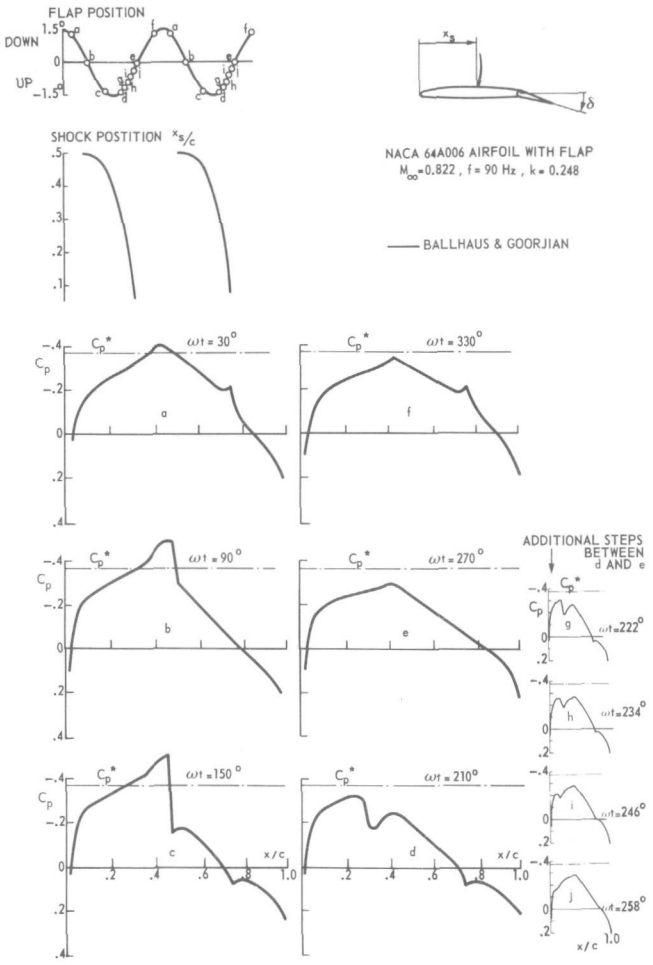

Fig. 13.17 Calculated instantaneous pressure distributions at the upper surface, showing type-C shock motion (reproduced from Ref. 165).

13.4 CONCLUDING REMARKS

From the preceding evaluation it is apparent that the inclusion of airfoil thickness, incidence, and transonic shock motions in inviscid-flow calculations leads to an improvement of the theoretical predictions in a qualitative sense. Quantitatively, a large discrepancy with the real flow remains as a result of the boundary layer, which determines the final location of the shock to a large extent, and by that the overall unsteady airloads. Because the modelling of unsteady boundary layers is only in its first stage (for a review of the present status, the reader is referred to reference 178), it is unlikely that in the near future sophisticated calculation methods will become available for this purpose. Therefore, an engineering type of approach has to be followed in the coming period. In this respect, the ideas developed by Magnus and Yoshihara (Ref. 121) deserve attention, since their relatively simple "viscous-ramp" model lends itself for easy implementation in inviscid calculation methods. In relation to the importance of the boundary layer, also the insight into the effects of the Reynolds number should be further increased.

Small-perturbation methods are very attractive from a computational point of view. Therefore, the limits of such methods should be investigated, in particular when they are applied to thick supercritical airfoils of the type considered in this investigation. In this respect, it is the opinion of the author that an improvement of the small-perturbation theories may be obtained - especially for theories in which a distinction is made between small unsteady perturbations superimposed upon a non-uniform steady flow field - if the

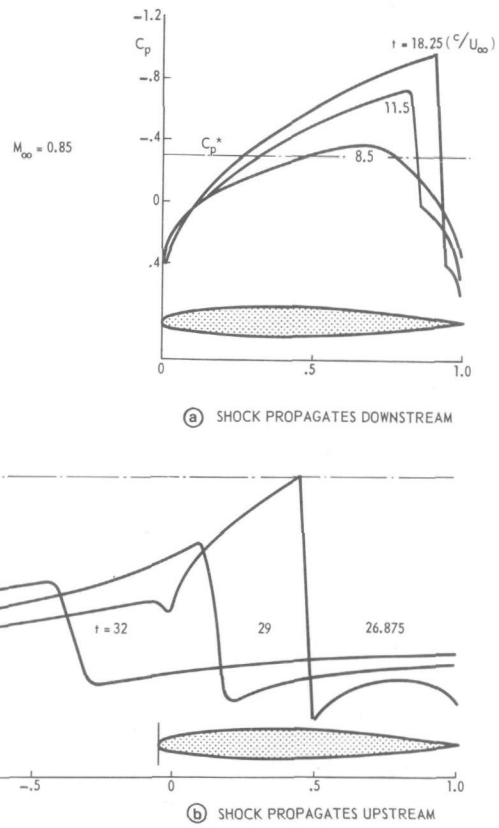

Fig. 13.18 Example of type-C shock-wave motion as calculated by Ballhaus and Steger (Ref. 127) for a parabolic airfoil with pulsating thickness.

steady flow field that forms part of the small-perturbation solution is replaced by a more accurate steady flow field. The latter flow field should be obtained from more advanced steady calculation methods that include boundary-layer effects, or from experiment. In this way, differences in unsteady airloads due to discrepancies in the steady flow field (such as differences in shock position and shock strength) may be suppressed.

Finally, from the considerations of the quasi-steady results (section 13.2) it has become clear that, in order to improve the reliability of comparisons between theory and wind-tunnel data, there is an urgent need for methods to assess the amount of wall interference in unsteady experiments in transonic test sections with slotted or porous walls.

14 IMPACT OF THE NLR INVESTIGATIONS AND FUTURE PROSPECTS

14.1 IMPACT OF THE NLR INVESTIGATIONS

As stated before, the aim of the NLR investigations was to explore the nature of two-dimensional unsteady transonic flows and to support the development of theoretical and semi-empirical prediction methods. In this respect, the investigations have proved to be successful. The physical insight gained from the experiments described here and partly published in previous papers has found already wide application in the literature that describes the characteristics of unsteady transonic flow (see, for instance, references 178-182). The measured pressure distributions of the NACA 64A006 airfoil served as the basis for comparison in various theoretical studies and, from discussions with specialists in the field of unsteady-flow calculation methods, it turned out that the NLR findings concerning the possible types of unsteady shock-wave motion had a considerable impact on the interpretation of calculated results.

14.2 FUTURE PROSPECTS

In the period to come, further evaluations of the various calculation methods are needed by means of mutual comparisons and by means of comparisons between theoretical and experimental results. Furthermore, calculation methods have to be developed that incorporate the effect of viscosity.

One of the examples that lends itself for further evaluations is the NLR 7301 airfoil. In this respect it is worth noting that for this airfoil calculations are planned with the accurate but very time-consuming method of Magnus and Yoshihara. In this way, a basis is created for comparison with faster but more approximative methods. The NLR 7301 airfoil will be a strong test case for small-perturbation methods, since it is rather thick and has a blunt nose, which may cause a violation of the small-perturbation assumption.

The value of the NLR 7301 airfoil as a basis for comparison will be increased further by the tests scheduled for a model of this airfoil in the 11-ft. transonic wind tunnel of NASA Ames Research Center. With these tests, not only an independent check on the NLR experiments is obtained, but also an extension of the range of the Reynolds number to 15 million, instead of 2 million at NLR.

When the present state of affairs is surveyed, it is the author's opinion that a satisfactory prediction of unsteady airloads in attached two-dimensional transonic flow will be possible within a couple of years.

The next and more complicated step will be the development of prediction methods for three-dimensional unsteady transonic flows. From a practical point of view, this is of high interest, since three-dimensional effects are known to be important in transonic flow. The first attempts in this direction have been published recently. Ruo and Theisen (Ref. 183), Isogai (Ref. 135) and

Dowell (Ref. 184) developed methods which take the effect of wing thickness into account at $M_\infty \approx 1.0$, although shock waves have not been included. For some rectangular wings it was shown (Refs. 135, 183) that wing thickness has a significant effect. Finite-difference methods for three-dimensional flow, which take shock waves into account, have been reported by Isom and Garadonna (Refs. 168, 169) for a helicopter rotor and by Weatherhill, Ehlers and Sebastian (Ref. 171) for a pitching rectangular wing with an NACA 64A006 cross section. Whether methods like these will become successful for practical applications will depend largely on the reduction of computing times that can be achieved, especially since in aeroelastic investigations usually a large number of combinations of Mach number, reduced frequency, and vibration modes have to be calculated (in common practice 50 to 100).

Projected against the state of affairs for three-dimensional steady transonic flows, where the calculations are still very lengthy, it has to be expected that for unsteady flow adequate three-dimensional finite-difference methods will not be available for routine calculations in the coming years. Therefore, more approximative but faster methods, which may be used to interpolate between a limited number of results of more advanced methods, seem to be attractive in the near future. In this respect, methods like those of Cunningham (Refs. 185 - 187), who combines subsonic and supersonic linear theory via a compatibility relation at the mean shock position, and the semi-empirical method of Garner (Ref. 188) should deserve attention.

15 REFERENCES

1. A.R. Collar - "Aeroelastic problems at high speed". Journal of the Royal Aeronautical Society, Vol. 51 (Jan. 1947) pp. 1-34.
2. E.G. Broadbent - "Aeroelastic problems in connection with high speed flight". Journal of the Royal Aeronautical Society, Vol. 60 (July 1956) pp. 459-475.
3. W.J. Mykytow - "The flight flutter status from a military standpoint". NASA SP-385 (1958).
4. I.E. Garrick - "Perspectives in aeroelasticity". (Fifth Theodore von Karman Lecture). Israel Journal of Technology, Vol. 10, No. 1-2 (1972).
5. J.R. Unangst - "Transonic flutter characteristics of an aspect ratio 4, 45° swept back, taper ratio 0.2 planform", NASA TM X-136 (1959).
6. M.C. Sandford, C.L. Ruhlin, I. Abel - "Transonic flutter study of a 50.5° cropped delta wing with two rearward mounted nacelles". NASA TN D-7544 (1974).
7. R.C. Goetz, R.V. Dogget jr. - "Some effects of tipfins on wing flutter characteristics". NASA TN D-7702 (1974).
8. A.R. Collar, E.G. Broadbent, E. Puttick - "An elaboration of the criterion for wing torsional stiffness". R & M, No.2154 (1946).
9. G.Y. Nieuwland - "Transonic potential flow around a family of quasi-elliptical aerofoil sections". Dissertation University of Groningen, the Netherlands (1967).
(Also NLR-TR T.172, 1967.)
10. J.W. Boerstoel - "Design and analysis of a hodograph method for the calculation of supercritical shock-free aerofoils". Dissertation Technical University Twenthe, the Netherlands (1977).
(Also NLR TR 77046 U, 1977.)
11. E.M. Murman - "Computational methods for inviscid transonic flows with embedded shock waves". AGARD Lecture series 48 "Numerical methods in fluid dynamics" (1972).
12. H. Yoshihara - " Some recent developments in planar inviscid transonic flow theory". AGARD-Agardograph No. 156 (1972).
13. G.Y. Nieuwland, B.M. Spee - "Transonic airfoils: recent developments in theory, experiment and design". Annual Review of Fluid Mechanics, Vol. 5 (1973) pp. 119-150.
14. F.R. Bailey - "On the computation of two- and three-dimensional steady transonic flows by relaxation methods". AGARD Lecture series 63 "Progress in Numerical Fluid Dynamics" (1974).
15. A. Jameson - "Numerical computation of transonic flows with shock waves". Symposium Transsonicum II, Göttingen (Eds. K. Oswatitsch and D. Rues; Springer Verlag, Berlin, 1976) pp. 384-422.
16. J.W. Boerstoel - "Review of the application of hodograph theory to transonic aerofoil design and theoretical and experimental analysis of shock-free aerofoils". Symposium Transsonicum II, Göttingen (Eds. K. Oswatitsch and D. Rues; Springer Verlag, Berlin, 1976) pp. 109-133.

17. D.W. Holder - "The transonic flow past two-dimensional aerofoils". Journal of the Royal Aeronautical Society, Vol. 68, No. 644 (Aug. 1964) pp. 501-516.

18. H.H. Pearcy - "The aerodynamic design of section shapes for swept wings". Advances in Aeronautical Sciences, Vol. 3 (London, 1962).

19. H.H. Pearcy, A.B. Haines, J. Osborne - "The interaction between local effects at the shock and rear separation". AGARD CP No. 35 "Transonic Aerodynamics" (1968).

20. B.M. Spee - "Investigations on the transonic flow around aerofoils". Dissertation Technical University Delft, the Netherlands (1969). (Also NLR TR 69122 U, 1969.)

21. H. Bergh - "A new method for measuring the pressure distribution on harmonically oscillating wings". Proc. 4th ICAS-Congress (Paris, 1964). (Ed. R. Dexter; Mac Millan, London, 1965). (Also NLR MP.224, 1964.)

22. H. Bergh, H. Tijdeman - "Theoretical and experimental results for the dynamic response of pressure measuring systems". NLR-TR F.238 (1965).

23. AGARD Manual on Aeroelasticity (1968).

24. M. Landahl - "Unsteady Transonic Flow". (Pergamon Press, New York/London, 1961).

25. R.L. Bisplinghoff, H. Ashley, R.L. Halfman - "Aeroelasticity". (Addison-Wesley Publ. Comp., Reading, Mass., 1957).

26. M. Landahl, V.J.E. Stark - "Numerical lifting surface theory - Problems and progress". AIAA Journal, Vol. 6, No.11 (Nov. 1968) pp. 2049-2060.

27. H.W. Försching - "Grundlagen der Aeroelastik". (Springer Verlag, Berlin, 1974).

28. D.L. Woodcock - "A comparison of methods used in lifting surface theory". AGARD report No. 583 (1971).

29. W.P. Rodden - "A comparison of methods used in interfering lifting surface theory". AGARD report No. 643 (1976).

30. J.H. Greidanus, A.I. v.d. Vooren, H. Bergh - "Experimental determination of the aerodynamic coefficients of an oscillating wing in incompressible, two-dimensional flow". NLR-reports F.101, F.102, F.103 and F.104 (1952).

31. W.R. Laidlaw - "Theoretical and experimental pressure distributions on oscillating low aspect ratio wings". MIT Aeroelastic and Structures Research Lab. report 51-2 (1954).

32. H. Bergh - "Unsteady pressure measurements on a wing with oscillating flap in two-dimensional flow". Proc. 3rd European Aeronautical Congress (Brussels, 1958).

33. B. Laschka - "Die Druck-, Auftriebs- und Momentenverteilungen an einem harmonisch schwingenden Pfeilflügel kleiner Streckung im niedrigen Unterschallbereich. Vergleich zwischen Theorie und Messung". Proc. 4th ICAS Congress (Paris, August 1964). (Ed. R. Dexter; Mac Millan, London, 1965).

34. R.J. Zwaan - "Calculated results for oscillating T-tails in subsonic flow and comparisons with experiment". NLR MP.253 (1967).

35. H. Hertrich - "Zur experimentellen Prüfung instationärer dreidimensionaler Tragflächentheorien bei inkompressibler Strömung". Mitt. d. Max Planck Inst. für Strömungsforschung, Nr. 40 (1967).

36. H. Bergh, H. Tijdeman - "Binary wing-control surface flutter calculations with theoretical and empirical aerodynamic derivatives for two-dimensional incompressible flow". NLR TR 68069 U (1968).

37. R. Roos, R.J. Zwaan - "Calculations of instationary pressure distributions and generalized forces with the doublet-lattice method". NLR TR 72037 U (1972).

38. J. Becker - "Interfering lifting surfaces in unsteady subsonic flow - Comparison between theory and experiment". AGARD report No. 614 (1974).

39. R. Destuynder, H. Tijdeman - "An investigation on different techniques for unsteady pressure measurements in compressible flow and comparison with lifting surface theory". AGARD report No. 617 (1974).

40. C.G. Lodge, H. Schmid - "Unsteady pressures due to control surface rotation at low supersonic speeds - Comparison between theory and experiment". AGARD report No. 647 (1976).

41. A.L. Erikson, R.C. Robinson - "Some preliminary results in the determination of aerodynamic derivatives of control surfaces in the transonic speed range by means of a flush type electrical pressure cell". NACA RM A8H03 (1948).

42. R.F. Thompson - "Investigation of a 42.7° swept back wing model to determine the effects of trailing edge thickness on the aileron hinge-moment and flutter characteristics at transonic speeds". NACA RM L50J06 (1950).

43. J.A. Wyss, R.M. Sorenson - "An investigation of the control surface flutter derivatives of an NACA 65_1-213 airfoil in the Ames 16-foot high speed wind tunnel". NACA RM A51J10 (1951).

44. A.B. Henning - "Results of a rocket-model investigation of control surface buzz on a 4 percent thick unswept wing and on 6, 9 and 12 percent thick swept wings at transonic speeds". NACA RM L53I29 (1953).

45. D.J. Martin, R.F. Thompson, C.W. Martz - "Exploratory investigation of the moments on oscillating control surfaces at transonic speeds". NACA RM L55E31b (1955).

46. D.E. Reese, W.C.A. Carlson - "An experimental investigation of the hinge moment characteristics of a constant chord control surface oscillating at high frequency". NACA RM A55J24 (1955).

47. R.F. Thompson, W.C. Moseley - "Oscillating hinge moments and flutter characteristics of a flap type control surface on a 4 percent thick unswept wing with low aspect ratio at transonic speeds". NACA RM L55K17 (1956).

48. S.A. Clevenson - "Some wind tunnel experiments on single degree of freedom flutter of ailerons in the high subsonic speed range". NACA TN 3687 (1956).

49. W.C. Martz - "Experimental hinge moments on freely oscillating flap type control surfaces". NACA RM L56G20 (1956).

50. R.F. Thompson, S.A. Clevenson - "Aerodynamics of oscillating control surfaces at transonic speeds". NACA RM L57D22b (1957).

51. R.F. Thompson, W.C. Moseley - "Effect of hinge-line position on the oscillating hinge moments and flutter characteristics of a flap type control at transonic speeds". NACA RM L57C11 (1957).

52. J.B. Bratt, J.W.C. Miles, R.F. Johnson - "Measurements of the direct hinge moment derivatives at subsonic and transonic speeds for a cropped delta wing with oscillating flap". R & M, No. 3163 (1957).

53. J.A. Wyss, R.M. Sorenson, B.J. Gambucci - "Effects of modifications to a control surface on a 6 percent thick unswept wing on the transonic control surface derivatives". NACA RM A58B04 (1958).

54. W.C. Moseley, R.F. Thompson - "Effect of control trailing edge thickness on the oscillating hinge moment and flutter characteristics of a flap type control at transonic speeds". NACA RM L58B25 (1958).

55. W.C. Moseley, T.G. Gainer - "Effect of wing thickness and sweep on the oscillating hinge moment and flutter characteristics of a flap type control at transonic speeds". NASA TM X-123 (1959).

56. J.A. Wyss, R.M. Sorenson, B.J. Gambucci - "Measurements of transonic flutter derivatives for a mid-span control surface on a modified delta wing". NASA TM X-157 (1960).

57. J.A. Wyss, R.E. Dannenberg, R.M. Sorenson, B.J. Gambucci - "Effect of boundary layer suction and spoilers on transonic flutter derivatives for a mid-span control surface on an unswept wing". NASA TM X-160 (1960).

58. W.C. Moseley, T.G. Gainer - "Some effects of control profile and control trailing edge angle on the oscillating hinge moment and flutter characteristics of flap type controls at transonic speeds". NASA TM X-170 (1960).

59. H. Loiseau - "Mesure de coefficients aérodynamique instationnaires de gouvernes en transsonique". La Recherche Aéronautique, No. 97 (Nov.-Dec. 1963).

60. Y. Nakamura, Y. Tanabe - "Some experiments on control surface buzz". National Aeronautical Laboratory (NAL) TR-72T (1964).

61. H. Loiseau - "Etude expérimentale des flottements à un degré de liberté en écoulement transsonique". ONERA NT 95 (1966).

62. Y. Nakamura - "Some contributions on a control surface buzz at high subsonic speeds". Journal of Aircraft, Vol. 5, No. 2 (March-April 1968) pp. 118-125.

63. Y. Nakamura, L. Woodgate - "Effects of Reynolds number and frequency parameter on control surface buzz at high subsonic speeds". NPL Aero report 1312 (1970).

64. J.B. Bratt, A. Chinneck - "Measurement of mid-chord pitching moment derivatives at high speeds". R & M, No. 2680 (1947).

65. A.J. Wyss, R. Herrera - "Effects of angle of attack and airfoil profile on the two-dimensional flutter derivatives for airfoils oscillating in pitch at high subsonic speeds". NACA RM A54H12 (1954).

66. A.J. Wyss, J.C. Montfort - "Effects of airfoil profile on the two-dimensional flutter derivatives for wings oscillating in pitch at high subsonic speeds". NACA RM A54C24 (1954).

67. J.C. Montfort, J.A. Wyss - "Effects of rigid spoilers on the two-dimensional flutter derivatives of airfoils oscillating in pitch at high subsonic speeds". NACA RM A54I22 (1954).

68. J.B. Bratt, W.G. Raymer, J.E.G. Townsend - "Measurements of the direct pitching moment derivatives for two-dimensional flow at subsonic and supersonic speeds and for a wing of aspect ratio 4 at subsonic speeds". R & M, No. 3257 (1959).

69. H.C. Lessing, J.L. Troutman, G.P. Meness - "Experimental determination of the pressure distribution on a rectangular wing oscillating in the first bending mode for Mach numbers from 0.24 to 1.30". NASA TN-D344 (1960).

70. S.A. Leadbetter, S.A. Clevenson, W.B. Igoe - "Experimental investigation of oscillatory aerodynamic forces, moments and pressures acting on a tapered wing oscillating in pitch at Mach numbers from 0.40 to 1.07". NASA TN-D1236 (1960).

71. H. Tijdeman, H. Bergh - "Analysis of pressure distributions measured on a wing with oscillating control surface in two-dimensional high subsonic and transonic flow". NLR-TR F.253 (1967).

72. H. Tijdeman, H. Bergh - "The influence of the main flow on the transfer function of tube-transducer systems used for unsteady pressure measurements". NLR MP 76052 U (1976).

73. J. Zwaaneveld - "Aerodynamic characteristics of the supercritical shock-free airfoil section NLR 7301". NLR TR 76052 U (1976).

74. A.H. Shapiro - "The dynamics and thermodynamics of compressible fluid flow", Vols. I and II. (The Ronald Press Company, New York, 1953).

75. W.R. Sears (ed.) - "General theory of high speed aerodynamics". Vol. VI: "High Speed Aerodynamics and Jet Propulsion". (Princeton University Press, Princeton, 1954).

76. G.Y. Nieuwland, B.M. Spee - "Transonic shock-free flow, fact or fiction?". AGARD CP No.35 "Transonic Aerodynamics" (1968).

77. J. Zierep - "Theorie der Schallnahen und der Hyperschallströmungen". (Verlag G. Braun, Karlsruhe, 1966).

78. J.W. Boerstoel, J.A. van Egmond - "Design of shock-free, basic aerofoils for a supercritical wing". NLR TR 75059 C (1975).

79. H. v. Helmholtz - "Verhandlungen der Naturhistorisch-Medizinischen Vereins zu Heidelberg vom Jahre 1863". Bd. III (1863) p. 16.

80. G. Kirchhoff - "Ueber den Einfluss der Wärmeleitung in einem Gase auf die Schallbewegung". Poggendorfer Annalen, Vol. 134, No. 6 (1868) pp. 177-193.

81. Lord Rayleigh - "The theory of sound", Vol. II, 2nd ed. (The Mc Millan Company, London, 1898) pp. 319-326.

82. H. Tijdeman - "On the propagation of sound waves in cylindrical tubes". Journal of Sound and Vibration, Vol. 39, No. 1 (1975) pp. 1-33.

83. D.E. Weston - "The theory of the propagation of plane sound waves in tubes". Proc. of the Physical Society, London, B.66 (1953) pp. 695-709.

84. W. Kerris - "Einfluss der Rohrleitung bei der Messung periodisch schwankender Drücke". Zentrallblatt für Wissenschaftliches Berichtswesen, Berlin-Adlerhof F.B. 1140 (1939).

85. C. Zwikker, C. Kosten - "Sound absorbing materials". (Elsevier, Amsterdam, 1949).

86. A.S. Iberall - "Attenuation of oscillatory pressures in instrument lines". Journal of Research of the National Bureau of Standards, Vol. 45 (July 1950) pp. 85-108.

87. C.P. Rohmann, E.C. Grogan - "On the dynamics of pneumatic transmission lines". Transactions of the American Society of Mechanical Engineers, Vol. 75 (1957) pp. 853-874.

88. J.T. Karam, M.E. Franke - "The frequency response of pneumatic lines". Journal of Basic Engineering, Transactions of the American Society of Mechanical Engineers, Series D, Vol. 91, No. 2(1969) pp. 371-378.

89. H.W. Helberg - "Zur Schallausbreitung in engen Rohren". Acustica, Vol. 4 (1954) pp. 578-586.

90. N.B. Nichols - "The linear properties of pneumatic transmission lines". Transactions of the Instrument Society of America, Vol. 1 (1962) pp. 5-14.

91. F.T. Brown - "The transient response of fluid lines". Journal of Basic Engineering, Transactions of the American Society of Mechanical Engineers, Vol. 84 (1962) pp. 547-553.

92. G.P. Watts - "An experimental verification of a computer programme for the calculation of oscillatory pressure attenuation in pneumatic transmission lines". Los Alamos Scientific Laboratory, report LA-3199-MS (1965).

93. H. Triebstein - "Entwicklung und Errichtung eines Versuchsstands zur Messung instationärer Druckverteilungen an schwingenden Modellen im transsonischen Windkanal der AVA". Teil III: "Theoretische und experimentelle Untersuchungen des dynamischen Verhaltens von Druckübertragungsleitungen". AVA-Bericht 68J04 (1968).

94. F.R. Goldschmied - "On the frequency response of viscous compressible fluids as a function of Stokes number". Journal of Basic Engineering, Transactions of ASME, Vol. 92 (1970) pp. 333-347.

95. P.H. Fuykschot, L.J.M. Joosten - "Dydra - data logger for dynamic measurements". NLR MP 69012 U (1969).

96. R. Poestkoke - "Hydraulic test rig for oscillating wind tunnel models". NLR MP 76020 U (1976).

97. "Facilities and Equipment at NLR". (NLR Brochure, 1971).

98. H. Tijdeman, P. Schippers - "Results of steady measurements on an NACA 64A006 airfoil with flap". NLR TR 73149 C (1973).

99. H. Tijdeman, P. Schippers - "Results of pressure measurements on an airfoil with oscillating flap in two-dimensional high subsonic and transonic flow (zero incidence and zero mean flap position)". NLR TR 73078 U (1973).

100. H. Tijdeman, P. Schippers - "Results of pressure measurements on a lifting airfoil with oscillating flap in two-dimensional high subsonic and transonic flow". NLR TR 73018 L (1973).

101. P. Schippers, H. Tijdeman, A.J. Persoon - "Results of unsteady pressure measurements on an oscillating supercritical airfoil". (to be published)

102. E.M. de Jager - "The aerodynamic forces and moments on an oscillating airfoil with control surface between two parallel walls". NLR report F.140 (1954).

103. A.L. Erickson, J.D. Stephenson - "A suggested method of analyzing for transonic flutter of control surfaces based on available experimental evidence". NACA RM A7F30 (1947).

104. A. Chinneck, D.W. Holder, C.J. Berry - "Observations of the flow round a two-dimensional airfoil oscillating in a high speed airstream". R & M, No. 2931 (1952).

105. N.C. Lambourne - "Some instabilities arising from the interaction between shock waves and boundary layers". AGARD report 182 (1958).

106. N.C. Lambourne - "Control surface buzz". R & M, No. 3364 (1962).

107. G.E.A. Meier - "Ein instationäres Verhalten transsonischer Strömungen". Mitteilungen Max Planck Institut/AVA Nr. 59 (1974). (Also: Shock induced flow oscillations, AGARD CP 168, paper 29; 1975.)

108. K. Finke - "Shock oscillations in transonic flows and their prevention". Symposium Transsonicum II (Ed. K. Oswatitsch und D. Rues; Springer Verlag, Berlin, 1976) pp. 57-65.

109. G. Coupry, G. Piazolli - "Etude du flottement en régime transsonique". Recherche Aéronautique, No. 63 (Mars/Avril 1958) pp. 19-28.

110. W. Eckhaus - "Two dimensional transonic unsteady flow with shock waves". OSR TR No. 59-491 (1959).

111. W. Fiszdon - "A simple qualitative estimation of the effect of an oscillating pressure on the detached shock wave shape". Fluid Dynamics Transactions, Vol. 2 (ed. W. Fiszdon; Pergamon Press, New York/London, 1965) pp. 89-93.

112. R. Dvořàk - "On the unsteady boundary layer-shock wave interaction in the lower transonic region". Fluid Dynamics Transactions, Vol. 2 (ed. W. Fiszdon; Pergamon Press, New York/ Londen, 1965) pp. 63-74.

113. E.V. Laitone - "Limiting velocity by momentum relations for hydrofoils near the surface and airfoils near sonic flow". Proceedings of the second U.S. National Congress of Applied Mechanics (Michigan, June 1954) pp. 751-753. (Published by the American Society of Mechanical Engineers.)

114. E.V. Laitone - "Local supersonic region on a body moving at subsonic speed". Symposium Transsonicum (Aachen, 1962) (Ed. K. Oswatitsch; Springer Verlag, Berlin, 1964) pp. 57-70.

115. J.H. Greidanus, A.I. v.d. Vooren, H. Bergh - "Experimental determination of the aerodynamic coefficients of an oscillating wing in incompressible, two-dimensional flow". NLR report F.101 (1952).

116. F. Bauer, P. Korn, D. Garabedian - "A theory of supercritical wing sections, with computer programs and examples". Lecture notes on Economics and Math. Systems, No. 66 (Springer Verlag, Berlin, 1972).

117. R. Houwink, R. Roos, C.M. Siebert - "The calculation of quasi-steady lift distributions on a pitching supercritical wing". NLR report (to be published).

118. F. Bauer, P. Garabedian, D. Korn, A. Jameson - "Supercritical wing sections II". Lecture notes on Economics and Math. Systems.No. 108 (Springer Verlag, Berlin, 1975).

119. R.J. Magnus, H. Yoshihara - "Finite difference calculations of the NACA 64A-410 airfoil oscillating sinusoidally in pitch at $M_\infty = 0.72$". Convair report NSC 74-004 (1974)

120. R.J. Magnus, H. Yoshihara - "Calculations of transonic flow over an oscillating airfoil". AIAA paper 75-98; 13th Aerospace Sciences Meeting (Pasadena, Jan. 1975).

121. R.J. Magnus, H. Yoshihara - "The transonic oscillating flap". AIAA paper 76-327; 9th Fluid and Plasma Dynamics Conference (San Diego, July 1976).

122. R.M. Beam, R.F. Warming - "Numerical calculations of two-dimensional unsteady transonic flow with circulation". NASA TN-D 7605 (1974).

123. P. Laval - "Calcul de l'écoulement instationnaire transsonique autour d'un profil oscillant par une méthode à pas fractionnaires". ONERA TP No. 1975-115 (1975).

124. A. Lerat, J. Sidès - "Calcul numérique d'écoulements transsoniques instationnaires". AGARD Specialists Meeting on "Unsteady Airloads in Separated and Transonic Flow" (Lisbon, Portugal, April 1977). (Also ONERA TP No. 1977-19E.)

125. K. Isogai - "Calculation of the unsteady transonic flow over oscillating airfoils using the full potential equation". AIAA paper 77-448; Dynamics Specialists Conference (San Diego, March 1977).

126. W.F. Ballhaus, H. Lomax - "The numerical simulation of low frequency unsteady transonic flow fields". Proc. 4th International Conference on Numerical Methods in Fluid Dynamics (Univ. of Colorado, Bolder, June 1974).

127. W.F. Ballhaus, J.L. Steger - "Implicit approximate factorization schemes for the low frequency transonic equation". NASA TM X-73.082 (1975).

128. J.A. Krupp, J.D. Cole - "Studies in transonic flow, IV - Unsteady transonic flow". UCLA-Eng-76104 (Oct. 1975).

129. S.T.K. Chan, H.C. Chen - "Finite element applications to unsteady transonic flow". AIAA paper 77-446; Dynamics Specialists Conference (San Diego, March 1977).

130. F.E. Ehlers - "A finite difference method for the solution of the transonic flow around harmonically oscillating wings". NASA CR-2257 (1973). (Also AIAA paper 74-543, 7th Fluid and Plasma Dynamics Conference (Palo Alto, June 1974).)

131. R.M. Traci, J.L. Farr, E. Albano - "Perturbation method for transonic flows about oscillating airfoils". AIAA paper 75-877; 8th Fluid and Plasma Dynamics Conference (Hartford, Connecticut, June 1975).

132. S.T.K. Chan, M.R. Brashear - "Finite element analysis of unsteady transonic flow". AIAA paper 75-875; 8th Fluid and Plasma Dynamics Conference (Hartford, Connecticut, June 1975).

133. S. Stahara, J.R. Spreiter - "Development of a nonlinear unsteady transonic flow theory". NACA CR-2258 (1973).

134. K. Isogai - "Unsteady transonic flow over oscillating circular arc airfoils". AIAA paper 74-360; AIAA/ASME/SAE 15th Structures Structural Dynamics and Material Conference (Las Vegas, April 1974).

135. K. Isogai - "A method for predicting unsteady aerodynamic forces on oscillating wings with thickness in transonic flow near Mach number 1; part I: Two-dimensional theory; part II: Rectangular wings". NAL report TR-368T (1974).

136. K.R. Kimble, J.M. Wu - "An approximate solution of unsteady transonic flow problems". AFFDL-TR-74-32 (1974).

137. E.H. Dowell - "A simplified theory of oscillating airfoils in transonic flow". Symposium on Unsteady Aerodynamics (ed. Kinney, R.B.; Univ. of Tucson, Arizona, 1975).

138. P.H. Park - "Calculation of aerodynamic derivatives in unsteady two-dimensional transonic flow using Dowell's linearization method". Princeton University, AMS report No. 1238-T (1975).
(See also AIAA Journal, Vol. 14, No. 10 (Oct. 1976) pp. 1345-1346.)

139. R.J. Zwaan - "Eine Studie der nichtstationären Druckverteilung an einem zweidimensionalem Flügel mit schwingendem Ruder im schallnahen Bereich". Fachtagung Aerodynamik (Berlin, 1968). DGLR Fachbuchreihe, Band 3 (Herausgabe DGLR, Braunschweig, März 1969).

140. D. Nixon - "A two-dimensional aerofoil oscillating at low frequency in high subsonic flow". ARC Current paper 1285 (1974).

141. D. Nixon - "A two-dimensional aerofoil with a control surface oscillating at low frequency in high subsonic flow". Aeronautical Quarterly (August 1974) pp 186-198.

142. K. Isogai - "Approximate method for calculating aerodynamic loadings on an airfoil oscillating in high subsonic flow". NAL TR-455T (1976).

143. H. Tijdeman, R.J. Zwaan - "On the prediction of aerodynamic loads on oscillating wings in transonic flow". AGARD report No. 612 (1974).

144. R. Roos - "Application of panel methods for unsteady flow". NLR MP 76010 U (1976).

145. J.P. Giesing, T.P. Kalman, W.P. Rodden - "Correction factor techniques for improving aerodynamic prediction methods". NASA CR-144967 (1976).

146. G.S. Deiwert - "Numerical simulation of high Reynolds number transonic flows". AIAA Journal, Vol. 13, No. 10 (1975) pp. 1354-1359.

147. G.S. Deiwert - "Computation of separated transonic turbulent flows". AIAA Journal, Vol. 14, No. 6 (1976) pp 735-740.

148. J.B. McDevitt, L.L. Levy, G.S. Deiwert - "Transonic flow about a thick circular-arc airfoil". AIAA paper 75-878; 8th Fluid and Plasma Dynamics Conference (Hartford, Connecticut, June 1975).

149. L.S. King, L. Walitt, J.A. Enos - "An investigation of computational time reduction methods for solving the Navier-Stokes equations". NASA TM X-73.012 (1975).

150. J. van der Vooren, J.W. Slooff - "On inviscid isentropic flow models used for finite difference calculations of two-dimensional transonic flows with embedded shocks about airfoils". NLR MP 73024 U (1973).

151. Y.C. Fung - "An introduction to the theory of aeroelasticity". (John Wiley & Sons, New York, 1955).

152. R.L. Bisplinghof, H. Ashley - "Principles of aeroelasticity". (Addison-Wesley Publ. Comp. Reading, Mass. 1957).

153. E. Albano, W.P. Rodden - "A doublet-lattice method for calculating lift distributions on oscillating surfaces in subsonic flows". AIAA Journal, Vol. 7, No. 2 (1965) pp. 279-285.

154. H. Ashley, W.S. Rowe - "On the unsteady aerodynamic loading of wings with control surfaces". Zeitschrift für Flugw., Band 18, Heft 9/10 (Sept. 1970) pp 321-330.

155. W.S. Rowe, B.A.Winther, M.C. Redman - "Numerical method for predicting unsteady aerodynamic loadings caused by control surface motions in subsonic flow". AIAA paper 73-315; AIAA Dynamics Specialists Conference (Williamsburg, Va, March 1973).

156. K. Oswatitsch - "Die Geschwindigkeitsverteilung bei lokalen Ueberschallgebieten an flachen Profilen". Zeitschrift für angewandte Mathematik und Mechanik, Band 30 (1950) pp. 17-24.

157. D. Nixon, G.J. Hancock - "Integral equation methods - a reappraisal". Symposium Transsonicum II, Göttingen (eds K. Oswatitsch and D. Rues; Springer Verlag, Berlin, 1976).

158. J.R. Spreiter, A. Alksne - "Thin airfoil theory based on an approximate solution of the transonic flow equation". NACA report 1359 (1958).

159. R.J. Magnus, H. Yoshihara - "Inviscid transonic flow over airfoils". AIAA Journal, Vol. 8, No. 12 (Dec. 1970) pp. 2157-2162.

160. E.M. Murman, J.D. Cole - "Calculation of plane steady transonic flows". AIAA Journal, Vol. 9, No. 1 (Jan. 1971) pp. 114-121.

161. J.L. Steger, H. Lomax - "Transonic flow about two-dimensional airfoils by relaxation procedures". AIAA Journal, Vol. 10, No. 1 (Jan. 1972) pp. 49-54.

162. H. Yoshihara, R. Magnus - "The transonic oscillating flap - A comparison of calculations with experiments". AGARD Specialists Meeting on "Unsteady Airloads in Separated and Transonic flow" (Lisbon, Portugal, April 1977).

163. R.M. Beam, W.F. Ballhaus - "Numerical integration of the small-disturbance potential and Euler equation for unsteady transonic flow", part III. NASA SP-347 (March 1975) pp. 789-809.

164. W.F. Ballhaus, R.J. Magnus, H. Yoshihara - "Some examples of unsteady transonic flow over airfoils". Symposium on "Unsteady Aerodynamics" (ed. Kinney, R.B.; Univ. of Tucson, Arizona, 1975).

165. W.F. Ballhaus, P.M. Goorjian - "Implicit finite difference computations of unsteady transonic flows about airfoils, including the treatment of irregular shock wave motions". AIAA paper 77-205, 15th Aerospace Sciences Meeting (Los Angeles, Jan. 1977).

166. W.F. Ballhaus, P.M. Goorjian - "Efficient solution of unsteady transonic flows about airfoils". AGARD Specialists Meeting on "Unsteady Airloads in Separated and Transonic flow" (Lisbon, Portugal, April 1977).

167. N.J. Yu, A.R. Seebass, W.F. Ballhaus - "An implicit shock-fitting scheme for unsteady transonic flow computations". AIAA paper 77-633, 3d Comp. Fluid Dynamics Conference (Albuquerque, New Mexico, June 1977).

168. M.P. Isom - "Unsteady subsonic and transonic potential flow over helicopter blades". NASA CR-2463 (1974).

169. F.X.Caradonna, M.P. Isom - "Numerical calculation of unsteady transonic potential flow over helicopter blades". AIAA paper 75-168, 13th Aerospace Sciences Meeting (Pasadena, Jan. 1975).

170. H. Tijdeman - "On the motion of shock waves on an airfoil with oscillating flap". Symposium Transsonicum II, Göttingen. (eds. K. Oswatitsch and D. Rues; Springer Verlag, Berlin 1976).

171. W.H. Weatherill, F.E. Ehlers, J.D. Sebastian - "Computation of the transonic perturbation flow fields around two- and three-dimensional oscillating wings". NACA CR-2599 (1975).

172. H. Tijdeman - "On the unsteady aerodynamic characteristics of oscillating airfoils in two-dimensional transonic flow". Paper presented at the ONR Transonic Flow Conference (Univ. of California, Los Angeles, March 1976).

173. H. Tijdeman, P. Schippers, A.J. Persoon - "Unsteady airloads on an oscillating supercritical airfoil". AGARD Specialists Meeting on "Unsteady Airloads in Separated and Transonic flow" (Lisbon, Porbugal, April 1977).

174. E.M. Murman - "Analysis of embedded shock waves calculated by relaxation methods". AIAA Journal, Vol. 12 (May 1974) pp. 626-633.

175. J. Smith - "Values of wall interference correction for the NLR Pilottunnel with 10 % open slotted test section". NLR int. report AC-74-01 (1974).

176. J.W. Kooi - "Investigation on the applicability of the Bauer, Garabedian, Korn and Jameson program for the calculation of the viscous pressure distributions on airfoils". NLR int. report AC-77-026 (in Dutch) (1977).

177. M.M. Hafez, M.H. Rizk, E.M. Murman - "Numerical solution of the unsteady small-disturbance equation". AGARD Specialists Meeting on "Unsteady Airloads in Separated and Transonic flow" (Lisbon, Portugal, April 1977).

178. W.J. McCroskey - "Some current research in unsteady fluid dynamics". Journal of Fluids Engineering, Vol. 99, No. 1 (March 1977) pp. 8-39.

179. J.R. Spreiter, S. Stahara - "Unsteady transonic aerodynamics - an aeronautical challenge". Symposium on "Unsteady Aerodynamics" (ed. R.B. Kinney; Univ. of Tucson, Arizona, 1975).

180. M.T. Landahl - "Some developments in unsteady transonic flow research". Symposium Transsonicum II, Göttingen. (eds. K. Oswatitsch and D. Rues; Springer Verlag, Berlin, 1976).

181. W.F. Ballhaus - "Some recent progress in transonic flow computations". Lecture series on Computational Fluid Dynamics (Von Karman Institute, Rhode-St.Genese, Belgium, March 1976).

182. J.M. Wu, T.H. Moulden - "A survey of transonic aerodynamics". AIAA paper 76-326; AIAA 9th Fluid and Plasma Dynamics Conference (San Diego, July 1976).

183. S.Y. Ruo, J.G. Theisen - "Calculation of unsteady transonic aerodynamics for oscillating wings with thickness". NASA CR-2259 (1973). (See also AIAA paper 73-316; Dynamics Specialists Conference (Williamsburg, March 1973).)

184. E.H. Dowell - "A simplified theory of oscillating airfoils in transonic flow: Review and extension". AIAA paper 77-445; Dynamics Specialists Conference (San Diego, March 1977).

185. A.M. Cunningham jr. - "The application of general dynamic lifting surface elements to problems in unsteady transonic flow". NASA CR-112264 (1973).

186. A.M. Cunningham jr. - "An oscillatory Kernel function method for lifting surfaces in mixed transonic flow". AIAA paper 74-359, AIAA/ASME/SAE 15th Structures, Structural Dynamics and Materials Conference (Las Vegas, April 1974).

187. A.M. Cunningham jr. - "Further developments in the prediction of oscillatory aerodynamics in mixed transonic flow". AIAA paper 75-99; 13th Aerospace Sciences Meeting (Pasadena, Jan. 1975).

188. H.G. Garner - "A practical approach to the prediction of oscillatory pressure distributions on wings in supercritical flow". RAE TR 74181 (1975).

APPENDICES

APPENDIX A : DEFINITION OF STEADY AND UNSTEADY AERODYNAMIC QUANTITIES

The steady and unsteady pressures are presented as dimensionless pressure coefficients and the resulting forces and moments, obtained by chordwise integration of the pressure coefficients, are reduced to dimensionless aerodynamic coefficients.

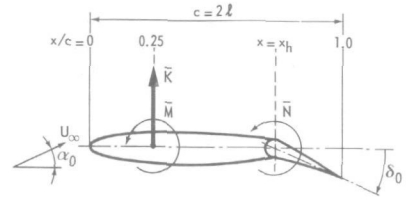

a: STEADY FORCE AND MOMENTS

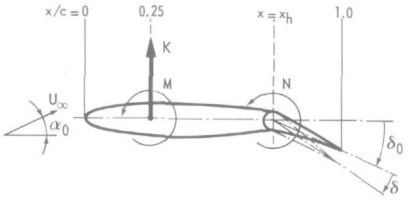

FLAP POSITION = $\delta_0 + \delta e^{i\omega t}$

b: UNSTEADY FORCE AND MOMENTS FOR AN AIRFOIL WITH OSCILLATING FLAP

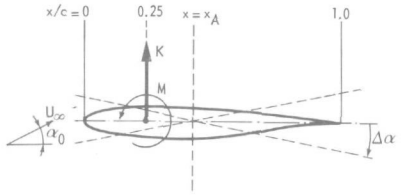

INCIDENCE = $\alpha_0 + \Delta\alpha e^{i\omega t}$

c: UNSTEADY FORCE AND MOMENT FOR AN AIRFOIL OSCILLATING IN PITCH

Fig. A.1 Definitions of steady and unsteady aerodynamic forces and moments.

A.1 STEADY FLOW

For steady flow, the pressures are reduced to pressure coefficients C_p, defined as:

$$C_p = (p - p_\infty)/q \ , \tag{A.1}$$

where q is the dynamic pressure and p_∞ the static pressure of the free-stream flow.
The corresponding steady force and moments are given as (Fig. A.1a):

Normal force:

$$\bar{K} = c_k \, q \, (2\ell), \qquad c_k = \int_0^1 (C_{p-} - C_{p+}) \, d(x/c) \ , \tag{A.2}$$

Moment about quarter chord:

$$\bar{M} = c_m \, q \, (2\ell)^2, \qquad c_m = \int_0^1 (C_{p-} - C_{p+}) \, (x/c - 0.25) \, d(x/c) \ , \tag{A.3}$$

Hinge moment:

$$\overline{N} = c_n \, q \, (2\ell)^2, \qquad c_n = \int_{x_h/c}^{1} (C_{p-} - C_{p+}) \, (x/c - x_h/c) \, d(x/c) \, . \tag{A.4}$$

Here the subscripts + and - denote upper and lower surface, respectively.

A.2 UNSTEADY FLOW

A.2.1 Airfoil with flap

In unsteady flow, the aerodynamic quantities have to be related to the motion of the airfoil. For the airfoil with oscillating flap, the following definitions apply (Fig. A.1b):

Unsteady pressure coefficient:

$$\Delta C_p = \Delta C_p' + i \, \Delta C_p'' = -\Delta p/q\delta \, , \tag{A.5}$$

where δ is the amplitude of the flap motion in radians.

Normal force:

$$K = 2\pi q\ell \, k_c \delta \, e^{i\omega t}, \qquad k_c = k_c' + i k_c'' = \frac{1}{\pi} \int_0^1 (\Delta C_{p+} - \Delta C_{p-}) \, d(x/c) \, , \tag{A.6}$$

Moment about quarter chord:

$$M = 2\pi q\ell^2 m_c \delta \, e^{i\omega t}, \qquad m_c = m_c' + i m_c'' = \frac{2}{\pi} \int_0^1 (\Delta C_{p+} - \Delta C_{p-}) \, (x/c - 0.25) \, d(x/c) \, , \tag{A.7}$$

Hinge moment:

$$N = 2\pi q\ell^2 n_c \delta \, e^{i\omega t}, \qquad n_c = n_c' + i n_c'' = \frac{2}{\pi} \int_{x_h/c}^1 (\Delta C_{p+} - \Delta C_{p-}) \, (x/c - x_h/c) \, d(x/c) \, . \tag{A.8}$$

A.2.2 Airfoil oscillating in pitch

For the airfoil oscillating in pitch, the unsteady aerodynamic pressures are described as (Fig. A.1c):

$$\Delta C_p = \Delta C_p' + i \, \Delta C_p'' = -\Delta p/q \, \Delta\alpha \, , \tag{A.9}$$

with $\Delta\alpha$ being the amplitude of the pitch oscillation in radians.

The definitions for the corresponding normal force and moment are:

Normal force:

$$K = 2\pi q \ell \, k_\alpha \, \Delta\alpha \, e^{i\omega t}, \quad k_\alpha = k'_\alpha + i k''_\alpha = \frac{1}{\pi} \int_0^1 (\Delta C_{p+} - \Delta C_{p-}) \, d(x/c) \, , \tag{A.10}$$

Moment about quarter chord:

$$M = 2\pi q \ell^2 m_\alpha \, \Delta\alpha \, e^{i\omega t}, \quad m_\alpha = m'_\alpha + i m''_\alpha = \frac{2}{\pi} \int_0^1 (\Delta C_{p+} - \Delta C_{p-}) \, (x/c - 0.25) \, d(x/c) \, . \tag{A.11}$$

The sign conventions for the unsteady aerodynamic forces and moments, as given in figures A.1b and A.1c, are according to the AGARD Manual on Aeroelasticity Vol. VI (Ref. 23).

APPENDIX B : THE DYNAMIC RESPONSE OF TUBE - TRANSDUCER SYSTEMS

B.1 THE PROPAGATION OF PRESSURE WAVES IN CYLINDRICAL TUBES

B.1.1 Formulation of the problem

To determine the dynamic response of a system of tubes and transducers, first the propagation of pressure waves in cylindrical tubes has to be considered. This problem is governed by the following equations, written in cylindrical coordinates:

(a) the Navier-Stokes equations, for a constant value of the viscosity, μ,

$$\bar{\rho}\left[\frac{\partial \bar{u}}{\partial t} + \bar{v}\frac{\partial \bar{u}}{\partial r} + \bar{u}\frac{\partial \bar{u}}{\partial x}\right] = -\frac{\partial \bar{p}}{\partial x} + \mu\left\{\left(\frac{\partial^2 \bar{u}}{\partial x^2} + \frac{\partial^2 \bar{u}}{\partial r^2} + \frac{1}{r}\frac{\partial \bar{u}}{\partial r}\right) + \frac{1}{3}\frac{\partial}{\partial x}\left(\frac{\partial \bar{u}}{\partial x} + \frac{\partial \bar{v}}{\partial r} + \frac{\bar{v}}{r}\right)\right\} \, ; \tag{B.1}$$

$$\bar{\rho}\left[\frac{\partial \bar{v}}{\partial t} + \bar{v}\frac{\partial \bar{v}}{\partial r} + \bar{u}\frac{\partial \bar{v}}{\partial x}\right] = -\frac{\partial \bar{p}}{\partial r} + \mu\left\{\left(\frac{\partial^2 \bar{v}}{\partial r^2} + \frac{1}{r}\frac{\partial \bar{v}}{\partial r} - \frac{\bar{v}}{r^2} + \frac{\partial^2 \bar{v}}{\partial x^2}\right) + \frac{1}{3}\frac{\partial}{\partial r}\left(\frac{\partial \bar{u}}{\partial x} + \frac{\partial \bar{v}}{\partial r} + \frac{\bar{v}}{r}\right)\right\} \, ; \tag{B.2}$$

(b) the equation of continuity,

$$\frac{\partial \bar{\rho}}{\partial t} + \bar{u}\frac{\partial \bar{\rho}}{\partial x} + \bar{v}\frac{\partial \bar{\rho}}{\partial r} + \bar{\rho}\left[\frac{\partial \bar{u}}{\partial x} + \frac{\partial \bar{v}}{\partial r} + \frac{\bar{v}}{r}\right] = 0 \, ; \tag{B.3}$$

(c) the equation of state for an ideal gas,

$$\bar{p} = \bar{\rho} \, R_o \, \bar{T} \, ; \tag{B.4}$$

(d) the energy equation,

$$\bar{\rho} \, C_p \left[\frac{\partial \bar{T}}{\partial t} + \bar{u}\frac{\partial \bar{T}}{\partial x} + \bar{v}\frac{\partial \bar{T}}{\partial r}\right] = \lambda\left[\frac{\partial^2 \bar{T}}{\partial r^2} + \frac{1}{r}\frac{\partial \bar{T}}{\partial r} + \frac{\partial^2 \bar{T}}{\partial x^2}\right] + \frac{\partial \bar{p}}{\partial t} + \bar{u}\frac{\partial \bar{p}}{\partial x} + \bar{v}\frac{\partial \bar{p}}{\partial r} + \mu \, \Phi \, , \tag{B.5}$$

where Φ is the viscous dissipation function,

$$\Phi = 2\left[\left(\frac{\partial \bar{u}}{\partial x}\right)^2 + \left(\frac{\partial \bar{v}}{\partial r}\right)^2 + \left(\frac{\bar{v}}{r}\right)^2\right] + \left[\frac{\partial \bar{v}}{\partial x} + \frac{\partial \bar{u}}{\partial r}\right]^2 - \frac{2}{3}\left[\frac{\partial \bar{u}}{\partial x} + \frac{\partial \bar{v}}{\partial r} + \frac{\bar{v}}{r}\right]^2 .$$

When it is assumed that:

$$\bar{u} = a_o\, u(x,r)\, e^{i\omega t} ,$$

$$\bar{v} = a_o\, v(x,r)\, e^{i\omega t} ,$$

$$\bar{p} = p_s \{ 1 + p(x,r)\, e^{i\omega t}\} = \{\rho_s a_o^2/\gamma\} \{ 1 + p(x,r)\, e^{i\omega t}\} ,$$

$$\bar{\rho} = \rho_s \{ 1 + \rho(x,r)\, e^{i\omega t}\} ,$$

$$\bar{T} = T_s \{ 1 + T(x,r)\, e^{i\omega t}\} , \qquad (B.6)$$

with u, v, p, ρ, and T being small sinusoidal perturbations of the static conditions, and by introduction

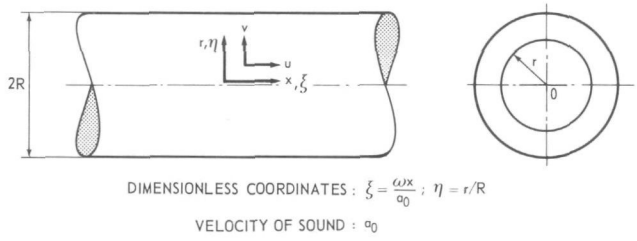

Fig. B.1 Coordinate system.

of the dimensionless coordinates (Fig. B.1)

$$\xi = \omega x/a_o , \qquad \eta = r/R \qquad (B.7)$$

the equations (B.1) - (B.5) can be rewritten as:

$$iu = -\frac{1}{\gamma}\frac{\partial p}{\partial \xi} + \frac{1}{s^2}\left[\left(\bar{k}^2\frac{\partial^2 u}{\partial \xi^2} + \frac{\partial^2 u}{\partial \eta^2} + \frac{1}{\eta}\frac{\partial u}{\partial \eta}\right) + \frac{1}{3}\bar{k}\frac{\partial}{\partial \xi}\left(\bar{k}\frac{\partial u}{\partial \xi} + \frac{\partial v}{\partial \eta} + \frac{v}{\eta}\right)\right] , \qquad (B.8)$$

$$i\bar{k}v = -\frac{1}{\gamma}\frac{\partial p}{\partial \eta} + \frac{\bar{k}}{s^2}\left[\left(\frac{\partial^2 v}{\partial \eta^2} + \frac{1}{\eta}\frac{\partial v}{\partial \eta} - \frac{v}{\eta^2} + \bar{k}^2\frac{\partial^2 v}{\partial \xi^2}\right) + \frac{1}{3}\frac{\partial}{\partial \eta}\left(\bar{k}\frac{\partial u}{\partial \xi} + \frac{\partial v}{\partial \eta} + \frac{v}{\eta}\right)\right] , \qquad (B.9)$$

$$i\bar{k}\rho = -\left(\bar{k}\frac{\partial u}{\partial \xi} + \frac{\partial v}{\partial \eta} + \frac{v}{\eta}\right) , \qquad (B.10)$$

$$p = \rho + T , \qquad (B.11)$$

$$iT = i\frac{\gamma-1}{\gamma}p + \frac{1}{\sigma^2 s^2}\left(\frac{\partial^2 T}{\partial \eta^2} + \frac{1}{\eta}\frac{\partial T}{\partial \eta} + \bar{k}^2\frac{\partial^2 T}{\partial \xi^2}\right) . \qquad (B.12)$$

These equations are valid if, together with the assumption of small perturbations, also the following conditions apply:

(a) homogeneous medium, which means that the wave length and the tube radius must be large in comparison with the mean free path; for air of normal atmospheric temperature and pressure, this condition breaks down if $f > 10^8$ Hz or $R < 10^{-5}$ cm;

(b) no steady flow

(c) tube long enough, so that end effects are negligible.

In the equations (B.9) - (B.12) the following four parameters can be distinguished:

$s = R\,(\rho_s \omega/\mu)^{\frac{1}{2}}$, the shear wave number

$\sigma = (\mu C_p/\lambda)^{\frac{1}{2}}$, the square root of the Prandtl number

$\bar{k} = \omega R/a_o$, the reduced frequency, being proportional to the ratio of tube radius to wave length

$\gamma = C_p/C_v$, the ratio of specific heats

As for a given gas σ and γ often can be considered as constants, the two important parameters are the shear wave number, s, and the reduced frequency, $\bar{k}$.

To obtain a solution of an infinitely long, rigid tube of constant circular cross-section, equations (B.8) - (B.12) have to satisfy the following boundary conditions and assumptions:

(a) at the tube wall the radial and the axial velocity must be zero: i.e.,

$$\text{at } \eta = 1 \,, \quad u = 0 \quad \text{and} \quad v = 0 \,; \tag{B.13}$$

(b) the radial velocity must be zero at the tube axis due to the axisymmetry of the problem: i.e.,

$$\text{at } \eta = 0 \,, \quad v = 0 \,; \tag{B.14}$$

and u, p, ρ, and T have to remain finite

(c) the heat conductivity of the tube wall is large in comparison with the heat conductivity of the fluid: i.e.,

$$\text{at } \eta = 1 \,, \; T = 0 \quad \text{(isothermal walls)} \tag{B.15}$$

B.1.2 Brief review of solutions given in the literature

The problem of solving equations (B.8) - (B.12) is a classical one, to which famous names are related like Helmholtz (Ref. 79), Kirchhoff (Ref. 80), and Rayleigh (Ref. 81). Since then many papers have been written on the subject, often in relation to studies dealing with the dynamic behaviour of pressure transmission lines. Recently the present author gave a review of the solutions given in the literature (Ref. 81). It appears that the solution for the pressure perturbation p in general can be put in the form

$$p = \{ A(\eta)\, e^{\Gamma\xi} + B(\eta)\, e^{-\Gamma\xi} \}\, e^{i\omega t} \,. \tag{B.16}$$

In this expression, two types of pressure waves can be distinguished, namely waves propagating in the positive ξ-direction and waves propagating in the opposite direction. An important quantity in this process is the propagation constant $\Gamma = \Gamma' + i\Gamma''$, which consists of a real part Γ', representing the attenuation of the waves over a unit distance ξ, and an imaginary part Γ'', being the phase shift over the same distance.

Once it was recognized that the problem is governed by the parameters s and $\bar{k}$, it appeared possible to rewrite the most significant analytical solutions for the propagation constant Γ in terms of these two parameters (Table B.1). The solutions collected in table B.1 can be divided roughly into two groups. The first group comprises solutions obtained as analytical approximations of the full solution of equations

TABLE B.1

Review of significant analytical solutions for the propagation constant

Author	Year	Formula for the propagation constant $\Gamma = \Gamma' + i\Gamma''$
Helmholtz (Ref. 79)	1863	$\Gamma = 1 + \frac{1+i}{\sqrt{2}} \frac{1}{s}$
Kirchhoff (Ref. 80) ("wide tube")	1868	$\Gamma = i + \frac{1+i}{\sqrt{2}} \left[\frac{\gamma-1+\sigma}{\sigma s}\right]$
Rayleigh (Ref. 81) ("narrow tube")	1896	$\Gamma = 2(1+i) \frac{\sqrt{\gamma}}{s}$
Kerris (Ref. 84)	1939	$\Gamma = \left[\frac{J_o(i^{3/2}s)}{J_2(i^{3/2}s)}\right]^{\frac{1}{2}}$
Zwikker and Kosten (Ref. 85) (independently also Iberall, 1950, Ref. 86)	1949	$\Gamma = \left[\frac{J_o(i^{3/2}s)}{J_2(i^{3/2}s)}\right]^{\frac{1}{2}} \left(\frac{\gamma}{n}\right)^{\frac{1}{2}}$, with $n = \left[1 + \frac{\gamma-1}{\gamma} \frac{J_2(i^{3/2}\sigma s)}{J_o(i^{3/2}\sigma s)}\right]^{-1}$
Weston (Ref. 83)	1953	$\Gamma' = 2\frac{\sqrt{\gamma}}{s}\left[1 - \frac{1}{48}s^2\left(4 - 3\frac{\gamma-1}{\gamma}\sigma^2\right) - \frac{1}{1536}s^4\left(-6 - 12\frac{\gamma-1}{\gamma}\sigma^2 + 13\frac{\gamma^2-1}{\gamma^2}\sigma^4\right)\right]$
Transition "narrow/wide" †		$\Gamma'' = 2\frac{\sqrt{\gamma}}{s}\left[1 - \frac{1}{48}s^2\left(4 - 3\frac{\gamma-1}{\gamma}\sigma^2\right) - \frac{1}{1536}s^4\left(-6 - 12\frac{\gamma-1}{\gamma}\sigma^2 + 13\frac{\gamma^2-1}{\gamma^2}\sigma^4\right) + \frac{1}{2304}s^4\left(4 - 3\frac{\gamma-1}{\gamma}\sigma^2\right)^2\right]^{-1}$
Transition "wide/narrow"		$\Gamma' = \frac{1}{\sqrt{2}}\left(\frac{\gamma-1+\sigma}{\sigma s}\right) + \frac{1}{s^2}\left(\frac{\gamma-1+\sigma}{\sigma} - \frac{\gamma(\gamma-1)}{2\sigma^2}\right) + \frac{1}{8\sqrt{2}}\frac{1}{s^3}\left(15 + 32\frac{\gamma-1}{\sigma} + \frac{12(\gamma-1)(\gamma-2)}{\sigma^2} + \frac{(\gamma-1)(4\gamma^2-12\gamma+7)}{\sigma^3}\right)$
		$\Gamma'' = \left[1 - \frac{1}{\sqrt{2}}\left(\frac{\gamma-1+\sigma}{\sigma s}\right) + \left(\frac{1}{\sqrt{2}}\right)^2\left(\frac{\gamma-1+\sigma}{\sigma s}\right)^2 - \left(\frac{1}{\sqrt{2}}\right)^3\left(\frac{\gamma-1+\sigma}{\sigma s}\right)^3 - \frac{1}{8\sqrt{2}}\frac{1}{s^3}\left(15 + 32\frac{\gamma-1}{\sigma} + \frac{12(\gamma-1)(\gamma-2)}{\sigma^2} + \frac{(\gamma-1)(4\gamma^2-12\gamma+7)}{\sigma^3}\right)\right]^{-1}$
Transition "wide/very wide"		$\Gamma' = \frac{1}{\sqrt{2}}\left(\frac{\gamma-1+\sigma}{\sigma s}\right) + \frac{1}{2}\frac{k^2}{s^2}\left(\frac{4}{3} + \frac{\gamma-1}{\sigma^2}\right) + \frac{1}{4}k^2\left(\frac{\gamma-1+\sigma}{\sigma s}\right)^2$
		$\Gamma'' = \left[1 - \frac{1}{\sqrt{2}}\frac{\gamma-1+\sigma}{\sigma s}\right]^{-1}$
Transition "very wide"		$\Gamma' = \frac{1}{2\sqrt{2}}\left(\frac{\gamma-1+\sigma}{\sigma s}\right) + \frac{1}{2}\frac{k^2}{s^2}\left(\frac{4}{3} + \frac{\gamma-1}{\sigma^2}\right) + \frac{1}{2}k^2\left(\frac{\gamma-1+\sigma}{\sigma s}\right)^2$
		$\Gamma'' = \left[1 - \frac{1}{2\sqrt{2}}\frac{\gamma-1+\sigma}{\sigma s}\right]^{-1}$
Rohmann and Grogan (Ref. 87)	1957	$\Gamma = \left[i\,(8/s^2) - \left(1 + \frac{1}{3}\exp\{-s^2/32\pi\}\right)\right]^{\frac{1}{2}}$
Karam and Franke (Ref. 88)	1969	$\Gamma = i + \frac{1}{\sqrt{2}}\left[\frac{\gamma-1+\sigma}{\sigma s}\right]$

† In reference 83, the solution for Γ' is a factor $\sqrt{2}$ in error.

(B.8) - (B.12), given by Kirchhoff in the form of a transcendental equation (Refs. 80, 81). The solutions in the second group were derived directly from the basic equations by the introduction of one or more simplifying assumptions.

The first approximations of the full Kirchhoff solution were produced by Kirchhoff himself for "wide" tubes and by Rayleigh for "narrow" tubes. Later, higher-order approximations were given by Weston (Ref. 83), who derived formulae for the transitions "narrow/wide", "wide/narrow", "wide/very-wide" and for "very-wide" tubes.

Analytical solutions in the second group, obtained directly from more or less simplified basic equations were presented by, among others, Kerris (Ref. 84), Zwikker and Kosten (Ref. 85), Iberall (Ref. 86), Rohmann and Grogan (Ref. 87), and by Karam and Franke (Ref. 88).

A closer examination of the formulae in table B.1 reveals that the expressions do not contain the reduced frequency, $\bar{k}$, except for the "wide/very-wide" and "very-wide" approximations of Weston (Ref. 83). In the last two cases the expressions for the attenuation, among other things, contain the term

$$\Gamma_{class} = \frac{1}{2} \{\bar{k}^2/s^2\} \{ \frac{4}{3} + (\gamma-1)/s^2\} , \qquad (B.17)$$

which equals the attenuation of plane waves in free air (Ref. 81), and which is independent of the tube radius.

In the "wide"-tube solution of Kirchhoff, the parameters s and σ are present, which indicates that both viscosity effects and heat conductivity have been accounted for. Putting $\gamma = 1$ (isothermal conditions) reduces the Kirchhoff solution to that of Helmholtz. For both solutions the result $\lim_{s\to\infty} \Gamma = i$ holds, this being the solution for plane waves in free air without dissipation.

The solution by Rayleigh for "narrow tubes", in which the diameter is assumed to be so small that heat is transferred freely from the center of the tube to the wall, does not contain the parameter σ, which indicates that only viscosity effects are involved.

As mentioned above, Weston's formulae are higher-order approximations of the full Kirchhoff solution, and therefore it is not surprising that the first terms of the "narrow/wide" approximation equal the Rayleigh solution, whereas the first term of the "wide/narrow" and "wide/very-wide" transitions show the characteristics of the "wide" tube of Kirchhoff.

The analytical solutions belonging to the second group, obtained directly from simplified basic equations, are of a different type, with the exception of the "high-frequency" solution of Karam and Franke (Ref. 88), which looks very similar to that of Kirchhoff.

The mutual relationship of the majority of the solutions to one another, except Weston's "wide/very-wide" and "very-wide" approximation, is shown in figure B.2, where the attenuation, Γ', and the phase shift, Γ'', are plotted as functions of the shear wave number s.

A point of interest revealed by figure B.2 is that the solution given for the first time by Zwikker and Kosten and designated here as the "low-reduced-frequency solution" passes continuously from Rayleigh's solution into the solution of Kirchhoff. This "low-reduced-frequency solution", to be derived in the next section, can be shown to be valid for $\bar{k} \ll 1$ and $\bar{k}/s \ll 1$. The solution covers all the solutions in table B.1, except for the "wide/very-wide" and "very-wide" approximations of Weston.

Another point of interest revealed by figure B.2 is that "narrow"-tube solutions are valid for low values of s and "wide"-tube solutions for high values of this parameter.

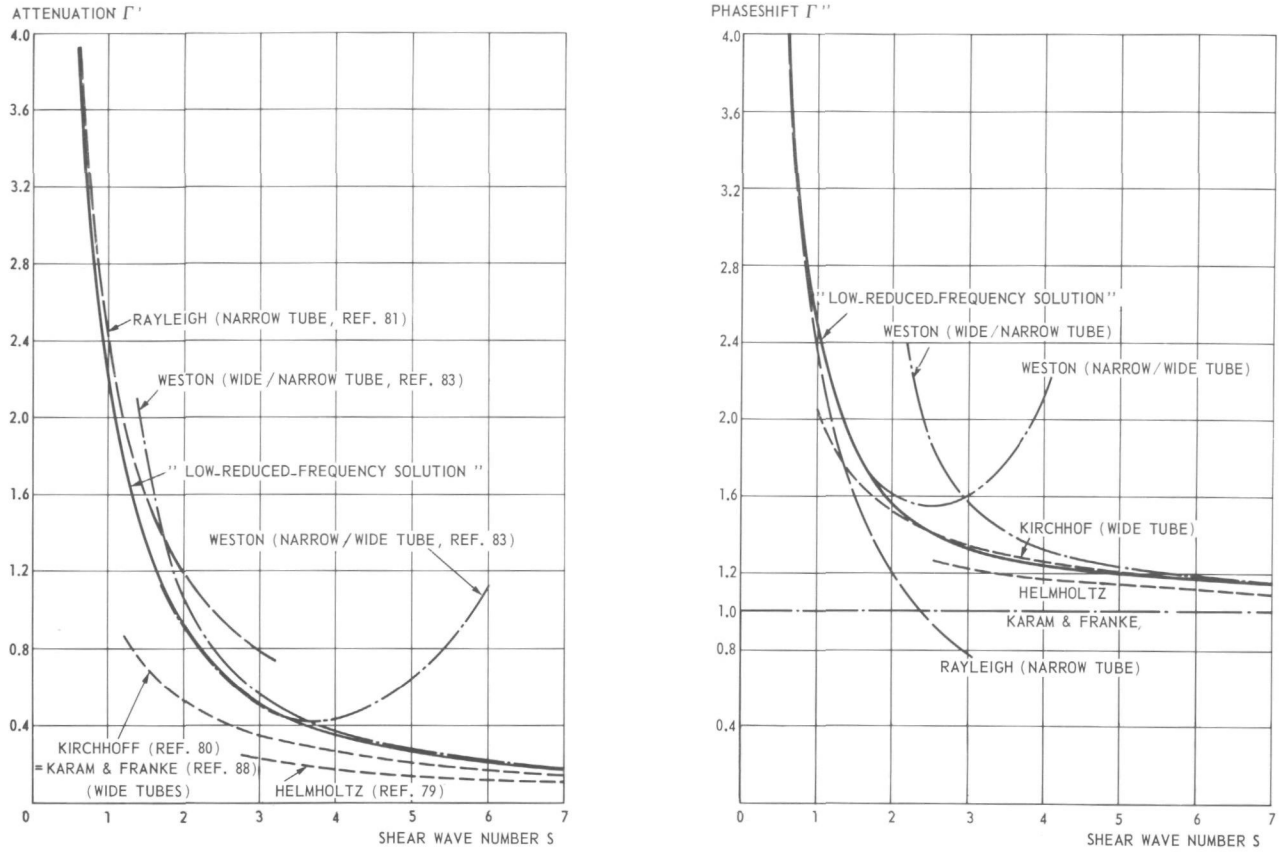

Fig. B.2 Propagation constant $\Gamma = \Gamma' + i\Gamma''$ as a function of shear wave number.

B.1.3 Derivation of the "low-reduced-frequency solution"

The formula for the propagation constant, Γ, according to the "low-reduced-frequency solution" was given for the first time by Zwikker and Kosten (Ref. 85), who obtained their solution in an intuitive way and without firm proof. Later, the solution was given more rigorously in references 22, 86, 89 - 91. In this section, a derivation of the "low-reduced-frequency solution" is given, which includes not only the complete set of acoustic variables, but explains also the conditions for which the solution is valid.

When the internal tube radius is small in comparison with the wave length and the radial velocity component, v, is small with respect to the axial velocity, u (i.e. $\bar{k} = \omega R/a_o \ll 1$ and $v/u \ll 1$) the basic equations (B.8) - (B.12) can be reduced to:

$$iu = -\frac{1}{\gamma}\frac{\partial p}{\partial \xi} + \frac{1}{s^2}\left[\frac{\partial^2 u}{\partial \eta^2} + \frac{1}{\eta}\frac{\partial u}{\partial \eta}\right], \tag{B.18}$$

$$0 = -\frac{1}{\gamma}\frac{\partial p}{\partial \eta}, \tag{B.19}$$

$$i\bar{k}\rho = -\left[\bar{k}\frac{\partial u}{\partial \xi} + \frac{\partial v}{\partial \eta} + \frac{v}{\eta}\right], \tag{B.20}$$

$$p = \rho + T, \tag{B.21}$$

$$iT = i\frac{\gamma-1}{\gamma}p + \frac{1}{\sigma^2 s^2}\left[\frac{\partial^2 T}{\partial \eta^2} + \frac{1}{\eta}\frac{\partial T}{\partial \eta}\right], \tag{B.22}$$

while the boundary conditions remain:

$$\text{at } \eta = 1 , \quad u = 0 , \quad v = 0 , \quad T = 0 ;$$

$$\text{at } \eta = 0 , \quad v = 0 . \tag{B.23}$$

From equation (B.19), it follows immediately that the amplitude of the pressure perturbation, p, depends only on the coordinate ξ.

Upon putting $u = f(\xi)\, h(z)$, with $z = i^{3/2}\, \eta s$, equation (B.18) can be rewritten as

$$\frac{\partial^2 h}{\partial z^2} + \frac{1}{z}\frac{\partial h}{\partial z} + h = \frac{i}{\gamma\, f(\xi)}\frac{dp}{d\xi} , \tag{B.24}$$

which yields the following solution

$$h(z) = C_1\, J_o(z) + C_2\, Y_o(z) + \frac{i}{\gamma\, f(\xi)}\frac{dp}{d\xi} . \tag{B.25}$$

To maintain a finite value of u for $\eta = 0$, the constant C_2 has to be zero.

From the condition $u = 0$ for $\eta = 1$ it follows that

$$f(\xi) = -\frac{i}{\gamma\, C_1\, J_o(i^{3/2}s)}\frac{dp}{d\xi} , \text{ wherefrom } \quad u = f(\xi)\, h(z) = \frac{i}{\gamma}\frac{dp}{d\xi}\left[1 - \frac{J_o(i^{3/2}\eta s)}{J_o(i^{3/2}s)}\right] . \tag{B.26 and B.27}$$

Equation (B.22) for the temperature perturbation, T, can be solved in a very similar way as the equation for the axial velocity. The solution that fulfils the requirement that T remains finite for $\eta = 0$ and vanishes for $\eta = 1$ is

$$T = \frac{\gamma - 1}{\gamma}\, p \left[1 - \frac{J_o(i^{3/2}\sigma\eta s)}{J_o(i^{3/2}\sigma s)}\right] . \tag{B.28}$$

Substitution of equation (B.28) into equation (B.21) gives

$$\rho = p - T = p\left[1 - \frac{\gamma - 1}{\gamma}\left(1 - \frac{J_o(i^{3/2}\sigma\eta s)}{J_o(i^{3/2}\sigma s)}\right)\right] . \tag{B.29}$$

Finally, the equation of continuity (B.20) has to be satisfied; thus

$$\frac{1}{\eta}\frac{\partial(v\,\eta)}{\partial\eta} = \bar{k}\left[i\rho + \frac{\partial u}{\partial\xi}\right] . \tag{B.30}$$

By using equations (B.27) and (B.29), this can be expressed as

$$\frac{1}{\eta}\frac{\partial(v\,\eta)}{\partial\eta} = i\bar{k}\left[p\left\{1 - \frac{\gamma - 1}{\gamma}\left(1 - \frac{J_o(i^{3/2}\sigma\eta s)}{J_o(i^{3/2}\sigma s)}\right)\right\} + \frac{1}{\gamma}\frac{d^2 p}{d\xi^2}\left(1 - \frac{J_o(i^{3/2}\eta s)}{J_o(i^{3/2}s)}\right)\right] . \tag{B.31}$$

After integration with respect to η, one has

$$v\eta = i\bar{k}\left[p\left\{\tfrac{1}{2}\eta^2 - \frac{\gamma-1}{\gamma}\left(\tfrac{1}{2}\eta^2 - \frac{\eta}{i^{3/2}\sigma s}\frac{J_1(i^{3/2}\sigma\eta s)}{J_o(i^{3/2}\sigma s)}\right)\right\} + \frac{1}{\gamma}\frac{d^2p}{d\xi^2}\left(\tfrac{1}{2}\eta^2 - \frac{\eta}{i^{3/2}s}\frac{J_1(i^{3/2}\eta s)}{J_o(i^{3/2}s)}\right) + F(\xi)\right] . \quad (B.32)$$

From the boundary condition $v = 0$ at $\eta = 1$, it follows that

$$-F(\xi) = \tfrac{1}{2}p\left\{1 + \frac{\gamma-1}{\gamma}\frac{J_2(i^{3/2}\sigma s)}{J_o(i^{3/2}\sigma s)}\right\} - \frac{1}{2\gamma}\frac{d^2p}{d\xi^2}\frac{J_2(i^{3/2}s)}{J_o(i^{3/2}s)} . \quad (B.33)$$

Due to the axial symmetry, $v = 0$ at $\eta = 0$, this requirement is fulfilled if $F(\xi) = 0$, or

$$p\left\{1 + \frac{\gamma-1}{\gamma}\frac{J_2(i^{3/2}\sigma s)}{J_o(i^{3/2}\sigma s)}\right\} - \frac{1}{\gamma}\frac{d^2p}{d\xi^2}\frac{J_2(i^{3/2}s)}{J_o(i^{3/2}s)} = 0 . \quad (B.34)$$

From the equation (B.34), one can solve for p:

$$p = A\,e^{\Gamma\xi} + B\,e^{-\Gamma\xi}, \quad \text{with} \quad \Gamma = \left[\frac{J_o(i^{3/2}s)}{J_2(i^{3/2}s)}\frac{\gamma}{n}\right]^{\frac{1}{2}}, \quad \text{and} \quad n = \left[1 + \frac{\gamma-1}{\gamma}\frac{J_2(i^{3/2}\sigma s)}{J_o(i^{3/2}\sigma s)}\right]^{-1} . \quad (B.35)$$

The solution for the other acoustic variables becomes

$$u = \frac{i\Gamma}{\gamma}\left[1 - \frac{J_o(i^{3/2}\eta s)}{J_o(i^{3/2}s)}\right]\left[A\,e^{\Gamma\xi} - B\,e^{-\Gamma\xi}\right], \quad (B.36)$$

$$v = i\bar{k}\left[\tfrac{1}{2}\eta\left\{1 + \frac{J_o(i^{3/2}s)}{J_2(i^{3/2}s)}\frac{\gamma}{n}\right\} + \frac{\gamma-1}{i^{3/2}\sigma s}\frac{J_1(i^{3/2}\sigma\eta s)}{J_o(i^{3/2}\sigma s)} - \frac{\gamma}{i^{3/2}\eta s}\frac{J_1(i^{3/2}\eta s)}{J_2(i^{3/2}s)}\right]\left[A\,e^{\Gamma\xi} + B\,e^{-\Gamma\xi}\right], \quad (B.37)$$

$$\rho = \left[1 - \frac{\gamma-1}{\gamma}\left\{1 - \frac{J_o(i^{3/2}\sigma\eta s)}{J_o(i^{3/2}\sigma s)}\right\}\right]\left[A\,e^{\Gamma\xi} + B\,e^{-\Gamma\xi}\right], \quad (B.38)$$

$$T = \frac{\gamma-1}{\gamma}\left[1 - \frac{J_o(i^{3/2}\sigma\eta s)}{J_o(i^{3/2}\sigma s)}\right]\left[A\,e^{\Gamma\xi} + B\,e^{-\Gamma\xi}\right] . \quad (B.39)$$

The constants A and B should be determined by specifying additional constraints at both ends of the tube. From the solution for the radial velocity, v, it can be verified a posteriori that the condition $v/u \ll 1$ is fulfilled if $\bar{k} \ll 1$ and $\bar{k}/s \ll 1$.

It appears that a solution identical to (B.35) can be obtained if, in the original set of equations, the equation of state and the energy equation (equation B.11 and B.12) are replaced by the single polytropic relation $\bar{p}/\bar{\rho}^{n} = \text{constant}$. Evidently, the thermodynamic process inside the tube can be considered to occur polytropically, with the (complex) polytropic constant, n, given by the expression (B.35). This polytropic constant is a function of the product σs, which means that the constant does not depend on the

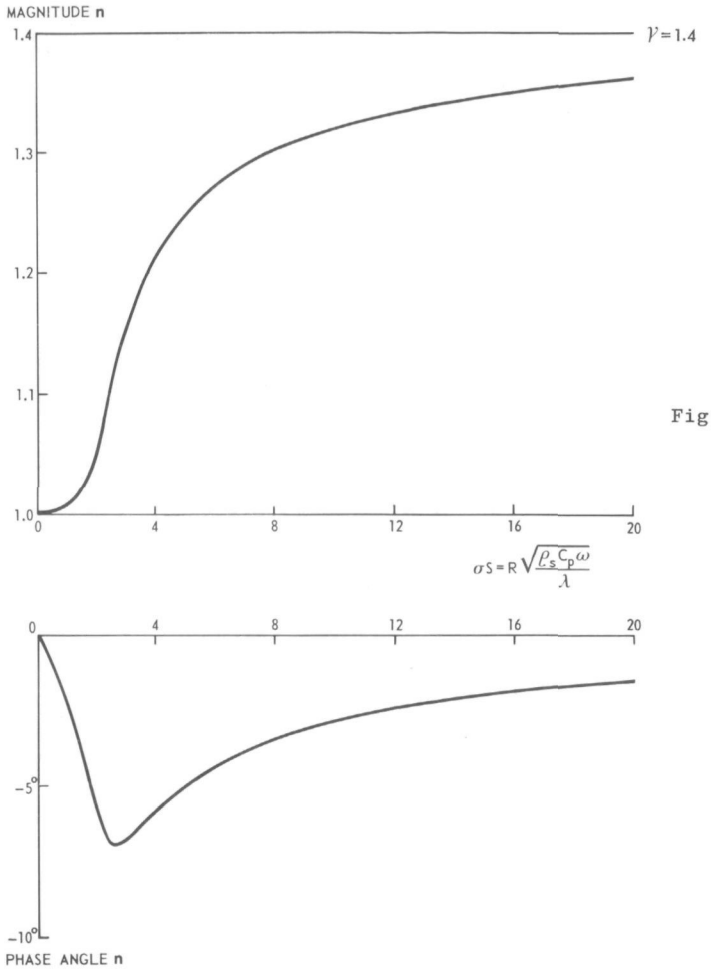

Fig. B.3 "Polytropic constant" n for the propagation of pressure waves in cylindrical tubes as a function of σs.

viscosity and only accounts for the effect of heat conduction. The development of the polytropic constant with σs is shown in figure B.3. Of interest are the asymptotic values of n:

$$\lim_{\sigma s \to 0} n = 1 \qquad \text{and} \qquad \lim_{\sigma s \to \infty} n = \gamma \ ,$$

which imply that the propagation of the pressure waves at very small values of σs (for instance at very low frequency) happens isothermally, whereas at high values of σs (for instance at very high frequency) the propagation takes place almost adiabatically.

B.1.4 Effect of the reduced frequency

The full solution of the basic equations (B.8) - (B.12), without the assumptions pertaining to the "low-reduced-frequency solution", is given in the original paper of Kirchhoff (Ref. 80). This solution is obtained in the form of a transcendental equation, which does not lend itself to further analytical treatment. Using the knowledge that the problem is governed by the four basic parameters s, $\bar{k}$, σ, and γ, the present author rewrote the original Kirchhoff solution into the more attractive form (Ref. 82):

$$F(\Gamma, s, \bar{k}, \sigma, \gamma) = 0 \ . \tag{B.40}$$

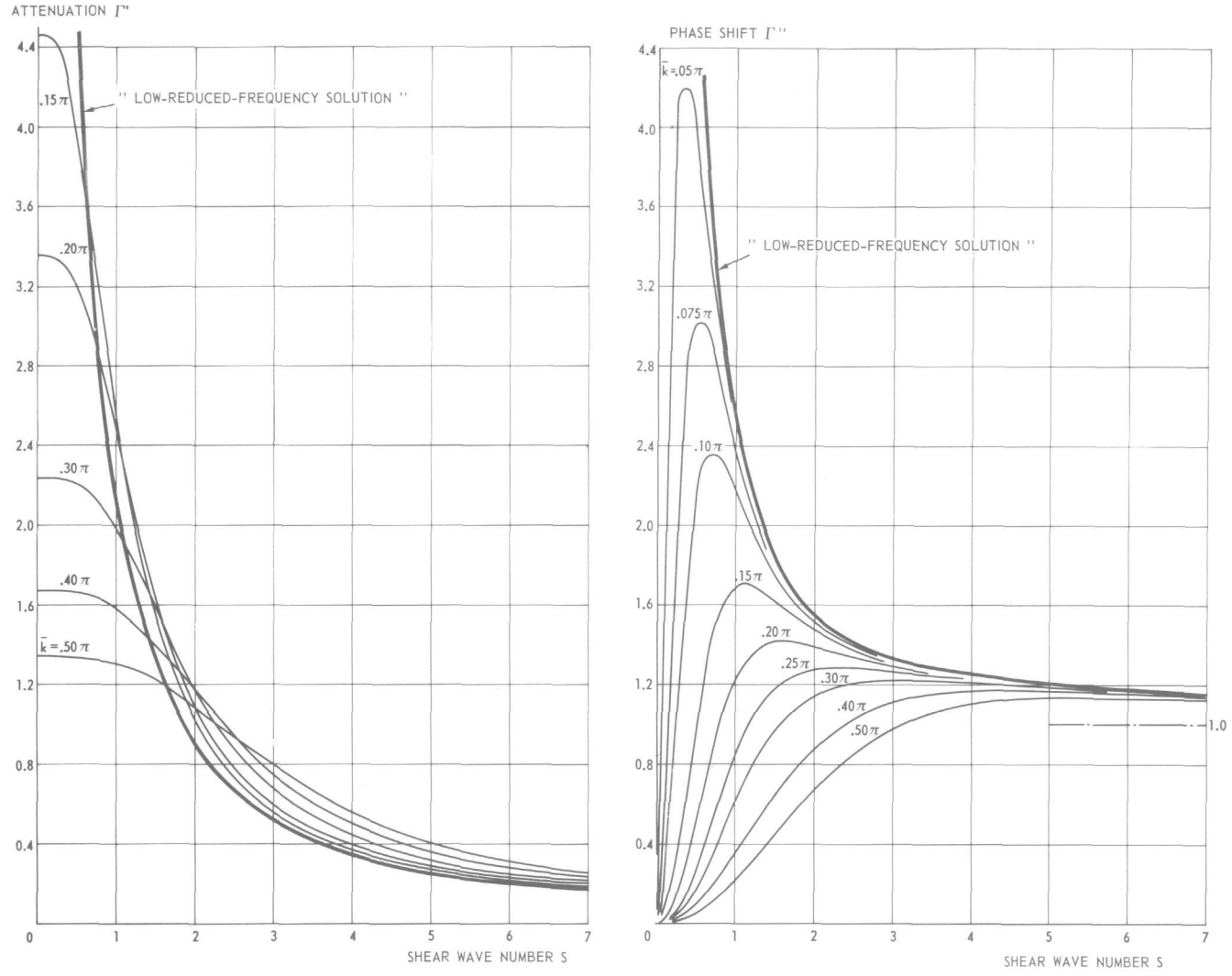

Fig. B.4 Exact solution of $\Gamma = \Gamma' + i\Gamma''$ as a function of shear wave number and reduced frequency.

This equation is solved numerically with the Newton-Raphson procedure. As a first estimate, the value of Γ resulting from the "low-reduced-frequency solution" has been used.

Some characteristic results, showing the influence of the reduced frequency, $\bar{k}$, on the propagation constant, Γ, are given in figure B.4. This figure reveals a large effect of the reduced frequency on both attenuation and phase shift, especially in the range of relatively low values of s ($s \lesssim 4$). For small values of $\bar{k}$, the exact value approaches the "low-reduced-frequency solution".
For the range of interest for the present investigation ($0 \leq \bar{k} \leq 0.007$), the effect of this parameter can be discarded.

B.2 DERIVATION OF THE FORMULAE FOR THE DYNAMIC RESPONSE OF TUBE-TRANSDUCER SYSTEMS

To arrive at the solution of tube-transducer systems, use is made of the "low-reduced-frequency solution". From this solution, both the expression for the pressure perturbation (B.35) and the expression for the perturbation in axial velocity (B.36) are needed. The latter expression is used to calculate the mean value of the velocity perturbation:

$$u_o = \frac{1}{\pi R^2} \int_o^R u\, 2\pi r\, dr = \frac{i\Gamma}{\gamma} \frac{J_2(i^{3/2}s)}{J_o(i^{3/2}s)} \left[A\, e^{(\omega x/a_o)\Gamma} - B\, e^{-(\omega x/a_o)\Gamma} \right] e^{i\omega t} \quad . \tag{B.41}$$

To determine the values of the constants A and B, the following boundary conditions are introduced. At the entrance of tube j of the general tube-transducer system of figure 5.2, the pressure perturbation equals the pressure perturbation in the preceding volume $V_{v,j-1}$, which in its turn equals the pressure perturbation at the end of tube j-1. Furthermore, for each volume $V_{v,j}$ the increase in mass at each moment has to be equal to the difference in mass leaving tube j and the mass entering tube j+1.
The first condition leads to:

$$x_j = 0, \qquad p_{j-1}(x_{j-1}=L_{j-1}) = p_j(x_j=0) = \text{pressure perturbation in } V_{v,j-1} \quad . \tag{B.42}$$

(This condition is valid for $j \geq 2$. For the entrance of the first tube (j = 1) a separate boundary condition has to be given, which will be discussed later.)
The second condition gives:

$$dm_{v,j}/dt = \pi R_j^2\, \rho_s\, u_{o,j}(x_j=L_j) - \pi R_{j+1}^2\, \rho_s\, u_{o,j+1}(x_{j+1}=0) \quad . \tag{B.43}$$

with $$m_{v,j} = V_{v,j}\, \rho_s\, (1 + \rho_j e^{i\omega t}) \quad \text{being the mass inside volume } V_{v,j} \quad . \tag{B.44}$$

In order to obtain a relation between the pressure perturbation p_j and the density perturbation ρ_j inside the volume, it is assumed that the gas inside the volume behaves polytropically, according to the relation

$$\left[p_s\, (1 + p_j\, e^{i\omega t})\right] \left[\rho_s\, (1 + \rho_j\, e^{i\omega t})\right]^{-n_v} = \text{constant} \quad , \tag{B.45}$$

with n_v a polytropic constant, which has to be chosen. At rest conditions, the constant reduces to $(p_s)(\rho_s)^{-n_v}$. For small perturbations, this implies that

$$p_j = n_v \rho_j \quad . \tag{B.46}$$

With the help of conditions (B.42) and (B.43) and the relations (B.35), (B.41), (B.44), and (B.46), the following recursion formula can be derived, which relates the pressure perturbation in volume j to the sinusoidal pressure perturbation in the preceding volume j-1 and the next volume j+1:

$$\frac{p_j}{p_{j-1}} = \left[\cosh\left\{\frac{\omega L}{a_o}\Gamma\right\}_j + \frac{V_{v,j}}{V_{t,j}} \frac{n_j}{n_{v,j}} \left\{\frac{\omega L}{a_o}\Gamma\right\}_j \sinh\left\{\frac{\omega L}{a_o}\Gamma\right\}_j + \right.$$

$$\left. + \frac{V_{t,j+1}}{V_{t,j}} \frac{a_{o,j}^2}{a_{o,j+1}^2} \frac{n_j}{n_{j+1}} \frac{\left\{\frac{\omega L}{a_o}\Gamma\right\}_j}{\left\{\frac{\omega L}{a_o}\Gamma\right\}_{j+1}} \frac{\sinh\left\{\frac{\omega L}{a_o}\Gamma\right\}_j}{\sinh\left\{\frac{\omega L}{a_o}\Gamma\right\}_{j+1}} \left(\cosh\left\{\frac{\omega L}{a_o}\Gamma\right\}_j - \frac{p_{j+1}}{p_j} \right) \right]^{-1} \quad . \tag{B.47}$$

where j = 2,3.....,N.

In still air, the boundary condition at the entrance of the first tube is dictated by the fact that the pressure perturbation for x = 0 equals the value p_i imposed upon the system (Fig. 5, 4a):

$$x_1 = 0 \ , \quad p_o = p_i \ . \tag{B.48}$$

This implies that no restriction is present for the oscillatory velocity u_o in the tube entrance, so that air is free to move in and out of the tube opening. In case an airflow blows across the tube entrance, however, the air leaving the tube has to displace the main flow, which leads locally to additional oscillatory pressures at the tube entrance (Fig. 5.4b). This leads to an adapted boundary condition:

$$x_1 = 0 \ , \quad p_o = p_i + \Delta p \ . \tag{B.49}$$

For the relation between Δp and the main flow parameters, the following expression has been introduced:

$$\Delta p = C \, \rho_s \, u_o \, U \tag{B.50}$$

with C being a constant yet unknown.

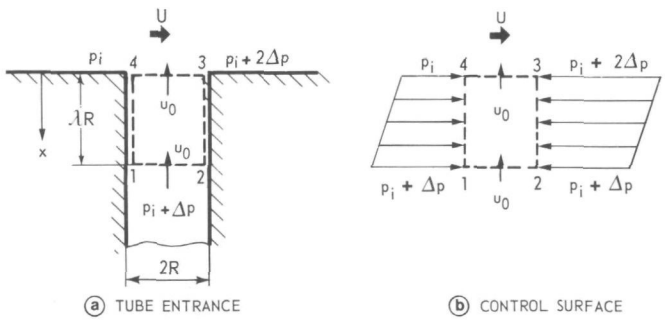

Fig. B.5 Momentum balance of the tube entrance.

Relation (B.50) can be made plausible as follows: let us assume, for convenience in a two-dimensional case, that the gradient in oscillatory pressure across the tube opening changes linearly inside the tube in such a way that at a distance λR from the opening the gradient is smoothed out (Fig. B.5a). From the momentum balance in U-direction, it then follows that

$$\rho_s \, u_o \, U \, 2R = -\tfrac{1}{2}(2p_i + \Delta p)\lambda R + \tfrac{1}{2}(2p_i + 3\Delta p)\lambda R = \Delta p \, \lambda R, \quad \text{or:} \quad \Delta p = \frac{2}{\lambda} \rho_s \, u_o \, U = C \, \rho_s \, u_o \, U \ .$$

Because λR can be expected to be of the order of a diameter, C will be of O(1).

When the boundary conditions (B.43) and (B.49) are applied and when expression (B.41) is used for the axial velocity u_o, the following formula for the dynamic response for the first tube (j = 1) can be derived:

$$\left\{\frac{p_1}{p_i}\right\}_{U\neq 0} = \left[\left\{\frac{p_1}{p_i}\right\}_{U=0}^{-1} + C \, \frac{U}{a_{o,1}} \frac{i\gamma}{n_1 \Gamma_1} \left\{ \sinh\left\{\frac{\omega L}{a_o}\Gamma\right\}_1 - \frac{n_1}{n_{v,1}} \left\{\frac{\omega L}{a_o}\Gamma\right\}_1 \frac{V_{v,1}}{V_{t,1}} \cosh\left\{\frac{\omega L}{a_o}\Gamma\right\}_1 + \right.\right.$$
$$\left.\left. + \frac{V_{t,2}}{V_{t,1}} \frac{a_{o,1}^2}{a_{o,2}^2} \frac{n_1}{n_2} \frac{\left\{\frac{\omega L}{a_o}\Gamma\right\}_1 \cosh\left\{\frac{\omega L}{a_o}\Gamma\right\}_1}{\left\{\frac{\omega L}{a_o}\Gamma\right\}_2 \sinh\left\{\frac{\omega L}{a_o}\Gamma\right\}_2} \left(\cosh\left\{\frac{\omega L}{a_o}\Gamma\right\}_2 - \left\{\frac{p_2}{p_1}\right\}_{U=0} \right) \right\} \right]^{-1} , \tag{B.51}$$

where $\left\{\frac{p_1}{p_i}\right\}_{U=0}$ and $\left\{\frac{p_2}{p_1}\right\}_{U=0}$

should be obtained from (B. 47).

By putting j = 1 and C = 0, the formula for the dynamic response of a single tube-transducer system (Fig. 5.3a) in still air is obtained:

$$\left\{\frac{p_1}{p_i}\right\}_{U=0} = \left[\cosh\left\{\frac{\omega L}{a_o}\Gamma\right\} + \frac{V_v}{V_t}\frac{n}{n_v}\left\{\frac{\omega L}{a_o}\Gamma\right\}\sinh\left\{\frac{\omega L}{a_o}\Gamma\right\}\right]^{-1} . \qquad (B.52)$$

This expression can be shown to be identical to the solution published by Iberall (Ref. 86). Detailed experimental verifications of this solution were published independently by Bergh and Tijdeman (Ref. 22), who cover a shear-wave-number range $0 \leq s \leq 8.5$, and by Watts (Ref. 92) for $0 \leq s \leq 100$. Later, additional comparisons between theory and experiment were given by Karam and Franke (Ref. 88) for $0 \leq s \leq 83$, by Triebstein (Ref. 93) for $0 \leq s \leq 9$, and by Goldschmiedt (Ref. 94) for $0 \leq s \leq 20$. In all these cases, a satisfactory agreement between the theoretical prediction and the experimental results was obtained for tubes that in the various investigations varied in length between 15 and 600 cm.

For a single tube-transducer system with a main flow across the tube entrance, the following formula holds (j = 1, $C \neq 0$):

$$\frac{p_1}{p_i} = \left[\left\{\frac{p_1}{p_i}\right\}^{-1}_{U=0} + C\frac{U}{a_o}\frac{i\gamma}{n\Gamma}\left(\sinh\left\{\frac{\omega L}{a_o}\Gamma\right\} - \frac{n}{n_v}\left\{\frac{\omega L}{a_o}\Gamma\right\}\frac{V_v}{V_t}\cosh\left\{\frac{\omega L}{a_o}\Gamma\right\}\right)\right]^{-1} . \qquad (B.53)$$

This formula has been verified in the course of the present investigation (Ref. 72).

APPENDIX C : DERIVATION OF THE QUASI - STEADY AND UNSTEADY SHOCK RELATIONS

To obtain the required relations between the flow quantities just upstream and downstream of a normal shock wave for quasi-steady and unsteady flow, the following well-known relations for steady flow have been applied:

$$p_2/p_1 = 1 + \frac{2\gamma}{\gamma+1}\{M_1^2 - 1\} , \qquad (C.1)$$

(Rankine-Hugoniot relation)

$$M_2^2 = \{(\gamma-1)M_1^2 + 2\}/\{2\gamma M_1^2 - (\gamma-1)\} \qquad (C.2)$$

$$U_2/U_1 = \{(\gamma-1)M_1^2 + 2\}/\{(\gamma+1)M_1^2\} . \qquad (C.3)$$

Here index 2 refers to the quantities just behind the shock wave, and index 1 to the quantities just ahead of the shock wave.

Under the assumption of isentropic flow, the local flow quantities ahead of the shock wave are related to the corresponding quantities under stagnation conditions, designated by index 0, as:

$$p_o/p_1 = \{1 + \tfrac{1}{2}(\gamma-1)M_1^2\}^{\gamma/(\gamma-1)} , \qquad (C.4)$$

$$a_o/a_1 = \{T_o/T_1\}^{\frac{1}{2}} = \{1 + \tfrac{1}{2}(\gamma-1)M_1^2\}^{\frac{1}{2}} , \qquad (C.5)$$

$$U_1 = a_1 M_1 . \qquad (C.6)$$

If the simplified flow model, discussed in section 9.1 (Fig. 9.7), is accepted and if it is assumed that the shock wave moves relatively to the airfoil with a velocity V ($V \ll a$), then relation (C.1) becomes:

$$\frac{\bar{p}_2}{\bar{p}_1} = 1 + \frac{2\gamma}{\gamma+1}\left[\left\{M_1 + \frac{\partial M_1}{\partial x}\Delta x - \frac{V}{a_1 + (\partial a_1/\partial x)\Delta x}\right\}^2 - 1\right]$$

$$\approx \left\{\frac{p_2}{p_1}\right\}_{x=x_s} + \frac{4\gamma M_1}{\gamma+1}\left\{\frac{\partial M_1}{\partial x}\Delta x - \frac{V}{a_1}\right\}, \qquad (C.7)$$

where $\bar{p}_2$ and $\bar{p}_1$ are the instantaneous pressures just downstream and upstream of the shock wave, respectively.

When a sinusoidal motion of the shock wave with frequency ω and amplitude x_o is considered, the following definitions apply:

$$\Delta x = x_o\, e^{i\omega t}\ ,$$
$$V = i\omega x_o\, e^{i\omega t}\ , \qquad (C.8)$$

Introduction of (C.8) gives the following relation for the instantaneous shock strength:

$$\bar{p}_2/\bar{p}_1 = \{p_2/p_1\}_{x=x_s} + \frac{4\gamma M_1}{\gamma+1}\left[\frac{\partial M_1}{\partial x} - \frac{i\omega}{a_1}\right] x_o\, e^{i\omega t}. \qquad (C.9)$$

To obtain the relation between the pressure perturbation behind the shock wave and the amplitude of the shock-wave motion, the left-hand side of (C.7) is written as:

$$\bar{p}_2/\bar{p}_1 = \{p_2(x_s) + \Delta p_2\} \,/\, \{p_1(x_s) + \Delta p_1\}\ . \qquad (C.10)$$

By putting $\Delta p_1 = (\partial p_1/\partial x)\Delta x$, it can be derived easily that

$$\frac{\Delta p_2}{p_1(x_s)} \approx \frac{1}{p_1(x_s)}\left\{\frac{p_2}{p_1}\right\}_{x=x_s}\frac{\partial p_1}{\partial x}\Delta x + \frac{4\gamma M_1}{\gamma+1}\left\{\frac{\partial M_1}{\partial x}\Delta x - \frac{V}{a_1}\right\}. \qquad (C.11)$$

When constant stagnation conditions are assumed, it can be shown by differentiation of the isentropic relation (C.4) that

$$\frac{\partial p_1}{\partial x} = -\,p_1\,\frac{\gamma M_1(\partial M_1/\partial x)}{1 + \frac{1}{2}(\gamma-1)M_1^2}\ . \qquad (C.12)$$

Substitution of (C.12) and (C.8) into (C.11) yields for a sinusoidal shock-wave motion:

$$\frac{\Delta p_2}{p_1(x_s)} \approx \frac{2\gamma M_1}{\gamma+1}\left[\left\{\frac{3 + \gamma - 2M_1^2}{2 + (\gamma-1)M_1^2}\right\}\frac{\partial M_1}{\partial x} - 2\,\frac{i\omega}{a_1}\right] x_o\, e^{i\omega t}. \qquad (C.13)$$

When equation (C.3) is used, the velocity ratio is found to be:

$$U_2/U_1 = \{U_2(x_s) + \Delta U_2 - V\} \,/\, \{U_1(x_s) + \Delta U_1 - V\} \approx$$
$$\approx \frac{1}{(\gamma+1)M_1^2}\left[2 + (\gamma-1)M_1^2 + \frac{4V}{a_1 M_1} - \frac{4}{M_1}(\partial M_1/\partial x)\Delta x\right]. \qquad (C.14)$$

By putting $\Delta U_1 = (\partial U_1/\partial x)\Delta x$ and using (C.5) and (C.6), it follows that

$$\Delta U_1 = \frac{2a_1(\partial M_1/\partial x)\Delta x}{2 + (\gamma-1)M_1^2}\ . \qquad (C.15)$$

Substitution of (C.15) into (C.14) yields for the velocity perturbation behind the shock wave:

$$\Delta U_2 = \frac{2}{(\gamma+1)M_1^2}\left[-a_1(\partial M_1/\partial x)\Delta x + V(1 + M_1^2)\right]\ . \qquad (C.16)$$

For a sinusoidal shock-wave motion, this velocity perturbation becomes:

$$\Delta U_2 = \frac{2}{(\gamma+1)M_1^2}\left[-a_1(\partial M_1/\partial x) + i\omega(1 + M_1^2)\right] x_o\, e^{i\omega t}. \qquad (C.17)$$

From (C.9), (C.13), and (C.17), the expressions for quasi-steady flow can be obtained simply by putting $\omega = 0$.

APPENDIX D : LIST OF SYMBOLS

A	constant defined in eq. (5.1)
A	constant defined in eq. (9.1b)
a	velocity of sound
a_o	undisturbed velocity of sound inside a pressure tube
a_j	coefficients defined in eq. (12.10)
B	constant defined in eq. (5.1)
c	chord length ($c = 2\ell$)
c_k	steady normal-force coefficient
c_ℓ	steady lift coefficient (for small incidences, $c_\ell \approx c_k$)
c_m	steady moment coefficient about quarter-chord point
c_n	steady hinge-moment coefficient
C_p	steady pressure coefficient
C_p^*	steady pressure coefficient for which $M_{loc} = 1$
C_p	specific heat at constant pressure
C_v	specific heat at constant volume
ΔC_p	unsteady pressure coefficients, defined in Appendix A
C	constant defined in eq. (5.4)
C	wall correction coefficient, defined in eq. (13.1)
D_{ij}	aerodynamic influence coefficient, defined in eq. (12.13)
e	energy per unit volume
f	frequency (Hz)
$f(x)$	airfoil thickness distribution
$g(x)$	mode of vibration
$g(x,t)$	time-dependent deformation
$H_j(x)$	pressure loading functions, defined in eq. (12.10)
$H_n^{(2)}$	Hankel function of second kind of order n
$i = \sqrt{-1}$	imaginary unit
J_n	Bessel function of first kind of order n
$\bar{K}$	steady normal force
K	unsteady normal force
$K(x_o,k,M_\infty)$	Kernel function for subsonic lifting-surface theory
K_{ij}	unsteady aerodynamic influence coefficient, defined in eq. (12.10)
k	reduced frequency ($k = \omega\ell/U_\infty$)
$\bar{k}$	reduced frequency (pressure tube) ($\bar{k} = \omega R/a_o$)
$k_\alpha = k'_\alpha + ik''_\alpha$	unsteady normal-force coefficient due to pitch oscillation
$k_c = k'_c + ik''_c$	unsteady normal-force coefficient due to flap oscillation
L	lift
L	wavelength
L	length of pressure tube
ΔL	variation in lift
ℓ	semi chord
$\bar{M}$	steady moment about quarter-chord point
M	unsteady moment about quarter-chord point
M	Mach number
M^*	critical Mach number
$m_\alpha = m'_\alpha + im''_\alpha$	unsteady moment coefficient about quarter-chord point due to pitch oscillation
$m_c = m'_c + im''_c$	unsteady moment coefficient about quarter-chord point due to flap oscillation
$\bar{N}$	steady hinge moment
N	unsteady hinge moment
N	number of pressure tubes in a series connection
n	polytropic constant for pressure tube, defined in eq. (5.2)
$n_c = n'_c + in''_c$	unsteady hinge-moment coefficient
n_v	polytropic constant for transducer volume
p	pressure
p_o	stagnation pressure
p_∞	static pressure of the free-stream flow
p_i	pressure perturbation at the entrance of a pressure tube
p_u	pressure perturbation in the scanning valve
p_s	mean pressure
$\Delta p = \Delta p' + i\Delta p''$	pressure perturbation at the airfoil surface
q	dynamic pressure ($q = \frac{1}{2}\rho_\infty U_\infty^2$)
R	tube radius
R	relaxation factor, defined in eq. (10.3)
Re	Reynolds number based on chord length ($Re = \rho_\infty c U_\infty/\mu$)
R_e	real part of a complex number
R_o	gas constant
r	coordinate in radial direction (pressure tube)
$S(x,y,t)$	airfoil contour

s	shear wave number ($s = R\{\rho_s \omega/\mu\}^{\frac{1}{2}}$)
s	semi span
T	temperature
T_s	mean temperature inside a pressure tube
t	time
U	velocity component in x-direction
U_∞	free-stream velocity
u	velocity perturbation in axial direction (pressure tube)
u_o	velocity in the entrance of a pressure tube
V	velocity component in y-direction
V	velocity of a shock wave relative to the airfoil
V_v	transducer volume
V_t	volume of pressure tube ($V_t = \pi R^2 L$)
v	velocity perturbation in radial direction (pressure tube)
w	normal wash
x	coordinate in axial direction (pressure tube)
x	coordinate in the direction of the free-stream flow
x_h	location of hinge axis
x_o	amplitude of shock-wave oscillation
x_o	distance between sending and receiving point ($x_o = x-\xi$)
x_s	shock position
Y_n	Neumann function of first kind of order n
y	coordinate normal to the free-stream direction
α	incidence
α_c	incidence corrected for wall interference
α_o	geometric (mean) incidence
$\Delta\alpha$	variation in incidence, amplitude of pitch oscillation
β_∞	$\beta_\infty = (1-M_\infty^2)^{\frac{1}{2}}$
$\Gamma = \Gamma' + i\Gamma''$	constant for the propagation of pressure waves through cylindrical tubes
γ	ratio of specific heats ($\gamma = C_p/C_v$)
δ	variation in flap angle, amplitude of flap oscillation
δ_o	geometric (mean) flap angle
η	coordinate in radial direction (pressure tube) ($\eta = r/R$)
λ	thermal conductivity
μ	absolute fluid viscosity
ξ	coordinate in axial direction (pressure tube) ($\xi = \omega x/a_o$)
ξ	coordinate in streamwise direction
ρ	air density
ρ_s	mean air density inside a pressure tube
σ^2	Prandtl number ($\sigma^2 = \mu C_p/\lambda$)
$\Phi(x,y,t)$	disturbance velocity potential
$\Phi_o(x,y)$	steady part of disturbance velocity potential
$\phi(x,y)e^{i\omega t}$	unsteady part of disturbance velocity potential
φ	phase angle
ω	frequency (rad/sec) ($\omega = 2\pi f$)

Subscripts:

∞	free-stream value
loc	local value
1	value just upstream of a shock wave
2	value just downstream of a shock wave

APPENDIX E : SAMENVATTING IN HET NEDERLANDS

Onder bepaalde omstandigheden kunnen de vleugel of de staartvlakken van een vliegtuig in een instabiele trilling geraken, waardoor de constructie meestal in korte tijd bezwijkt. Dit verschijnsel, dat veroorzaakt wordt door het samenspel van de elastische en massatraagheidskrachten van de constructie en de luchtkrachten op het betreffende deel, wordt "flutter" genoemd. Vanwege het gevaarlijke karakter van flutter is een vliegtuigfabrikant verplicht om aan te tonen dat de snelheid waarbij dit verschijnsel optreedt voldoende ver buiten het snelheidsbereik van het desbetreffende vliegtuig ligt. In dit opzicht dient een vliegtuig aan stringente luchtwaardigheidseisen te voldoen.

Om genoemde reden wordt in de luchtvaartindustrie veel aandacht besteed aan de ontwikkeling van betrouwbare methoden voor het voorspellen van de fluttereigenschappen van vliegtuigen. De betrouwbaarheid van deze methoden hangt voornamelijk af van de nauwkeurigheid waarmee de luchtkrachten op trillende draagvlakken (de zogenaamde "instationaire luchtkrachten") kunnen worden bepaald. Voor subsone en supersone snelheden zijn hiervoor inmiddels goede rekenmethoden beschikbaar, maar voor het transsone snelheidsgebied, waarin gecompliceerde stromingspatronen met zowel subsone als supersone snelheden, vaak gescheiden door schokgolven, optreden, is dit nog niet het geval. Deze situatie is weinig bevredigend, vooral omdat de ervaring heeft geleerd dat flutterproblemen relatief vaak optreden in het transsone snelheidsgebied.

Door de in de laatste jaren sterk toegenomen belangstelling voor het vliegen bij transsone snelheid (met name door de ontwikkeling van zogenaamde "superkritieke" of "schokvrije" vleugels, waarbij door een speciale vormgeving een gedeeltelijk supersone stroming zonder schokgolven wordt verkregen), is er ook een sterk toegenomen behoefte ontstaan aan methoden waarmee de luchtkrachten op trillende draagvlakken in transsone stroming voorspeld kunnen worden. Op verschillende plaatsen is men dan ook begonnen met het ontwikkelen van numerieke methoden om de gecompliceerde vergelijkingen voor de transsone stroming op te lossen.

Het succes van dergelijke methoden hangt sterk af van de betrouwbaarheid waarmee het typisch transsone karakter van de stroming kan worden beschreven. Om dit te kunnen beoordelen is het nodig te beschikken over experimentele resultaten die voldoende gedetailleerd zijn om basisveronderstellingen in de rekenmethoden te verifiëren en berekende resultaten te toetsen. Experimentele gegevens voor dit doel waren echter niet of nauwelijks aanwezig op het moment dat het in dit proefschrift beschreven onderzoek werd gestart.

Om het inzicht in het gedrag van transsone stromingen om trillende profielen te vergroten en experimentele resultaten te verkrijgen voor de ondersteuning van de genoemde ontwikkeling op theoretisch gebied, is op het Nationaal Lucht- en Ruimtevaartlaboratorium (NLR) een verkennend windtunnelonderzoek uitgevoerd aan trillende modellen van twee verschillende vleugelprofielen. Met behulp van een speciale meettechniek, zijn gedetailleerde stationaire en instationaire drukken gemeten op een conventioneel profiel met een trillend roer en op een door het NLR ontworpen "schokvrij" transsoon profiel dat draaitrillingen kon uitvoeren.

Het proefschrift, dat dit onderzoek beschrijft en waarin de nadruk is gelegd op de interpretatie van de resultaten, is onderverdeeld in vier delen, waarvan de inhoud hieronder is samengevat.

Deel I begint met een beschrijving van de stroming om trillende vleugelprofielen, gevolgd door een beschouwing over de specifieke problemen die bij transsone snelheden optreden. Het blijkt dat, anders dan bij gematigd subsone en supersone stromingen, in een transsone stroming een essentiële koppeling bestaat tussen het stationaire en het instationaire stromingsveld. Hierdoor kunnen beide stromingsproblemen niet langer onafhankelijk van elkaar worden behandeld. In verband met deze koppeling, wordt deel I afgesloten met een samen-

vatting van de belangrijkste kenmerken van de stationaire transsone stroming om profielen (hoofdstuk 3).

Deel II beschrijft de windtunnelproeven, waarbij wordt ingegaan op de door het NLR ontwikkelde techniek voor het meten van instationaire drukken op harmonisch trillende windtunnelmodellen (hoofdstuk 5). Vervolgens worden, in de hoofdstukken 6 en 7, de modellen, de meetopstellingen en de meetprogramma's beschreven.

Deel III bevat een analyse van de verkregen resultaten, waarbij de nadruk is gelegd op de aspecten die typerend zijn voor het transsone gebied, namelijk het mechanisme van de interactie tussen het stationaire en het instationaire stromingsveld en de aanwezigheid van periodiek bewegende schokgolven (hoofdstuk 8). In hoofdstuk 9 wordt het bestaan gesignaleerd van drie verschillende typen van periodieke schokgolfbewegingen. Deze typen worden verklaard met behulp van een eenvoudig rekenmodel. In hoofdstuk 10 worden enkele aspecten van het instationair aërodynamisch gedrag van het schokvrije NLR-profiel besproken. Speciale aandacht wordt hierbij besteed aan de situatie waarin het profiel trilt om de invalshoek, waarbij in het stationaire geval de schokvrije stromingstoestand optreedt. Tenslotte wordt in hoofdstuk 11 de voor het flutteronderzoek belangrijke vraag behandeld in hoeverre in praktische toepassingen het instationaire stromingsprobleem beschouwd kan worden als een lineaire verstoring op een gegeven stationair stromingsveld.

Deel IV begint met een overzicht van theorieën voor het berekenen van de luchtkrachten op trillende profielen in hoog-subsone en transsone stromingen. Hierbij is de nadruk gelegd op de recente ontwikkelingen op dit gebied. Het blijkt dat de laatste jaren aanzienlijke vorderingen zijn gemaakt bij het ontwikkelen van numerieke methoden voor de berekening van transsone stromingen. De op het NLR uitgevoerde proeven hebben deze ontwikkeling ondersteund; de NLR-gegevens worden dan ook veelvuldig gebruikt ter verificatie van rekenmethoden. Deze situatie, met zijn vele stimulerende contacten, bood de auteur de gelegenheid het proefschrift te besluiten met een evaluatie van de mogelijkheden en beperkingen van een aantal nieuwe methoden voor het berekenen van instationaire transsone stromingen (hoofdstuk 13).

STELLINGEN

bij het proefschrift

INVESTIGATIONS OF THE TRANSONIC FLOW AROUND OSCILLATING AIRFOILS

van

H. TIJDEMAN

21 december 1977

1 De benamingen "narrow-tube solution", "wide-tube solution", "high-frequency solution", enz., die in de literatuur worden gehanteerd voor oplossingen van het probleem van de voortplanting van geluidsgolven door met gas gevulde buizen met een cirkelvormige doorsnede, geven aanleiding tot verwarring en dienen derhalve vermeden te worden. De verwarring wordt voorkomen door de oplossingen te beschrijven met behulp van het "shear wave number", zoals gedefinieerd in hoofdstuk 5 van dit proefschrift.

H. Tijdeman - "On the propagation of sound waves in cylindrical tubes". Journal of Sound and Vibration, Vol. 35, No. 1 (1975) pp. 1-33.

2 De door Karam en Franke gegeven "high-frequency solution" voor de voortplanting van geluidsgolven in met gas gevulde buizen is minder nauwkeurig dan de "wide-tube solution" welke een eeuw eerder door Kirchhoff werd afgeleid.

J.T. Karam, M.E. Franke - "The frequency response of pneumatic lines". Journal of Basic Engineering, Transactions of ASME, Series D, Vol. 91, No. 2 (1969) pp. 371-378.
G. Kirchhoff - "Ueber den Einfluss der Wärmeleitung in einem Gase auf die Schallbewegung". Poggendorfer Annalen, Vol. 134, No. 6 (1868) pp. 177-193.

3 Het door Coupry en Piazolli, Eckhaus, en Landahl gebruikte model voor de berekening van de instationaire luchtkrachten op een profiel met trillend roer is geen fysisch reëel model voor de situatie waarbij de schokgolven op het roer staan.

G. Coupry, G. Piazolli - "Etude du flottement en régime transsonique". Recherche Aéronautique No. 63 (Mars/Avril 1958) pp. 19-28.
W. Eckhaus - "Two-dimensional transonic unsteady flow with shock waves". OSR TR No. 59-491 (1959).
M. Landahl - "Unsteady transonic flow". (Pergamon Press, 1961).

4 De bewering van Yoshihara dat flutterspecialisten moeten afzien van hun lineaire systemen wordt, zeker als het om vleugels met een grote slankheid gaat, niet voldoende ondersteund door de tot nu toe door hem gepubliceerde numerieke oplossingen van de transsone stromingsvergelijkingen.

E.A. Murman, H. Yoshihara, D. Korn - "AIAA Course on transonic aerodynamics" (June 14-15, 1975, Hartford, Connecticut) Ch. 12, p. 19.

5 De in dit proefschrift beschreven type-C schokgolfbeweging, waarbij de schokgolf van het profiel afvliegt en zich voortplant in de vliegrichting, vormt een belangrijke lawaaibron bij helikopters, indien de stroming om de tippen van de rotorbladen periodiek transsoon wordt.

6 Het toepassen van "striptheorie" voor het berekenen van de instationaire transsone luchtkrachten op draagvlakken die uitgerust zijn met roeren over een deel van de spanwijdte, kan aanleiding geven tot resultaten die sterk afwijken van de werkelijkheid.

H. Bergh, H. Tijdeman, R.J. Zwaan - "High subsonic and transonic effects on pressure distributions measured for a swept wing with oscillating control surface". Z. Flugwiss. 18, Heft 9/10 (1970) pp. 339-347.

7 Bij de interpretatie van windtunnelresultaten waarbij variaties in het getal van Reynolds worden verkregen door variatie van de luchtdruk, dient men er op te letten dat effecten tengevolge van de elastische vervorming van het model niet geïnterpreteerd worden als effecten tengevolge van het getal van Reynolds.

8 Het hinderlijke lawaai dat een lege imperiaal boven op een rijdende personenauto kan veroorzaken, wordt voor een belangrijk deel onderdrukt door de voorste dwarsstaven spiraalsgewijs met een touwtje te omwikkelen.

9 Het feit dat op het NLR de aëroëlastische afdeling deel uitmaakt van de hoofdafdeling "Stromingen" en niet van de hoofdafdeling "Constructies en Materialen", zoals elders meestal het geval is, heeft in belangrijke mate bijgedragen tot de vooraanstaande positie welke het NLR inneemt op het gebied van de instationaire aërodynamica.

10 De gemoedsrust van vele vliegtuigpassagiers zou er mee gebaat zijn, als de bij de luchtvaartmaatschappijen gebruikelijke mededeling "Dames en Heren, wij nemen afscheid van U en danken U dat U met onze maatschappij heeft gevlogen" niet tijdens de naderingsvlucht, doch na de landing zou worden gedaan.

11 Indachtig de oude wijsheid "een gezonde geest in een gezond lichaam" verdient het aanbeveling promovendi de keus te laten tussen het schrijven van stellingen en het met goed gevolg afleggen van een zogenaamde "Cooper conditietest".

K.H. Cooper - "The new aerobics". (M. Evans and Company, New York, 1970).

cover design: jaap kuipers